

**THE APPLICATION OF NICKEL COMPLEXES TO
HALOGEN BONDING
AND HYDROFLUOROARYLATION**

VARGINI GAYATHRI THANGAVADIVALE

Doctor of Philosophy

**University of York
Chemistry**

June, 2015

ABSTRACT

The N-heterocyclic carbene complex, (1,5-hexadiene)Ni(IPr) (IPr = 1,3-bis(2,6-diisopropylphenyl)-4,5-dihydro-2H-imidazol-2-ylidene) was found to catalyse the hydrofluoroarylation reaction of alkynes at lower temperatures and more cleanly compared to the Ni(PR₃)₂ (R =Cyp and Cy) catalysts reported in the literature. Kinetic studies of the hydrofluoroarylation reaction using the above catalyst was carried out to obtain more information of the mechanism, which is addressed in chapters 2 and 3. The reaction followed in-situ by ¹H-NMR spectroscopy using 4,4-dimethylpentyne and C₆F₅H as the substrates catalysed by (1,5-hexadiene)Ni(IPr), suggested saturation kinetics with respect to the alkyne and first order dependence on the fluoroarene and the catalyst. The results also suggests an initial coordination of the alkyne to nickel Ni(IPr)(alkyne), the active species that reacts with the fluoroarene. The mechanistic understanding gained from this study, is similar to that proposed in the literature based on the DFT calculations using Ni-PR₃ as the catalyst.

Chapter 4 details the synthesis and study of two series of self-complementary nickel complexes Ni(X)(PEt₃)₂(y-C₆F₄I) (X=F⁻, Cl⁻, Br⁻ and I⁻ and y= ortho and para) exhibiting intermolecular halogen bonding interactions. X-ray crystallographic studies revealed the strength of the halogen bonding interaction decreases in the following order, with different XB acceptors; F⁻>Cl⁻≈Br⁻>I⁻. The XB interaction occurs at an angle of 180° for Ni-F⁻⋯I and ranges from 139° to 147° for Ni-X⁻⋯I, where X=Cl, Br and I). When PEt₃ ligand were substituted with PEt₂Ph ligand the halogen bonding interaction was observed to weaken. The higher number of fluorines ortho to the halogen bond donor strengthened the interaction. Investigation of the Ni-F⁻⋯I interactions by solid state NMR spectroscopy upon the ¹⁹F nuclei showed a downfield shift in the fluoride resonance when compared to its analogous complex without the halogen bonding interaction. The thermodynamic study of the halogen and hydrogen bonding interactions of nickel fluoride complexes, ligated to N-heterocyclic carbene ligands are reported in chapter 5. Interactions of indole and C₆F₅I have been studied with Ni(F)(ⁱ-Pr₂Im)₂(C₆F₅) using ¹⁹F-NMR spectroscopic titrations (For C₆F₅I, K₃₀₀ =7.2; ΔS° =-50.2±1.2 J/(mol.K); ΔH° =-23.9±0.3 kJ/mol and for indole K₃₀₀ =33; ΔS° = -53.6±1.7 J/ (mol.K); ΔH° =-32.7±0.5 kJ/mol).

TABLE OF CONTENTS

Abstract	ii
List of figures	ix
List of Schemes	xvi
List of tables	xx
Acknowledgement	xxiii
Declaration	xxv

CHAPTER 1

ACTIVATION OF FLUOROAROMATICS VIA PHOSPHINE AND N-HETEROCYCLIC CARBENE LIGATED Ni(0) COMPLEXES

1.1	Introduction	1
1.1.1	Is fluorine so special?	1
1.1.2	Transition metal-mediated activation of fluoroaromatics	3
1.1.2.1	Group 10 Metal-phosphines in the activation of fluoroaromatics	3
1.1.2.2	The role of phosphines	5
1.1.2.3	The reactivity of fluoroaromatics with Ni(0)-PR ₃ complexes	7
1.1.2.4	Activation of fluoroaromatics by Pd(0) and Pt(0) complexes	8
1.1.3	Tuning the kinetic and thermodynamic accessibility of C-H and C-F bonds	11
1.1.4	C-F bond activation via phosphine assisted pathways	15
1.1.5	N-heterocyclic carbenes as an alternative ligand to phosphines	19
1.1.5.1	The steric and electronic factors of N-heterocyclic carbenes	19
1.1.5.2	N-heterocyclic ligated Ni(0) - reactivity and use as catalysis	21
1.1.6	Hydrofluoroarylation of alkynes	23
1.1.6.1	Hydroarylation of heteroarenes	23
1.1.6.2	Hydrofluoroarylation of alkynes	24
1.2	Summary	26
1.3	References	27

CHAPTER 2

THE SEARCH FOR A SYSTEM TO STUDY THE MECHANISM OF HYDROFLUOROARYLATION OF ALKYNES

2.1.	Introduction	33
2.1.1.	Proposed mechanisms for the hydrofluoroarylation reaction	34
2.1.2.	Nickel-Alkyne complexes	40
2.2.	Results	42
2.2.1.	Synthesis of Ni(PCy ₃) ₂ (η^2 -alkyne)	43
2.2.2.	Reaction of Ni(PCy ₃) ₂ (η^2 -alkyne) with C ₆ F ₅	44
2.2.2.1	Formation of the Ni-H and the arylalkene in the reaction between C ₆ F ₅ H and Ni(PCy ₃) ₂ (η^2 -alkyne)	46
2.2.2.2	Formation of Ni-F in the reaction-C ₆ F ₅ H and Ni(PCy ₃) ₂ (η^2 -alkyne)	47
2.2.3.	Reaction of Ni(PCy ₃) ₂ (η^2 -alkyne) with 1,2,4,5-C ₆ F ₄ H ₂	52
2.2.4.	Synthesis of Ni(L)(1,5-hexadiene)	54
2.2.4.1	Synthesis and reactions of (1,5-hexadiene)Ni(PR ₃)	55
2.2.4.2	Reactions of Ni(PR ₃)(1,5-hexadiene) with C ₆ F ₅ H and alkynes	56
2.2.4.3	Synthesis and reactions of (1,5-hexadiene)Ni(IPr)	57
2.2.4.4	Reaction of C ₆ F ₅ H and alkyne catalysed Ni(IPr)(1,5-hexadiene)	58
2.3.	Discussion	64
2.3.1.	Introduction: Nickel(0) precursors	64
2.3.2.	Can Ni-PR ₃ be used to study the hydrofluoroarylation reaction?	65
2.3.3.	Ni-NHC -an alternative to Ni-PR ₃ to study the hydrofluoroarylation	69
2.4.	Summary	71
2.5.	References	72

CHAPTER 3

KINETIC ANALYSIS OF THE HYDROFLUOROARYLATION OF ALKYNES CATALYSED BY NI(0) LIGATED TO N-HETEROCYCLIC CARBENES

3.1	Introduction	75
3.1.1	Rate law of a reaction	75
3.1.2	Construction of the rate law for a reaction	77
3.1.3	Catalytic reactions	78
3.1.3.1	Reaction Progress Kinetic Analysis	79
3.1.3.2	Catalytic reactions involving two substrates	80
3.1.3.3	Saturation Kinetics	82
3.2	Results	83
3.2.1	Introduction	83
3.2.2	Choice of reactants	84
3.2.2.1	Choice of fluoroarene	84
3.2.2.2	Choice of alkyne	86
3.2.2.3	Conditions of data collection	88
3.2.3	Reaction progress kinetic analysis	89
3.2.3.1	Integral Method	89
3.2.4	Induction period	92
3.2.5	Catalyst deactivation or product inhibition	93
3.2.6	Stoichiometric reaction between fluoroarene and alkyne	95
3.2.7	The dependence of the rate of the reaction on [catalyst]	96
3.2.8	The order of the reaction with respect to C ₆ F ₅ H	101
3.2.8.1	Isolation method – C ₆ F ₅ H order	101
3.2.9	The dependence of the rate of the reaction on [alkyne]	104
3.2.10	Kinetic analysis at a low temperature	106
3.2.11	RPKA – Excess alkyne conditions	108
3.2.12	Modelled kinetic data	114
3.3	Discussion	118

3.3.1	The role of the catalyst	119
3.3.2	The dependence of the rate of the reaction on the substrates	120
3.3.2.1	The dependence of the rate on C ₆ F ₅ H	120
3.3.2.2	The role of the alkyne in the hydrofluoroarylation reaction	120
3.3.3	Mechanistic understanding of the hydrofluoroarylation reaction	122
3.4	Summary	125
3.5	Reference	126

CHAPTER 4

INTERMOLECULAR HALOGEN BONDING INTERACTIONS OF NICKEL HALIDE COMPLEXES AND THEIR PENDANT HALOGEN BOND DONORS IN THE SOLID STATE

4.1.	Introduction	129
4.1.1	A brief look into the history of halogen bonding interactions	129
4.1.2	General features and applications of XB interactions	130
4.2.	Results	139
4.1.3	Synthesis and characterization of Ni(X)(PCy ₃) ₂ (2,3,5,6-C ₆ F ₄ I)	139
4.2.1.1	Synthesis of Ni(X)(PCy ₃) ₂ (2,3,5,6-C ₆ F ₄ I)	139
4.2.1.2	Characterisation of trans-Ni(I)(PCy ₃) ₂ (2,3,5,6-C ₆ F ₄ I)	140
4.2.1.3	Characterization of trans-Ni(F)(PCy ₃) ₂ (2,3,5,6-C ₆ F ₄ I)	141
4.1.4	Synthesis and characterization of Ni(X)(PEt ₃) ₂ (2,3,5,6-C ₆ F ₄ I)	143
4.2.1.4	Synthesis of trans-Ni(X)(PEt ₃) ₂ (2,3,5,6-C ₆ F ₄ I)	143
4.2.1.5	Characterization of trans-Ni(I)(PEt ₃) ₂ (2,3,5,6-C ₆ F ₄ I)	144
4.2.1.6	X-ray crystallographic studies of 2-I	148
4.2.1.7	Characterization of trans-Ni(F)(PEt ₃) ₂ (2,3,5,6-C ₆ F ₄ I)	150
4.2.1.8	X-ray crystallographic studies of 2-F	152
4.2.1.9	Synthesis and characterization of Ni(Cl)(PEt ₃) ₂ (2,3,5,6-C ₆ F ₄ I)	153
4.2.1.10	X-ray crystallographic studies of 2-Cl	154
4.2.1.11	Characterization of trans-Ni(Br)(PEt ₃) ₂ (2,3,5,6-C ₆ F ₄ I)	156
4.2.1.12	X-ray crystallographic studies of 2-Br	156

4.2.1.13 Formation of $[\text{Ni}(\text{Br})(\text{PEt}_3)_2]_2(\text{C}_6\text{F}_4)$	158
4.1.5 Synthesis and characterization of trans- $\text{Ni}(\text{X})(\text{PEt}_2\text{Ph})_2(2,3,5,6\text{-C}_6\text{F}_4\text{I})$, X = I and F	161
4.2.1.14 Synthesis of trans- $\text{Ni}(\text{X})(\text{PEt}_2\text{Ph})_2(2,3,5,6\text{-C}_6\text{F}_4\text{I})$, X = I and F	161
4.2.1.15 Characterisation of trans- $\text{Ni}(\text{I})(\text{PEt}_2\text{Ph})_2(2,3,5,6\text{-C}_6\text{F}_4\text{I})$	162
4.2.1.16 X-ray crystallographic studies of 3-I	163
4.2.1.17 Characterization of trans- $\text{Ni}(\text{F})(\text{PEt}_2\text{Ph})_2(2,3,5,6\text{-C}_6\text{F}_4\text{I})$	165
4.1.6 Synthesis and characterization of $\text{tNi}(\text{X})(\text{PEt}_3)_2(2,3,4,5\text{-C}_6\text{F}_4\text{I})$, X = I, Br, Cl and F	166
4.2.1.18 Synthesis of $\text{Ni}(\text{X})(\text{PEt}_3)_2(2,3,4,5\text{-C}_6\text{F}_4\text{I})$, X = I, Br, Cl and F	166
4.2.1.19 Characterisation of trans- $\text{Ni}(\text{I})(\text{PEt}_3)_2(2,3,4,5\text{-C}_6\text{F}_4\text{I})$	168
4.2.1.20 X-ray crystallographic studies of 4-I	170
4.2.1.21 Characterization of trans- $\text{Ni}(\text{F})(\text{PEt}_3)_2(2,3,4,5\text{-C}_6\text{F}_4\text{I})$	171
4.2.1.22 X-ray crystallographic studies of 4-F	174
4.2.1.23 Unexpected Formation of $\text{Ni}(\text{PEt}_3)_2(\text{C}_6\text{F}_4)$	175
4.2.1.24 Characterization of trans- $\text{Ni}(\text{Cl})(\text{PEt}_3)_2(2,3,4,5\text{-C}_6\text{F}_4\text{I})$	177
4.2.1.25 X-ray crystallographic studies of 4-Cl	178
4.2.1.26 Characterization of trans- $\text{Ni}(\text{Br})(\text{PEt}_3)_2(2,3,4,5\text{-C}_6\text{F}_4\text{I})$	179
4.1.7 Solid State NMR spectroscopic studies	181
4.1.8 Variable Temperature X-ray crystallographic studies of 2-F	185
4.3 Discussion	189
4.4 Summary	195
4.5 References	196

CHAPTER 5

SOLUTION STUDIES OF HYDROGEN AND HALOGEN BONDING TOWARDS NICKEL FLUORIDES

5.1 Introduction	200
5.2 NMR spectroscopic studies of halogen bonding interactions of $\text{Ni}(\text{F})(\text{PEt}_3)_2(2\text{-C}_5\text{F}_4\text{N})$ with iodoperfluorohexane	202

5.2.1	Background /Aim	202
5.2.2	Results	203
5.3	NMR spectroscopy studies of Ni(F)(<i>i</i> -Pr ₂ Im) ₂ (C ₆ F ₅) as a Halogen and Hydrogen bond acceptor	204
5.3.1	Introduction	204
5.3.2	Results	208
5.3.2.1	NMR spectroscopy studies of Halogen bonding of trans-Ni(F)(<i>i</i> -Pr ₂ Im) ₂ (C ₆ F ₅)	208
5.3.2.2	NMR spectroscopy studies of Hydrogen bonding of trans-Ni(F)(<i>i</i> -Pr ₂ Im) ₂ (C ₆ F ₅)	211
5.4	Discussion	214
5.5	Summary	216
5.6	References	216
CHAPTER 6		
	Conclusions and further development	219
CHAPTER 7		
	Experimental	226
	Appendix	257
	Abbreviation	259
	References	262

LIST OF FIGURES

CHAPTER 1

- Figure 1-1** Some of the top selling pharmaceutical drugs in the market. 2
- Figure 1-2** Schematic demonstration of the cone angle used by Tolman to quantify the steric effects of PR_3 6
- Figure 1-3** Potential energy surface diagram for possible phosphine assisted C-F activation pathways of pentafluoropyridine by $Ni(PMe_3)_2$ leading to activation at 4- and 2-position 17
- Figure 1-4** The first “bottleable” N-heterocyclic carbene synthesised 19
- Figure 1-5** The selectivity of the activation of C-H bond ortho to fluorine 25

CHAPTER 2

- Figure 2-1** The ^{19}F -NMR spectrum (470 MHz, C_6D_6) of the reaction mixture between 1-P and C_6F_5H after an hour at $50^\circ C$ in toluene 46
- Figure 2-2** The ^{31}P -NMR spectrum (202 MHz, C_6D_6) of the reaction between 1-P and C_6F_5H after 24 hours at $50^\circ C$ in toluene 47
- Figure 2-3** The ^{19}F -NMR spectrum (470 MHz, C_6D_6) (fluoride region) of the reaction between 1-P and C_6F_5H after 24 hours at $50^\circ C$ in toluene 48
- Figure 2-4** The ^{31}P -NMR spectrum (202 MHz, C_6D_6) of the purified solid from the reaction between 1-P and C_6F_5H in hexane 49
- Figure 2-5** The ^{31}P -NMR spectrum (202 MHz, C_6D_6) of the solution decanted from the reaction between 1-P and C_6F_5H in hexane 49
- Figure 2-6** The LIFDI mass spectrum of the reaction between $trans-Ni(F)(PCy_3)_2(C_6F_4H)$ and 1-P 51
- Figure 2-7** LIFDI mass spectrum - the isotopic pattern of complex 4-P 55
- Figure 2-8** LIFDI mass spectrum of the complex 5-C 58
- Figure 2-9** The ^{19}F -NMR spectrum (470 MHz, C_6D_6) of the reaction mixture C_6F_5H and 4-octyne, catalysed by 5-C, after 7 hours at $55^\circ C$ 60

Figure 2-10 The $^1\text{H-NMR}$ spectrum (500 MHz, C_6D_6) of the reaction mixture $\text{C}_6\text{F}_5\text{H}$ and 4-octyne, catalysed by 5-C, after 3 hours at 55°C	60
Figure 2-11 Complexes used in literature as sources of $\text{Ni}(\text{PR}_3)_2$	64
Figure 2-12 Complex $(2,6\text{-Me}_2\text{C}_5\text{H}_3\text{N})\text{Ni}(\eta^2\text{-PhC}\equiv\text{CSiMe}_3)_2$	70

CHAPTER 3

Figure 3-1 $^1\text{H-NMR}$ spectrum of the reaction mixture of $\text{CH}_3\text{C}\equiv\text{CC}(\text{CH}_3)_3$ with $\text{C}_6\text{F}_5\text{H}$ catalysed by $(1,5\text{-hexadiene})\text{Ni}(\text{IPr})$ after 2 hours at 322.8 K (48% conversion) (labels in above scheme)	85
Figure 3-2 $^{19}\text{F-NMR}$ spectrum of the reaction mixture of $\text{CH}_3\text{C}\equiv\text{CC}(\text{CH}_3)_3$ with $\text{C}_6\text{F}_5\text{H}$ catalysed by $(1,5\text{-hexadiene})\text{Ni}(\text{IPr})$ after 12 hours at 55°C	86
Figure 3-3 Percentage conversion of the reactant and the formation of the product monitored for the reaction of 2B with 1A catalysed by $(1,5\text{-hexadiene})\text{Ni}(\text{IPr})$ in C_6D_6 at 322.8 K	89
Figure 3-4 'Graphical rate equation' - A plot of the rate of the reaction against $[1\text{A}]$ constructed from the data collected by monitoring $^1\text{H-NMR}$ spectroscopy for the reaction of 2B with 1A catalysed by $(1,5\text{-hexadiene})\text{Ni}(\text{IPr})$ in C_6D_6 at 322.8 K	91
Figure 3-5 A plot of the rate of the reaction against time constructed from the data collected by monitoring $^1\text{H-NMR}$ spectroscopy for the reaction of 1A with 2B catalysed by $(1,5\text{-hexadiene})\text{Ni}(\text{IPr})$ in C_6D_6 at 322.8 K	92
Figure 3-6 A plot of the rate of the reaction against $[1\text{A}]$ constructed from the data collected for the reactions of 1A with 2B catalysed by $(1,5\text{-hexadiene})\text{Ni}(\text{IPr})$ in C_6D_6 at 322.8 K	94
Figure 3-7 A plot of $1/[1\text{A}]^2$ against time constructed from the data collected by $^1\text{H-NMR}$ spectroscopy for the reaction of 1A with 2B catalysed by $(1,5\text{-hexadiene})\text{Ni}(\text{IPr})$ in C_6D_6 at 322.8 K	95

- Figure 3-8** A plot of $1/[1A]$ against time constructed from the data collected by $^1\text{H-NMR}$ spectroscopy for the reaction of 1A with 2B catalysed by (1,5-hexadiene)Ni(IPr) in C_6D_6 at 322.8 K 96
- Figure 3-9** A plot of k_{obs} as a function of [catalyst] from the data collected by $^1\text{H-NMR}$ spectroscopy for the hydrofluoroarylation reaction of 1A with 2B under different catalyst loading in C_6D_6 at 322.8 K 98
- Figure 3-10** A plot of the TOF as a function of the substrate concentration constructed from the data collected by $^1\text{H-NMR}$ spectroscopy for reactions of 1A with 2B, with different catalyst loading in C_6D_6 at 322.8 K 100
- Figure 3-11** A plot of $1/[1A]$ against time for the reaction of 1A with 2B (ratio 1 : 35) catalysed by (1,5-hexadiene)Ni(IPr) in C_6D_6 at 322.8 K (catalyst loading 12 mol%). 101
- Figure 3-12** A plot of k_{obs} as a function of [2B] for the reaction of 1A with different excesses of 2B catalysed by (1,5-hexadiene)Ni(IPr), in C_6D_6 at 322.8 K 103
- Figure 3-13** A plot of $\ln[2B]$ against time for the reaction of 1A with 2B (ratio 11 : 1) catalysed by (1,5-hexadiene)Ni(IPr) in C_6D_6 at 322.8 K (catalyst loading 10 mol%) 104
- Figure 3-14** A plot of $1/[1A]^2$ against time for the reaction of 1A with 2B catalysed by (1,5-hexadiene)Ni(IPr) in C_6D_6 at 306.4 K 105
- Figure 3-15** A plot of $\ln[2B]$ against for the reaction of 1A with excess 2B catalysed by (1,5-hexadiene)Ni(IPr) in C_6D_6 at 306.4 K (catalyst loading 5 mol%) 106
- Figure 3-16** A plot of k_{obs} as a function of [1A] for the reaction of 2B with different excesses of 1A catalysed by (1,5-hexadiene)Ni(IPr), at 306.4 K 107
- Figure 3-17** A plot of the TOF against [2B] for two reaction of 2B with excess 1A catalysed by (1,5-hexadiene)Ni(IPr) in C_6D_6 at 322.8 K (catalyst loading 10 mol%) 110

- Figure 3-18** A plot of the rate against the concentration of 2B for a reaction with the ratio 2B : 1A = 1 : 11 catalysed by (1,5-hexadiene)Ni(IPr) in C₆D₆ at 322.8 K (catalyst loading 10 mol%) 111
- Figure 3-19** A plot of the k_{obs} as a function of the ratio [1A]: [2B] for a series of hydrofluoroarylation reactions with different [1A] catalysed by (1,5-hexadiene)Ni(IPr) in C₆D₆ at 322.8 K 112
- Figure 3-20** A plot of the 1/k_{obs} as a function of 1/[1A] for a series of hydrofluoroarylation reactions with different [1A] catalysed by (1,5-hexadiene)Ni(IPr) in C₆D₆ at 322.8 K 114
- Figure 3-21** The percentage conversion of reactant as a function of time for a stoichiometric reaction of 1A : 2B = 1 : 1 at 322.8 K the experimental data and the fit based on the proposed model (catalyst loading 14.8 mol%) 116

CHAPTER 4

- Figure 4-1** Intermolecular halogen bond leading to the formation of the 1:1 adduct of bromine and 1,4-dioxane. 130
- Figure 4-2** Halogen bonding interactions exhibited in metal systems demonstrated by Brammer and co-workers. 133
- Figure 4-3** Pincer palladium halides acting as halogen bond acceptors with various halogen bond donors. 134
- Figure 4-4** Ion-pair recognition receptor designed with podand groups and XB-donor site. 135
- Figure 4-5** Intermolecular halogen bonding network in self-complementary systems 136
- Figure 4-6** ³¹P-NMR (202 MHz) spectrum of the reaction of 1,4-C₆F₄I₂ with Ni(COD)₂ and PCy₃ in C₆D₆. 140
- Figure 4-7** ³¹P-NMR (202 MHz) spectrum of the reaction of 1-I with CsF in C₆D₆. 141
- Figure 4-8** ¹⁹F-NMR (470 MHz) spectrum (in the region δ -300 to -440) of the reaction of reaction of 1-I with CsF in C₆D₆. 141
- Figure 4-9** ³²P-NMR (202 MHz) spectrum of 2-I in C₆D₆. 145

Figure 4-10 ^{19}F -NMR (470 MHz) spectrum of 2-I in C_6D_6	145
Figure 4-11 ^{31}P -NMR (202 MHz) spectrum of 2-I in C_6D_6 after purification	146
Figure 4-12 trans-[Ni(I)(PEt ₃) ₂] ₂ (2,3,5,6-C ₆ F ₄)	147
Figure 4-13 LIFDI mass spectrum showing the isotopic pattern of trans-[Ni(I)(PEt ₃) ₂] ₂ (2,3,5,6-C ₆ F ₄).	147
Figure 4-14 Molecular structure of 2-I. Thermal ellipsoids set at 50% level and hydrogen atoms are omitted for clarity. Torsional angle between the two adjacent metal centre planes of 2-I.	149
Figure 4-15 ^{31}P -NMR (202 MHz) spectrum of 2-F in C_6D_6 .	150
Figure 4-16 ^{19}F -NMR (470 MHz) spectrum of 2-F in C_6D_6 .	150
Figure 4-17 ^{19}F -NMR (470 MHz) spectrum of 2-F in C_6D_6 .	151
Figure 4-18 LIFDI mass spectrum showing the isotopic pattern of 2-F	152
Figure 4-19 Molecular structure of 2-F. Thermal ellipsoids set at 50% level. Hydrogen atoms are omitted for clarity.	153
Figure 4-20 Molecular structure of 2-Cl. Thermal ellipsoids set at 50% level and hydrogen atoms are omitted for clarity. Torsional angle between the two adjacent metal centre planes of 2-Cl	155
Figure 4-21 Molecular structure of 2-Br. Thermal ellipsoids set at 50% level. Hydrogen atoms are omitted for clarity. Torsional angle between the two adjacent metal centre planes of 2-Br.	157
Figure 4-22 Molecular structure of [Ni(Br)(PEt ₃) ₂] ₂ (2,3,5,6-C ₆ F ₄), thermal ellipsoids set at 50% level and hydrogen atoms are omitted for clarity.	158
Figure 4-23 ^{31}P -NMR (202 MHz) spectrum of 3-I in C_6D_6 .	163
Figure 4-24 ^{19}F -NMR (470 MHz) spectrum of 3-I in C_6D_6 .	163
Figure 4-25 Molecular structure of 3-I. Thermal ellipsoids set at 50% level. Hydrogen atoms are omitted for clarity.	164
Figure 4-26 ^{31}P -NMR (202 MHz) spectrum of 3-F in C_6D_6 .	165
Figure 4-27 ^{19}F -NMR (470 MHz) spectrum of 3-F in C_6D_6 .	165
Figure 4-28 ^{31}P -NMR (202 MHz) spectrum of 4-I in C_6D_6 .	169

Figure 4-29 ^{19}F -NMR (470 MHz) spectrum of 4-I in C_6D_6 .	169
Figure 4-30 Molecular structure of 4-I, Thermal ellipsoids set at 50% level and hydrogen atoms are omitted for clarity. Torsional angle between the two adjacent metal centre planes of 4-I.	170
Figure 4-31 ^{31}P -NMR (202 MHz) spectrum of 4-F in C_6D_6 .	172
Figure 4-32 ^{19}F -NMR (470 MHz) spectrum of 4-F in C_6D_6 .	172
Figure 4-33 ^{19}F -NMR (470 MHz) spectrum of 4-F in C_6D_6 .	173
Figure 4-34 Molecular structure of 4-F. Thermal ellipsoids set at 50% level and hydrogen atoms are omitted for clarity. Torsional angle between the two adjacent metal centre planes of 4-F.	174
Figure 4-35 Molecular structure of $\text{Ni}(\text{PEt}_3)_2(\text{C}_6\text{F}_4)$. Thermal ellipsoids set at 50% level and hydrogen atoms are omitted for clarity. Selected bond lengths (\AA) and angles ($^\circ$) given in table above for $\text{Ni}(\text{PEt}_3)_2(\text{C}_6\text{F}_4)$.	176
Figure 4-36 ^{19}F -NMR (470 MHz) spectrum of the sample containing $\text{Ni}(\text{PEt}_3)_2(\text{C}_6\text{F}_4)$.	176
Figure 4-37 Molecular structure of 4-Cl. Thermal ellipsoids set at 50% level. Hydrogen atoms and the end methyl groups are omitted for clarity	178
Figure 4-38 ^{19}F -MAS SSNMR spectrum of complex 2-F. The black dots indicate the peaks corresponding to the fluoride resonance	181
Figure 4-39 ^{19}F -MAS SSNMR spectrum of complex 4-F. The black dots indicate the peaks corresponding to the fluoride resonance	183
Figure 4-40 ^{19}F -MAS SSNMR spectrum of $\text{trans-Ni}(\text{F})(\text{PEt}_3)_2(\text{C}_6\text{F}_5)$. The black dots indicate the peaks corresponding to the fluoride resonance	183

CHAPTER 5

Figure 5-1 Fit of the titration curves at 300 K showing $\Delta\delta_{\text{F}}$ versus the ratio of the molar concentrations of $\text{C}_6\text{F}_{13}\text{I}$ and $\text{Ni}(\text{F})(\text{PEt}_3)_2(\text{C}_5\text{F}_4\text{N})$ in toluene- d_8 .	203
Figure 5-2 Predicted curves for a 1:1 host-guest binding system, for different concentrations of host and guest.	207

- Figure 5-3** Species used for the study; indole, pentafluorobenzene, trans- $\text{Ni}(\text{F})(i\text{-Pr}_2\text{Im})_2(\text{C}_6\text{F}_5)$ 207
- Figure 5-4** Fit of the titration curves for different temperatures showing $\Delta\delta_{\text{F}}$ versus the ratio of the molar concentrations of $\text{C}_6\text{F}_5\text{I}$ and trans- $\text{Ni}(\text{F})(i\text{-Pr}_2\text{Im})_2(\text{C}_6\text{F}_5)$ (~7 mM) in toluene- d_8 . 209
- Figure 5-5** Van't Hoff plot of the equilibrium constants from the NMR titration of $\text{C}_6\text{F}_5\text{I}$ and $\text{Ni}(\text{F})(i\text{-Pr}_2\text{Im})_2(\text{C}_6\text{F}_5)$ in toluene- d_8 . 210
- Figure 5-6** Fit of the titration curves for different temperatures showing $\Delta\delta_{\text{F}}$ versus the ratio of the molar concentrations of indole and $\text{Ni}(\text{F})(i\text{-Pr}_2\text{Im})_2(\text{C}_6\text{F}_5)$ (~1.6 mM) in toluene- d_8 . 211
- Figure 5-7** Van't Hoff plot of the equilibrium constants from the NMR titration of indole and $\text{Ni}(\text{F})(i\text{-Pr}_2\text{Im})_2(\text{C}_6\text{F}_5)$ in toluene- d_8 . 213

LIST OF SCHEMES

CHAPTER 1

- Scheme 1-1** First reported example of a nickel-catalysed cross coupling reaction by Kumada and co-workers in 1973 6
- Scheme 1-2** Contrasting behaviour of in-situ generated Ni(PEt₃)₂ towards variously substituted fluoroarenes 9
- Scheme 1-3** Synthesis and reactivity of Pd(F)(Pi-Pr₃)₂(C₅F₄N) towards various silanes and the stannane, Bu₃SnCH=CH₂ 10
- Scheme 1-4** Suzuki coupling of phenylboronic acid and monofluorobenzene catalysed by Pd, in the presence of PMe₃ and Cr(CO)₃ 11
- Scheme 1-5** Cross coupling of polyfluoroarenes and aryl Grignard reagents catalysed by Pd 11
- Scheme 1-6** Cross-coupling of aryl halides and fluorobenzenes catalysed by palladium 12
- Scheme 1-7** The reactivity of Ni(PEt₃)₂(η²-C₁₄H₁₀) with C₆F₅H 14
- Scheme 1-8** Catalytic cross coupling via C-F bond activation mediated by Ni(0) 16
- Scheme 1-9** Reactivity of Ni(0) and Pt(0) phosphine complexes with C₅F₅N 17
- Scheme 1-10** The formation of the *cis*-Ni(PEt₃)₂(F)(3,5,6-C₅F₃NH) 19
- Scheme 1-11** C-F bond activation of C₆F₆ by a Ni(0)-NHC complex 22
- Scheme 1-12** A base-free Suzuki-Miyaura cross-coupling of fluoroarenes to aryl boronates using [Ni(ⁱ-Pr₂Im)₂]₂(COD) as the catalyst 22
- Scheme 1-13** Hydroarylation of unactivated olefins catalysed by Ni(0)-NHC complex 23
- Scheme 1-14** Hydroarylation observed as a side product in the arylocyanation of alkynes 24

Scheme 1-15 η^2 -coordination of Ni(0)-NHC at C3-C4 of the pyridyl ring in the presence of AlMe ₃	25
Scheme 1-16 Hydrofluoroarylation of alkynes catalysed by Ni(0)-PR ₃	26
CHAPTER 2	
Scheme 2-1 Hydrofluoroarylation of the alkyne catalysed by Ni(0)	34
Scheme 2-2 Stoichiometric reactions carried out using [(PCy ₃) ₂ Ni] ₂ N ₂ with C ₆ F ₅ H and 4-octyne	34
Scheme 2-3 Mechanism of hydrofluoroarylation proposed by Nakao et al	35
Scheme 2-4 Mechanism postulated based on the result from DFT calculations	39
Scheme 2-5 Formation of Ni(P ^{<i>i</i>} -Pr ₃) ₂ (η^2 -EtC≡CEt) ₃	42
Scheme 2-6 Formation of Ni(PR ₃) ₂ (alkyne) complexes	43
Scheme 2-7 The products resulting from the reaction between Ni(PCy ₃) ₂ (η^2 -alkyne) and C ₆ F ₅ H	45
Scheme 2-8 The products resulting from the reaction between Ni(PCy ₃) ₂ (η^2 -alkyne) and 1,4-C ₆ F ₄ H ₂	52
Scheme 2-9 Synthesis of (1,5-hexadiene)Ni(L)	54
Scheme 2-10 The reactions of (1,5-hexadiene)Ni(PR ₃) with C ₆ F ₅ H and alkynes	56
Scheme 2-11 Coupling reaction of C ₆ F ₅ H and alkyne catalysed by 5-C	59
Scheme 2-12 Double C-F activation of pentafluoropyridine	66
Scheme 2-13 The resultant products from two separate reactions aiming for the formation of Ni(F)(PCy ₃) ₂ [(C ₆ F ₄)PhC=CPh(H)]	68

CHATER 3

Scheme 3-1 Schematic diagram of a one substrate enzyme catalytic system	79
Scheme 3-2 Schematic diagram of a two substrate catalytic system	80
Scheme 3-3 The substrates and the standard conditions of the hydrofluoroarylation reaction used to collect data for the kinetic analysis	85
Scheme 3-4 The substrates and the standard conditions of the hydrofluoroarylation reaction used to collect data for the kinetic analysis	86
Scheme 3-5 A schematic diagram of the hydrofluorarylation catalytic cycle for 1A and 2B catalysed by (1,5-hexadiene)Ni(IPr) in C ₆ D ₆	90
Scheme 3-6 A schematic diagram of the catalytic cycle for the hydrofluoroarylation reaction of 1A and 2B catalysed by (1,5-hexadiene)Ni(IPr)	108
Scheme 3-7 Schematic diagram of a two substrate catalytic system	122
Scheme 3-8 Schematic diagram of the catalytic cycle proposed based on the kinetic analysis of the hydrofluoroarylation of alkynes	124

Chapter 4

Scheme 4-1 Structural motif targeted in this study that shows the envisaged intermolecular halogen bonding interaction.	137
Scheme 4-2 Formation of 1-I and 1-F	139
Scheme 4-3 The formation of complexes 2-I, 2-F, 2-Cl and 2-Br	144
Scheme 4-4 Formation of complexes 3-I and 3-F at room temperature	162
Scheme 4-5 Synthesis of complexes 4-I, 4-F, 4-Cl and 4-Br	168

Scheme 4-6 Scheme of the anisotropic charge distribution around the halogen depending on their environment and the resulting electrostatic attraction of electrophiles or nucleophiles respectively 192

Scheme 4-7 Schematic diagram of the Ni-X...I angles of the para-iodo complexes 192

Chapter 5

Scheme 5-1 Group 10 metal fluorides used for halogen bonding interactions studies. 201

Scheme 5-2 trans-Ni(F)(ⁱ-Pr₂Im)₂(C₆F₅) acting as a Lewis base towards C₆F₅I and indole. 208

LIST OF TABLES

CHAPTER 2

Table 2-1 NMR spectroscopic data for the nickel complexes formed in the reaction of C ₆ F ₅ H with 1-P or 2-P	53
Table 2-2 The spectral data for the products of the hydrofluoroarylation – 1af, 2af and 3af	62

CHAPTER 3

Table 3-1 The rate laws and the integrated rate equations	76
Table 3-2 The modified rate equation of a two substrate catalytic system under certain limiting cases	83
Table 3-3 The observed third order rate constants for stoichiometric reactions where the [2B] : [1A] ratio = 1 : 1 at 322.8 K	98
Table 3-4 The observed pseudo second order rate constants for reactions varying the [2B]: [1A] ratio by using excess 2B	102
Table 3-5 The observed pseudo first order rate constants for reactions varying the [2B] : [1A] ratio at 306.4 K	107
Table 3-6 The observed rate constants obtained from pseudo 1st order rate equations for experiments varying the [1A]:[2B] ratio at 322.8 K	112
Table 3-7 Rate constants obtained from the model fitting the experimental kinetic data	116
Table 3-8 Rate constants obtained from the simplified model fitting the experimental kinetic data	117

CHAPTER 4

Table 4-1 Complexes prepared to study the halogen bonding interactions in the solid state.	138
Table 4-2 Selected bond lengths (Å) and angles (°) of 2-l.	148

Table 4-3 Selected bond lengths (Å) and angles (°) of 2-F.	153
Table 4-4 ³¹ P and ¹⁹ F-NMR data for complex 2-Cl.	154
Table 4-5 Selected bond lengths (Å) and angles (°) of 2-Cl.	155
Table 4-6 ³¹ P and ¹⁹ F-NMR data for complex 2-Br.	156
Table 4-7 Selected bond lengths (Å) and angles (°) of 2-Br.	158
Table 4-8 Selected bond lengths (Å) and angles (°) of complex [Ni(Br)(PEt ₃) ₂] ₂ (2,3,5,6-C ₆ F ₄).	159
Table 4-9 Crystal data for complexes 2-I, 2-F, 2-Cl and 2-Br.	160
Table 4-10 Selected bond lengths (Å) and angles (°) of 3-I.	164
Table 4-11 Selected bond lengths (Å) and angles (°) of 4-I.	171
Table 4-12 ³¹ P and ¹⁹ F-NMR data for complex 4-F.	173
Table 4-13 Selected bond lengths (Å) and angles (°) of 4-F	175
Table 4-14 ³¹ P and ¹⁹ F-NMR spectroscopy data for complex 4-Cl	177
Table 4-15 Selected bond lengths (Å) and angles (°) of 4-Cl.	178
Table 4-16 ³¹ P and ¹⁹ F-NMR data for complex 4-Br	179
Table 4-17 Crystal data for complexes 3-I, 4-I, 4-F and 4-Cl.	180
Table 4-18 Isotropic chemical shifts of trans-Ni(F)(PEt ₃) ₂ (C ₆ F ₅), 2-F and 4 F in solution and solid state NMR spectroscopy.	184
Table 4-19 ¹⁹ F-MAS-SSNMR parameters for trans-Ni(F)(PEt ₃) ₂ (C ₆ F ₅), 2-F and 4-F	184
Table 4-20 Variable temperature X-ray crystallographic data for complex 2-F, selected intermolecular bond lengths are given for comparison purposes.	185
Table 4-21 Crystal data and structure refinement for 2-F at variable temperatures.	186
Table 4-22 Intermolecular distances and the angles of complexes 2-I, 2-F, 2-Cl, 2-Br, 3-I, 4-I, 4-F and 4-Cl.	187

CHAPTER 5

- Table 5-1** Summary of the thermodynamic data for halogen bonding for complex $\text{Ni}(\text{F})(\text{PEt}_3)_2(\text{C}_5\text{F}_4\text{N})$ with $\text{C}_6\text{F}_{13}\text{I}$ at 300 K in toluene- d_8 204
- Table 5-2** Thermodynamic data for XB and HB for complexes $\text{Ni}(\text{F})(i\text{-Pr}_2\text{Im})_2(\text{C}_6\text{F}_5)$ from previous studies in the group 205
- Table 5-3** Equilibrium constants and the downfield shift of the co-ordinated fluoride resonance from that of the free fluoride resonance measured at various temperatures for adduct formation between $\text{trans-Ni}(\text{F})(i\text{-Pr}_2\text{Im})_2(\text{C}_6\text{F}_5)$ and $\text{C}_6\text{F}_5\text{I}$ in toluene. 210
- Table 5-4** Equilibrium constants and the downfield shift of the coordinated fluoride resonance from that of the free fluoride resonance measured at various temperatures for adduct formation with indole in toluene. 212
- Table 5-5** Summary of the thermodynamic data obtained for hydrogen and halogen bonding of $\text{Ni}(\text{F})(i\text{-Pr}_2\text{Im})_2(\text{C}_6\text{F}_5)$ with indole and $\text{C}_6\text{F}_5\text{I}$ respectively, in toluene- d_8 . 213
- Table 5-6** Thermodynamic data for XB and HB for complexes $\text{Ni}(\text{F})(i\text{-Pr}_2\text{Im})_2(\text{C}_6\text{F}_5)$ studies here and the literature values for $\text{Ni}(\text{F})(\text{PCy}_3)_2(\text{C}_5\text{NF}_4)$ and $\text{Ni}(\text{F})(\text{PEt}_3)_2(\text{C}_5\text{NF}_4)$ in toluene 214

ACKNOWLEDGEMENT

My heartfelt gratitude goes to my supervisor, Prof. Robin Perutz for his support throughout the past few years. His vast knowledge and his amazing experience in the field was truly a privilege to work with. Prof. Robin, was a very supportive supervisor who always found time for discussions and the useful advice and suggestions he has given on many occasions have made this work possible. But most importantly, his patience with me was surprising and is much appreciated.

A very special “thank you” for Dr. Dan A Smith, the “cheerful and simple” post-doctoral fellow who joined the group to work on halogen and hydrogen bonding interactions. Being one of the ‘rare’ talented chemists, he was full of useful suggestions and skilful techniques which I benefitted greatly from. Some of the questions he asked me has been “eye-opening” and has led to some of the good work in the thesis. His advice and patience in proof reading the thesis is greatly appreciated! It will not be just not to say that this may not have been possible without all the moral support from him, thanks Dan! ☺

Thank you to Adrian, Sam and Dan for the crystal structures, especially Adrian for tackling very difficult structures. A warm thank you for Heather Fish, for the support with the NMR spectroscopy, Pedro for the help with the SS NMR spectroscopy and for the simulation spectra obtained. Grate for elemental analysis. The friendly services of Abby, from the workshops, Steve and Mike in the chemical stores is much appreciated. A huge thank you for Karl for the excellent services extended by him on the mass spectrometry. Karl was always ready to listen and help, adjusting according to the experimental needs, which makes a researcher’s life so much easier! Thank you to the present and past RNP group members and laboratory technicians, whom I’ve worked with. The overseas research scholarship, University of York is greatly appreciated for the funding.

For God almighty, whose love and grace makes everything possible. My patron saint, St. Anthony, for his love and guidance in every step. Most importantly, my family. The greatest privilege a child could have is good parents, I am blessed with parents who have never feared to go beyond their capacity to support my endeavours. Everything I have ever achieved is because of their constant and vital support. My heart's gratitude goes to my Appa and Amma, whose unceasing faith in me and their inspiration from miles away kept me going in the most desperate of times. My lovely sisters, Praveena and Scholia who I could always count on, who were always there for a laugh or to listen to my troubles without judging me. My brother Ginger, whose constant patience and unceasing love has never failed to put a smile on my face and who is the very reason for my existence.

AUTHOR'S DECLARATION

I declare that this thesis is a presentation of original work and I am the sole author. This work has not previously been presented for an award at this, or any other, University. All sources are acknowledged as References.

Vargini G Thangavadivale

CHAPTER ONE

INTRODUCTION

Activation of fluoroaromatics via phosphine and N-heterocyclic carbene ligated Ni(0) complexes

1.1 Introduction

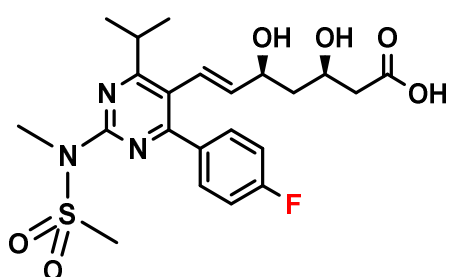
1.1.1 Is fluorine so special?

The successful isolation of fluorine by Henri Moissan in 1886, earned him the Nobel prize in 1906.¹ The electrolysis method developed by Moissan is still in use to produce fluorine gas by certain industries.¹ However, given the poisonous nature of the few naturally occurring fluorine containing organic molecules, the phenomenon of introducing fluorine into natural products for improved therapeutic efficiency was unheard of until the 1950s.¹ The observation by Fried and Sabo in 1954 of the glucocorticoid activity of fludrocortisone (*sic*), the first fluorine containing pharmaceutical, exceeding nearly 10 times that of its parent hormones paved the path for fluorine containing organic molecules for enhanced biological activity.²

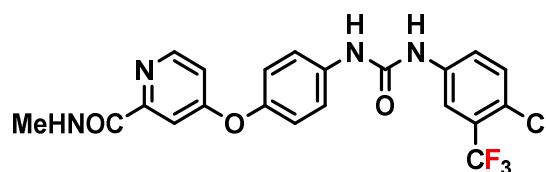
Organic molecules with fluorine motifs are continuously on the rise in the market of bio-active molecules.³ This is attributable to the fact that introduction of a fluorine into an organic molecule alters the physical and chemical properties of the molecule dramatically.⁴ Replacing a hydrogen atom by a more electronegative fluorine atom alters the polarity and the acidity of the resulting molecule without significantly altering the steric demand of the molecule and hence fluorine is often considered a good bioisostere for hydrogen.^{1,5,6}

At least one fluorine is incorporated in nearly 40% of the agrochemicals in the market and the influence of fluorine containing pharmaceutical drugs in the market is seen by the growth seen in the last few decades, resulting in nearly a 25% occurrence of fluorine containing drugs in the current market.¹ These numbers include several drugs that topped the sales market (Figure 1-1).^{1,3,7} Incorporation of a fluorine atom in an organic molecule results in an increase in the lipophilicity and for a pharmaceutical drug often the metabolic stability

and solubility. The presence of fluorine atoms can also enhance the delivery of a drug molecule to the desired target through the interaction with biological media by non-covalent interactions such as hydrogen bonding that are facilitated by the fluorine atom on the drug molecule.³ Another important reason that fluorine containing drugs are attractive is the potential for an increase in the drug efficiency that allows for lower doses.³



Rosuvastatin
marketed as 'Crestor' by
Astra-Zeneca -
treatment of
hypercholesterolemia
(total sales reached
\$6622 billion in 2011)



Sorafenib
marketed as 'Nexavar' by
Bayer and Onyx -
treatment of kidney, liver and
thyroid cancer
(total sales reached
\$1.01 billion in 2011, with a year to
year increase of 2.8 %).

Figure 1-1 Some of the top selling pharmaceutical drugs in the market.¹

In the absence of naturally occurring fluorinated aromatics, all fluoroaromatic molecules of interest have to be synthesised.³ Currently the fluoroarenes are widely accessed via non transition metal-mediated processes. These processes include the Halex reaction and Balz-Schiemann reaction. These methods require high temperatures and harsh conditions. In addition, copper-mediated oxidative fluorination which recycles the by-products and Cu catalyst, also uses harsh conditions for the process.⁶ These processes are energy consuming and the functional group tolerance is poor due to the harsh conditions used, making them unsuitable for fluorination at a late stage in multi-step synthesis.⁶

1.1.2 Transition metal-mediated activation of fluoroaromatics

1.1.2.1 Group 10 Metal-phosphine complexes in the activation of fluoroaromatics

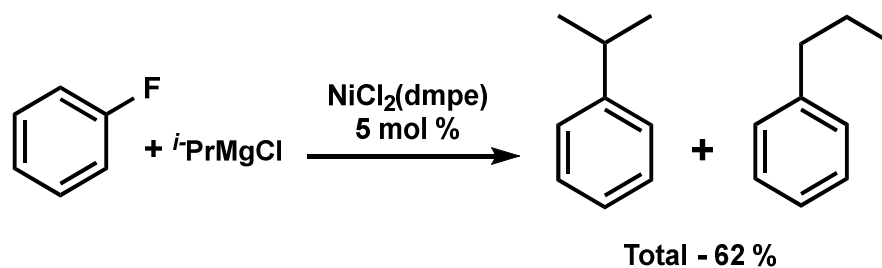
The aromatic C-F bond is the strongest bond the carbon atom can make with a heteroatom ($D_{\text{Ph-F}}$ 126 kcal/mol) and the activation of this bond can prove to be challenging, especially in the presence of weaker bonds.⁸ However, the breakage of this bond is done frequently with the help of transition metals, this can be attributed to the stronger bond formation between transition metals and fluorine on the cleavage of the C-F bond.^{3,7,9,10}

Metal-mediated catalysis as a synthetic route to fluorinated organic molecules has enjoyed significant attention in the recent past.^{8,10} Out of all the possibilities, the two most promising routes forward are fluorination of an organic molecule and C-F bond functionalization. Metal-mediated fluorination, a method where fluorine atoms or the fluorine containing motifs are introduced in the molecule at a later stage in the synthesis. C-F bond functionalization techniques are often carried out via activation and derivatization of a fluorine containing molecule to the desired target molecule.¹⁰ Fluorination techniques involve nucleophilic fluorination, electrophilic fluorination and radical fluorination.¹¹ Nucleophilic fluorination where the substrate acts as the electrophile, is carried out using alkali metal fluorides (e.g. KF, CsF), tetraalkylammonium fluorides (e.g. TMAF, TBAF) and others such as HF/pyridine, silicates and deoxofluorinating reagents.¹¹ Electrophilic fluorination on the other hand involves a substrate that would act as a nucleophile (e.g. arenes or Grignard reagents) and some of the commonly used fluorinating agents involve N-fluoropyridinium salts or other similar reagents bearing N-F motifs.¹¹ Radical fluorination is carried out by creating a C-F bond by generating radicals in-situ.¹¹

The latter method of accessing fluoroarenes, the C-F bond activation is conducted either by hydrodefluorination, which is the process of replacing a fluorine atom by a hydrogen or by another motif through cross-coupling

reactions to give C-C, C-S, C-O, C-N, C-P or C-X (X= halogens) bonds.¹⁰ The higher fluorinated arenes are more likely to undergo hydrodefluorination compared to the less fluorinated arenes; this is attributed to the stronger C-F bond in hexafluorobenzene compared to monofluorobenzene.¹⁰ Hydrodefluorination is also sought as a method to dehalogenate fluorocarbons which have a prolonged life in the environment.^{10,12} The cross-coupling techniques focused on activating the C-H bonds present in the fluoroarenes, although achieved in certain instances, is challenging due to the lack of selectivity when there is more than one C-H bond present.⁶ The activation of the C-H bond ortho to fluorine atoms is more favourable than the other C-H bonds in metal-mediated reactions. This behaviour can be attributed to the stronger M-C bond.¹³ DFT calculations performed by Perutz and co-workers on the influence of fluorine substituents on the M-C_(aryl) bond and the H-C_(aryl) bond provided evidence that the increase in the bond energy of the M-C_(aryl) bond is much larger compared to the increase in the bond energy of the H-C_(aryl) when ortho fluorine substituents are present.¹³

Efficient synthesis of substituted arylalkenes with selective stereochemistry has attracted increasing attention due to the presence of this motif in several natural products, pharmaceuticals and in organic materials.¹⁴ The most attractive synthetic route to arrive at such substituted arylalkenes are the metal-catalysed synthetic methods. This advantage can be attributed to the milder conditions used and the resulting atom efficiency, which are features that are often sought by industries. Cross-coupling reactions catalysed by a transition metal were reported as early as 1973, by Kumada and co-workers, where a nickel catalyst is demonstrated to catalyse the coupling of isopropyl magnesium chloride to monofluorobenzene (Scheme 1-1).¹⁵



Scheme 1-1 First reported example of a nickel-catalysed cross-coupling reaction by Kumada and co-workers in 1973.

1.1.2.2 The role of phosphines

Tertiary phosphines play an important role as ligands in metal-mediated catalytic transformations and therefore, along with N-heterocyclic carbenes and cyclopentadienyls are widely known as catalytically useful ligands.¹⁶ The ability of these ligands to be tuned according to their steric and electronic requirement makes them attractive for altering the outcome of catalytic reactions.^{16,17} Phosphines unlike amines, cannot be regarded as pure σ -donors due to their π -bonding ability.¹⁷ The π -acidity of the phosphines (PR₃) depend heavily on the substituent R group, with weak π -acidity observed for alkyl phosphines and strong π -acidity comparable to CO in the case of PF₃.¹⁷

The R group of the phosphine can influence the electronic effect and the steric effect of the metal, which has been quantified by Tolman.¹⁸ The electronic effect of various R groups was quantified by measuring the CO stretching frequencies, $\nu(\text{CO})$, of complexes of the type, Ni(PR₃)(CO)₃.¹⁸ The electron density at the metal centre is increased by strong donors, which results in the increase in back donation from the metal to the π^* -orbital of the CO ligand. This back donation into the π^* -orbital of CO weakens the C≡O bond and hence lowers the IR stretching frequency.¹⁸

The steric factors of the phosphines affect the number of phosphine ligands that fit in the coordination sphere of the metal.¹⁷ This has been quantified with the cone angle by Tolman (Figure 1-2).¹⁸ The cone angle was obtained by measuring the angle of the cone that consisted of the ligand in the metal phosphine model, in which the R groups had been folded back to its maximum.^{17,18}

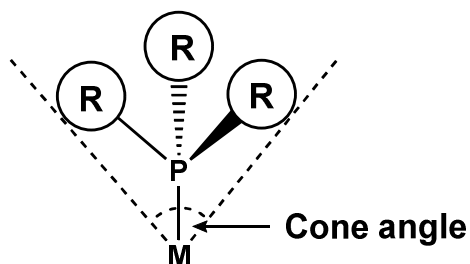


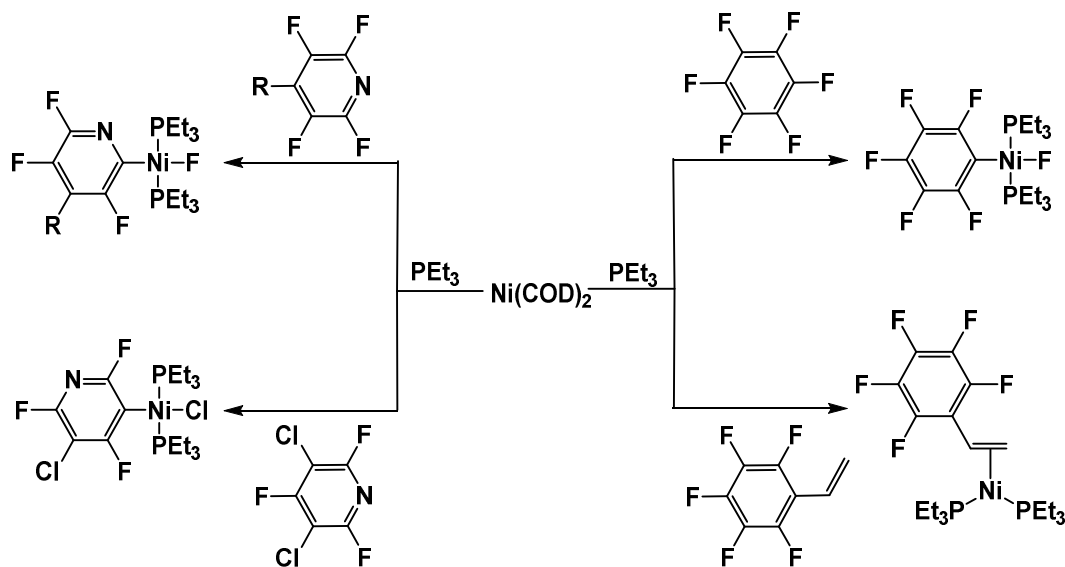
Figure 1-2 Schematic demonstration of the cone angle used by Tolman to quantify the steric effects of PR₃

In a recent computational studies done by Gusev on the electron donor properties of two electron donors, an argument was presented stating that comparing the Tolman electronic parameter alone is not sufficient when different groups of ligands are compared.¹⁹ The study was performed with the complexes IrCp(CO)L and IrCp(H₂C=CH₂)L. The complexes were chosen so that the CO ligand would not have significant trans effect from the ligand, L and influence of the steric hindrance on the studies caused by bulky ligands is minimal.¹⁹ The results from the study pointed out that the CO stretching frequency are often interpreted best when they correspond to the change in their C≡O bond distances.¹⁹ The study also pointed out that when amine and ether were used as the ligands in the complex, IrCp(CO)L, they acted as stronger electron donors than the N-heterocyclic carbene ligands. This property can be attributed to the pure σ -donation and poor π -acceptor character of those ligands.¹⁹

1.1.2.3 The reactivity of fluoroaromatics with Nickel(0)–phosphine complexes

As early as the late seventies, the reactivity of sources of Ni(0) towards fluoroaromatics has been investigated. The complex Ni(F)(PEt₃)₂(C₆F₅) was first reported in 1977, as a result of a reaction between Ni(COD)₂ and C₆F₆ in the presence of PEt₃ in a yield of 7%.²⁰ The only evidence provided for the formation was the IR spectroscopic data and elemental analysis.²⁰ The full characterization of the complex was performed later by Perutz and co-workers in 1997 (Scheme 1-2).²¹ The reaction was postulated to proceed via a Ni(PEt₃)₂(COD) species which subsequently reacted with hexafluorobenzene. It was also observed that upon dissolution of the isolated species, Ni(PEt₃)₄ in hydrocarbon solvents gave rise to a purple solution. This purple solution resulted from the dissociation of a phosphine group to produce Ni(PEt₃)₃ which was found to be more reactive than the Ni(PEt₃)₂(COD) species.²⁰ However, the reaction of Ni(PEt₃)₄ with halo-aromatics was observed to give rise to competing reactions resulting in the formation of paramagnetic Ni(I) species, Ni(X)(PEt₃)₃ (X = Cl, Br and I).²²

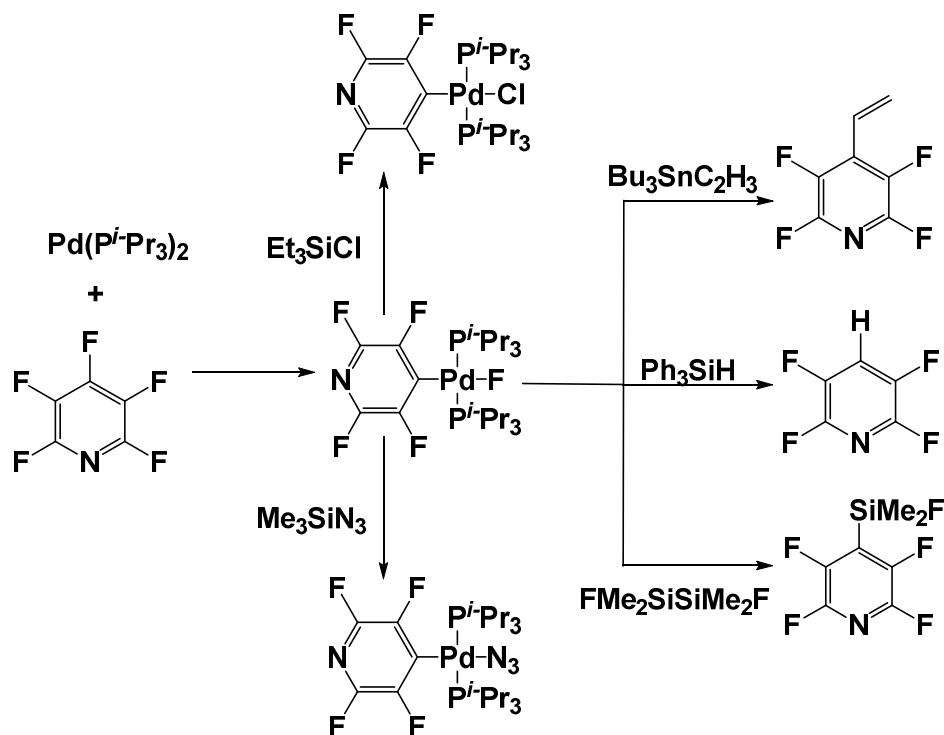
In addition to characterizing the compound, Ni(F)(PEt₃)₂(C₆F₅), the reactivity of Ni(0) complexes was tested with other fluoroaromatics including fluoropyridines by Perutz et al. in 1997. The studies showed that the fluoropyridines reacted more rapidly with Ni(0) resulting in better yields and was found to be more selective for C-F bonds over C-H bonds. The predominant product of the fluoropyridine reaction was observed to be C-F activation at 2-position, unlike the analogous Pt(0) and Pd(0) complexes where activation occurred at 4-position.²¹



Scheme 1-2 Contrasting behaviour of in-situ generated Ni(PEt₃)₂ towards variously substituted fluoroarenes²¹

1.1.2.4 Activation of fluoroaromatics by Pd(0) and Pt(0) complexes

The reactivity studies of fluoropyridines were extended to Pd and Pt by Perutz, Braun and co-workers. The stoichiometric reactions of Pd(0) and Pt(0) complexes were observed to give rise to C-F activation with pentafluoropyridine exclusively at the 4-position, unlike the Ni(0) analogue where a mixture of all three possible isomers were observed where the predominant species was activation at the 2-position.²³ Catalytic and stoichiometric reactions of the Pd(II)-F complex with various silanes and the stannane Bu₃SnCH=CH₂ were reported by Braun and co-workers (Scheme 1-3).⁹

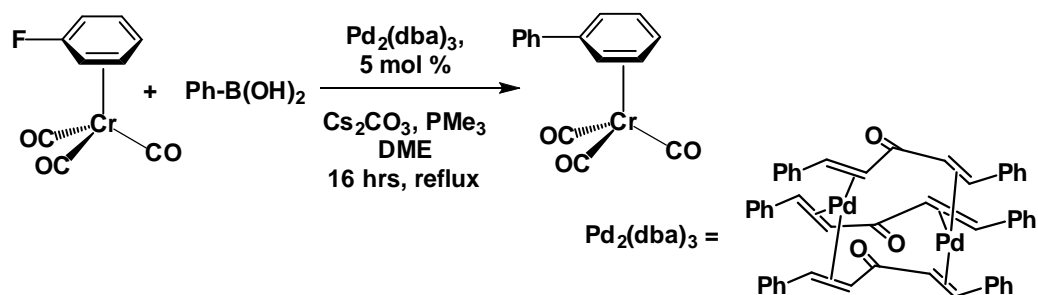


Scheme 1-3 Synthesis and reactivity of Pd(F)(P^{*i*}-Pr₃)₂(C₅F₄N) towards various silanes and the stannane, Bu₃SnCH=CH₂⁹

In a separate study by Crespo, Martinez and co-workers, the stoichiometric C-F bond activation was demonstrated to be facilitated via the imine group in the stoichiometric reaction between a Pt dimer, [Me₂Pt(μ-SMe₂)]₂ and aryl imines. The mechanistic studies showed that the reaction proceeded via C-F oxidative addition ortho to the imine even in the presence of weaker aryl C-Cl and C-Br bonds.²⁴

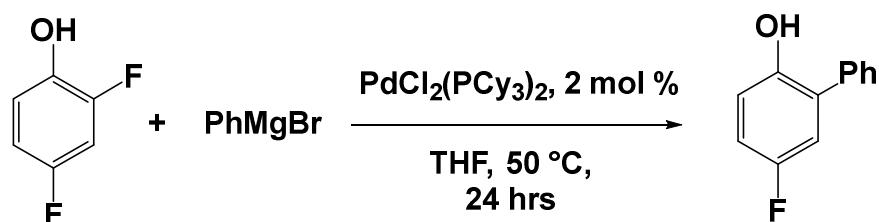
Catalytic carbon-carbon cross-coupling via activation of C-F bonds has been demonstrated in the past with group 10 metals. The nickel fluoride complex, Ni(F)(PEt₃)₂(2-C₅F₄N) catalysed the cross-coupling reaction of C₅F₅N and 2,3,5,6-C₅F₄NH with vinyl tin reagents in the presence of PEt₃ and Cs₂CO₃.²⁵ The nickel fluoride complex Ni(F)(PPh₃)₂(4-C₄N₂ClF₂) was reported to catalyse Suzuki-Miyaura cross coupling reactions, which proceeded via a selective C-F bond activation in the presence of significantly weaker C-Cl bonds.²⁶

The first cross-coupling reaction of a monofluorobenzene and phenylboronic acid catalysed by a Pd catalyst in the presence of PMe₃ was reported in 1999 by Widdowson et al. where fluoroarenes were activated via the C-F bonds (Scheme 1-4).²⁷ Tricarbonylchromium(0) was an essential additive in the reaction which they believed to lead to a coordination to the fluoroarene, increasing the feasibility of the C-F activation.^{6,27}



Scheme 1-4 Suzuki coupling of phenylboronic acid and monofluorobenzene catalysed by Pd, in the presence of PMe₃ and Cr(CO)₃ (DME = dimethoxyethane).²⁷

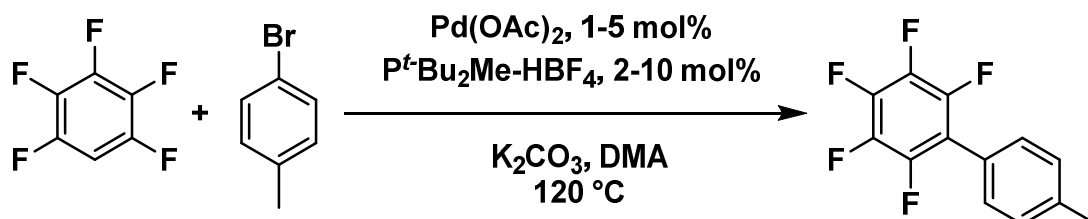
In 2008, Manabe and co-workers reported a cross-coupling reaction of polyfluoroarenes and aryl Grignard reagents (Scheme 1-5). The reaction, which was one of the earliest examples of polyfluoroarene activation, was found to selectively activate the C-F bond ortho to the hydroxyl group even in the presence of C-F and C-Cl bonds on other positions.²⁸



Scheme 1-5 Cross-coupling of polyfluoroarenes and aryl Grignard reagents catalysed by Pd

In 2006, Fagnou and co-workers reported a direct arylation reaction of fluorobenzene catalysed by palladium (Scheme 1-6).²⁹ The cross-coupling reaction was reported to be possible with aryl halides (bromide, chloride and

iodide) in the presence of electron withdrawing, electron donating groups and heteroaryl halides.²⁹ The reaction was found to selectively activate the C-H bond ortho to the fluorine atoms in the case of less fluorinated arenes (C₆F_nH, n = 1,2,3 and 4). This observation was attributed by Fagnou and co-workers to the acidity of the C-H bond and not to intermediate stabilization by fluorines.²⁹



Scheme 1-6 Cross-coupling of aryl halides and fluorobenzenes catalysed by palladium.²⁹

The mechanism of the reaction was proposed to occur via a concerted metalation deprotonation mechanism (CMD) involving either a bromine or a carbonate based on the results from the DFT calculation performed.²⁹ The kinetic isotopic effect of the reaction was found to be 3.0 suggesting the involvement of the C-H bond in the step corresponding to the highest energy barrier.²⁹

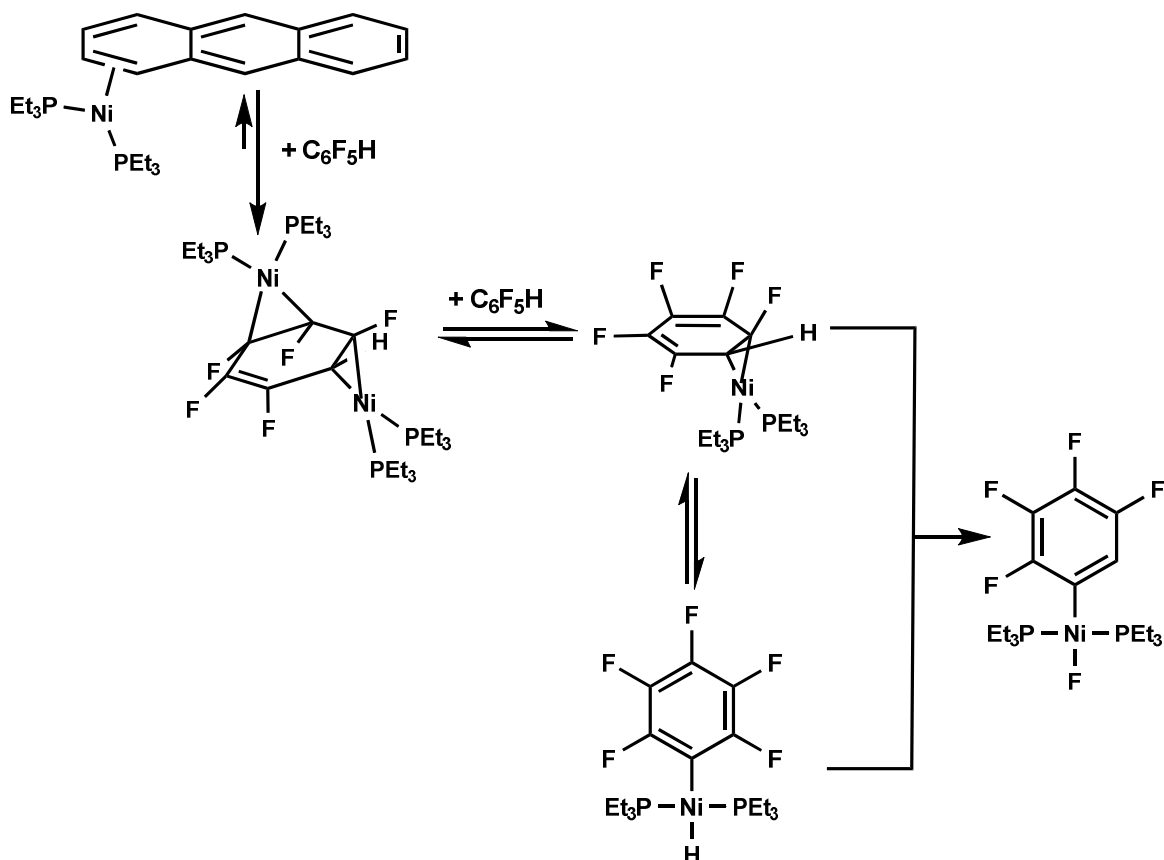
1.1.3 Tuning the kinetic and thermodynamic accessibility of C-H and C-F bonds - The choice of phosphines and the choice of fluoroarenes

The activation of the C-F bond in a partially fluorinated arene is thermodynamically more favourable with nickel complexes compared to palladium and platinum, according to both experimental and theoretical evidence.³⁰⁻³² However, the C-H bonds in the partially fluorinated arenes are accessible kinetically by nickel complexes.³² This has been demonstrated by various stoichiometric reactions with certain phosphines^{31,33} and kinetic

activation of the C-H bond has been demonstrated through several catalytic processes.³⁴ This observation demonstrates that selective activation of the C-F and C-H is possible by tuning the ligands on nickel and choosing the correct fluoroarene.

The reaction of Ni(COD)₂ with C₆F₅H in the presence of 5 equivalents of PEt₃ was studied by Perutz and co-workers and was found to result in all three isomers of *trans*-Ni(F)(PEt₃)₂(C₆F₄H) (in the ratio 7: 2: 1). In addition to this, difluorophosphoranes and 1,2,4,5-C₆F₄H₂ were observed in the reaction mixture.²¹ Johnson and co-workers believed that the observation of difluorophosphoranes suggested the interference of excess phosphine in the reaction mixture.³⁵ Excess phosphine in the reaction mixture can push the equilibrium to decrease the amount of Ni(PEt₃)₂ and Ni(PEt₃)₃ species in the solution and increase the amount of the coordinatively saturated Ni(PEt₃)₄ species, which was believed to only be suitable for oxidative additions that involve electron transfer.^{22,35}

To avoid the problems caused by excess phosphine, a more well-defined nickel(0) source, Ni(PEt₃)₂(η²-C₁₄H₁₀) (C₁₄H₁₀ = anthracene in this case) was used by Johnson and co-workers to study the reactivity with C₆F₅H. The reaction of Ni(PEt₃)₂(η²-C₁₄H₁₀) with 4 equivalents of C₆F₅H resulted in the dinuclear Ni(PEt₃)₂ adduct of C₆F₅H, [Ni(PEt₃)₂]₂(μ-η²:η²-C₆F₅H).³⁵ This dinuclear species is in equilibrium with the mono-nuclear species, Ni(PEt₃)₂(η²-C₆F₅H) and the nickel hydride, *trans*-Ni(H)(PEt₃)₂(C₆F₅) (Scheme 1-7).



Scheme 1-7 The reactivity of Ni(PEt₃)₂(η^2 -C₁₄H₁₀) with C₆F₅H.

The reaction of the dinuclear species, [Ni(PEt₃)₂]₂(μ - η^2 : η^2 -C₆F₅H) with C₆F₅H gave rise to C-F bond activation with a rare selectivity, where the C-F bond ortho to the hydrogen was selectively activated.³⁵ This was in contrast to the reaction of Ni(PEt₃)₄ with C₆F₅H, which resulted in all three possible C-F bond activated products, with the C-F bond para to the hydrogen activated product. The complex Ni(F)(PEt₃)₂(2,3,5,6-C₆F₄H) was observed as the major product (65%) and the ortho C-F bond to the hydrogen activated product, Ni(F)(PEt₃)₂(3,4,5,6-C₆F₄H) was observed as the minor product (12%) in the reaction.³⁵

The reaction of the Ni(PEt₃)₂ phenanthrene adduct, Ni(PEt₃)₂(η^2 -C₁₄H₁₀) with 1,2,4,5-C₆F₄H₂ gave rise to the C-H bond activated product, Ni(H)(PEt₃)₂(2,3,5,6-C₆F₄H) initially before the transformation to C-F activated

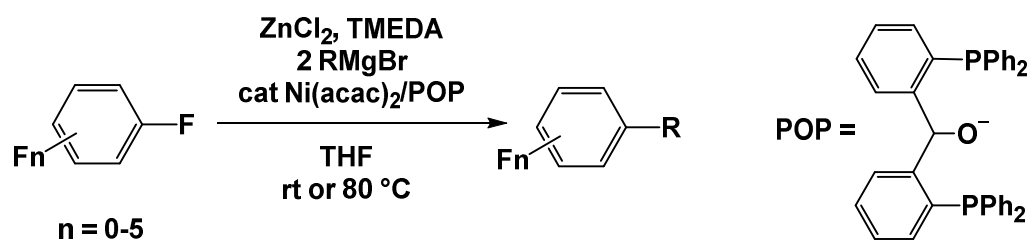
products.³⁰ The reaction was observed to give rise to C-F bond activated products of the C-H rearranged 1,2,4,5-C₆F₄H₂ and products of hydrodefluorination.³⁰

Changing the phosphine from PEt₃ to P^{*i*}-Pr₃ showed a general trend towards the formation of more stable C-H activated products. This was seen in the reaction of 1,2,4,5-C₆F₄H₂ with Ni(P^{*i*}-Pr₃)₂(η²-C₁₄H₁₀) which resulted in the C-H bond activation and no evidence of C-F bond activation was seen upon heating the reaction mixture at 100 °C for 3 hours.³³ The absence of C-F bond activation was believed to be the result of either a high energy barrier involved in the C-F bond activation or the formation of a very stable nickel hydride, *trans*-Ni(H)(P^{*i*}-Pr₃)₂(2,3,5,6-C₆F₄H₂) compared to the adduct, Ni(P^{*i*}-Pr₃)₂Ni(η²-1,2,4,5-C₆F₄H₂), which is believed to be the general intermediate for C-H and C-F bond activation.³³ However, the change of the fluoroarene from 1,2,4,5-C₆F₄H₂ to 1,2,3,5-C₆F₄H₂ showed initial C-H activation which gradually converted into a C-F bond activated product upon prolonged heating for several days.³³ The same behaviour was observed when C₆F₅H was used as the fluoroarene, giving rise to a stable C-H bond activated nickel hydride which gradually converted into the thermodynamically more favourable C-F activated nickel fluoride at room temperature over several weeks.³³

The reactions of the Ni(P^{*i*}-Pr₃)₂ motif with the fluoroaromatics give rise to stable nickel hydrides, which gradually convert to C-F activated nickel fluorides. This is in contrast to the situation when the Ni(PEt₃)₂ motif is used, where the C-H activation is converted to C-F activated products faster.^{30,33,35} This observation of the kinetically accessible C-H bond activation being more accessible with tri(sec-alkyl)phosphines is also exhibited in catalytic reactions occurring via a C-H bond activation catalysed by Ni(0) ligated to tri(sec-alkyl)phosphines, hydrofluoroarylation of alkynes and C-H bond stannylation reactions.^{34,36}

On the other hand, cross-coupling via C-F bond activation has been possible in partially fluorinated benzenes catalysed by Ni(0) ligated to a diphosphine ligand that had two phosphine groups and an alkoxide group (Scheme 1-8).³⁷ This enhancement in selective activation of a C-F bond of a partially

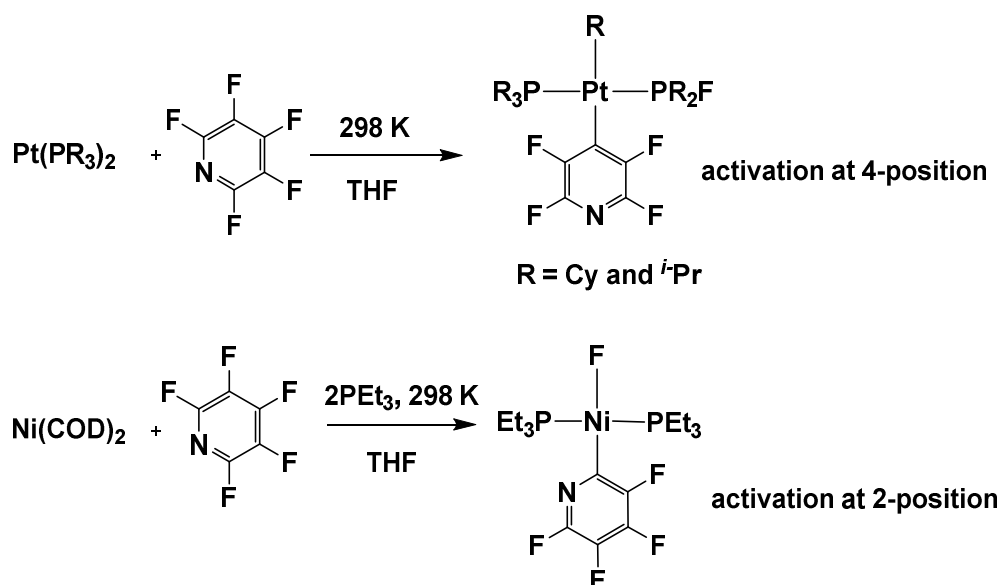
fluoroaromatic was observed upon the incorporation of an alkoxide group into a phosphine.^{38,39}



Scheme 1-8 Catalytic cross-coupling via C-F bond activation mediated by Ni(0)

1.1.4 C-F bond activation in fluoropyridines via phosphine-assisted pathways

The major product observed in the reaction of Ni(PEt₃)₂ with pentafluoropyridine and 2,3,5,6-tetrafluoropyridine is the C-F bond activation at the 2-position, in contrast to the activation at 4-position observed with Pt(P^{*i*}-Pr₃)₂ (Scheme 1-9).⁴⁰ DFT calculation results supported the possibility of the C-F bond activation occurring via a phosphine-assisted pathway, where the fluorine is first transferred to the phosphorus atom and then on to the metal.



Scheme 1-9 Reactivity of Ni(0) and Pt(0) phosphine complexes with pentafluoropyridine.^{40,41}

Metal-fluoride bonds in some complexes undergo rearrangements involving phosphorus to give rise to metallophosphorane species; however these pathways are not possible for analogous metal bonds with hydrides, chlorides, bromides or iodides.⁴⁰ The calculations were performed for four possible pathways, the oxidative addition pathway and three phosphine-assisted pathways that involve either a metallophosphorane species or metal alkyl intermediates.⁴⁰

The DFT calculation results showed that, despite its weak basicity, the pyridyl N can participate in the reaction at Ni(0), lowering the barrier for C-F activation at 2-position, if the mechanism of the reaction proceeds through a metallophosphorane intermediate (Figure 1-3). Therefore due to the involvement of the pyridyl nitrogen the phosphine-assisted mechanism can be more favourable than the oxidative addition reaction through stabilisation of both the metallophosphorane intermediate and the transition state that follows. In the phosphine-assisted mechanism, the fluorine is first transferred to the phosphorus atom of the phosphine ligand and then on to the metal. If the phosphines in the nickel complex are replaced by carbenes the C-F bond at

4-position is activated as the carbenes cannot support the migrating fluorine atom.⁴⁰

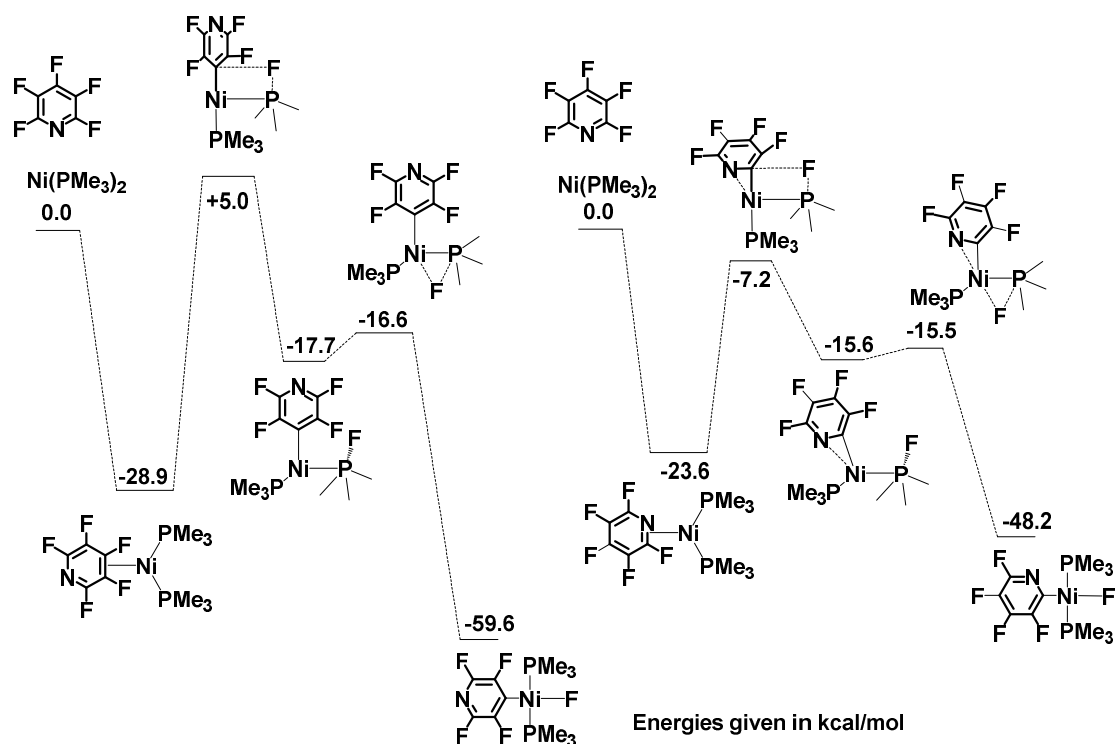
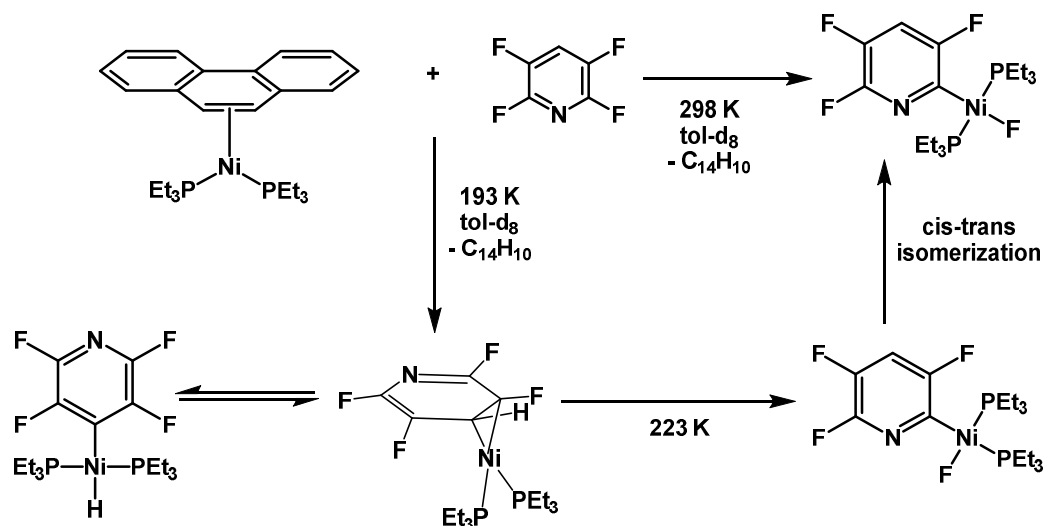


Figure 1-3 Potential energy surface diagram for possible phosphine-assisted C-F activation pathways of pentafluoropyridine by Ni(PMe₃)₂ leading to activation at 4- and 2-position.⁴⁰

In Pt complexes it has been shown that the phosphine ligands take part in the reaction by acting as F-atom acceptors, leading to platinum alkyls. However no such alkyl complexes have been observed for Ni so far. DFT calculations conducted for an oxidative addition mechanism for the reaction of Ni(PEt₃)₂ with C₅F₅N showed that the mechanism is initiated by the coordination of the pyridine to the nickel centre. This is followed by the formation of the transition state for the oxidative addition and then the formation of a cis Ni-F complex, where the two phosphine groups are cis to each other. In contrast the phosphine-assisted pathway goes straight through to the trans isomer.⁴⁰ Experimentally the trans Ni-F complex was seen, which is due to the fact that

the trans isomer is more stable than the cis isomer. However, recently Johnson et al. have been able to observe the cis isomer in a reaction with Ni(PEt₃)₂ with 2,3,5,6-tetrafluoropyridine (Scheme 1-10).⁴²



Scheme 1-10 The formation of the cis isomer Ni(PEt₃)₂(F)(3,5,6-C₅F₃NH).⁴²

In a reaction of 2,3,5,6-tetrafluoropyridine with the Ni(PEt₃)₂(anthracene) adduct the cis isomer of Ni(PEt₃)₂(F)(3,5,6-C₅F₃NH) was observed. This led them to suggest that the reaction proceeds through a concerted oxidative addition. However they also suggested that the failure to confirm the phosphine-assisted mechanism, predicted by DFT calculations might be due to the different phosphine used versus the one used in the calculations and the different substrate. The reaction of C₅F₅N with the Ni(PEt₃)₂(anthracene) adduct, however, showed no evidence of a cis-isomer of the Ni(II)-F. The reaction gave rise to the trans Ni(F)(PEt₃)₂C₅F₄N and to double C-F activated products, where both the C-F activations occur at ortho position to the N-atom.⁵

1.1.5 N-heterocyclic carbenes as an alternative ligand to phosphines

The synthesis of the first isolable carbene stabilised by adjacent phosphorus and silicon substituents was reported in 1988 by Bertrand and co-workers.⁴³ The synthesis of a stable “bottleable” N-heterocyclic carbene was reported in 1991 by Arduengo and co-workers (Figure 1-4), with adamantyl substituents on the nitrogen.⁴⁴

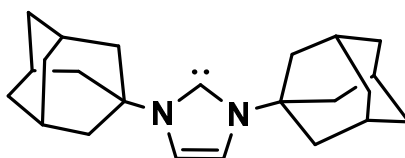


Figure 1-4 The first “bottleable” N-heterocyclic carbene synthesised

The use of NHCs in controlling organometallic homogenous catalysis has now been expanding for more than two decades.⁴⁵ In the early days of carbene development it was believed that the carbenes were simple sterically more demanding substitutions for phosphine ligands. However, the dramatic rise of the use of NHC ligands in catalysis has shown complex and unique properties making them useful ligands in metal-mediated catalytic transformations.¹⁶ An attractive feature of the N-heterocyclic carbenes over phosphines is their reluctance to dissociate from a metal centre especially in the case of electron rich transition metals. This feature can be attributed to the thermodynamic instability of free NHCs in solution.^{17,46}

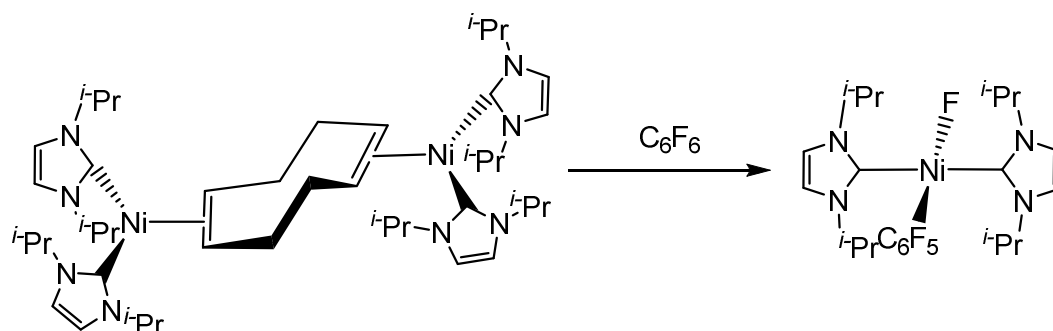
1.1.5.1 The steric and electronic factors of N-heterocyclic carbenes

The substituents on the NHCs are not directly on the atom that is bound to the metal, unlike the phosphines. Therefore the change in the substituents has not been reported to have a dramatic change in the electronic effects in literature and has not been studied in detail so far.¹⁶ To attain a change in the electronics

a modification in the azole ring is possibly the most successful route.¹⁶ The change in the substituent on the other hand has significant effects on the steric factor.¹⁶

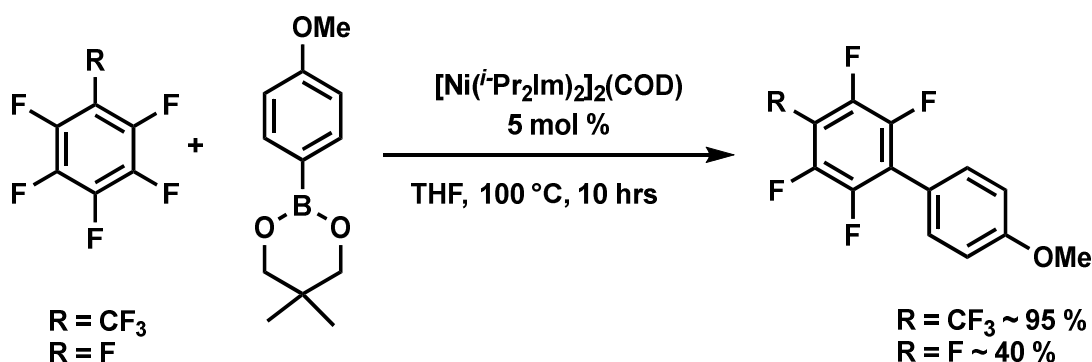
In general N-heterocyclic carbene ligands are more σ -donating than phosphines to metals.⁴⁷ The π -acceptor property of the NHC is dependent on the substituents of the other ligands on the metal and the metal it is ligated to.⁴⁷ The trans effect of the NHC ligands is higher than that of the tertiary phosphine ligands, as exhibited in the Grubbs' catalyst, when the phosphine ligand is changed to a NHC ligand. The resulting catalyst used in metathesis shows a higher activity which is driven by the enhanced binding of the metal to the olefin over the phosphine, which was dissociated from the metal at an earlier step.^{16,48} The computational study performed by Gusev on two electron donor ligands the NHCs with less bulky substituents such as methyl groups on the nitrogen atoms showed donor properties similar to phosphines such as PMe₃ and PEt₃ for both saturated and unsaturated NHCs.¹⁹ The unsaturated carbenes with bulkier substituents such as butyl groups on nitrogen exhibited donor properties such as trialkylphosphines.¹⁹ A study performed based on computational calculations and calorimetric measurements comparing saturated and unsaturated NHC complexes of Ru by Nolan and co-workers showed a very small difference in the bond dissociation energies (1 kcal/mol). The study also showed that the smallest changes in the NHC ligands can still contribute significantly to the overall change in its catalytic properties.⁴⁹

1.1.5.2 N-heterocyclic ligated Ni(0) - reactivity and uses in catalysis



Scheme 1-11 Stoichiometric C-F bond activation of C₆F₆ by a Ni(0)-NHC complex.

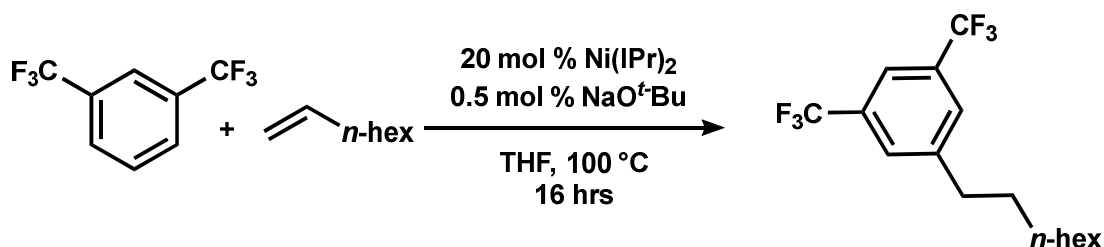
Stoichiometric C-F bond activation of hexafluorobenzene was achieved by Radius and co-workers with an electron rich Ni(0)-NHC complex (Scheme 1-11), [Ni(*i*-Pr₂Im)₂]₂(COD) giving rise to the first transition metal fluoride pentafluorophenyl complex bearing an NHC ligand, Ni(F)(*i*-Pr₂Im)₂(C₆F₅).⁵⁰ The work was extended to use the Ni(0) complex as a catalyst in cross-coupling of fluoroarenes to phenyl boronic acids where trimethylamine was used as the base. The aryl group selectively added to the fluoroarene in the para position.⁵¹ A base-free Suzuki-Miyaura cross-coupling of fluoroarenes to aryl boronates was reported by Ogoshi and co-workers recently using the same Ni-NHC complex, [Ni(*i*-Pr₂Im)₂]₂(COD) as the catalyst (Scheme 1-12). The reaction was reported to use aryl boronates instead of aryl boronic acids.⁵²



Scheme 1-12 A base-free Suzuki-Miyaura cross-coupling of fluoroarenes to aryl boronates using [Ni(*i*-Pr₂Im)₂]₂(COD) as the catalyst

More recently the use of complexes of Ni(0) ligated to only one NHC ligand as homogenous catalysts has become popular as an alternative to bis-NHC Ni(0) complexes.⁵³⁻⁵⁵ The mono-NHC Ni(0) complexes are more attractive compared to the Ni(NHC)₂ mainly due to the difficulty in substituting the NHC ligands which therefore limits the use of Ni(NHC)₂ complexes as precursors.⁵³ The mono-NHC ligand would be a sterically demanding molecule and the other coordination sphere is often completed by labile ligands that are easily displaced by other molecules when subjected to reactions.⁵³ In 2012, Hazari et al. reported the synthesis of a thermally stable Ni(0)-(NHC) complex, (1,5-hexadiene)Ni(IPr) and demonstrated in stoichiometric reactions that the 1,5-hexadiene ligand can be easily replaced.⁵³ In addition, it was also demonstrated that this (1,5-hexadiene)Ni(IPr) acts as a homogenous catalyst for hydrogenation of olefins.⁵³

Addition of benzene to 1-octene was observed via a hydroarylation reaction with un-activated terminal olefins, catalysed by Ni(COD)₂ with IPr as the ligand by Hartwig and co-workers (IPr = 1,3-bis(2,6-diisopropylphenyl)-1,3-dihydro-2H-imidazol-2-ylidene).⁵⁵ The reaction was extended to more reactive arenes in this study and it was also observed that the regioselectivity at the arene was primarily dependent on steric hindrance.⁵⁵ The catalyst resting state was found to be Ni(IPr)(norbornene)₂ suggesting the active catalyst to have only one IPr ligated to the metal centre.⁵⁵ The hydrogen transfer from the arene to the alkene was proposed to occur via a ligand to ligand hydrogen transfer and does not involve a nickel hydride intermediate.

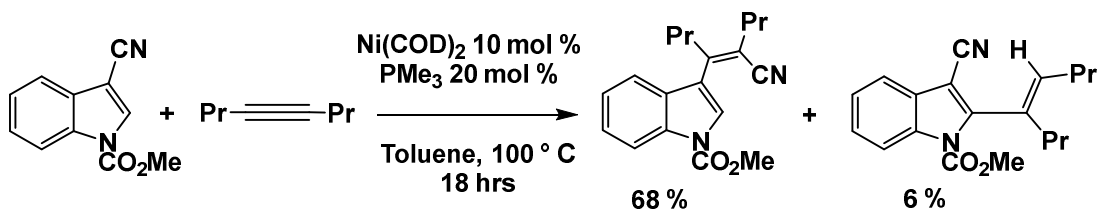


Scheme 1-13 Hydroarylation of unactivated olefins catalysed by Ni(0)-NHC

A similar Ni(0) complex ligated to a mono-NHC has been observed to catalyse the amination of aryl tosylates. A Ni-IPr complex stabilized by two styrene ligands, Ni(IPr)(C₆H₅CH=CH₂)₂ was introduced as a modification of the Ni(IPr)(allyl)Cl catalyst which was used for the room-temperature Buchwald-Hartwig aminations of aryl and heteroaromatic chlorides. The active Ni(0)-IPr species was believed to be generated in-situ in the presence of the base NaO^tBu.⁵⁴

1.1.6 Hydroarylation of alkynes

In 2008, Nakao and co-workers while investigating the arylation of alkynes catalysed by nickel(0), observed that the hydroarylated alkyne was formed in low quantities as a side product. This led to further investigation and it was found that nickel catalysts are capable of catalysing hydroarylation of alkynes (Scheme 1-14). It was observed that when sec-alkyl phosphines such as PCyp₃ were used as ligands for nickel, the arylation reaction was suppressed and hydroarylation was observed.¹⁴

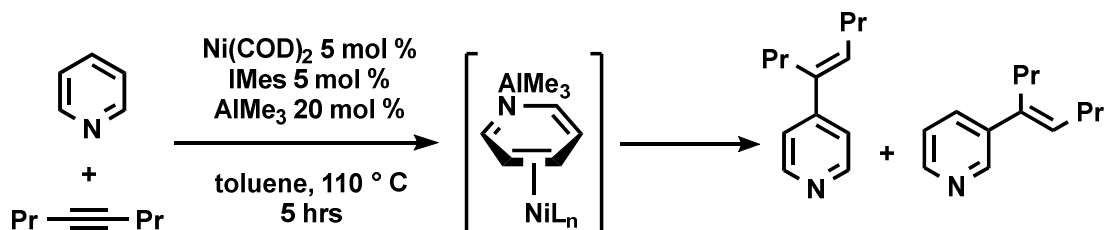


Scheme 1-14 Hydroarylation observed as a side product in the arylation of alkynes.

1.1.6.1 Hydroarylation of heteroarenes

Hydroarylation of 5 and 6 membered heterocycles was investigated by Nakao and co-workers.¹⁴ Benzo-fused heteroarenes such as caffeine, purine, benzofuran, benzimidazole and thiazole were found to alkenylate at the C2

position of the ring. The presence of an electron withdrawing group at C3 was observed to be vital for successful alkenylation at C2 in indoles.¹⁴ The alkenylation of *N*-methylimidazole was found to yield better results when AlMe₃ was used as a co-catalyst.¹⁴



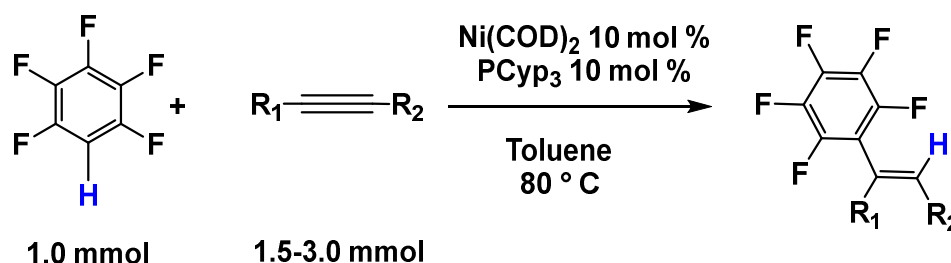
Scheme 1-15 η²-coordination of Ni(0)-NHC at C3-C4 of the pyridyl ring in the presence of AlMe₃

When electron deficient six-membered heteroarenes were used for this study, it was observed that pyridine-*N*-oxides undergo alkenylation selectively at the C2 position and under mild conditions and the resulting alkenylated pyridine-*N*-oxides were easily converted to substituted pyridines.¹⁴ In addition, it was also observed that the C3 substituted pyridines alkenylated at C2 due to steric hindrance. The use of a N-heterocyclic carbene as the ligand and AlMe₃ resulted in alkenylation at C3 and C4 which was attributed to the η²-coordination at C3-C4 of Ni(0)-NHC.¹⁴

1.1.6.2 Hydrofluoroarylation of alkynes

Nakao and co-workers were successful in expanding their hydroarylation reactions of the electron deficient heteroarenes to fluoroarenes.^{14,31,34} The results showed successful hydrofluoroarylation of alkynes in the presence of Ni(COD)₂ and PCy₃. The hydrofluoroarylation reaction occurred via a selective activation of the C-H bond in the fluoroarene adding the fluoroarene across the triple bond of the alkyne. Although the oxidative addition of the electron rich

Ni(0) complexes is thermodynamically favourable for C-F bonds over C-H bonds in partially fluorinated arenes, the hydrofluoroarylation reaction was observed to occur via a chemo-selective C-H bond activation. This C-H bond activation is kinetically accessible for partially fluoroarenes.



Scheme 1-16 Hydrofluoroarylation of alkynes catalysed by Ni(0)-PR₃
(R = Cyp, Cy)

The choice of phosphine used as the ligand played a significant role on the yield of the hydrofluoroarylation reaction. The highest yield was obtained when tri(sec-alkyl)phosphines were used as the ligand, with ~99% yield observed with tricyclopentylphosphines.^{31,34} Tri-primary and tri-tertiary alkyl phosphines (e.g.: P(*n*-Bu)₃, P(*t*-Bu)₃) resulted in only trace amounts of the arylalkene and triaryl and diarylalkylphosphines (e.g.: PPh₃, PCy₂Ph) proved to be equally ineffective.³¹

When fluoroaromatics with more than one reactive site were used in the reaction, formation of dialkenylated products too was observed. The formation of the dialkenylated product was found to be dominant when the reaction was done with 4 equivalents of alkyne.³¹ When unsymmetrical alkynes were used in the reaction good regioselectivity was observed where the fluoroarene was added to the carbon with the less bulky substituent in the alkyne molecule.³¹

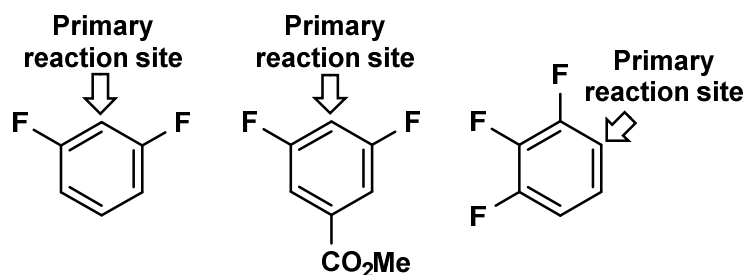


Figure 1-5 The selectivity of the activation of C-H bond ortho to fluorine

The higher the number of fluorine substituents, the higher the reactivity of the fluoroarenes. Both electron withdrawing substituents and electron donating substituents were observed to tolerate the reaction to give multifunctionalized arylalkenes.³¹ The C-H bonds ortho to fluorine atoms are activated, (Figure 1-5) regardless of the other electron withdrawing or donating group substituents on the ring due to the following reasons:

- a) Increase in the acidity of the C-H bond
- b) And the increase in the bond strength of the M-C bond by ortho fluorines.¹³

The mechanism of the reaction was pursued by Nakao et al. experimentally by stoichiometric reactions with a Ni(PR₃)₂ source, [Ni(PCy₃)₂]₂N₂ and C₆F₅H. The mechanism thus proposed was postulated to proceed via the formation of the nickel hydride which further reacts with the alkyne.³¹ However, the DFT calculations performed on the hydrofluoroarylation reaction by Perutz and co-workers were found to support a different mechanism rather than the one proposed by Nakao et al. The mechanistic aspects of the reaction and the proposed mechanisms are discussed in more detail in Chapter 2.

1.2 Aims and Objectives

The difference in the mechanisms proposed based on the results from experimental studies and the DFT calculations stimulated the investigation of the mechanism further. The hydrofluoroarylation of alkynes has been a significant coupling reaction of fluoroaromatics catalysed by Ni(0). Therefore it is vital to gain a proper understanding of the mechanism in order to understand the catalytic behaviour of Ni(0) towards such systems. The absence of very unique intermediates that do not lead to other side products or a reversible product (e.g. the nickel hydride) in the mechanisms proposed suggested to

seek a different method of studying the mechanism. As Crabtree states, the presence of plausible intermediates seen by spectroscopy in the catalytic reaction mixture does not necessarily indicate that they are true intermediates and relying solely on spectroscopic methods can often be misleading.¹⁷ Showing that the mechanisms proposed are kinetically possible is often the most reliable and informative evidence.¹⁷

- The initial aim of the project was to find a suitable catalytic system to study the hydrofluoroarylation reaction. The work carried out in order to achieve this goal is presented in chapter 2.
- Once a suitable system is obtained, kinetic analysis of the hydrofluoroarylation reaction was targeted in order to obtain more mechanistic information of the reaction. The kinetic analysis carried out is described in detail in chapter 3.

Although the solid state analysis of metal-halide systems exhibiting halogen bonding interactions has been reported in detail for chloride, bromide and iodide, the description of the metal-fluoride halogen bonding interactions in the solid state were still absent. The literature review on halogen bonding interaction is included at the beginning of Chapter 4.

- The aim of the project was to design a series of self-complementary molecules exhibiting intermolecular halogen bonding interaction, where the metal halides would act as the XB acceptor. This objective of this is to obtain solid state analysis of metal fluoride complexes as XB acceptors and to compare its acceptor capability with other halides.
- The objective of chapter 5 was to obtain reliable thermodynamic data in solution phase for a strong XB interaction by changing the working concentrations of host and guest in the titrations. The literature review on this is included at the beginning of Chapter 4.

1.3 References

- (1) Wang, J.; Sánchez-Roselló, M.; Aceña, J. L.; del Pozo, C.; Sorochinsky, A. E.; Fustero, S.; Soloshonok, V. A.; Liu, H. *Chem. Rev. (Washington, DC, U. S.)* **2014**, *114*, 2432.
- (2) Fried, J.; Sabo, E. F. *J. Am. Chem. Soc.* **1954**, *76*, 1455.
- (3) Sun, A. D.; Love, J. A. *Dalton Trans.* **2010**, *39*, 10362.
- (4) Braun, T.; Perutz, R. N. In *Perspectives in Organometallic Chemistry*; Screttas, C. G., Steele, B. R., Eds.; The Royal Society of Chemistry: 2003, p 136.
- (5) Kuehnel, M. F.; Lentz, D.; Braun, T. *Angew. Chem. Int. Ed. Engl.* **2013**, *52*, 3328.
- (6) Keyes, L.; Love, J. A. In *C-H and C-X Bond Functionalization: Transition Metal Mediation*; The Royal Society of Chemistry: 2013, p 159.
- (7) Grushin, V. V. *Acc. Chem. Res.* **2010**, *43*, 160.
- (8) Weaver, J.; Senaweera, S. *Tetrahedron* **2014**, *70*, 7413.
- (9) Braun, T.; Izundu, J.; Steffen, A.; Neumann, B.; Stammer, H.-G. *Dalton Trans.* **2006**, 5118.
- (10) Ahrens, T.; Kohlmann, J.; Ahrens, M.; Braun, T. *Chem. Rev. (Washington, DC, U. S.)* **2015**, *115*, 931.
- (11) Champagne, P. A.; Desroches, J.; Hamel, J.-D.; Vandamme, M.; Paquin, J.-F. *Chem. Rev. (Washington, DC, U. S.)* **2015**.
- (12) Hughes, R. P. *Eur. J. Inorg. Chem.* **2009**, *2009*, 4591.
- (13) Clot, E.; Besora, M.; Maseras, F.; Megret, C.; Eisenstein, O.; Oelckers, B.; Perutz, R. N. *Chem. Commun. (Cambridge, U. K.)* **2003**, 490.
- (14) Nakao, Y. *The Chemical Record* **2011**, *11*, 242.
- (15) Kiso, Y.; Tamao, K.; Kumada, M. *J. Organomet. Chem.* **1973**, *50*, C12.
- (16) Crabtree, R. H. *J. Organomet. Chem.* **2005**, *690*, 5451.
- (17) Crabtree, R. H. In *The Organometallic Chemistry of the Transition Metals*; John Wiley & Sons, Inc.: 2005, p 235.
- (18) Tolman, C. A. *Chem. Rev. (Washington, DC, U. S.)* **1977**, *77*, 313.

- (19) Gusev, D. G. *Organometallics* **2009**, *28*, 763.
- (20) Fahey, D. R.; Mahan, J. E. *J. Am. Chem. Soc.* **1977**, *99*, 2501.
- (21) Cronin, L.; Higgitt, C. L.; Karch, R.; Perutz, R. N. *Organometallics* **1997**, *16*, 4920.
- (22) Tsou, T. T.; Kochi, J. K. *J. Am. Chem. Soc.* **1979**, *101*, 6319.
- (23) Jasim, N. A.; Perutz, R. N.; Whitwood, A. C.; Braun, T.; Izundu, J.; Neumann, B.; Rothfeld, S.; Stammler, H.-G. *Organometallics* **2004**, *23*, 6140.
- (24) Crespo, M.; Martinez, M.; Sales, J. *Organometallics* **1993**, *12*, 4297.
- (25) Braun, T.; Perutz, R. N.; Sladek, M. I. *Chem. Commun. (Cambridge, U. K.)* **2001**, 2254.
- (26) Steffen, A.; Sladek, M. I.; Braun, T.; Neumann, B.; Stammler, H.-G. *Organometallics* **2005**, *24*, 4057.
- (27) A. Widdowson, D.; Wilhelm, R. *Chem. Commun. (Cambridge, U. K.)* **1999**, 2211.
- (28) Manabe, K.; Ishikawa, S. *Synthesis* **2008**, *2008*, 2645.
- (29) Lafrance, M.; Rowley, C. N.; Woo, T. K.; Fagnou, K. *J. Am. Chem. Soc.* **2006**, *128*, 8754.
- (30) Johnson, S. A.; Huff, C. W.; Mustafa, F.; Saliba, M. *J. Am. Chem. Soc.* **2008**, *130*, 17278.
- (31) Kanyiva, K. S.; Kashihara, N.; Nakao, Y.; Hiyama, T.; Ohashi, M.; Ogoshi, S. *Dalton Trans.* **2010**, *39*, 10483.
- (32) Reinhold, M.; McGrady, J. E.; Perutz, R. N. *J. Am. Chem. Soc.* **2004**, *126*, 5268.
- (33) Hatnean, J. A.; Beck, R.; Borrelli, J. D.; Johnson, S. A. *Organometallics* **2010**, *29*, 6077.
- (34) Nakao, Y.; Kashihara, N.; Kanyiva, K. S.; Hiyama, T. *J. Am. Chem. Soc.* **2008**, *130*, 16170.
- (35) Johnson, S. A.; Taylor, E. T.; Cruise, S. J. *Organometallics* **2009**, *28*, 3842.

- (36) Doster, M. E.; Hatnean, J. A.; Jeftic, T.; Modi, S.; Johnson, S. A. *J. Am. Chem. Soc.* **2010**, *132*, 11923.
- (37) Nakamura, Y.; Yoshikai, N.; Ilies, L.; Nakamura, E. *Org. Lett.* **2012**, *14*, 3316.
- (38) Yoshikai, N.; Mashima, H.; Nakamura, E. *J. Am. Chem. Soc.* **2005**, *127*, 17978.
- (39) Yoshikai, N.; Matsuda, H.; Nakamura, E. *J. Am. Chem. Soc.* **2009**, *131*, 9590.
- (40) Nova, A.; Reinhold, M.; Perutz, R. N.; Macgregor, S. A.; McGrady, J. E. *Organometallics* **2010**, *29*, 1824.
- (41) Nova, A.; Erhardt, S.; Jasim, N. A.; Perutz, R. N.; Macgregor, S. A.; McGrady, J. E.; Whitwood, A. C. *J. Am. Chem. Soc.* **2008**, *130*, 15499.
- (42) Hatnean, J. A.; Johnson, S. A. *Organometallics* **2012**, *31*, 1361.
- (43) Igau, A.; Grutzmacher, H.; Baceiredo, A.; Bertrand, G. *J. Am. Chem. Soc.* **1988**, *110*, 6463.
- (44) Arduengo, A. J.; Harlow, R. L.; Kline, M. *J. Am. Chem. Soc.* **1991**, *113*, 361.
- (45) Herrmann, W. A.; Elison, M.; Fischer, J.; Köcher, C.; Artus, G. R. *J. Angewandte Chemie International Edition in English* **1995**, *34*, 2371.
- (46) Herrmann, W. A.; Goossen, L. J.; Köcher, C.; Artus, G. R. *J. Angewandte Chemie International Edition in English* **1996**, *35*, 2805.
- (47) Perrin, L.; Clot, E.; Eisenstein, O.; Loch, J.; Crabtree, R. H. *Inorg. Chem.* **2001**, *40*, 5806.
- (48) Love, J. A.; Sanford, M. S.; Day, M. W.; Grubbs, R. H. *J. Am. Chem. Soc.* **2003**, *125*, 10103.
- (49) Hillier, A. C.; Sommer, W. J.; Yong, B. S.; Petersen, J. L.; Cavallo, L.; Nolan, S. P. *Organometallics* **2003**, *22*, 4322.
- (50) Schaub, T.; Radius, U. *Chemistry – A European Journal* **2005**, *11*, 5024.
- (51) Schaub, T.; Backes, M.; Radius, U. *J. Am. Chem. Soc.* **2006**, *128*, 15964.

(52) Ohashi, M.; Saijo, H.; Shibata, M.; Ogoshi, S. *Eur. J. Org. Chem.* **2013**, 2013, 443.

(53) Wu, J.; Faller, J. W.; Hazari, N.; Schmeier, T. J. *Organometallics* **2012**, 31, 806.

(54) Iglesias, M. J.; Blandez, J. F.; Fructos, M. R.; Prieto, A.; Álvarez, E.; Belderrain, T. R.; Nicasio, M. C. *Organometallics* **2012**, 31, 6312.

(55) Bair, J. S.; Schramm, Y.; Sergeev, A. G.; Clot, E.; Eisenstein, O.; Hartwig, J. F. *J. Am. Chem. Soc.* **2014**, 136, 13098.

CHAPTER TWO

THE SEARCH FOR A SYSTEM TO STUDY THE MECHANISM OF HYDROFLUOROARYLATION OF ALKYNES

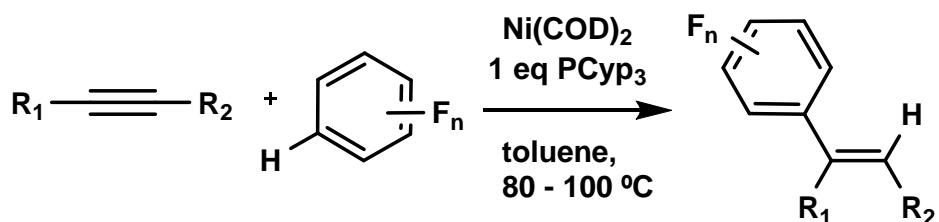
The search for a system to study the mechanism of hydrofluoroarylation of alkynes

2.1. Introduction

Over the past decade attempts to incorporate fluorine containing motifs into organic molecules have been triggered as a result of the unique chemical physical and biological properties achieved by fluorine in pharmaceutical agrochemicals polymer and material science.^{1,2} Although, traditional methods of fluorination are possible by electrophilic and nucleophilic attack, direct functionalization of the C-H or C-F bond of fluorine-containing molecules by the use of transition metal catalysts has caught the attention of many due to the possible usage of mild conditions and atom efficiency.^{2,3}

Late transition metals including Pd and Cu have been used in direct coupling of fluoroarenes to aryl and alkenyl halides by C-H activation of the partially fluorinated arenes.^{4,5} Nickel(0)-phosphine complexes are attractive catalysts in reactions involving C-F activation because of their ability to preferentially activate the C-F bonds while in the presence of C-H bonds that are also available in partially fluorinated arenes. DFT calculations and experiments over the past years have shown the C-F activation by nickel to be thermodynamically favourable over the C-H bond activation in these partially fluorinated arenes.^{6,7} However, despite this, various reactions have now been reported, where selective activation of the C-H bond is achieved kinetically, by Ni-PR₃ complexes in partially fluorinated arenes.^{1,3}

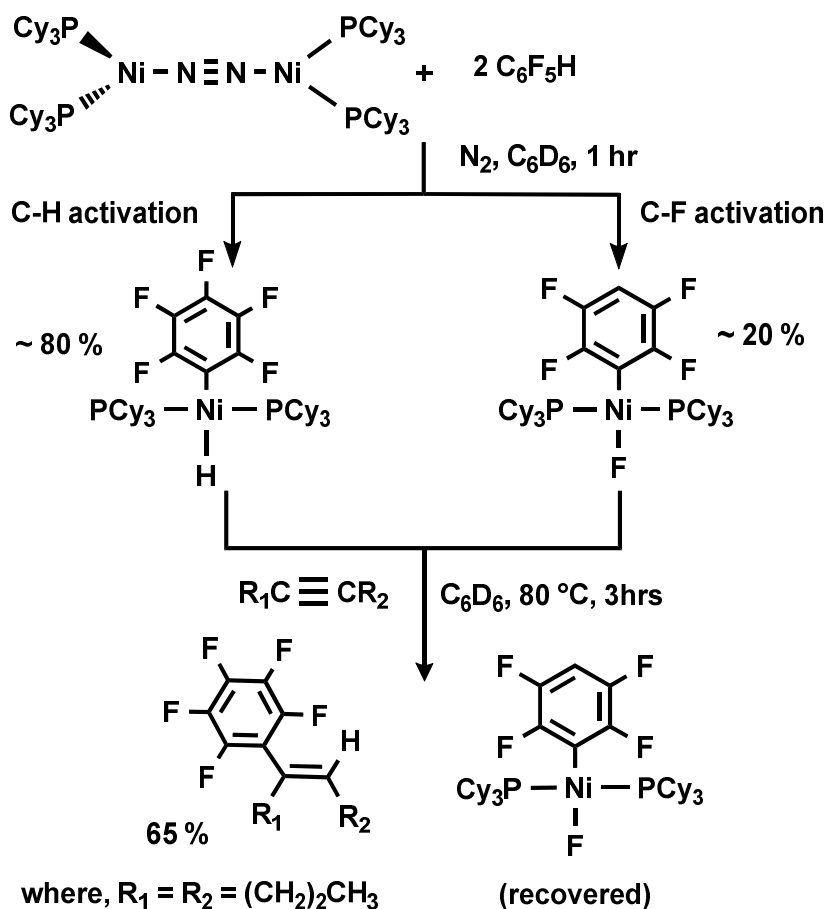
In 2008, a nickel catalyst was used to couple an alkyne molecule to a partially fluorinated arene by Nakao et al.¹ This hydrofluoroarylation reaction proceeds by chemo-selectively activating the C-H bond of the partially fluorinated arene. Ni(COD)₂ with one equivalent of phosphine was used as the nickel-phosphine source to catalyse the hydrofluoroarylation (Scheme 2-1).



Scheme 2-1 Hydrofluoroarylation of the alkyne catalysed by Ni(0).¹

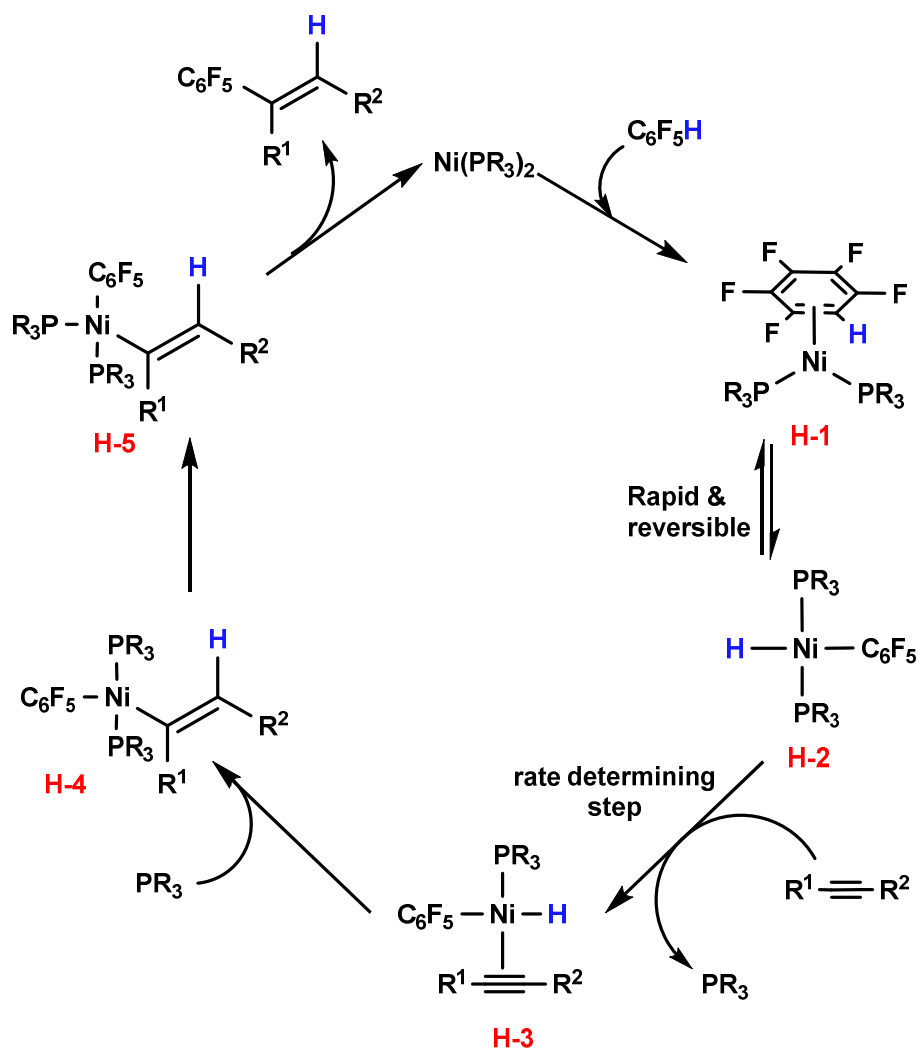
2.1.1. Proposed mechanisms for the hydrofluoroarylation reaction

In an attempt to study the mechanism of the hydrofluoroarylation reaction, the known complex, $[\text{Ni}(\text{PCy}_3)_2]_2\text{N}_2$,^{2,8} was used by Nakao et al., as the nickel(0)-phosphine source. A series of stoichiometric experiments were performed with the nickel complex, fluoroarene and the alkyne to understand the mechanism of the reaction.



Scheme 2-2 Stoichiometric reactions carried out using $[(\text{PCy}_3)_2\text{Ni}]_2\text{N}_2$ with $\text{C}_6\text{F}_5\text{H}$ and 4-octyne.²

Upon addition of C_6F_5H to $[(PCy_3)_2Ni]_2N_2$, two oxidative addition reactions were observed: of the C-H bond to nickel and the para C-F bond of the fluoroarene. This resulted in a mixture of *trans*-Ni(H)(PCy₃)₂(C₆F₅) and *trans*-Ni(F)(PCy₃)₂(C₆F₄H), which after an hour was found in the ratio 4:1, respectively. Both oxidative addition processes mentioned above, are proposed to proceed via a possible η^2 -complex formed by the co-ordination of the fluoroarene to the Ni(PR₃)₂ unit. When 4-octyne was added to this mixture of nickel hydride and nickel fluoride complexes, and heated (80 °C), the decay of the nickel hydride was observed with concurrent formation of the arylalkene. The nickel fluoride *trans*-Ni(F)(PCy₃)₂(C₆F₄H) was found to be inert in this reaction.



Scheme 2-3 Mechanism proposed by Nakao et al. for hydrofluoroarylation of alkynes.²

A mechanism for the hydrofluoroarylation reaction was proposed by Nakao et al. based on the results obtained from the stoichiometric reactions mentioned above. The reaction was proposed to be initiated by the coordination of the fluoroarene to the metal centre $\text{Ni}(\text{PR}_3)_2$ species to form a η^2 -fluoroarene complex (**H-1** in Scheme 2-3). The second step suggested was the activation of the C-H bond of the fluoroarene, giving rise to, *trans*- $\text{Ni}(\text{H})(\text{PCy}_3)_2(\text{C}_6\text{F}_5)$ (**H-2** in Scheme 2-3). This oxidative addition step was proposed to be rapid and reversible.² The next step in the mechanism was predicted to be a ligand exchange step where one of the coordinated phosphine groups on the metal centre dissociates and an alkyne associates. This is followed by a migratory insertion of the coordinated alkyne into the nickel hydride bond giving rise to a fluoroaryl-Ni(II)-alkenyl intermediate (**H-4** in Scheme 2-3). It was noted for unsymmetrical alkynes, where different stereoisomers are possible, that the alkenyl intermediate produced was the one with steric interactions minimised, i.e. the bulkier substituent trans to nickel. The last step would be the reductive elimination step that gives the coupled arylalkene product and re-generates the catalyst.²

It was observed by Nakao et al. that increasing the phosphine equivalents in the reaction had a detrimental effect on the final yield of the hydrofluoroarylated alkyne. The change in the ratio of $\text{Ni}:\text{PR}_3$ from 1:1 to 1:2, resulted in the reduction of the yield from 99% to 62% and the rate of the reaction. In the proposed mechanism (Scheme 2-3) the ligand exchange step replacing one of the phosphines on nickel with an alkyne was expected to be retarded by excess phosphine. Hence it was postulated that this ligand exchange step is the rate determining step.²

Following this, in 2012 a computational study was performed on the hydrofluoroarylation reaction by Perutz, Eisenstein et al. for a clearer understanding of the mechanism involved. The DFT calculations sought to address 3 main issues unclear in the mechanism of the reaction.

- 1) The absence of interference from C-F bond activation in the catalytic reaction which was done at 80 °C, although C-F bond activation with

nickel phosphine has been reported to be thermodynamically more favoured in partially fluorinated arenes.³

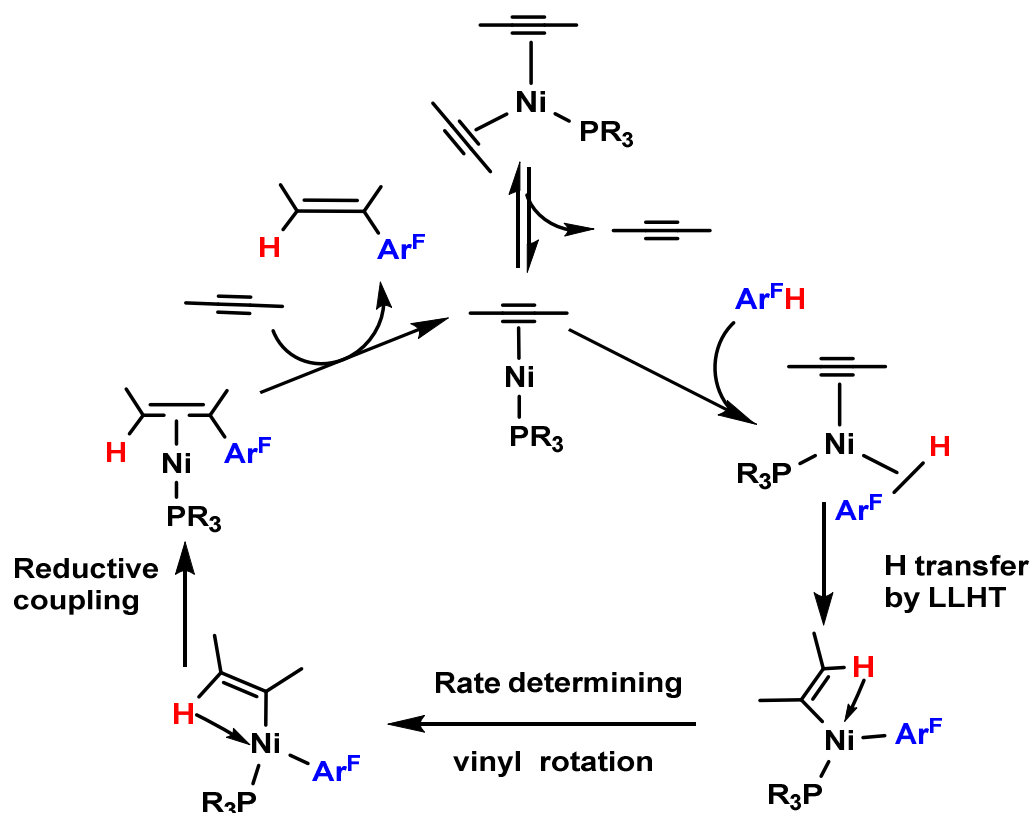
- 2) Whether the regioselectivity observed in the reaction is attributable also to the strength of the nickel-carbon bond rather than just the C-H bond acidity as suggested by Nakao et al.
- 3) To compare the conditions used by Nakao et al. in the catalytic and stoichiometric reactions used to postulate the mechanism. The conditions were different in the nickel: phosphine stoichiometry, where the catalytic conditions involved a Ni:PR₃ ratio of 1:1 whereas the stoichiometric reactions used to postulate the mechanism, the ratio was 1:2.

The DFT calculations were modelled for both the stoichiometric and catalytic conditions used by Nakao et al., where the dominant species in each case would be Ni(PR₃)₂ and Ni(PR₃) respectively. The best phosphine for the reaction, tricyclopentylphosphine was modelled by PMe₃ and the alkyne 4-octyne was replaced by 2-butyne in the DFT calculations to save computational time. The outcomes from the DFT calculations were as follows. In the presence of C₆F₅H and CH₃C≡CCH₃, both in the catalytic and stoichiometric conditions, the coordination of the alkyne to Ni(PR₃)₂ (or to NiPR₃ in the catalytic condition, where R = CH₃) was found to be preferred over the fluoroarene. The energetic preference for alkyne over C₆F₅H was calculated to be 38.5 kJ/mol under stoichiometric conditions⁹ and was attributed to a preference for the back donation of Ni(0) into the π* orbital of the alkyne over the back donation into the π* orbital of the fluoroarene. This coordination of alkyne to Ni(PR₃)₂ was also more favourable than the C-H bond activation of the fluoroarene. The nickel-alkyne complex was energetically more favourable than the C-H activated complex, *trans*-Ni(H)(PMe₃)₂(C₆F₅).

However, the C-F activation was found to be preferred over the coordination of the alkyne. Although the initial alkyne coordination was preferred over the C-H oxidative addition, a pathway proceeding via a *trans* or *cis* Ni(H)(PMe₃)₂(C₆F₅) complex reacting with alkyne was analysed. The results

pointed out that the ligand exchange between an alkyne and a phosphine did not yield a stable complex for the complex with the hydride and alkyne cis to each other. The trans complex was found to be more stable than the cis complex and had a Gibbs coordination energy of the alkyne close to nil, it was therefore not suitable to yield the vinyl complex and it was concluded that even if the formation of the nickel hydride was possible this hydride complex was not capable of reacting with the alkyne.⁹

Since alkyne was in excess in the medium, a bis(alkyne) complex, $\text{Ni}(\text{PMe}_3)(\text{MeC}\equiv\text{CMe})_2$ was also considered. The mono and the bis alkyne complexes, $\text{Ni}(\text{PMe}_3)(\text{MeC}\equiv\text{CMe})$ and $\text{Ni}(\text{PMe}_3)(\text{MeC}\equiv\text{CMe})_2$ were found to be in equilibrium with a slight preference for the mono alkyne complex, $\text{Ni}(\text{PMe}_3)(\text{MeC}\equiv\text{CMe})$. Coordination of $\text{C}_6\text{F}_5\text{H}$ was found to occur through a $\sigma\text{-C-H}$ bond. The hydrogen transfer occurs via a ligand-to-ligand hydrogen transfer (LLHT) resulting in a nickel(aryl) vinyl complex. This complex was found to have the Ni-C bond of the $\text{Me}(\text{H})\text{C}=\text{CMe}$ and C_6F_5 ligands trans to each other, which required an isomerization step for reductive elimination. This isomerization step requires an intermediate that has a high Gibbs energy relative to the reactants and hence was the rate determining step of the pathway. Based on the results obtained from the DFT calculations, an alternative mechanism for hydrofluoroarylation was proposed by Perutz, Eisenstein et al. (Scheme 2-4).



Scheme 2-4 Mechanism postulated based on the result from DFT calculations.⁹

Although the C-F bond activation is thermodynamically preferred over the C-H bond activation, no C-F activated product has been reported in the catalytic reaction. This was attributed to the fact that the cleavage of C-F bond has a transition state with higher Gibbs energy than the highest transition state of the catalytic cycle for hydrofluoroarylation of MeC≡CMe.⁹

The two mechanisms disagree with one another in two main steps:

- 1) The initial coordination to nickel is by the alkyne in the mechanism proposed by Perutz, Eisenstein et al., and by C₆F₅H in the mechanism proposed by Nakao et al.
- 2) The hydrogen transfer is by a LLHT in the Perutz-Eisenstein mechanism and in the latter the hydrogen is first transferred onto the metal and then to the alkyne.

The final step for both mechanisms would be the reductive elimination. The rate-determining step in the mechanism proposed from DFT calculations was the isomerization step, whereas in the other mechanism it was the ligand exchange between a phosphine and alkyne.

2.1.2. Nickel-Alkyne complexes

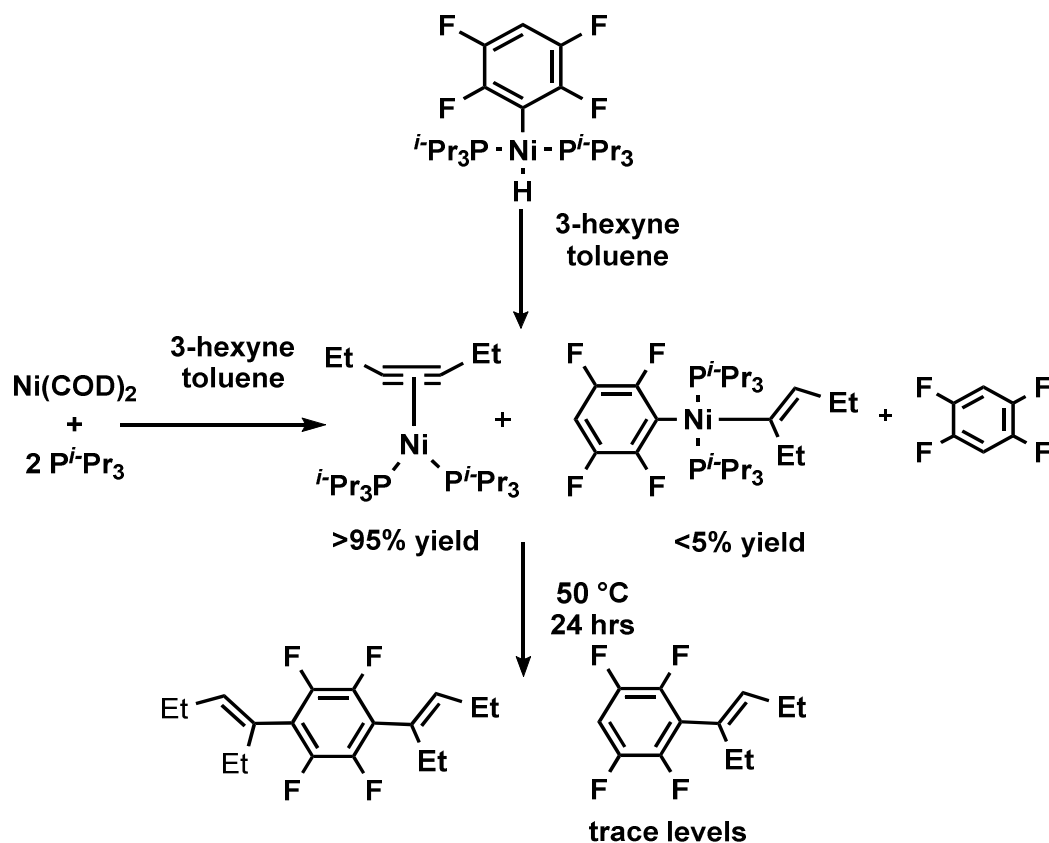
Although the interest in the nickel-alkyne complexes has existed for a long time due to their contribution in the coupling reactions of alkynes, there is a scarcity of very well defined stable complexes, from which one could choose to gain mechanistic insight.^{10,11} Nickel-alkyne complexes such as, $\text{Ni}(\text{PR}_3)(\text{HC}\equiv\text{CH})_n$ ($\text{R} = \text{Ph}, \text{Cy}$ and $n = 2,3$) decompose above 0°C and have therefore proven difficult to use in mechanistic studies. Homoleptic complexes of the nature, $\text{Ni}(\text{HC}\equiv\text{CH})_n$ ($n = 2,3$) are believed to be sterically unfavourable unlike its ethylene analogue, $\text{Ni}(\text{H}_2\text{C}=\text{CH}_2)_n$ ($n = 2,3$). Complexes such as $\text{Pt}(\text{PhC}\equiv\text{CPh})_2$ which have been synthesised,¹² are believed to adopt a pseudo-tetrahedral geometry with the bulky phenyl groups having a bend-back angle of 27° as a result of the steric effect. In the complex $\text{Ni}(\text{HC}\equiv\text{CH})_3$, hydrogens, which are not bulky, are calculated to have a H-C-C bend-back angle hypothesised as 5° , based on the optimised structure for $\text{Ni}(\pi\text{-C}_2\text{H}_2)$.¹³ The complex, with a planar D_{3h} geometry, tends to have a considerable steric hindrance between the hydrogens of neighbouring carbon atoms compared to the same in the nickel-ethylene complex, $\text{Ni}(\text{H}_2\text{C}=\text{CH}_2)_3$.¹⁴

The problem of steric hindrance restricting two or more alkynes ligating to nickel has been overcome in the past years by replacing the two alkynes by a chelating alkyne ligand in complex, $\text{Ni}(\text{PR}_3)(\eta^2, \eta^2\text{-C}_7\text{H}_8)$ ($\text{R} = \text{Me}, \text{Et}$ and Ph).¹⁰ Although $\text{Ni}(\text{HC}\equiv\text{CH})_n$ ($n = 2, 3$) is believed to be unstable, a complex replacing the acetylenes with cyclotriyne has been reported.^{10,14,15}

The co-ordination of ethyne to $\text{Ni}(0)$ was believed to be stabilized by ligands like phosphines, phosphites, t-butyl isocyanides.¹¹ The number of alkynes

permitted to be bonded to the Ni-PR₃ centre is highly dependent on the phosphine cone angle; two alkynes are likely to coordinate only if the cone angle is less than 145°. ¹¹ Depending on the phosphine attached to the Ni, different complexes are possible, e.g. for t-butyl isocyanides and phosphites the only complex possible is of the type (L)₂Ni(HC≡CH). Dinuclear complexes are possible for PPh₃ but not for PCy₃ and Pⁱ-Pr₃. ¹¹

Johnson et al. isolated and characterised a nickel alkyne complex, which resulted from a reaction which was intended to give the arylalkene from hydrofluoroarylation of the alkyne. ³ The reaction of *trans*-Ni(H)(Pⁱ-Pr₃)₂(C₆F₄H) (the nickel hydride obtained from 1,4-C₆F₄H₂) with 3-hexyne was observed to give rise to the alkyne-coordinated complex, (Pⁱ-Pr₃)₂Ni(η²-CH₃CH₂C≡CCH₂CH₃) as the major product, and the alkyne inserted product (Pⁱ-Pr₃)₂Ni(CH₃CH₂C=CHCH₂CH₃)(2,3,5,6-C₆F₄H) in trace amounts (Scheme 2-5). This mixture remained unchanged even in the presence of excess 1,2-C₆F₄H₂. Heating the reaction mixture at 50 °C gave rise to the arylalkene resulting from the hydrofluoroarylation of the alkyne and the doubly substituted reductively eliminated arylalkene product was observed on further heating (Scheme 2-5). The reaction of 3-hexyne with the nickel-hydride, Ni(H)(Pⁱ-Pr₃)₂(C₆F₅) resulted in equal amounts of the alkyne inserted product (Pⁱ-Pr₃)₂Ni(CH₃CH₂C=CHCH₂CH₃)(C₆F₅) and the Ni-alkyne complex, (Pⁱ-Pr₃)₂Ni(η²-CH₃CH₂C≡CCH₂CH₃). In a similar reaction with 1,2,3,4-C₆F₄H₂, only the final hydrofluoroarylated alkyne product was observed and no intermediates were observed. Johnson et al. believed that this was a result of faster reactions as the Ni-C bond is less stable for compounds with one ortho fluorine compared to two ortho fluorine atoms. When the bulky iso-propyl groups of the phosphine were replaced by less bulky ethyl groups in the complex, (PEt₃)₂Ni(η²-CH₃CH₂C≡CCH₂CH₃) similar reactivity was observed. It was also reported that the (Pⁱ-Pr₃)₂Ni(η²-EtC≡CEt) complex could also be synthesized more conveniently through the reaction of Ni(COD)₂, 2 equivalents of Pⁱ-Pr₃ and 3-hexyne (Scheme 2-5). ³



Scheme 2-5 Formation of $\text{Ni}(\text{P}^i\text{-Pr}_3)_2(\eta^2\text{-EtC}\equiv\text{CEt})^3$

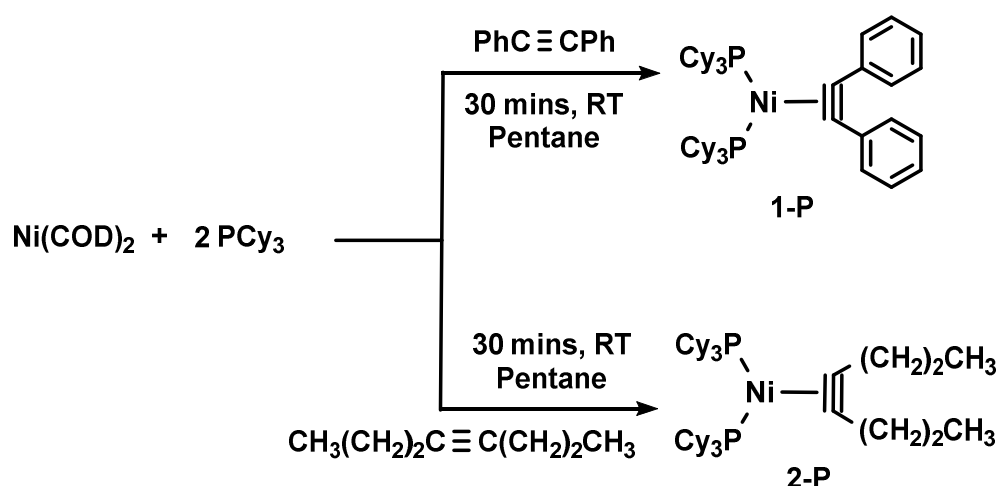
2.2. Results

The previous mechanistic studies performed to explore the hydrofluoroarylation of alkynes by Ni(0) catalysts have proven to exhibit contradictory features to one another, leaving the mechanism an unsolved mystery. The difference in the mechanisms postulated by experiments and DFT calculations was intriguing. The reactivity is strongly dependent on the number of phosphine ligands attached to Ni(0), which is shown by experiments and DFT calculations.^{2,3,9} Hence an attempt was made to look more closely at the mechanism involved, taking this into account. As the bis-phosphine Ni(0) source known complexes, such as $[\text{Ni}(\text{PCy}_3)_2]_2\text{N}_2$ and the alkyne coordinated complex, $\text{Ni}(\text{PR}_3)_2(\text{alkyne})$ were used.^{3,8} The recently reported complex, $(1,5\text{-hexadiene})\text{Ni}(\text{P}^i\text{-Pr}_3)$, which had only one phosphine

ligated to the metal centre was attractive as the source of mono-phosphine Ni(0). Work was carried out attempting to study the reactivity of these complexes with fluoroarenes and alkynes. The interest of this chapter lies in being able to design a system that would overcome the problems faced in studying the reaction.

2.2.1. Synthesis of Ni(PCy₃)₂(η^2 -alkyne) (alkyne = diphenylacetylene and 4-octyne)

The Ni(PCy₃)₂(η^2 -alkyne) was prepared in a similar manner to the analogous complex Ni(P^{*i*}Pr₃)₂(η^2 -hexyne) reported previously,³ by reacting 1 equivalent of alkyne (4-octyne or diphenylacetylene) with a stirred suspension of Ni(COD)₂ and two equivalents of phosphine (Scheme 2-6). The triisopropylphosphine groups were replaced by tricyclohexylphosphine groups as the hydrofluoroarylation reaction was reported to be equally effective for both phosphine groups. The product was observed to precipitate from the reaction mixture, which was purified by washing with pentane and was analysed by multinuclear NMR spectroscopy and LIFDI mass spectrometry.

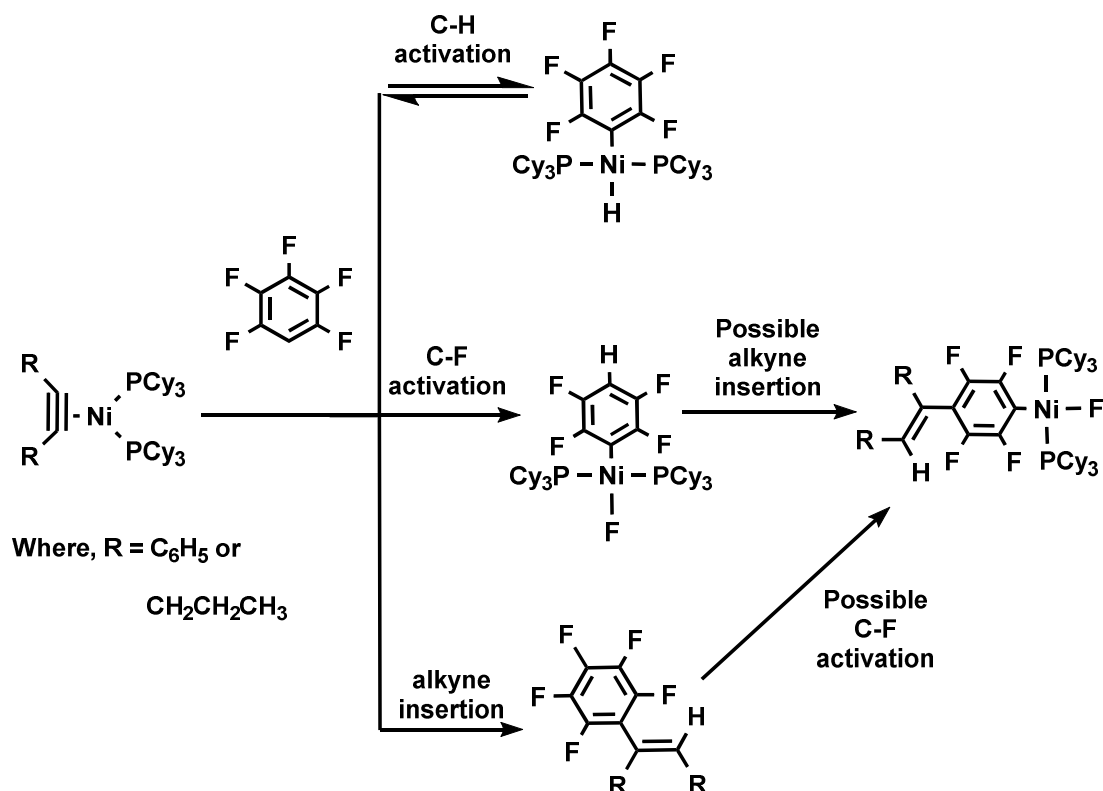


Scheme 2-6 Formation of Ni(PR₃)₂(alkyne) complexes.

The $\text{Ni}(\text{PCy}_3)_2(\eta^2\text{-PhC}\equiv\text{CPh})$ (**1-P**) could be isolated in excellent yields (92%) as an orange solid, that exhibited a singlet resonance at δ 41.2 in the ^{31}P -NMR spectrum. The LIFDI mass spectrum gave the molecular ion peak $[\text{M}]^+$ at 796.51 as the base peak (100%). The other peaks were at m/z 797.5, 798.5, 799.5, 800.5 and 801.5 which are consistent with the isotopic pattern of **1-P**. The $(\text{PCy}_3)_2\text{Ni}(\eta^2\text{-CH}_3(\text{CH}_2)_2\text{C}\equiv\text{C}(\text{CH}_2)_2\text{CH}_3)$ (**2-P**) was isolated as a bright yellow solid in very good yield (91.5%), that was analysed by ^{31}P -NMR spectrum, which exhibited a singlet at δ 44.4. The LIFDI mass spectrum of the product gave the molecular ion peak $[\text{M}]^+$ at 728.53 as base peak (100%). The other peaks were at 730, 731 and 732 which are consistent with the isotopic pattern expected for **2-P**.

2.2.2. Reaction of $\text{Ni}(\text{PCy}_3)_2(\eta^2\text{-alkyne})$ (alkyne = diphenylacetylene and 4-octyne) with $\text{C}_6\text{F}_5\text{H}$

The reaction of **1-P** with $\text{C}_6\text{F}_5\text{H}$ at 50 °C in toluene, gave rise to four different products after an hour, a C-H bond-activated nickel-hydride, arylalkene and two different C-F bond-activated nickel fluorides (Scheme 2-7). The major product in the reaction mixture after an hour at 50 °C, was the alkyne inserted product, $\text{Ph}(\text{H})\text{C}=\text{C}(\text{C}_6\text{F}_5)\text{Ph}$, which could be seen in the ^{19}F -NMR spectrum. The reaction mixture consisted of 46% of the alkyne inserted product, 36% of the nickel hydride and 18% of the nickel fluorides after an hour at 50 °C.



Scheme 2-7 The products resulting from the reaction between Ni(PCy₃)₂(η²-alkyne) and C₆F₅H

Upon heating the reaction mixture further at 50 °C for 48 hours, the number of products present was reduced to three. The nickel hydride was removed from the reaction mixture and the nickel fluoride resonance exhibited in the ³¹P-NMR spectrum was observed to grow. This is in agreement with observations made in literature, stating that the kinetically favoured C-H activation product, nickel hydride, is formed rapidly and reversibly and gives rise to the thermodynamically favoured C-F activation product, nickel fluoride. Both C-H bond and C-F bond activation are suggested to proceed via a similar intermediate, (PR₃)₂Ni(η²-C₆F₅H).^{2,16}

2.2.2.1. Formation of the nickel hydride and the arylalkene in the reaction between C₆F₅H and Ni(PCy₃)₂(η^2 -alkyne) (alkyne = diphenylacetylene and 4-octyne)

The major product of the reaction of **1-P** with C₆F₅H, after an hour at 50 °C in toluene, was observed to be the Ph(H)C=C(C₆F₅)Ph, which is the coupled product of the fluoroarene and the alkyne. The ¹⁹F-NMR spectrum exhibited a resonance at δ -143.7 (dd, J = 23 Hz and 2 Hz) for the ortho fluorine atoms, δ -157.3 (t, J = 22 Hz) for the para fluorine atom and δ -166.1 (td, J = 21 Hz, 8 Hz) for meta fluorine atoms (Figure 2-1). The vinyl hydrogen resonance was seen as a singlet at δ 5.8 in the ¹H-NMR spectrum which was in agreement with literature.²

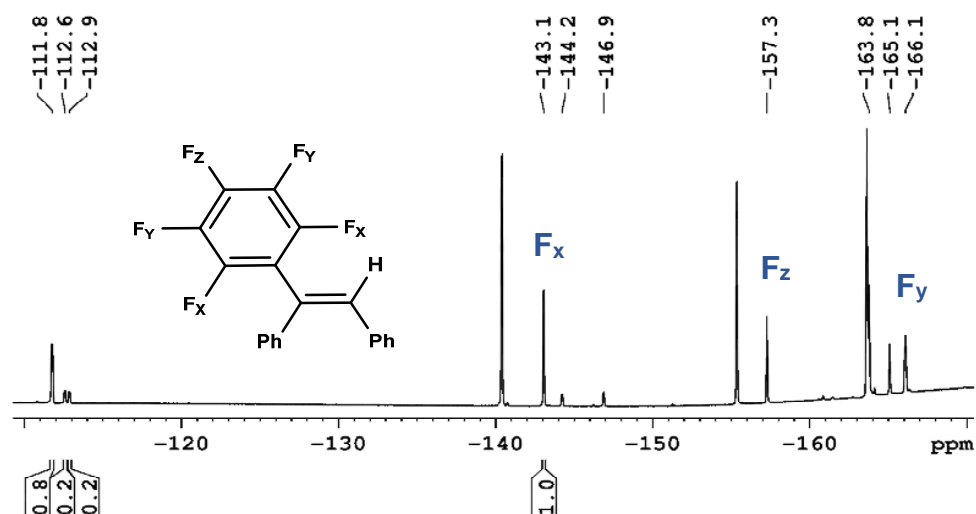


Figure 2-1 The ¹⁹F-NMR spectrum (470 MHz, C₆D₆) of the reaction mixture between **1-P** and C₆F₅H after an hour at 50 °C in toluene.

After an hour at 50 °C of reaction between **1-P** and C₆F₅H, the ¹H-NMR spectrum showed a triplet at δ -16.3 with a coupling constant of J = 68 Hz. The corresponding phosphorus resonance was observed at δ 39.1 in the

$^{31}\text{P}\{^1\text{H}\}$ -NMR spectrum, which was further confirmed by ^1H - ^{31}P -2D NMR spectroscopy. The ^{19}F -NMR spectrum of the reaction mixture showed a triplet at δ -163.8 ($J = 20$ Hz) and two unresolved multiplets at δ -111.8 and -165.1, for the five fluorine atoms of the aromatic ring (Figure 2-1). The data obtained for this nickel hydride is in agreement with the well-known complex (Scheme 2-7).¹⁶ The hydride formation is observed almost immediately (also under ambient conditions) in the reaction and decays upon heating the reaction mixture.

2.2.2.2. Formation of nickel fluorides in the reaction between $\text{C}_6\text{F}_5\text{H}$ and $\text{Ni}(\text{PCy}_3)_2(\eta^2\text{-alkyne})$ (alkyne = diphenylacetylene and 4-octyne)

The ^{19}F -NMR spectrum of the reaction in toluene, after an hour at 50 °C mixture exhibited two major triplets in the fluoride region at δ -403.7 and -404.3, suggesting two metal fluoride species, which were observed to grow with time. The $^{31}\text{P}\{^1\text{H}\}$ -NMR spectrum exhibited two doublets overlapping at δ 18.2 (Figure 2-2). In addition to this, another triplet at δ -409.0 was also observed in trace amounts in the ^{19}F -NMR spectrum, which could be attributed to an isomer of the *trans*- $\text{Ni}(\text{F})(\text{PCy}_3)_2(\text{C}_6\text{F}_4\text{H})$ (Figure 2-3).

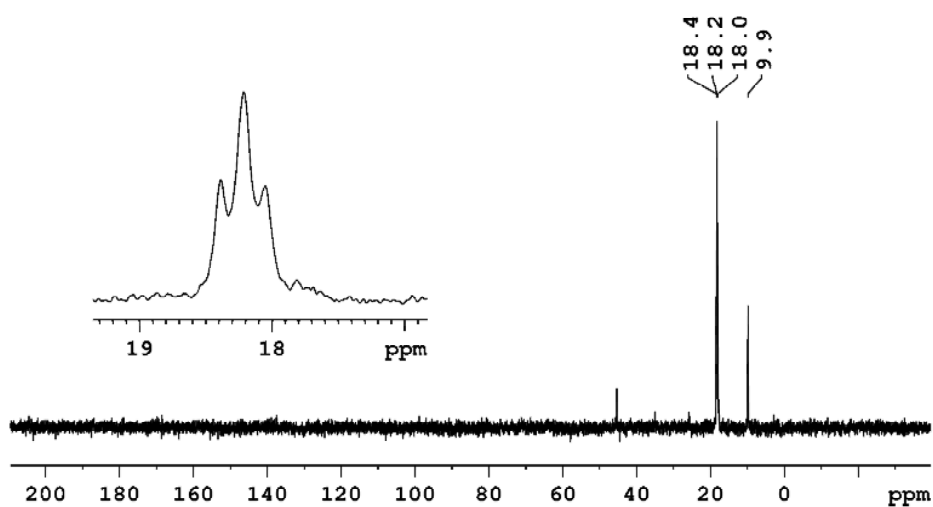


Figure 2-2 The ^{31}P -NMR spectrum (202 MHz, C_6D_6) of the reaction between **1-P** and $\text{C}_6\text{F}_5\text{H}$ after 24 hours at 50 °C in toluene.

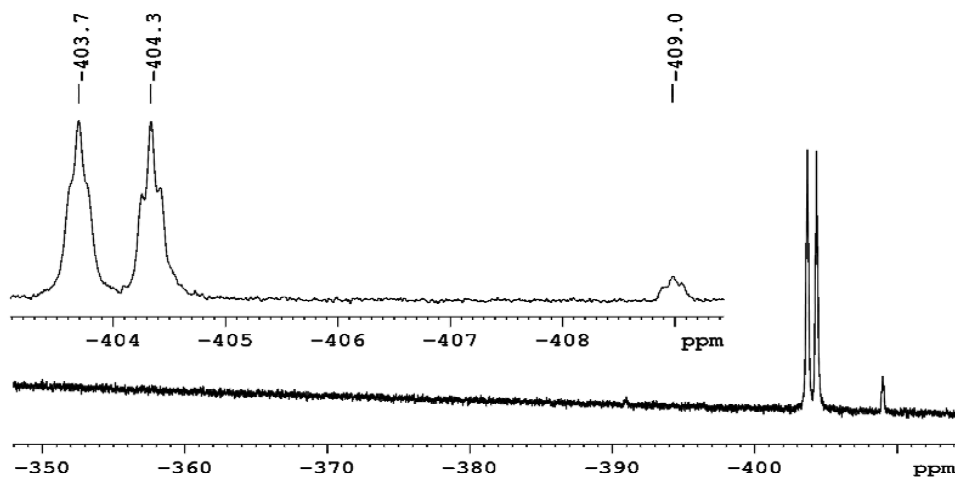


Figure 2-3 The ^{19}F -NMR spectrum (470 MHz, C_6D_6) (fluoride region) of the reaction between **1-P** and $\text{C}_6\text{F}_5\text{H}$ after 24 hours at 50 °C in toluene.

In order to identify the C-F activation products formed in the reaction, the reaction was repeated using hexane as the solvent. Upon heating at 50 °C a reaction mixture for two days containing one equivalent of **1-P** with one equivalent of $\text{C}_6\text{F}_5\text{H}$, a yellow precipitate with a yellow solution resulted. The yellow solid was separated, washed with cold pentane and was analysed by NMR spectroscopy and LIFDI mass spectrometry. The ^{19}F -NMR spectrum in C_6D_6 showed a triplet at δ -404.4, with a coupling constant of 39 Hz, which is consistent with a ^2J phosphorus fluorine coupling. The corresponding phosphorus resonance was observed at δ 18.3 as a doublet with a coupling of $J = 38$ Hz (Figure 2-4). The aromatic region of the ^{19}F -NMR spectrum showed two multiplets at δ -112.9 and δ -144.2 with unresolved multiplicity, suggesting C-F bond activation para to the hydrogen. The LIFDI mass spectrum of the purified solid from the reaction showed a peak at 786.44, which corresponds to the molecular mass of $\text{Ni}(\text{F})(\text{PCy}_3)_2(\text{C}_6\text{F}_4\text{H})$. The data obtained from multinuclear NMR spectroscopy and LIFDI mass spectrometry of the solid, are in good agreement to the literature known complex, *trans*- $\text{Ni}(\text{F})(\text{PCy}_3)_2(\text{C}_6\text{F}_4\text{H})$ (Scheme 2-7).¹⁷

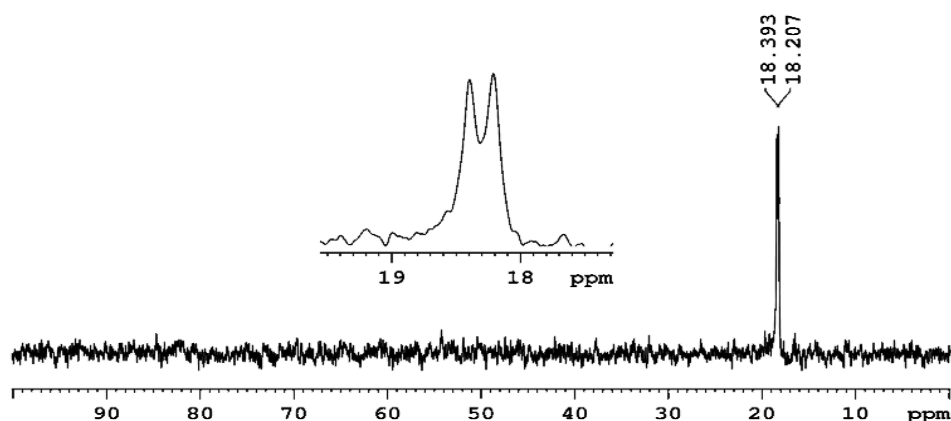


Figure 2-4 The ^{31}P -NMR spectrum (202 MHz, C_6D_6) of the purified solid from the reaction between **1-P** and $\text{C}_6\text{F}_5\text{H}$ in hexane.

The solution decanted from the reaction mixture of **1-P** with one equivalent of $\text{C}_6\text{F}_5\text{H}$ in hexane, was analysed by multinuclear NMR spectroscopy and LIFDI mass spectrometry. The two doublets observed to be overlapping in the $^{31}\text{P}\{^1\text{H}\}$ -NMR spectrum at δ 18.2, for the same reaction in toluene were now resolved into two doublets at δ 18.1 and δ 17.7 with coupling constants of 39 Hz and 44 Hz respectively (Figure 2-5). The peak at δ 9.9 corresponds to the free PCy_3 and the peak at δ 16.4, was an impurity not identified and absent in other reactions. The ^{19}F -NMR spectrum exhibited two triplets in the fluoride region similar to the same reaction in toluene mentioned above.

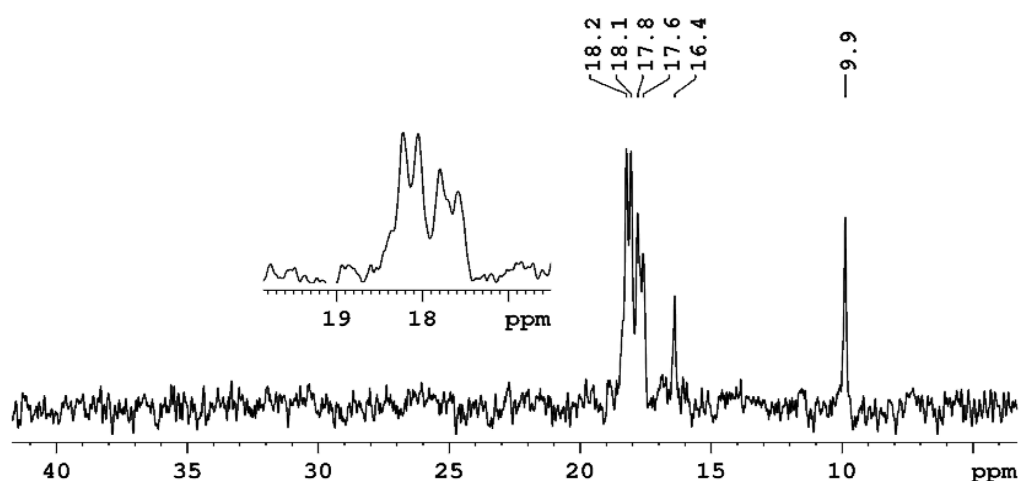


Figure 2-5 The ^{31}P -NMR spectrum (202 MHz, C_6D_6) of the solution decanted from the reaction between **1-P** and $\text{C}_6\text{F}_5\text{H}$ in hexane.

The LIFDI mass spectrum of the solution decanted showed two peaks at m/z 786.44 and 964.50. The peak at m/z 786.44 was identified as arising from *trans*-Ni(F)(PCy₃)₂(C₆F₄H). The peak at 964.50 which had isotopic peaks at 965.50, 966.50, 967.51, 968.50 and 969.50 was in good agreement with the molecular mass of the species Ni(F)(PCy₃)₂(C₆F₄PhC=CPhH) which could be the result of the C-F bond activated product of the arylalkene. This could be formed by the hydrofluoroarylation of PhC≡CPh or by the alkyne inserting (via hydrofluoroarylation reaction) into the C-H bond of the nickel fluoride species *trans*-Ni(F)(PCy₃)₂(C₆F₄H). The aromatic region of the ¹⁹F-NMR spectrum exhibited two resonances at δ -112.6 and δ -146.9 with AA'XX' spin systems for the unknown fluoride species, suggesting magnetically inequivalent environments for the aromatic fluorine atoms. This too fits well for the above hypothesised nickel fluoride species.

In order to confirm the identity of this species, several experiments were performed. The reaction was repeated with **2-P** with one equivalent of C₆F₅H in hexane. The LIFDI mass spectrum of the solution now had a peak at 729.3 which is consistent with the molecular formula Ni(F)(PCy₃)₂[C₆F₄(CH₃CH₂CH₂C=CHCH₂CH₂CH₃)], which is the expected product molecule obtainable by replacing the PhC≡CPh with 4-octyne.

Further, a reaction was done with one equivalent of C₆F₅H with Ni(COD)₂ in the presence of two equivalents of PCy₃. The reaction gave rise to a nickel hydride, *trans*-Ni(H)(PCy₃)₂(C₆F₅), and nickel fluoride, *trans*-Ni(F)(PCy₃)₂(C₆F₄H), which was observed by multinuclear NMR spectroscopy, after 3 hours at 50 °C. To this reaction mixture, one equivalent of PhC≡CPh was added and heated at 50 °C, overnight. The resulting reaction mixture was analysed by multinuclear NMR spectroscopy and LIFDI mass spectrometry. The ¹⁹F-NMR spectrum in the fluoride region showed the formation of a new fluoride resonance, which corresponds to the species, Ni(F)(PCy₃)₂[(C₆F₄)PhC=CPh(H)]. In addition to this, the formation of the alkyne-inserted product, Ph(H)C=C(C₆F₅)Ph, is observed in the ¹⁹F-NMR spectrum. The LIFDI mass spectrum of the resultant reaction mixture

exhibited a molecular ion peak at 964.46 corresponding to the molecular mass of $\text{Ni}(\text{F})(\text{PCy}_3)_2[(\text{C}_6\text{F}_4)\text{PhC}=\text{CPh}(\text{H})]$ (Scheme 2-7).

The alkyne-inserted product, $\text{Ph}(\text{H})\text{C}=\text{C}(\text{C}_6\text{F}_5)\text{Ph}$, was prepared according to literature² and was purified. This purified product was reacted with one equivalent of $\text{Ni}(\text{COD})_2$ and two equivalents of PCy_3 . The reaction mixture was heated at 80 °C for several weeks. However the ^{19}F -NMR spectrum showed no resonance in the fluoride region. The ^{31}P and ^1H -NMR spectra of the reaction mixture was not obtained as a result of poor shimming. Alternatively, the nickel fluoride, *trans*- $\text{Ni}(\text{F})(\text{PCy}_3)_2(\text{C}_6\text{F}_4\text{H})$ was prepared by heating a reaction mixture containing, $\text{Ni}(\text{COD})_2$, two equivalents of PCy_3 and one equivalent of $\text{C}_6\text{F}_5\text{H}$, at 80 °C for 48 hours. The nickel fluoride thus obtained was reacted with one equivalent of **1-P**, and was heated at 80 °C for 3 hours. The resulting reaction mixture, showed the formation of $\text{Ni}(\text{F})(\text{PCy}_3)_2[(\text{C}_6\text{F}_4)\text{PhC}=\text{CPh}(\text{H})]$, which was observed by the appearance of the new fluoride at δ -403.7 and the new peak observed at 964.50 in the LIFDI mass spectrum (Figure 2-6), which was consistent with the molecular mass and the isotopic pattern of $\text{Ni}(\text{F})(\text{PCy}_3)_2[(\text{C}_6\text{F}_4)\text{PhC}=\text{CPh}(\text{H})]$.

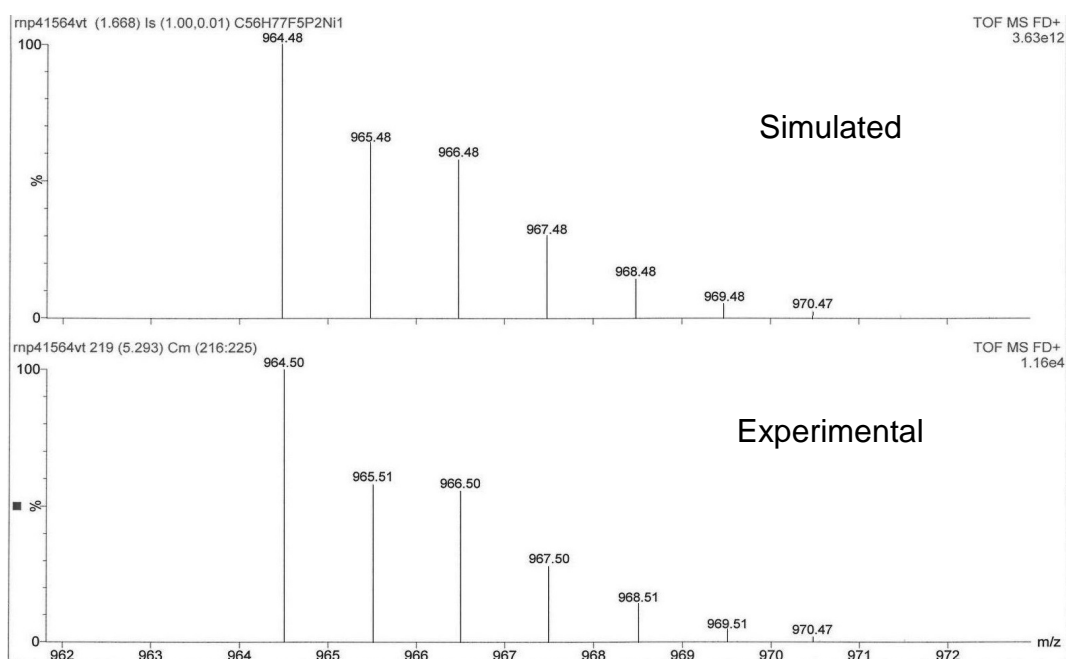
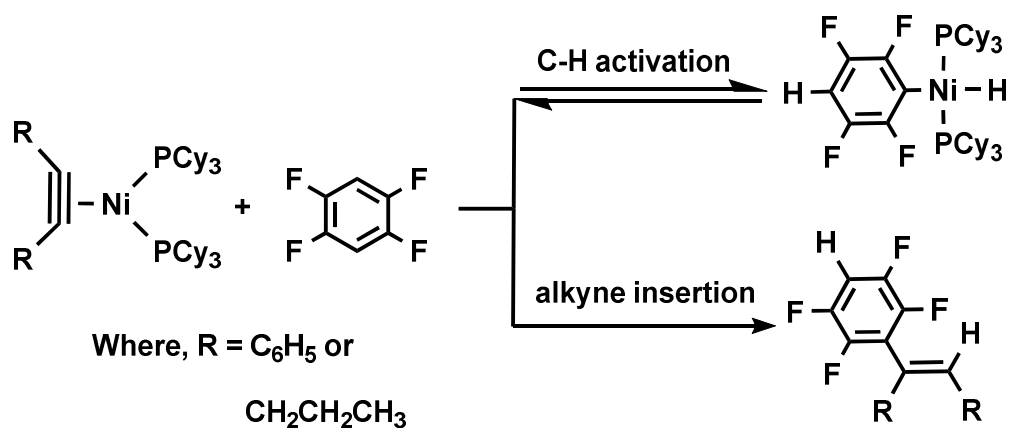


Figure 2-6 The LIFDI mass spectrum of the reaction between *trans*- $\text{Ni}(\text{F})(\text{PCy}_3)_2(\text{C}_6\text{F}_4\text{H})$ and **1-P**.

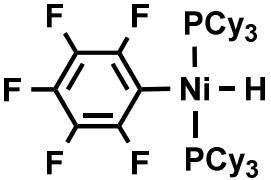
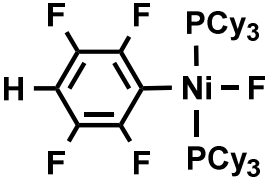
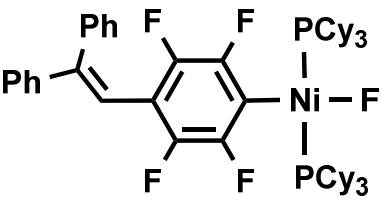
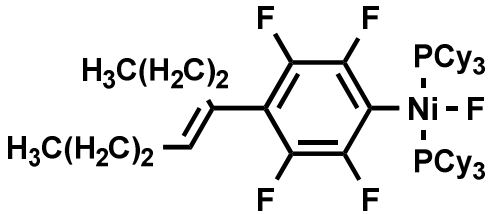
2.2.3. Reaction of Ni(PCy₃)₂(η^2 -alkyne) (alkyne = diphenylacetylene and 4-octyne) with 1,2,4,5-C₆F₄H₂

The reaction of **1-P** with 1,4-C₆F₄H₂ gave rise to the hydrofluoroarylated alkyne product and the C-H bond activated nickel hydride within an hour at ambient temperature (Scheme 2- 8). The ¹⁹F-NMR spectrum of the reaction mixture after an hour at 50 °C showed the equal amounts of the nickel hydride, *trans*-Ni(H)(PCy₃)₂(C₆F₄H) and the arylalkene, Ph(H)C=C(C₆F₄H)Ph. The *trans*-Ni(H)(PCy₃)₂(C₆F₄H) was identified by the hydride resonance observed at δ -16.1 (t, J = 68 Hz). The corresponding singlet resonance in the decoupled ³¹P{¹H}-NMR spectrum was observed at δ 39.7 and the ¹⁹F-NMR spectrum exhibited two multiplets at δ -114.0 and at δ -144.4. The hydrofluoroarylated alkyne, was observed by both ¹H and ¹⁹F-NMR spectroscopy. The vinyl hydrogen was observed in the ¹H-NMR spectrum at δ 5.3 as a singlet and the ¹⁹F-NMR spectrum exhibited two multiplets at δ -140.5 and at δ -143.1 for the aromatic fluorine atoms. The reaction did not give rise to C-F bond activation after an hour at 50 °C, but raising the temperature to 80 °C for an hour showed trace levels of nickel fluoride, *trans*-Ni(F)(PCy₃)₂(C₆F₃H₂), which was observed in the ¹⁹F-NMR spectrum at δ -386.4 as a triplet (J = 42 Hz). The same was observed with the 4-octyne nickel complex, **2-P**.



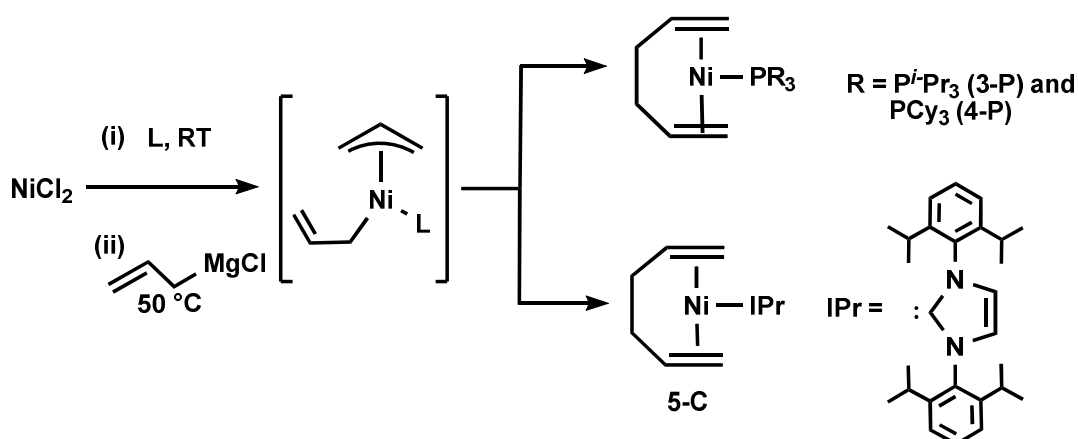
Scheme 2- 8 The products resulting from the reaction between Ni(PCy₃)₂(η^2 -alkyne) and 1,4-C₆F₄H₂.

Table 2-1 NMR spectroscopic data for the nickel complexes formed in the reaction of C₆F₅H with **1-P** or **2-P**

	¹ H-NMR	³¹ P-NMR	¹⁹ F-NMR
	δ -16.3 (t, J = 68 Hz)	δ 39.1 (s)	δ -163.8 (J = 20 Hz) δ - 111.8 (m) - 165.1(m)
	δ 6.4 (m)	δ 18.3 (d, J = 38 Hz)	δ -404.4, (t, J = 39 Hz), δ -112.9 (m), δ - 144.2 (m)
	δ 5.8 (t, J = 7 Hz)	δ 17.7 (d, J = 44 Hz)	δ -403.7, (t, J = 43 Hz), δ -112.6 (AA'XX'), δ -146.9 (AA'XX')
	δ 5.7 (t, J = 7 Hz)	δ 18.0 (d, J = 41 Hz)	δ -403.4, (t, J = 40 Hz), δ -113.2 (AA'XX'), δ -147.4 (AA'XX')

2.2.4. Synthesis of Ni(L)(1,5-hexadiene) (L = Pⁱ-Pr₃, PCy₃ and IPr)

A new straightforward route to prepare various N-heterocyclic carbenes and Pⁱ-Pr₃ ligated Ni(0)-hexadiene complexes was reported by Hazari in 2012.¹⁸ The synthesis did not involve any thermally unstable intermediates and is believed to proceed via the intermediate (η^1 -allyl)(η^3 -allyl)Ni(NHC)¹⁹ (Scheme 2-9). The complexes were found to stable up to 60 °C. Stoichiometric reactions of (1,5-hexadiene)Ni(L) (where L = NHC or Pⁱ-Pr₃) performed by Hazari et al., demonstrated that the 1,5-hexadiene ligand can be easily replaced with other ligands such as phosphines, CO, isonitriles and olefins.



Scheme 2-9 Synthesis of (1,5-hexadiene)Ni(L).¹⁸

This suggested the complex to be a promising precursor for complexes having a single N-heterocyclic carbene or phosphine. This new complex was attractive as the mono-phosphine-Ni(0) source, which would enable further studies in the hydrofluoroarylation reaction. The reaction has been extended in this work to prepare analogous tricyclohexylphosphines giving rise to (1,5-hexadiene)Ni(PCy₃) (**4-P**) (Scheme 2-9). The (allyl)MgCl used in the synthesis is used to both reduce the Ni(II) and to form the 1,5-hexadiene ligand.¹⁸

2.2.4.1. Synthesis and reactions of (1,5-hexadiene)Ni(PR₃) (R = isopropyl and cyclohexyl)

The orange product resulting from the synthesis of (1,5-hexadiene)Ni(P^{*i*}-Pr₃) (**3-P**) (Scheme 2-9) was analysed by NMR spectroscopy and was in good agreement with the literature values.¹⁶ The ³¹P-NMR spectrum exhibited a singlet resonance at δ 54.4. However, the product could not be isolated as a solid free of solvent. All attempts to remove the solvent completely from the solid were fruitless. As an attempt to obtain a solid product, the triisopropylphosphine was replaced by tricyclohexylphosphine, in a similar reaction. The product was obtained as a yellow solid by precipitation in pentane. The solid product thus obtained from the reaction was analysed by NMR spectroscopy and LIFDI mass spectrometry. The LIFDI mass spectrum of the solid showed a molecular ion peak at 420.25 (Figure 2-7), which corresponds to the molecular mass of complex (1,5-hexadiene)Ni(PCy₃). The other peaks were at *m/z* 421.25, 422.25, 423.25 and 424.24 which matches the isotopic pattern of **4-P**.

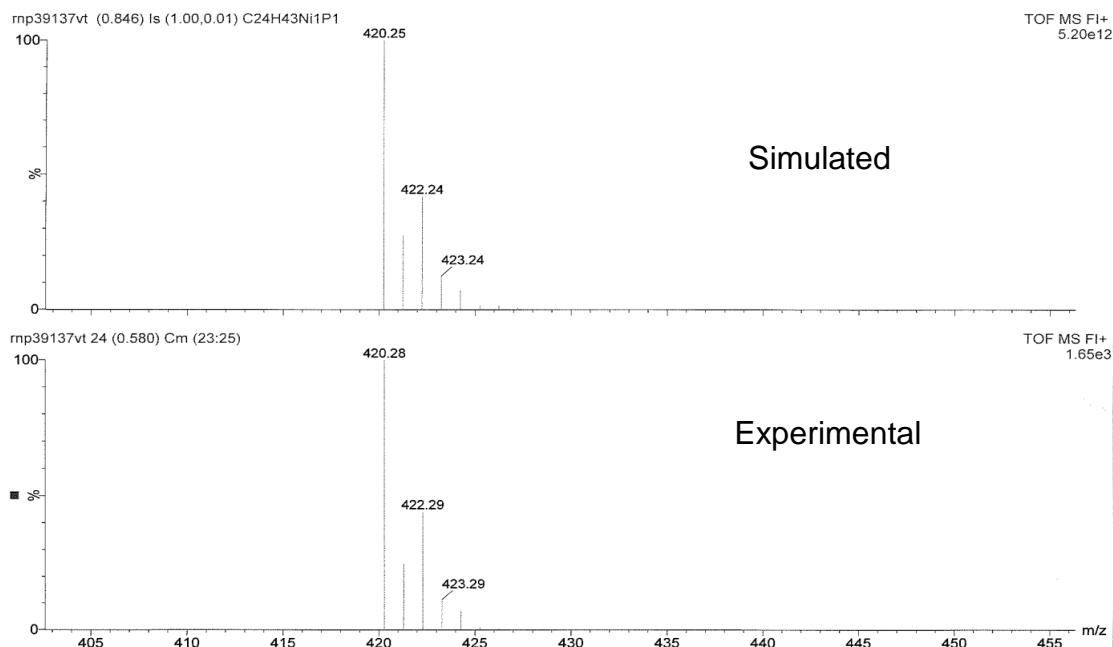
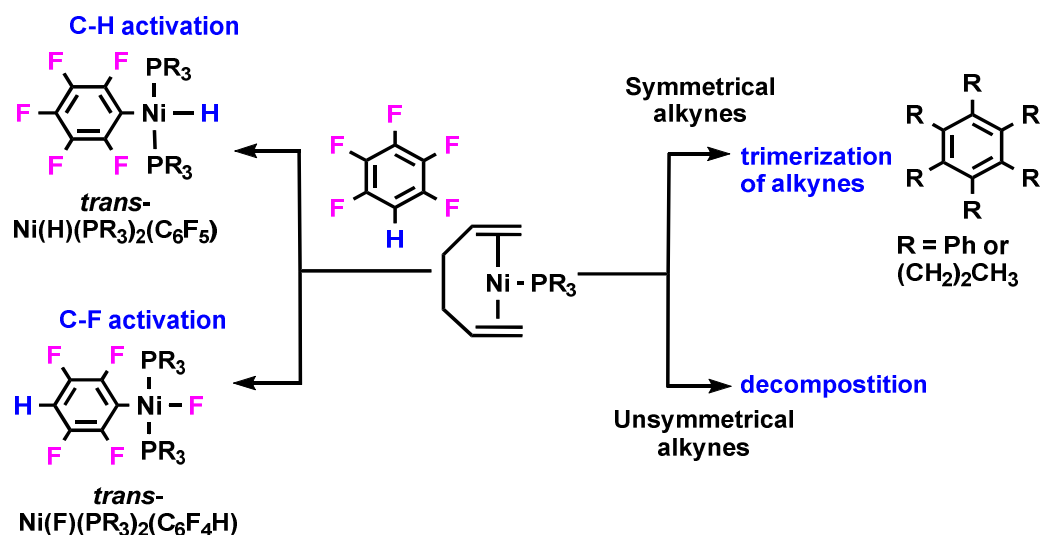


Figure 2-7 LIFDI mass spectrum illustrating the isotopic pattern of complex **4-P**.

2.2.4.2. Reactions of Ni(PR₃)(1,5-hexadiene) with C₆F₅H and alkynes (R = isopropyl and cyclohexyl)

2.2.4.2.1. Reaction of Ni(PR₃)(1,5-hexadiene) with C₆F₅H (R = isopropyl and cyclohexyl)

The reaction of (1,5-hexadiene)Ni(PR₃) (where R = *i*-Pr and Cy) with C₆F₅H, at room temperature, gave rise to C-H and C-F activation immediately at room temperature (Scheme 2-10). The reaction mixture was analysed by multinuclear NMR spectroscopy. The ¹H-NMR spectrum of the reaction mixture of **4-P** with C₆F₅H showed a triplet at δ -16.4, with a coupling constant of 68 Hz and the corresponding phosphorus resonance was seen in the ³¹P{¹H}-NMR spectrum at δ 39.2, which suggests the formation of a nickel hydride ligated to two phosphine groups, *trans*-Ni(H)(PCy₃)₂(C₆F₅). The ¹⁹F-NMR spectrum of the reaction mixture had a triplet at δ -404, with a coupling constant of 37 Hz, indicating the formation of the C-F activated species, *trans*-Ni(F)(PCy₃)₂(C₆F₄H). The same behaviour was observed when the complex **3-P** was reacted with C₆F₅H.



Scheme 2-10 The reactions of (1,5-hexadiene)Ni(PR₃) with C₆F₅H and alkynes.

2.2.4.2.2. Reaction of Ni(PR₃)(1,5-hexadiene) with alkynes.

The reaction of (1,5-hexadiene)Ni(PR₃) with alkynes was investigated with both symmetrical and unsymmetrical alkynes (Scheme 2-10). The reaction of one equivalent of (1,5-hexadiene)Ni(PR₃) with one equivalent of PhC≡CPh gave rise to a red solution at room temperature, that could not be analysed by NMR spectroscopy probably due to paramagnetic components. The solution was analysed by LIFDI mass spectrometry. The LIFDI mass spectrum obtained had a molecular ion peak at 872.4, suggesting [Ni(PCy₃)] coordinated to a trimerized alkyne unit C₆Ph₆. As an attempt to suppress trimerization of alkynes, the reaction was repeated with an unsymmetrical alkyne. The reaction of one equivalent of (1,5-hexadiene)Ni(PCy₃) with one equivalent of PhC≡CSi(CH₃)₃ did not show any reaction at low temperature and upon heating up the solution, decomposition was observed.

2.2.4.3. Synthesis and reactions of (1,5-hexadiene)Ni(IPr)

The reactions for the mono-phosphine complex, (1,5-hexadiene)Ni(PR₃) (as mentioned above) with C₆F₅H and alkyne were similar to the reactions observed with bis-phosphine Ni(0) complexes, offering no new information. This was due to the phosphine ligands attached to nickel being labile and hence giving rise to bis-phosphine Ni(0) motifs which then takes part in reactions. To overcome this, the analogous N-heterocyclic carbene Ni(0) complex, (1,5-hexadiene)Ni(IPr) (**5-C**) (also reported by Hazari et al.) was sought as a replacement. The complex was chosen with the anticipation that the N-heterocyclic carbene ligands would be far less labile than the phosphine ligands when bound to Ni(0) and also that the bulky carbene ligand would not favour the coordination of another bulky carbene ligand on Ni(0), hence the complex would act as a nickel-mono carbene motif.

The complex **5-C**, was prepared and isolated as an orange solid in a reasonable yield (69%), by following the synthetic route followed in literature

(Scheme 2-9).¹⁸ The ¹H-NMR spectrum of the product was in good agreement with literature.¹⁸ The LIFDI mass spectrum of the solid showed a molecular ion peak at 528.30, which corresponds to the molecular mass of complex **5-C**. The other peaks were at m/z 529.31, 530.30, 531.31 and 532.30 which matches the isotopic pattern of **5-C** (Figure 2-8).

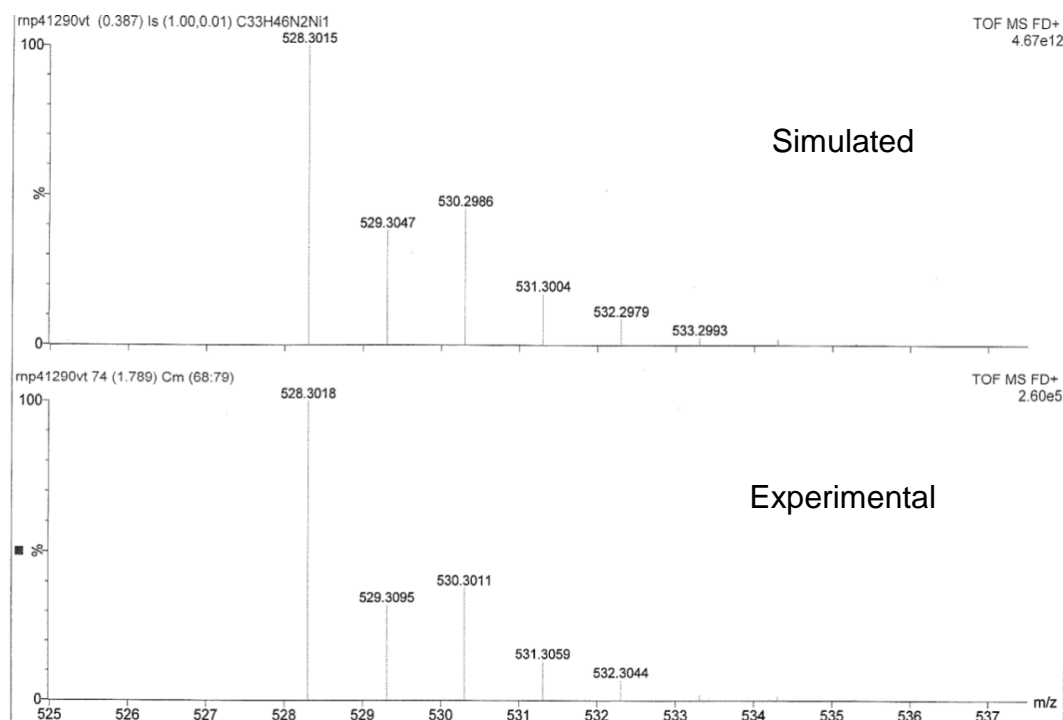
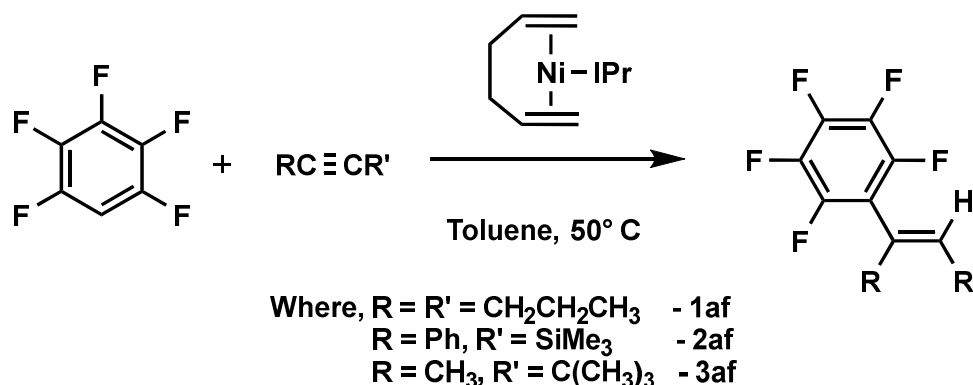


Figure 2-8 LIFDI mass spectrum of the complex **5-C**.

2.2.4.4. Reaction of C₆F₅H and alkyne in the presence of Ni(IPr)(1,5-hexadiene)

The reaction of C₆F₅H with alkynes, in the presence of **5-C** gave rise to coupled product, arylalkene, at room temperature (Scheme 2-11). The reaction mixture was analysed by ¹H and ¹⁹F-NMR spectroscopy. The reaction was followed under both stoichiometric and catalytic conditions of the Ni(0) complex and the hydrofluoroarylation of the alkyne was observed

clearly at both conditions. Both symmetrical and unsymmetrical alkynes were used for the study.



Scheme 2-11 Coupling reaction of C₆F₅H and alkyne catalysed by **5-C**.

2.2.4.4.1. Reaction of C₆F₅H with symmetrical alkynes catalysed by **5-C**.

Using **5-C** as the catalyst (10 mol %) the reaction of C₆F₅H with 4-octyne to give the coupled product, pentafluoro(4-octenyl)benzene, was complete within 7 hours at 50 °C (Scheme 2-11). The ¹H-NMR spectrum exhibited a triplet with a coupling constant of J = 7 Hz at δ 5.3, characteristic of the vinyl hydrogen on the arylalkene product (literature, δ 5.5, J = 7.4 Hz) (Figure 2-10). The ¹⁹F-NMR spectrum (Figure 2-9) exhibited three resonances in the aromatic region for the product (Table 2-2).

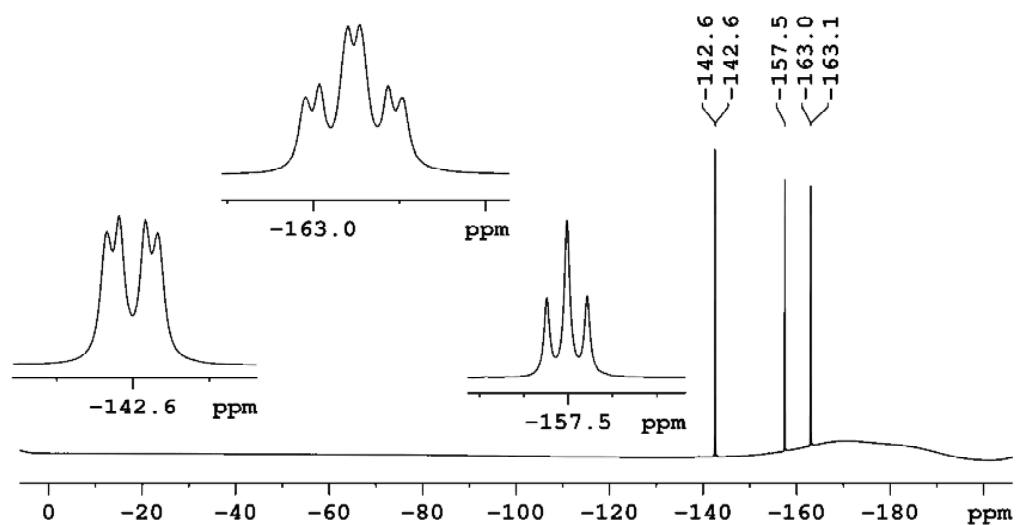


Figure 2-9 The ^{19}F -NMR spectrum (470 MHz, C_6D_6) of the reaction mixture $\text{C}_6\text{F}_5\text{H}$ and 4-octyne, catalysed by **5-C**, after 7 hours at 55 °C.

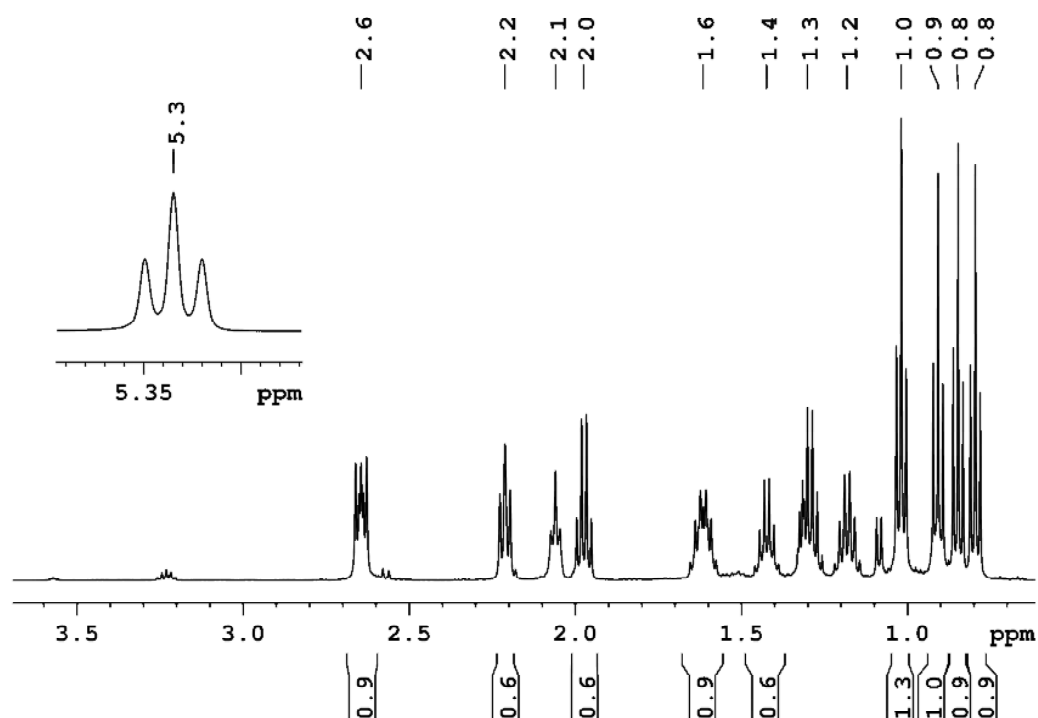


Figure 2-10 The ^1H -NMR spectrum (500 MHz, C_6D_6) of the reaction mixture $\text{C}_6\text{F}_5\text{H}$ and 4-octyne, catalysed by **5-C**, after 3 hours at 55 °C.

The ^1H -NMR spectrum of the reaction mixture showed that in addition to the hydrofluoroarylation reaction, giving rise to the desired coupled product pentafluoro(4-octenyl)benzene (**1af**), the product of trimerization of the

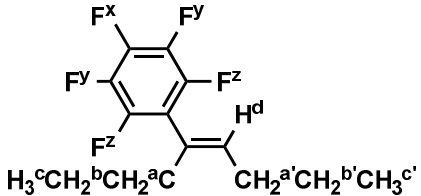
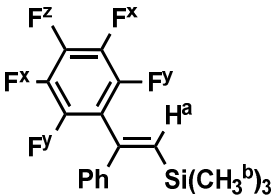
alkyne, 4-octyne was present too. The $^1\text{H-NMR}$ spectrum exhibited two multiplets at δ 2.6, 1.6 and a triplet at δ 1.0 with a coupling constant of 7 Hz (Figure 2-10). The product ratio of arylalkene to trimerized alkyne was observed to be 1:0.2 after 3 hours at 55 °C (Figure 2-10). The alkyne trimerization was observed to initiate even at ambient temperature within an hour. The same was observed when other symmetrical alkynes such as 3-hexyne and diphenylacetylene were used.

2.2.4.4.2. Unsymmetrical alkynes ($\text{PhC}\equiv\text{CSiMe}_3$ and $\text{CH}_3\text{C}\equiv\text{CC}(\text{CH}_3)_3$)

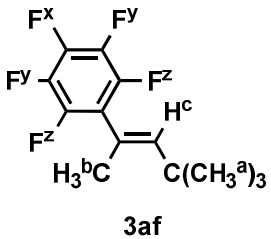
The reaction of $\text{C}_6\text{F}_5\text{H}$ with $\text{PhC}\equiv\text{CSiMe}_3$, in the presence of **5-C** was observed to initiate hydrofluoroarylation even at ambient temperature (Scheme 2-11). The reaction mixture was followed by ^1H and $^{19}\text{F-NMR}$ spectroscopy. (Table 2-2) The reaction mixture did not lead to any trimerization of the alkyne even after 24 hours at 55 °C. However, as the reaction proceeded, the product (**2af**) was observed to decay, which was revealed by the decrease in the intensity of the product resonance in the $^1\text{H-NMR}$ spectrum with respect to the internal standard, $(\text{CF}_3)_2\text{C}_6\text{H}_4$.

The reaction was repeated replacing $\text{PhC}\equiv\text{CSiMe}_3$ by $\text{CH}_3\text{C}\equiv\text{CC}(\text{CH}_3)_3$ as the alkyne (Scheme 2-11). The ^1H and $^{19}\text{F-NMR}$ spectra of the reaction mixture showed the formation of the product (**3af**) of the hydrofluoroarylation reaction within an hour at ambient temperature (Table 2-2). Even when the reaction mixture heated at 55 °C for 36 hours, alkyne trimerization reactions were still absent and the coupled product was found to be stable.

Table 2-2 The spectral data for the products of the hydrofluoroarylation – **1af**, **2af** and **3af**.

	¹ H-NMR spectra	¹⁹ F-NMR spectra
 <p style="text-align: center;">1af</p>	<p>Experimental (500 MHz, C₆D₆) : 5.3 (t, J = 7 Hz, 1, H_d), 2.2 (t, J = 7 Hz, 2 H_a), 2.0 (q, J = 7 Hz, 2 H_{a'}), 1.4 (sext, J = 7 Hz, 2 H_b), 1.2 (sext, J = 7 Hz, 2 H_{b'}), 0.9 (t, J = 7 Hz, 3 H_c), 0.8 (t, J = 7 Hz, 3 H_{c'})</p> <p>Literature (400 MHz, CDCl₃) : 5.51 (t, J = 7.4 Hz, 1 H_d), 2.35 (t, J = 7.6 Hz, 2 H_a), 2.22 (q, J = 7.3 Hz, 2 H_{a'}), 1.48 (sext, J = 7.4 Hz, 2 H_b), 1.29 (sext, J = 7.4 Hz, 2 H_{b'}), 0.97 (t, J = 7.4 Hz, 3 H_c), 0.90 (t, J = 7.3 Hz, 3 H_{c'})</p>	<p>Experimental (470 MHz, C₆D₆) : -142.4 (dd, J = 23 Hz, 2 F_z), -156.6 (t, J = 22 Hz, 1 F_x), -162.7 (td, J = 24 Hz, 2 F_y)</p> <p>Literature (282 MHz, CDCl₃) : -142.2 (dd, J = 23, 8 Hz, 2 F), -157.0 (t, J = 21 Hz, 1 F), -163.1 (td, J = 22, 8 Hz, 2 F)</p>
 <p style="text-align: center;">2af</p>	<p>Experimental (500 MHz, C₆D₆) : 5.9 (s, 1 H_a), 0.3 (s, 9 H_b), 7.5-7.4 (m, 3 H_{phenyl}), 7.2- 7.1 (m, overlapping with solvent, 5 H_{phenyl})</p>	<p>Experimental (470 MHz, C₆D₆) : -142.4 (dd, J = 23.3, 8.2 Hz, 2 F_y), -156.6 (t, J = 21.4 Hz, 1 F_z), -162.66 (td, J = 23, 8 Hz, 2 F_x)</p>

Hydrofluorarylation of alkynes

	Literature (400 MHz, CDCl ₃) : 6.06 (s, 1 H _a), 0.03 (s, 9 H _b), 7.34-7.29 (m, 3 H) 7.27-7.21 (m, 2 H)	Literature (282 MHz, CDCl ₃) : -142.2 (dd, J = 22.7, 8.2 Hz, 2 F), -157.0 (t, J = 20.6 Hz, 1F), -163.1 (td, J = 21.9, 8.2 Hz, 2 F)
 <p style="text-align: center;">3af</p>	Experimental (500 MHz, C ₆ D ₆) : 5.4 (m, 1 H _c), 1.8 (m, 3 H _b), 1.1 (s, 9 H _a)	Experimental (470 MHz, C ₆ D ₆) : -143.9 (dd, J = 22 Hz, 8 Hz, 2 F _z), -158.3 (t, J = 21 Hz, 1 F _x), -163.2 (td, J = 23 Hz, 8 Hz, 2 F _y)
	Literature (400 MHz, CDCl ₃) : 5.52-5.49 (m, 1 H), 2.05-2.02 (m, 3 H), 1.22 (s, 9 H)	Literature (282 MHz, CDCl ₃) : -143.7 (dd, J = 22.7, 8.2 Hz, 2 F _z), -158.7 (t, J = 20.6 Hz, 1 F _y), -163.6 (td, J = 22.0, 7.5 Hz, 2 F _x)

2.3. Discussion

2.3.1. Introduction: Nickel(0) precursors

Although many organic reactions are catalysed by Ni(0), there are few suitable Ni(0) precursors that enable one to gain a deep insight into the mechanisms involved. The commonly used precursor for nickel(0), Ni(COD)₂, is relatively difficult to handle and thermally unstable. In addition, one major problem is that the COD is very difficult to remove from the reaction and as a result the involvement of COD in side reactions has been reported in several cases.³ Complexes of the type Ni-N-heterocyclic carbenes are relatively stable, but ligand substitution is not easily achieved and hence limits their use as Ni(0) precursors.

The necessity for the species, Ni(PR₃)₂ arises mainly due to the interference caused by excess phosphine in reactions, which has been observed by the formation of difluorophosphoranes as side products and the lack of selectivity which has been observed in the reaction of C₆F₅H with Ni(PEt₃)₄, where the formation of all three possible C-F activation took place.¹⁶ Over the past few decades, various complexes have been used as sources of Ni(PR₃)₂ by various groups to study the reactivity of fluorinated arenes (Figure 2-11). The Ni(PR₃)₂ adducts of phenanthrene, anthracene and isobutene, Ni(PR₃)₂(η²-C₁₄H₁₀), Ni(PR₃)₂(η²-H₂CCMe₂) (where R = Et, *i*-Pr), are complexes used by Johnson to study the reactivity of fluoroarene. In solution the complexes readily give rise to the bis-phosphine-nickel adduct, which is then available for reaction with a fluoroarene.^{3,16,20}

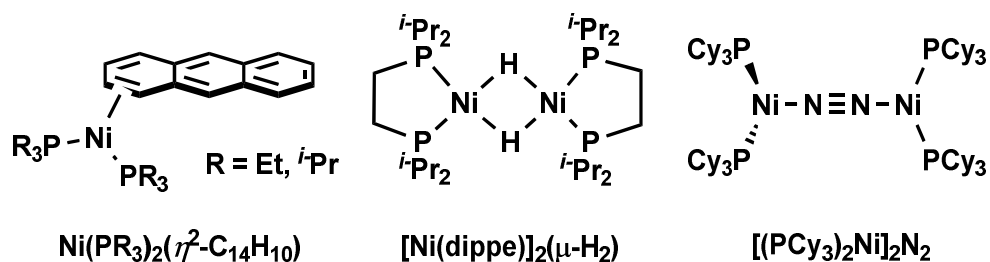


Figure 2-11 A selection of complexes used in literature as sources of Ni(PR₃)₂.^{2,3,21}

A bridging hydrogen complex, $[\text{Ni}(\text{dippe})(\mu\text{-H}_2)]_2$, is another example of a complex used as a Ni-bisphosphine source by Jones, where the phosphine was a chelating bidentate ligand 1,2-bis(diisopropylphosphino)ethane.²¹ To study the mechanism of the hydrofluoroarylation reaction, the dinitrogen complex, [bis(bis-tricyclohexylphosphine)nickel) dinitrogen], was used by Nakao et al. The deep red complex $[(\text{PCy}_3)_2\text{Ni}]_2\text{N}_2$ has two $\text{Ni}(\text{PCy}_3)_2$ units bonded end-on to N_2 . The N_2 is surrounded by a cage-like arrangement formed by the cyclohexyl rings of the phosphine and this is believed to be the main reason for the stability of the complex.² The N_2 is easily lost in solution to give rise to the $\text{Ni}(\text{PCy}_3)_2$ species of interest.^{8,22}

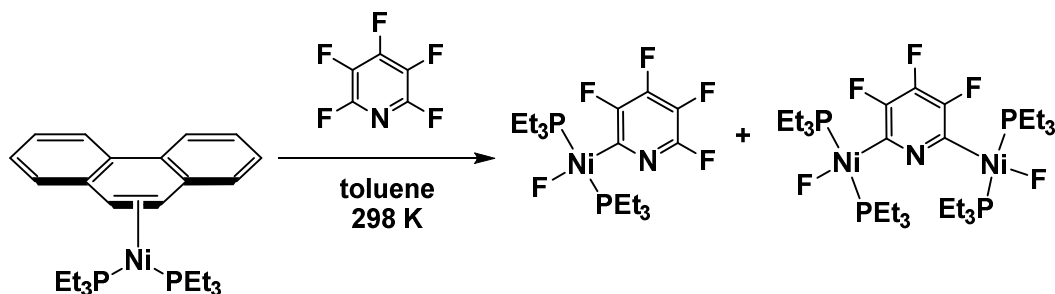
2.3.2. Can nickel-phosphine complexes be used to study the mechanism of hydrofluoroarylation?

As an attempt to understand the mechanism of hydrofluoroarylation several complexes were used. As the source of nickel bis-phosphine species, $\text{Ni}(\text{PR}_3)_2$, the dinitrogen complex, $[(\text{PCy}_3)_2\text{Ni}]_2\text{N}_2$, and the alkyne coordinated complex, $\text{Ni}(\text{PR}_3)_2(\text{alkyne})$, were used. The complex $\text{Ni}(\text{PR}_3)_2(\text{alkyne})$ proved to be far easier to handle and the synthesis and the stability was far more convenient than that of the dinitrogen complex. In addition to this, $\text{Ni}(\text{PR}_3)_2(\text{alkyne})$ already possesses the alkyne coordinated to the metal centre and hence was of interest to study the reactivity with fluoroarenes.

The reactivity of the complex $\text{Ni}(\text{PR}_3)_2(\text{alkyne})$ (where R = cyclohexyl and alkyne = $\text{PhC}\equiv\text{CPh}$ and 4-octyne) with fluoroarenes was studied by independent reactions with $\text{C}_6\text{F}_5\text{H}$ and 1,4- $\text{C}_6\text{F}_4\text{H}_2$. Both fluoroarenes gave rise to hydrofluoroarylation of the alkyne as expected. However, it was not possible to use the system as a model for the wider study of the mechanism of hydrofluoroarylation due to interference from side reactions. When $\text{C}_6\text{F}_5\text{H}$ was used as the fluoroarene, there were two major side reactions: C-H bond and C-F bond activation of fluoroarenes by $\text{Ni}(\text{PR}_3)_2$ motifs. These could not be ignored and made it difficult to distinguish the hydrofluoroarylation

Hydrofluorarylation of alkynes reaction for further studies. The widely known complex, *trans*-Ni(H)(PR₃)₂(C₆F₅) was the result of the C-H bond activation. The outcome of the C-F activation were two different products, where one of them was the well-known complex, *trans*-Ni(F)(PR₃)₂(C₆F₄H). Several possibilities were hypothesized and were pursued for the second unknown nickel fluoride observed to arise from the reaction. The possibility of this product being an isomer of the complex, *trans*-Ni(F)(PR₃)₂(C₆F₄H) was eliminated by the absence of similar resonances in the multinuclear NMR spectra to those found, in the reaction mixture of Ni(COD)₂ with C₆F₅H in the presence of two equivalents of PR₃, which gave rise to C-F activation ortho, meta and para to the hydrogen.

There is also a possibility that the unknown C-F activated product arising from the reaction between **1-P** and C₆F₅H is the result of double C-F activation. Double C-F activated products have been reported by Johnson et. al. in a reaction between Ni(PEt₃)₂(η²-C₁₄H₁₀) with pentafluoropyridine (Scheme 2-12).²⁰ The product of double C-F activation observed by Johnson, exhibited a doublet for the phosphorus resonance, which had a very close chemical shift to the phosphorus resonance of the mono C-F activated product in the ³¹P-NMR spectrum, which is observed to overlap in low resolution spectra. Attempts made to synthesize the double C-F activated product by reacting the mono C-F activated product, Ni(F)(PEt₃)₂(C₅F₄N) with excess Ni(PEt₃)₂(η²-C₁₄H₁₀) or Ni(PEt₃)₄ by Johnson was fruitless.

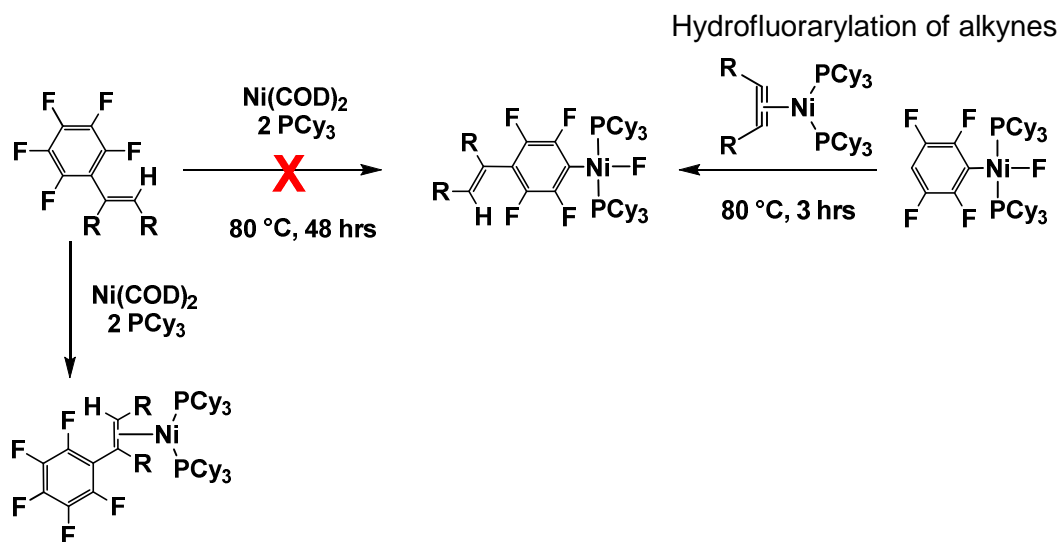


Scheme 2-12 Double C-F activation of pentafluoropyridine.²⁰

Since two doublets of phosphorus resonance was observed to overlap in the ^{31}P -NMR spectrum of the reaction of **1-P** with $\text{C}_6\text{F}_5\text{H}$, the possibility of this being the unknown fluoride arose. As an attempt to observe a double C-F activated product, one equivalent of $\text{C}_6\text{F}_5\text{H}$ was reacted with 2 equivalents of $\text{Ni}(\text{COD})_2$ in the presence of 4 equivalents of PCy_3 . The same reaction was done in two steps where the *trans*- $\text{Ni}(\text{F})(\text{PCy}_3)_2(\text{C}_6\text{F}_4\text{H})$ was then reacted with excess amounts of $\text{Ni}(\text{COD})_2$ and PCy_3 . However, all the attempts were fruitless and no such product was observed in either case.

Another possibility for the unknown nickel fluoride species observed in the reaction of **1-P** with $\text{C}_6\text{F}_5\text{H}$ could be the C-F activated arylalkene product, $\text{Ni}(\text{F})(\text{PR}_3)_2[(\text{C}_6\text{F}_4)\text{RC}=\text{CR}(\text{H})]$ (where $\text{R} = \text{C}_6\text{H}_5$ or $\text{CH}_3(\text{CH}_2)_2$). The LIFDI mass spectrum of the reaction mixture showed a molecular ion peak corresponding to the molecular mass of this species and the isotopic pattern matched the calculated isotopic pattern of this molecular mass and hence this possibility was investigated more to confirm its identity. The LIFDI mass spectrum of the reaction mixture replacing $\text{PhC}\equiv\text{CPh}$ with 4-octyne exhibited the molecular ion peak expected, which was the initial evidence to our hypothesis.

In an attempt to prove the identity of this hypothesised product, C-F bond activation of the reductively eliminated arylalkene product was attempted. The purified product from the hydrofluoroarylation reaction, pentafluoro(4-octenyl)benzene was reacted with $\text{Ni}(\text{COD})_2$ and PCy_3 in toluene and heated first at $50\text{ }^\circ\text{C}$ and then at $80\text{ }^\circ\text{C}$ for several days (Scheme **2-13**). However, no formation of the unknown nickel fluoride was observed in the fluoride region of the ^{19}F -NMR spectrum. The ^{31}P -NMR spectrum exhibited broad peaks impossible to analyse, attempts made to purify this mixture from para-magnetic species were fruitless. However, this absence of fluoride formation could be attributed to a similar observation made in literature, where pentafluorostyrene when reacted with $\text{Ni}(\text{COD})_2$ and PEt_3 , the observed product was $\text{Ni}(\text{PEt}_3)_2(\eta^2\text{-CH}_2\text{CH}(\text{C}_6\text{F}_5))$ and no C-F bond activation was observed.¹⁷



Scheme 2-13 The resultant products from two separate reactions aiming for the formation of $\text{Ni(F)(PCy}_3)_2[(\text{C}_6\text{F}_4)\text{PhC=CPh(H)}]$.¹⁷

The second possibility was to try the reverse of the reaction, where the alkyne insertion occurs into the C-F activated nickel fluoride, $\text{trans-Ni(F)(PCy}_3)_2(\text{C}_6\text{F}_4\text{H})$ (Scheme 2-13). The nickel fluoride, $\text{trans-Ni(F)(PCy}_3)_2(\text{C}_6\text{F}_4\text{H})$, when treated with $\text{Ni(PCy}_3)_2(\eta^2\text{-alkyne)}$ gave rise to the unknown fluoride, $\text{Ni(F)(PCy}_3)_2[(\text{C}_6\text{F}_4)\text{PhC=CPh(H)}]$, whose identity was confirmed by NMR spectroscopy and LIFDI mass spectrum. These results suggest that there is a high possibility that the alkyne is inserted via hydrofluoroarylation into the C-H bond in the nickel fluoride, $\text{trans-Ni(F)(PCy}_3)_2(\text{C}_6\text{F}_4\text{H})$ rather than that hydrofluoroarylation product undergoes a C-F bond activation.

2.3.3. Ni-NHC as an alternative to Ni-PR₃ to study the mechanism of hydrofluoroarylation

The (1,5-hexadiene)Ni(IPr) was synthesised as the carbenes would be less labile than the phosphines when bound to nickel and hence makes the complex more stable. This complex was synthesised as an alternative to (1,5-hexadiene)Ni(PR₃), where the phosphine ligands proved to be too labile to study the hydrofluoroarylation reaction with one ligand on the nickel centre. The results obtained from the reaction of these mono-phosphine complexes were similar to the results obtained through the bis-phosphine complexes mentioned before and hence were less promising.

The N-heterocyclic carbene Ni(0) alternative, **5-C** on the other hand exhibited surprisingly promising results to gain more insight into the hydrofluoroarylation mechanism. Results showed that the **5-C** acts as a catalyst in the hydrofluoroarylation reaction coupling the alkyne to the fluoroarene. The reaction catalysed by **5-C** was free of paramagnetic species unlike the original reaction published by Nakao et al., which was catalysed by Ni(0)-PR₃, and therefore this opened the opportunity to follow the reaction in-situ by NMR spectroscopy. The catalytic reaction reported by Nakao et al. catalysed by Ni-PR₃, contained paramagnetic species and hence had to be purified in order to observe the products by NMR spectroscopy.

Ni(0) catalysts are widely known for their ability to catalyse alkyne polymerizations. The **5-C** complex used as the catalyst in hydrofluoroarylation in this work has been reported to catalyse terminal alkyne polymerization of 1-propyne to give 1,2,4-trimethylbenzene.¹⁸ Nakao used 4-octyne as the alkyne molecule for his mechanistic studies and the highest yield of 99% was obtained.¹ In the hydrofluoroarylation reaction catalysed by **5-C**, a 100% conversion of 4-octyne was observed within 7 hours at 55 °C. However, the ¹H-NMR spectrum showed that trimerization of 4-octyne was competitive with hydrofluoroarylation (also observed at ambient

Hydrofluorarylation of alkynes (temperature). The same was observed when 3-hexyne and diphenylacetylene were used as substrates for hydrofluoroarylation.

Although alkyne coupling reactions are catalyzed by nickel, it is suggested that mere coordination of two alkynes at a Ni(0) center is not sufficient to induce a coupling reaction between the two alkynes.¹⁰ It is also suggested that the naked nickel atom bears the highest coupling activity and that this activity is reduced by any N or P donor ligands. The coupling reaction between the alkynes is very unlikely to occur when the alkynes concerned are di-substituted alkynes.¹⁰ The problem of trimerization of alkynes in the presence of Ni(0) was addressed by Rosenthal et al., in 1998.¹⁰ He suggests that this could be overcome by using unsymmetrical alkynes, and demonstrated by reaction of $\text{PhC}\equiv\text{CSiMe}_3$ to report a stable complex $(2,6\text{-Me}_2\text{C}_5\text{H}_3\text{N})\text{Ni}(\eta^2\text{-PhC}\equiv\text{CSiMe}_3)_2$. The X-ray crystal structure of the complex revealed that the carbon atoms of the $\text{C}\equiv\text{C}$ bonds were twisted out of the trigonal plane of the metal centre with a torsion angle N-Ni-D1-C1 of 23° due to the steric repulsions (where D1 is the mid-point between the two triple bond carbon atoms attached to the trimethylsilyl groups).¹⁰

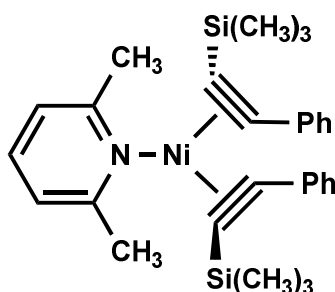


Figure 2-12 Complex $(2,6\text{-Me}_2\text{C}_5\text{H}_3\text{N})\text{Ni}(\eta^2\text{-PhC}\equiv\text{CSiMe}_3)_2$.¹⁰

Taking this suggestion by Rosenthal et al. into account, $\text{PhC}\equiv\text{CSiMe}_3$ was used as the substrate for hydrofluoroarylation catalysed by **5-C**. The reaction mixture gave rise to hydrofluoroarylation and no sign of trimerization of the alkyne was observed. However, the product of the hydrofluoroarylation was observed to decay as the reaction proceeded. This may be an outcome of the trimethylsilyl groups not being able to withstand pro-longed heating.

When PhCCSiMe_3 was replaced with another unsymmetrical alkyne, 4,4-dimethylpentyne the $^1\text{H-NMR}$ spectrum showed no signs of alkyne polymerization during the reaction time of interest. This was confirmed by starting the coupling reaction with excess of the alkyne and heating the reaction at $55\text{ }^\circ\text{C}$ for 10 hours. Then more $\text{C}_6\text{F}_5\text{H}$ was added into the reaction until all the remaining alkyne was consumed, suggesting that there was no other processes such as polymerization competing with the hydrofluoroarylation reaction that consumes the alkyne. The $^1\text{H-NMR}$ and the $^{19}\text{F-NMR}$ spectra both showed evidence of the formation of only one isomer after heating the reaction mixture at $55\text{ }^\circ\text{C}$ for 24 hours. Furthermore there is no evidence of any C-H bond or C-F bond activation of the fluoroarene during the reaction time of interest. This reaction will be discussed in more detail in the next chapter.

2.4. Summary

The mechanism of the hydrofluoroarylation of alkynes was of interest to study in more detail. The results of the DFT calculations performed for the hydrofluoroarylation of alkynes differ from the mechanism postulated based on experimental results, leaving several issues in the mechanism unclear. Mainly three different species were studied in order to obtain a system that would enable to gain more insight into the mechanism.

The bis-phosphine nickel(0) complex gave rise to C-H activation and C-F activation to give rise to *trans*- $\text{Ni(H)(PCy)}_3(\text{C}_6\text{F}_5)$ and *trans*- $\text{Ni(F)(PCy)}_3(\text{C}_6\text{F}_4\text{H})$ respectively, in addition to the hydrofluoroarylation reaction. The experimental evidence shows the formation of a new fluoride species, $\text{Ni(F)(PCy)}_3(\text{C}_6\text{F}_4\text{PhC=CPhH})$. The experiments suggest that this species is formed by the alkyne insertion into the C-H bond of the nickel fluoride and not vice versa.

Unfortunately the mono-phosphine nickel complexes, $(1,5\text{-hexadiene})\text{Ni(PR}_3)$ (where $\text{R} = \text{Cy}$ and $i\text{-Pr}$) used behaved as bis-phosphine nickel sources and therefore gave no further information about the reactivity. This was attributed

Hydrofluoroarylation of alkynes to the labile nature of the phosphine groups attached to nickel and hence the phosphine complex was substituted by the N-heterocyclic carbene complex, (1,5-hexadiene)Ni(IPr) (**5-C**, also reported in literature¹⁸). It has also been demonstrated that complex **5-C** acts as a catalyst for the hydrofluoroarylation reaction. It was also observed that the symmetrical and unsymmetrical alkynes behaved differently when used in the hydrofluoroarylation reaction. The hydrofluoroarylation reaction catalysed by **5-C** was free of paramagnetic substances and hence the possibility of following the reaction in-situ by NMR spectroscopy arose, making it a suitable model to study the reaction in detail. Further studies undertaken to understand the mechanism of hydrofluoroarylation using the system obtained in this chapter are reported in the chapter to follow.

2.5. References

- (1) Nakao, Y.; Kashiwara, N.; Kanyiva, K. S.; Hiyama, T. *J. Am. Chem. Soc.* **2008**, *130*, 16170.
- (2) Kanyiva, K. S.; Kashiwara, N.; Nakao, Y.; Hiyama, T.; Ohashi, M.; Ogoshi, S. *Dalton Trans.* **2010**, *39*, 10483.
- (3) Hatnean, J. A.; Beck, R.; Borrelli, J. D.; Johnson, S. A. *Organometallics* **2010**, *29*, 6077.
- (4) Lafrance, M.; Rowley, C. N.; Woo, T. K.; Fagnou, K. *J. Am. Chem. Soc.* **2006**, *128*, 8754.
- (5) Do, H.-Q.; Daugulis, O. *J. Am. Chem. Soc.* **2008**, *130*, 1128.
- (6) Nova, A.; Reinhold, M.; Perutz, R. N.; Macgregor, S. A.; McGrady, J. E. *Organometallics* **2010**, *29*, 1824.
- (7) Braun, T.; Perutz, R. N. In *Perspectives in Organometallic Chemistry*; Screttas, C. G., Steele, B. R., Eds.; The Royal Society of Chemistry: 2003, p 136.
- (8) Jolly, P. W.; Jonas, K.; Krüger, C.; Tsay, Y. H. *J. Organomet. Chem.* **1971**, *33*, 109.
- (9) Guihaumé, J.; Halbert, S.; Eisenstein, O.; Perutz, R. N. *Organometallics* **2012**, *31*, 1300.

- (10) Rosenthal, U.; Pulst, S.; Kempe, R.; Pörschke, K.-R.; Goddard, R.; Proft, B. *Tetrahedron* **1998**, *54*, 1277.
- (11) Poerschke, K. R. *J. Am. Chem. Soc.* **1989**, *111*, 5691.
- (12) Green, M.; Grove, D. M.; Howrd, J. A.; Spencer, J. L.; Stone, F. G. A. *J. Chem. Soc., Chem. Commun.* **1976**, 759.
- (13) Upton, T. H.; Goddard, W. A. *J. Am. Chem. Soc.* **1978**, *100*, 321.
- (14) Ozin, G. A.; McIntosh, D. F.; Power, W. J.; Messmer, R. P. *Inorg. Chem.* **1981**, *20*, 1782.
- (15) Guo, L.; Bradshaw, J. D.; Tessier, C. A.; Youngs, W. J. *Organometallics* **1995**, *14*, 586.
- (16) Johnson, S. A.; Taylor, E. T.; Cruise, S. J. *Organometallics* **2009**, *28*, 3842.
- (17) Cronin, L.; Higgitt, C. L.; Karch, R.; Perutz, R. N. *Organometallics* **1997**, *16*, 4920.
- (18) Wu, J.; Faller, J. W.; Hazari, N.; Schmeier, T. J. *Organometallics* **2012**, *31*, 806.
- (19) Wu, J.; Faller, J.; Hazari, N.; Schmeier, T. *Organometallics* **2012**, *31*, 806.
- (20) Hatnean, J. A.; Johnson, S. A. *Organometallics* **2012**, *31*, 1361.
- (21) Ateşin, T. A.; Li, T.; Lachaize, S.; García, J. J.; Jones, W. D. *Organometallics* **2008**, *27*, 3811.
- (22) Darensbourg, M. Y.; Ludwig, M.; Riordan, C. G. *Inorg. Chem.* **1989**, *28*, 1630.

CHAPTER THREE

KINETIC ANALYSIS OF THE HYDROFLUOROARYLATION OF ALKYNES CATALYSED BY NI(0) LIGATED TO N-HETEROCYCLIC CARBENES

Kinetic analysis of the hydrofluoroarylation of alkynes catalysed by Ni(0) ligated to N-heterocyclic carbenes

3.1 Introduction

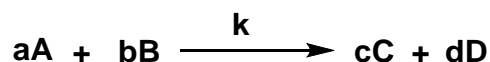
Multi-step catalytic cycles are comprised of a sequence of simple elementary steps.¹ In a reaction mechanism that involves more than one step the rate of the reaction is often determined by the step with the highest energy barrier.² However, mechanisms often consist of more than one step that contributes to the rate of the reaction, this arises when another step in the cycle has an energy barrier that is still significant.³ The rate of the reaction is also controlled by other physical factors such as temperature and pressure in gaseous reactions.^{2,3}

Kinetic analysis has proven to be a powerful tool in understanding catalytic mechanisms.^{4,5} In-situ data collection for kinetic analysis is done by several direct and indirect methods; indirect methods such as IR spectroscopy, NMR spectroscopy and direct methods such as calorimetry are some of the techniques used in the past for this purpose.^{3,6,7}

3.1.1 Rate law of a reaction

The progress of the reaction experimentally obtained by the consumption of the reactants or the formation of the products, with time allows the determination of the rate of the reaction.² For reactions that are dependent on the reactants, the rate of the reaction is proportional to the concentration of the reactants raised to a certain power. The power to which the concentration of the reactants are raised is termed the order of the reaction with respect to that reactant.² Excluding concerted one-step reactions, the order of the reactants is often different from the stoichiometry of the reactants involved in the chemical equation of the reaction. The order of the reaction with respect to individual reactants suggests the reactants and the number of molecules involved in the step that has the highest energy barrier. The rate law of the reaction expresses the relationship between the individual species

involved in the reaction and the rate of the reaction. This can be expressed for a general reaction as shown below. The powers m and n in the rate equation (equation 3-1) are the order of the reactants A and B respectively.



$$\text{rate} = k[A]^m[B]^n \text{ where } k = \text{rate constant}$$

equation 3-1²

The overall order of the reaction is generally the total number of reactants involved in the step with the highest energy barrier, which could be expressed as $(m+n)$ in equation 3-1. This overall order is generally derived from the integrated rate equations. The rate constant k is independent from the reactants concentrations. The integrated rate equations, which are obtained by integrating the rate law of a reaction, enables one to fit the kinetic data obtained experimentally. The best fit obtained for the kinetic data will provide the overall order and rate constant of the reaction (Table 3-1).

Table 3-1 The rate laws and the integrated rate equations

Order	Rate law	Integrated rate equation
Zero-order	Rate = k	
First-order	Rate = $k[A]$ Or Rate = $k[B]$	$\ln[A]_t = -kt + \ln[A]_0$
Second order	Rate = $k[A]^2$ Or Rate = $k[B]^2$ Or Rate = $k[A][B]$	$\frac{1}{[A]} = \frac{1}{[A]_0} + kt$
n^{th} order	Rate = $k[A]^n$	$\frac{1}{[A]^{n-1}} = \frac{1}{[A]_0^{n-1}} + (n-1)kt$

3.1.2 Construction of the rate law for a reaction

The rate law for a reaction is constructed from the dependence of the rate of the reaction on individual species present in the medium. The quantitative measure of this dependence is often given by the order with respect to each species. The individual orders with respect to the reactants are experimentally determined in different ways. Isolation method and Initial rate method are methods that are used frequently to determine the order of the reactants and hence the rate law of the reaction.²

The isolation method as the term implies, is carried out by isolating the concentration change in one species at a time to study the dependence of the rate of the reaction on that particular species. Experimentally, this is achieved by using large excess of reactants compared to the species of interest, which would make the change in the concentration of all other reactants negligible and hence the concentration is fixed as a constant.²

For the following reaction, [B] is added in large excess to [A]



This would modify the rate law of the reaction as follows,

$$rate = k_{obs}[A]^m \text{ where } k_{obs} = k[B]^n$$

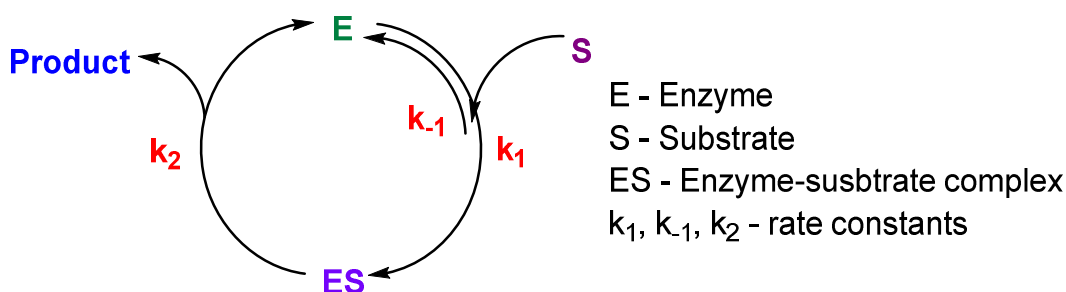
The resulting rate law is termed the pseudo rate law and the resulting rate is dependent only on the concentration of reactant **A**, hence the order of the reaction with respect to **A** is obtained. The same method is followed for other reactants in order to construct the overall rate law.²

The second method to obtain the order of the reactants, which is often used to study the kinetics of a catalytic system is the initial rate method. The initial rate methodology is often used along with the isolation method.² This methodology deals with the initial rate of the reactions at different concentration of the reactants. Experimentally this is performed by collecting a series of kinetic data where the initial concentration of the species of interest (e.g. **A**) is different. The data thus obtained is used to construct a plot

of the log of the initial rate as a function of log [A]. The graph thus obtained would exhibit a linear relationship with the slope as the order with respect to the species A.

3.1.3 Catalytic reactions

Unlike simple elementary reactions, analysis of kinetic data obtained for a catalytic reaction involving a multistep mechanism can be far more complex. Therefore, several approaches have been undertaken in the past to obtain simplified methods of interpretation of the catalyst kinetics.³ One such simplified method followed for enzyme kinetics, is the double reciprocal of the Michaelis-Menten equation (equation 3-2) giving rise to linear relationship plots for enzymatic systems obtained by Lineweaver and Burk (equation 3-3). This reciprocal method has enabled one to obtain linear relationships for both enzymatic and non-enzymatic catalytic systems.^{3,8} Enzymes are often looked upon as biological catalysts and hence treating a non-biological catalytic system as an enzymatic system with caution is widely acceptable.³



Scheme 3-1 Schematic diagram of a one substrate enzyme catalytic system.³

$$v = \frac{v_{max}[S]}{K_{MM} + [S]}, \quad \text{where, } v = \text{rate of reaction,}$$

v_{max} = maximum rate,
 K_{MM} = Michaelis Constant,
[S] = substrate concentration

equation 3-2

$$\frac{1}{v} = \frac{1}{v_{max}} + \frac{K_{MM}}{v_{max}} \frac{1}{[S]}$$

equation 3-3

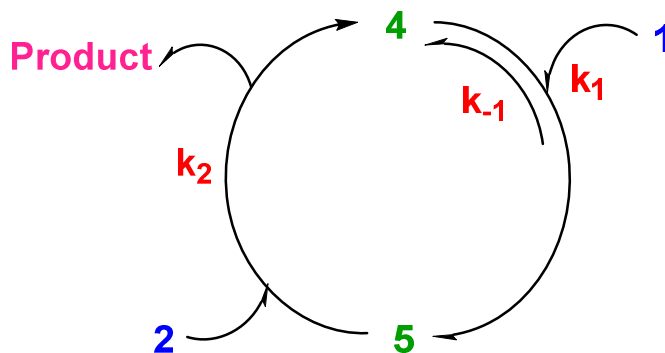
3.1.3.1 Reaction progress kinetic analysis

Reaction progress kinetic analysis (RPKA) demonstrated by Blackmond in 2005, is one such technique of simplifying the interpretation of the kinetic analysis of catalytic systems.³ This methodology is comparable to the enzymatic catalytic approaches and provides more kinetic detail using only a few experiments compared to classical kinetic approaches. RPKA in contrast to initial rate kinetic analysis, deals with the kinetics involved as the reaction proceeds, which is more practical with respect to the industrial world, where reactions are run to the end. In addition to this, the methodology also addresses time-dependent processes that occur as the reaction proceeds rather than simply ignoring them, which gives a better understanding of the dependence of the rate and yield of the product on such time-dependent processes.³

The RPKA requires an in-situ analysis to derive the rate of the reaction as the reaction proceeds. This could either be a direct measurement of the rate of the reaction, such as the heat flow or an indirect method such as spectroscopy which would enable one to calculate the rate of the reaction from the concentration of the species. The RPKA gives similar results to the Michaelis-Menten approach for a simple one substrate catalytic system. This is further expanded to a catalytic reactions involving two reactants. The kinetic analysis carried out with RPKA with two substrates demonstrated by Blackmond³ is discussed in detail below.

3.1.3.2 Catalytic reaction involving two substrates- Reaction progress kinetic analysis

Polymerization, decomposition and hydrogenation reactions under constant pressure are the most common reactions involving only one substrate. Excluding these, the majority of the catalytic reactions involve bringing two or more different molecules together to form a product. This is shown in Scheme 3-2 where the two substrates are denoted by **1** and **2**.³ The rate of the system described below is given in equation 3-4, where **[1]** and **[2]** are the concentrations of substrates **1** and **2**; **[4_{total}]** is the total concentration of the catalyst in all forms present in the reaction mixture; k_1 and k_{-1} are the rate constants for the binding of substrate **1** to the catalyst and k_2 is the rate constant involved with the second substrate.



Scheme 3-2 Schematic diagram of a two substrate catalytic system.

$$v = \frac{k_1 k_2 [1][2][4_{total}]}{k_{-1} + k_1 [1] + k_2 [2]}$$

equation 3-4³

In a catalytic reaction involving two substrates the concentration of both substrates **1** and **2** change simultaneously during the course of the reaction. This complexity of two species changing at the same time in the rate equation (equation 3-4) is simplified by Blackmond by defining a parameter called the “excess”.³ This term “excess” is the difference in the concentration of the two substrates **1** and **2** at any given time. If experiments are carried out in a manner so that this difference in concentrations, termed “excess” is kept

the same, at any given time the only variable in the rate equation would be [1] (equation 3-5 to equation 3-7). This simplifies the rate equation and gives one the opportunity to analyse the reaction without the added complexity arising from the simultaneous concentration change of two substrates.³

$$[2] - [1] = \textit{“excess”}$$

equation 3-5³

Therefore at any given time, [2] can be given as;

$$[2] = [2_0] - [1_0] + [1] = \textit{excess} + [1]$$

equation 3-6

Hence the rate equation can be modified to;

$$v = a' \frac{[\textit{excess}][1] + [1]^2}{[1] + b'[1]} [4_{total}]$$

equation 3-7³

$$\textit{where } a' = \frac{k_1 k_2}{k_{-1} + k_2 [\textit{excess}]}$$

$$\textit{and } b' = \frac{k_1 + k_2}{k_{-1} + k_2 [\textit{excess}]}$$

equation 3-8³

The term “excess” for a constant volume reaction does not change and can be a positive or negative value or zero.³ The kinetic data for the analysis is obtained either from experiments with same “excess” or different “excess” depending on the requirement of the analysis. The experiments with the same “excess” provides with the information of any time-dependent secondary processes such as catalyst deactivation or product inhibition during the course of the reaction while the experiments with the different

“excess” experiments helps to postulate the order of the reaction and the steps involved in the mechanism.³

3.1.3.3 Saturation Kinetics

In certain mechanisms of a two-substrate catalytic system, the catalyst is predominantly found coordinated to substrate **1**, which makes **5** the catalyst resting state (Scheme 3-2). This situation normally results from a rate constant k_1 being much larger than k_2 , the rate constant of the second step in the catalytic cycle in Scheme 3-2. This makes the term ' $k_1[1]$ ' in the denominator in equation 3-4 the dominating term. This limiting situation is termed 'saturation kinetics in substrate 1' and the rate equation can be modified as follows;

$$v = k_2[2][4_{total}]$$

equation 3-9³

Saturation kinetics in **1**, can be graphically shown by plotting the rate of two reactions (where the “excess” is different) as a function of **[2]** on the same graph. If the graphs result in linear plots where both plots overlay each other, the reaction is believed to follow saturation kinetics with respect to **1** (Table 3-2). This can be further proven by another graph where (rate/**[2]**) is plotted as a function of **[1]**. When the catalyst is predominantly found as the free catalyst **4** (Scheme 3-2), the reaction follows saturation kinetics with respect to substrate **2**. This is a result of the of the step involving substrate **2** being very fast (rate constant k_2 a large value). The resulting rate equation and the graphical rate equation are derived in a similar manner to the saturation kinetics with respect to **1** (Table 3-2). If neither k_1 nor k_2 is not significantly large enough to be the dominating species in the denominator in equation 3-4, then all the terms in the denominator are significant and hence affect the rate of the reaction. In this case, the reaction doesn't have a significant rate determining step and both steps contribute towards the rate of the reaction. The catalyst in this case would be present in almost equal amounts as **4** & **5**

in the catalytic cycle. In such cases it is essential to plot various other forms of the graphical rate equations until a reasonable equation is obtained (Table 3-2). Once this is achieved the mechanism of the reaction can then be postulated based on the rate equation obtained from the graphs.

Table 3-2 The modified rate equation of a two substrate catalytic system under certain limiting cases

Catalyst predominant state	Dominating term in rate equation 3-4	Rate equation	Graphical rate equation	
			x-axis	y-axis
5	k_1	$v = k_2[2][4_{total}]$	[2]	v
			[1]	$\frac{v}{[2]}$
4	k_2	$v = k_1[1][4_{total}]$	[1]	v
			[2]	$\frac{v}{[1]}$
4 & 5	All terms contribute	$v = \frac{k_1 k_2 [1][2][4_{total}]}{k_{-1} + k_1[1] + k_2[2]}$		

3.2 Results

3.2.1 Introduction

The hydrofluoroarylation of alkynes catalysed by Ni(0)-PR₃ has been studied by Nakao, Perutz and Johnson in the past with two mechanisms postulated.⁹⁻

¹¹ The mechanisms proposed, however, differ from each other in the following two steps:

- 1) The initial coordination of substrate – The coordination of alkyne was found to be preferred over the fluoroarene in the results from the DFT calculations performed by Perutz et al, in contrast to the suggested initial fluoroarene coordination by Nakao et al.^{9,10}
- 2) Hydrogen transfer – In the mechanism proposed by Nakao et al. the fluoroarene coordination is followed by the formation of the nickel hydride which then transfers the hydrogen to the alkyne. However, the DFT calculations found that the coordination of alkyne was favoured over the fluoroarene and the concomitant Ni-H formation. Therefore the hydrogen transfer was proposed to occur via a ligand to ligand hydrogen transfer (LLHT).^{9,10}

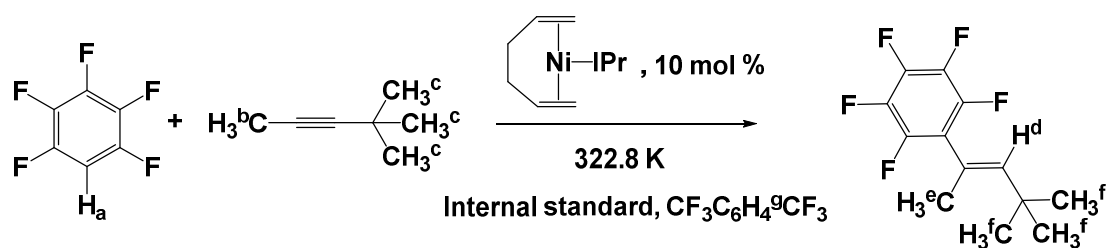
This difference stimulated the investigation of the mechanism in more detail. The hydrofluoroarylation reaction catalysed by Ni-PR₃ could not be followed by NMR spectroscopy as a result of paramagnetic species formed. However when the nickel-heterocyclic carbene complex, (1,5-hexadiene)Ni(IPr)¹² was used as the catalyst for the same reaction, it was observed that the reaction did not give rise to any paramagnetic species, enabling the reaction to be followed clearly by NMR spectroscopy. One explanation for the absence of paramagnetic species is the lower temperatures involved with the Ni-NHC catalysed reaction (55 °C) compared to when Ni-PR₃ was used as the catalyst (80-100 °C).¹³ The opportunity to follow the reaction in-situ by NMR spectroscopy opened the possibility of obtaining data for kinetic analysis of the reaction.

3.2.2 Choice of reactants

3.2.2.1 Choice of fluoroarene

The hydrofluoroarylation of alkynes reported by Nakao in 2008¹³ was found to proceed via a selective oxidative addition of the C-H bonds ortho to C-F bonds in partially fluorinated arenes.⁹ The rate of the reaction and the yield of the hydrofluoroarylated product was found to be dependent on the number of

fluorine atoms on the ring, with the highest yield recorded for C_6F_5H and a poor yield for mono-fluorobenzene.⁹ Given the higher yield observed for C_6F_5H (**2B**), this fluoroarene was chosen for our kinetic studies. Another major advantage of C_6F_5H was the presence of a single C-H bond and therefore only one regio-isomer could be formed in contrast to the less fluorinated arenes, $C_6F_nH_{6-n}$ (where $n = 4,3,2$ and 1) (Scheme 3-3, Figure 3-1 and Figure 3-2).



Scheme 3-3 The substrates and the standard conditions of the hydrofluoroarylation reaction used to collect data for the kinetic analysis.

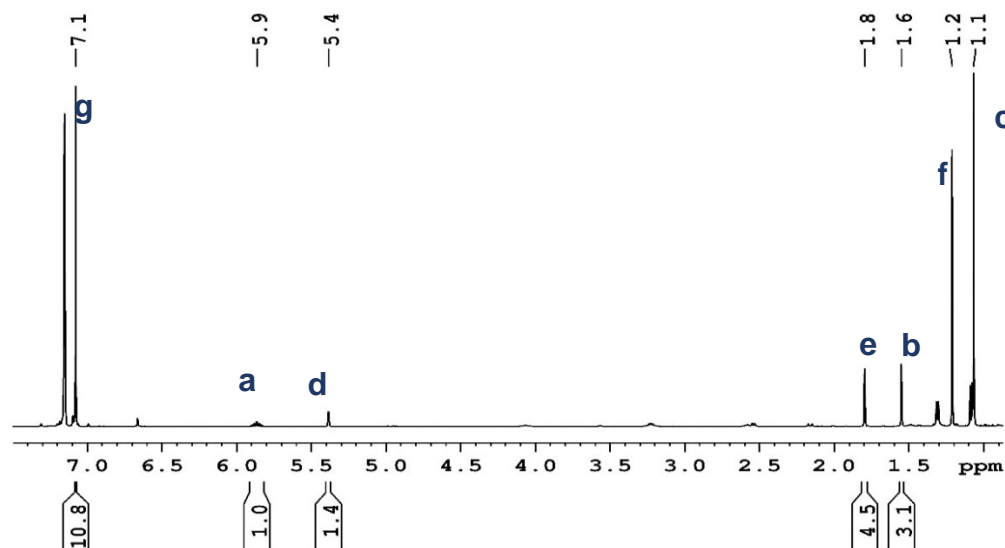
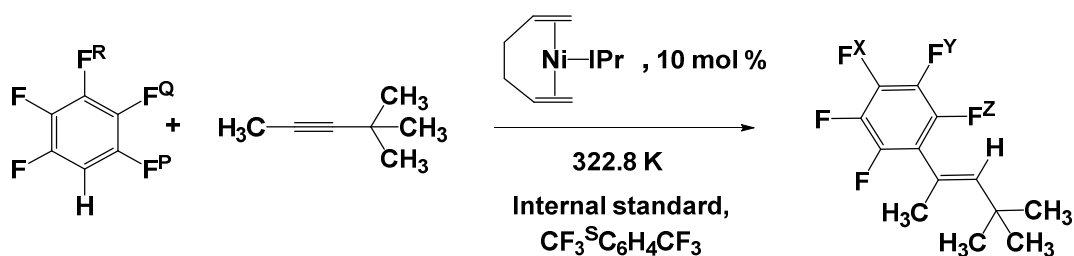


Figure 3-1 1H -NMR (500 MHz, C_6D_6) spectrum of the reaction mixture of $CH_3C\equiv CC(CH_3)_3$ with C_6F_5H catalysed by (1,5-hexadiene)Ni(IPr) after 2 hours at 322.8 K (48% conversion) (labels in above scheme).



Scheme 3-4 The substrates and the standard conditions of the hydrofluoroarylation reaction used to collect data for the kinetic analysis

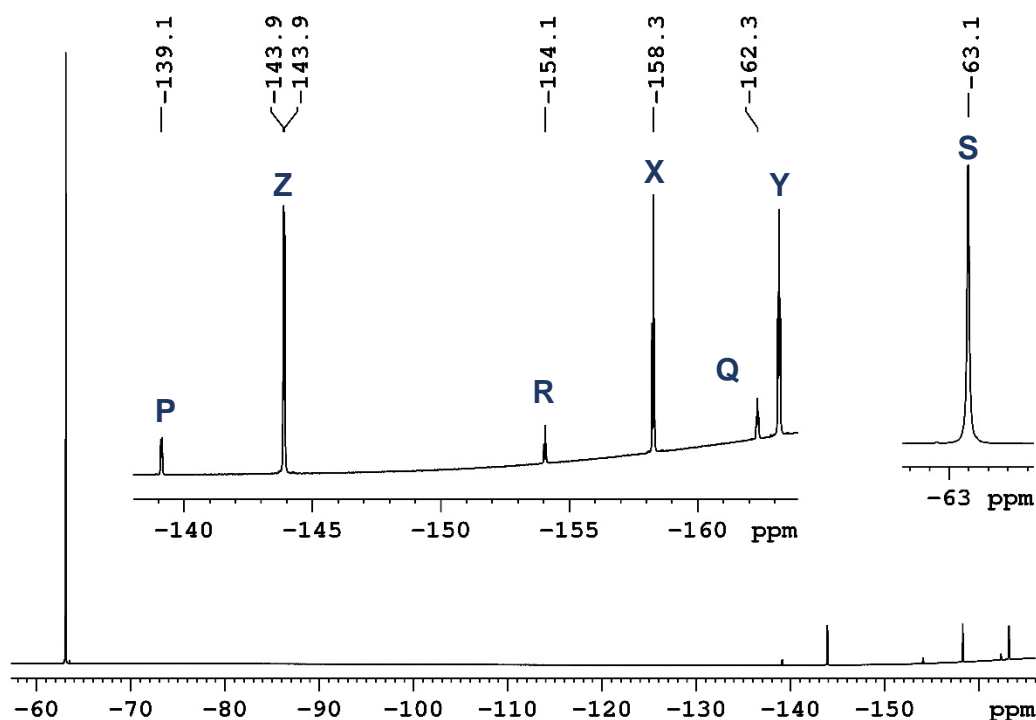


Figure 3-2 ^{19}F -NMR (470 MHz) spectrum of the reaction mixture of $\text{CH}_3\text{C}\equiv\text{CC}(\text{CH}_3)_3$ with $\text{C}_6\text{F}_5\text{H}$ catalysed by $(1,5\text{-hexadiene})\text{Ni}(\text{IPr})$ after 12 hours at 55°C (labels in above scheme).

3.2.2.2 Choice of alkyne

The hydrofluoroarylation of alkynes was carried out successfully with both symmetrical and unsymmetrical alkynes by Nakao et al.^{9,13} An exception to this was found with terminal alkynes that were observed to undergo rapid oligomerization in the presence of the nickel-phosphine catalyst.⁹ This

problem of trimerization was also pronounced in alkynes such as diphenylacetylene and the necessity of slow addition of alkyne or excess alkyne was required to provide good yields.⁹ Nakao et al. used 4-octyne in their mechanistic studies of hydrofluoroarylation. The catalytic reaction conducted with 1.5 equivalent of 4-octyne with one equivalent of C₆F₅H gave the highest yield of ~99%. However, the ¹H-NMR spectrum showed the presence of competing trimerization reactions when 4-octyne was used as the alkyne for the hydrofluoroarylation reaction catalysed by (1,5-hexadiene)Ni(IPr). To avoid hindrance by complications arising in the analysis, an unsymmetrical alkyne was chosen for the kinetic studies. This as discussed in detail in chapter 2, is in agreement to the observation made by Rosenthal that using unsymmetrical alkynes will avoid the trimerization of the alkyne in the presence of nickel.¹⁴ The alkyne 4,4-dimethylpentyne (**1A**) was reported to give a good yield of 89% of the hydrofluoroarylated alkyne within 3 hours at 80 °C.⁹ Hence, 4,4-dimethylpentyne was chosen as the alkyne for the kinetic studies performed.

When the hydrofluoroarylation reaction of **1A** with **2B** was done using (1,5-hexadiene)Ni(IPr) as the catalyst, the reaction showed no evidence of trimerization of **1A** and no observation was made in the ¹H and ¹⁹F-NMR spectra of C-H bond or C-F bond activation of **2B** by the nickel complex (Figure 3-1 and Figure 3-2). Therefore this reaction between **1A** and **2B** was examined in detail by ¹H and ¹⁹F-NMR spectroscopy and found that no side reactions occur for these substrates catalysed by (1,5-hexadiene)Ni(IPr). This is supported further by the graph plotted with the percentage decay of the reactants and the percentage formation of the product (Figure 3-3), which provided the evidence that the reactants were converted only to the desired product and no other process consumed the reactants. Furthermore, the ¹H and ¹⁹F-NMR spectra both showed evidence of only one regioisomer formed in the reaction between **2B** and **1A** heated at 55 °C for 24 hours.

3.2.2.3 Conditions of data collection

The data collection for the kinetic analysis was done by an integral method, where the concentrations of the species were found by NMR spectroscopy and were then converted into the rate of the reaction. The ^1H -NMR spectroscopy was chosen over ^{19}F -NMR spectroscopy mainly due to the ease and accuracy of integration. The peaks in the ^1H -NMR spectrum were well defined and isolated from each other making it possible to integrate them accurately (Figure 3-1). The catalyst, (1,5-hexadiene)Ni(IPr) was reported to have a decomposition temperature of $60\text{ }^\circ\text{C}$ ¹² and hence the data collection for the kinetic studies was done at 322.8 K ($\sim 50\text{ }^\circ\text{C}$). The standard catalyst loading (excluding special cases that required different catalyst loadings) was kept at $10\text{ mol } \%$, which was found to give the most efficient conversion of the reactants to product in the desired time.

The ^1H -NMR spectral data were collected at regular intervals, based on the requirements in individual cases. The delay time between pulses was set to 10 seconds to ensure adequate relaxation for the integrals to be accurate. The internal standard chosen was 1,4-bis(trifluoromethyl)benzene because of its inertness towards the catalyst and its NMR spectroscopic resonances were distinct in chemical shift to that of the reactants and product. The internal standard was found to be inert to the catalyst and to all reactants used in the studies. The integrals were normalized against the internal standard. Deuterated benzene was used as the solvent for data collection as toluene was found to be the best solvent for the hydrofluoroarylation reaction by Nakao et al.⁹

Only the data collected up to 55% conversion was used for the kinetic analysis in order to avoid any secondary processes that may occur at the later stages of the reaction, and may affect the results. However, it was observed that there was no significant change in the final result regardless of whether the cut-off was made at 40% conversion or at 65% conversion. The percentage decay of the reactant, **1A** and the percentage formation of the product when plotted on the same graph (Figure 3-3) as a function of time,

showed no signs of any other side reactions that consumed the reactant nor any loss of the product formed by the hydrofluoroarylation.

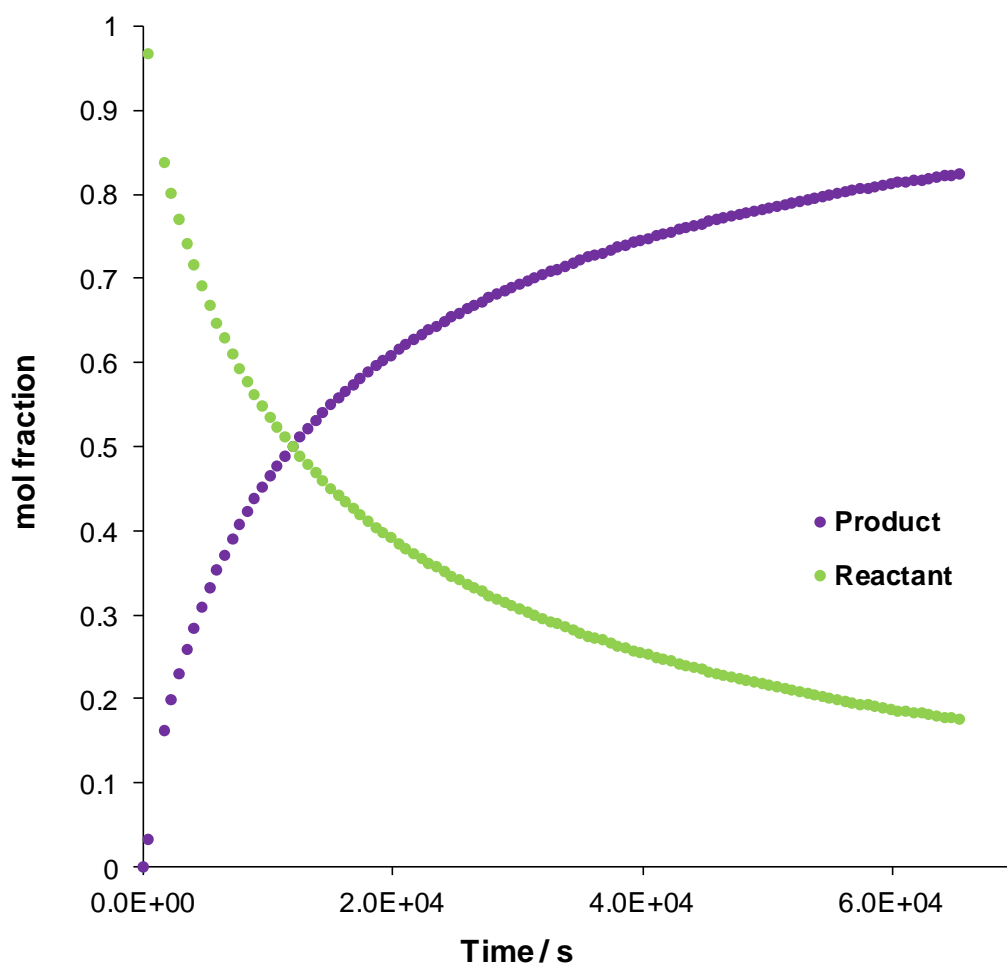


Figure 3-3 Percentage conversion of the reactant **1A** (green) and the formation of the product (purple) monitored by $^1\text{H-NMR}$ spectroscopy for the reaction of **2B** with **1A** catalysed by (1,5-hexadiene)Ni(IPr) in C_6D_6 at 322.8 K

3.2.3 Reaction progress kinetic analysis

3.2.3.1 Integral Method

Analysis methods that involve measuring the concentration of the species in the reaction indirectly by a measurable parameter are generally termed as the integral method.³ The rate of the reaction in such methods is obtained by

differentiating the concentration versus time data obtained from the measurable parameter. The concentration of the substrate can be calculated as follows:

$$[S] = [S_0](1 - x)$$

equation 3-10³

Where, **[S]** = concentration of substrate at time t

[S₀] = initial concentration of substrate

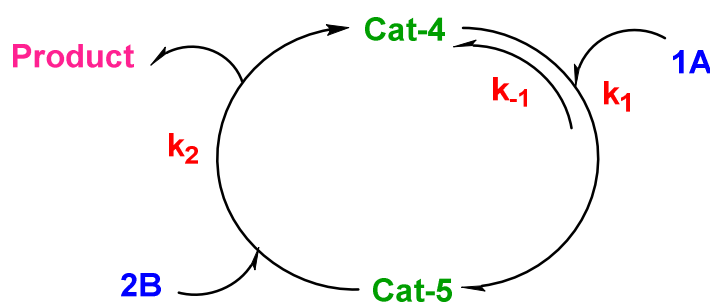
x = fraction conversion

And hence the rate of the reaction (*v*) can be given as:

$$v = \frac{d[S]}{dt} = -[S_0] \frac{dx}{dt}$$

equation 3-11³

The hydrofluoroarylation of **1A** with **2B** can be schematically shown as follows, where Cat-4 is the free catalyst in its active form that initiates the reaction. Cat-5 is the catalyst bound to **1A** in an equilibrium step with the rate constants, *k*₁ and *k*₋₁. This further reacts with the second substrate present in the medium, **2B** to give the final product in the step with a rate constant of *k*₂.



Scheme 3-5 A schematic diagram of the hydrofluoroarylation catalytic cycle for **1A** and **2B** catalysed by (1,5-hexadiene)Ni(IPr) in C₆D₆.

The rate of the reaction can be given as;

$$v = \frac{k_1 k_2 [1A][2B][4_{total}]}{k_{-1} + k_1 [1A] + k_2 [2B]}$$

equation 3-12

A plot can be generated from the rate of the reaction derived from the experiment as a function of the substrate concentration. This is termed as a “*graphical rate equation*”.³ The graphical rate equation is constructed by plotting the rate of the reaction as a function of the concentration of the substrate, the reaction proceeds from right to left (Figure 3-4).

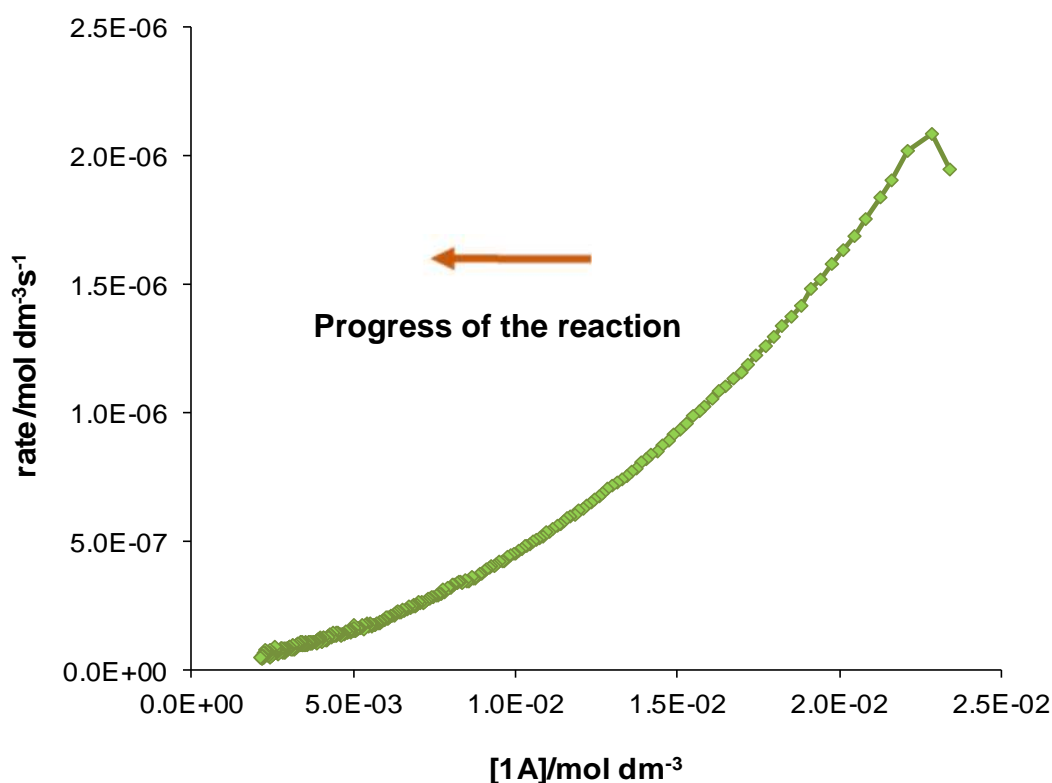


Figure 3-4 ‘*Graphical rate equation*’ - A plot of the rate of the reaction against [1A] constructed from the data collected by monitoring ¹H-NMR spectroscopy for the reaction of 2B with 1A catalysed by (1,5-hexadiene)Ni(IPr) in C₆D₆ at 322.8 K.

3.2.4 Induction period

A reaction with positive order kinetics with respect to the substrates will exhibit a trend of decreasing rate with time. However, this may not hold true at the initial stage of the reaction and this can be the result of various factors including the catalyst being added as a pre-catalyst rather than in its active form and the time taken for the catalytic system to attain steady state.³ This time taken for the reaction to achieve its steady state is known as the induction time. The RPKA deals with the data of the reaction obtained in its steady state as the reaction rate and concentration are accurately known in this period and the data involved in the induction period is generally ignored throughout the rest of the kinetic analysis.³

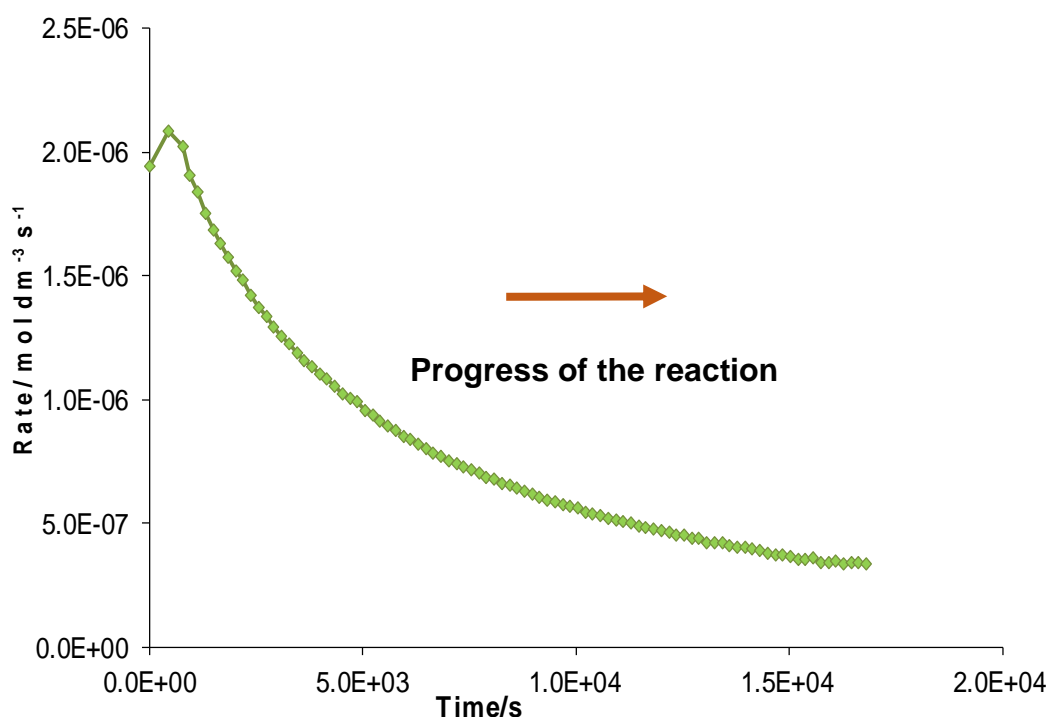


Figure 3-5 A plot of the rate of the reaction against time constructed from the data collected by monitoring ¹H-NMR spectroscopy for the reaction of **1A** with **2B** catalysed by (1,5-hexadiene)Ni(IPr) in C₆D₆ at 322.8 K.

The rate of the reaction between **1A** and **2B** catalysed by (1,5-hexadiene)Ni(IPr) at 322.8 K was plotted as function of time (Figure 3-5).

The graph shows that the rate at the beginning of the reaction does not show a direct proportional relationship with the concentration of the substrates (as the [substrate] decreases with time, the rate decreases with time). This induction period lasts for ~ 10-12% conversion. This time taken for the reaction to attain steady state can be due to the fact that the catalyst, (1,5-hexadiene)Ni(IPr) is not in its active form or this might be due to other factors such as time taken for mixing or other physical factors. The data collected in this region is avoided in the kinetic analysis performed.

3.2.5 Catalyst deactivation or product inhibition

There are also processes that are commonly associated with the latter stages of a reaction such as catalyst deactivation or product inhibition of the catalyst. These time-dependent secondary processes have the tendency to complicate the analysis.

One common method used to avoid this problem is to discard the data after 40-50% conversion which has proven to be successful in many cases, However, discarding the latter part of the data may be misleading in some cases.³ With RPKA, rather than ignoring such secondary processes one is able to account for them.³ Analysing the data obtained from two different experiments by RPKA enables one to identify the presence of any time-dependent secondary processes and also helps to identify whether it is caused by product inhibition or catalyst deactivation that is accountable for the observation made. The two different experiments are carried out under the following conditions. The concentrations of the individual reactants are different in each experiment but the difference in concentration of the individual reactants are essentially the same in the two different experiments.³ In our particular case, this could be stated as follows:

In experiment **1**- $[C_6F_5H] = [2B_1]$ and $[CH_3C\equiv C(CH_3)_3] = [1A_1]$:

In experiment **2**- $[C_6F_5H] = [2B_2]$ and $[CH_3C\equiv C(CH_3)_3] = [1A_2]$:

- i. $[2B_1] \neq [2B_2]; [1A_1] \neq [1A_2]$
- ii. But, $[2B_1]-[1A_1] = [2B_2]-[1A_2]$

The rates calculated for the two different experiments are then plotted as a function of the substrate concentration. If the resulting curves overlay each other, time-dependent secondary processes are absent. However if the two curves deviate from each other, a follow up experiment where the final product is already added to the initial reaction mixture is done. The rate of this reaction plotted on the same graph will indicate whether this secondary process is a product inhibition or a catalyst deactivation.³

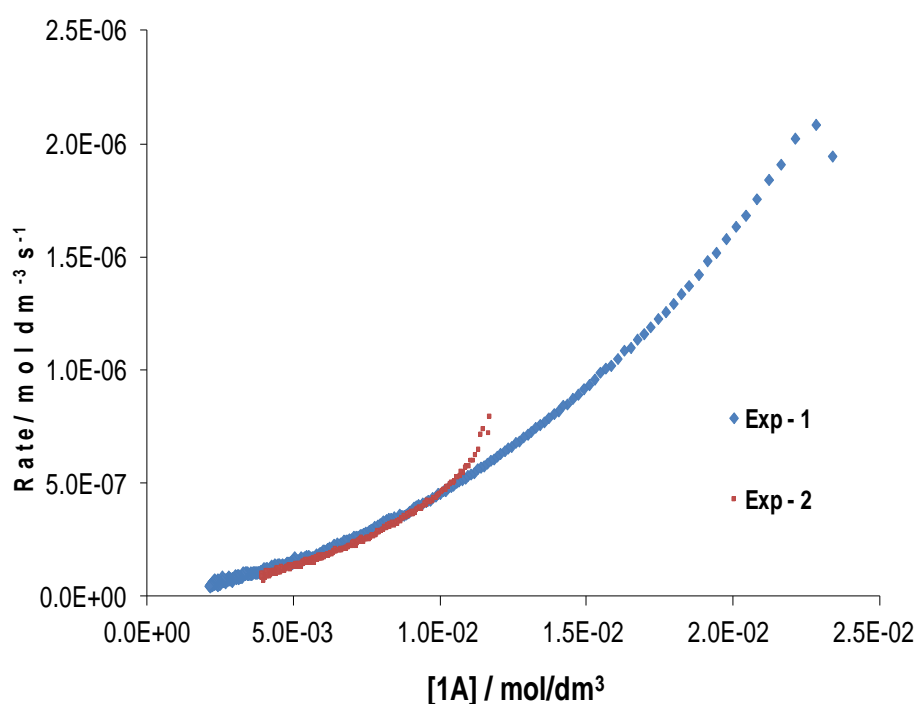


Figure 3-6 A plot of the rate of the reaction against $[1A]$ constructed from the data collected for the reactions of $1A$ with $2B$ catalysed by (1,5-hexadiene)Ni(IPr) in C_6D_6 at 322.8 K, where the “excess” is kept the same.³ (The conditions of Exp-1 and Exp-2 are stated in the text above)

When the rates of the reaction of experiments **1** and **2** are plotted against the substrate concentration ($2B$), the two curves are observed to overlay each other. This overlay suggests the presence of no such time-dependent secondary processes. The initial rates of the two reactions exhibit a slight

deviation from one another in the above graph. However, this is most likely due to the time taken for the system to attain steady state and can be ignored.

3.2.6 Stoichiometric reaction between 1A and 2B

The data obtained for a stoichiometric reaction between **2B** and **1A** catalysed by (1,5-hexadiene)Ni(IPr) at 322.8 K was analysed by classical kinetic methods, by fitting to the 1st order 2nd order (Figure 3-8) and 3rd order integrated rate equations. A linear relationship for the stoichiometric reaction at 322.8 K was observed when the data was treated as a 3rd order system (Figure 3-7).

A graph plotted treating the data to follow the third order integrated rate law equation

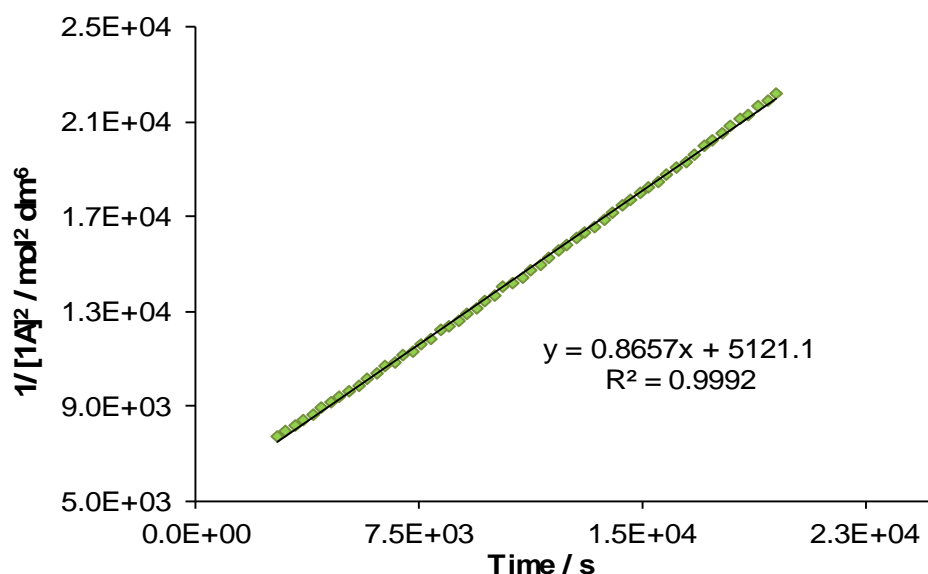


Figure 3-7 A plot of $1/[1A]^2$ against time constructed from the data collected by $^1\text{H-NMR}$ spectroscopy for the reaction of **1A** with **2B** catalysed by (1,5-hexadiene)Ni(IPr) in C_6D_6 at 322.8 K.

A graph plotted treating data as second order using second order integrated rate equation

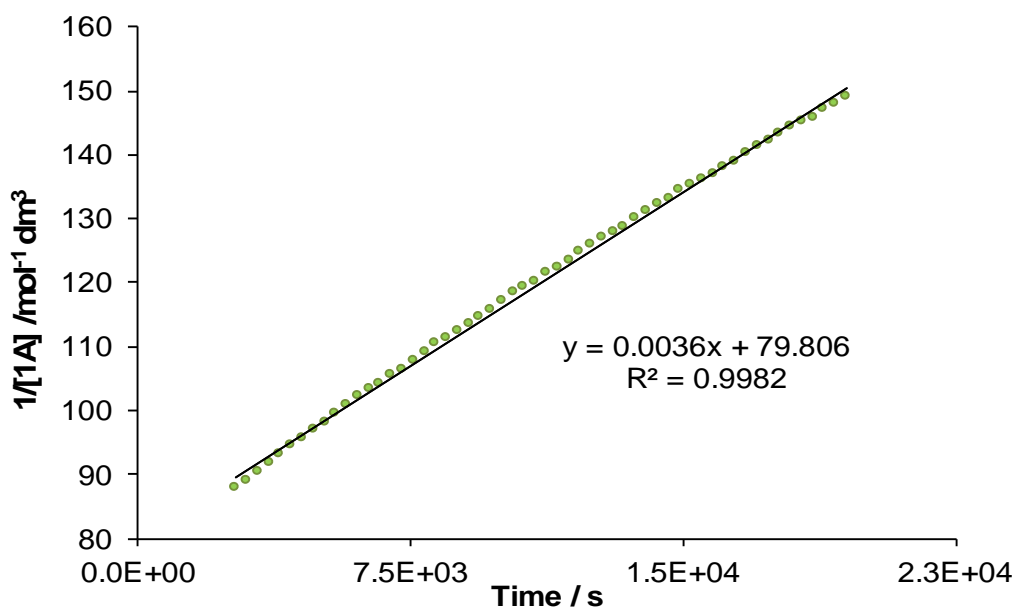


Figure 3-8 A plot of $1/[1A]$ against time constructed from the data collected by $^1\text{H-NMR}$ spectroscopy for the reaction of **1A** with **2B** catalysed by (1,5-hexadiene)Ni(IPr) in C_6D_6 at 322.8 K.

This preliminary observation suggested an overall third order dependence of the rate of the reaction on the substrates **2B** and **1A**. However, in order to express the rate law of the reaction with respect to individual substrates with some degree of confidence more detailed experiments are necessary. The experiments and the results obtained are laid out in detail in the following sections.

3.2.7 The dependence of the rate of the reaction on the concentration of the catalyst

The dependence of the reaction on the catalyst is experimentally determined by the order with respect to the catalyst concentration. However, the integrated rate equation of the rate law does not include the catalyst order as

the total concentration of the catalyst remains a constant throughout the reaction.³ Although the integrated rate law does not directly provide the dependence of the rate of the reaction on the catalyst concentration, the rate constant obtained experimentally should include this dependence. The experimental procedure performed to obtain this relationship is explained below.

Several stoichiometric reactions where, **2B:1A** was 1:1 were performed, varying only the catalyst loading at 322.8 K. The data thus obtained was used to plot a graph for the 3rd order integrated rate equation, plotting $1/[\mathbf{1A}]^2$ as a function of time. This was done as the experimental results obtained fitted best for a 3rd order rate equation. The gradient of these plots according to the 3rd order integrated rate law would be $2k$, where k would be the observed rate constant that would incorporate the term [catalyst] (equation 3-13). If the dependence of the reaction with respect to the [catalyst] was 1st order, a graph plotted with the observed rate constants $2k$ (which is derived from experiments with different catalyst loading) as a function of the catalyst concentration, a linear relationship should be observed.

$$k_{obs} = k[\mathbf{Catalyst}]$$

equation 3-13

Stoichiometric reactions between **2B** and **1A** varying the catalyst loading from 6-26 mol % (Table 3- 3). The graph plotted with the k_{obs} as a function of the catalyst concentration were fitted by a linear regression giving R^2 0.991 (Figure 3-9). The last few data points of the graph below corresponding to lower catalyst loadings were erroneous due to the errors in obtaining a good quality NMR spectra which was due to the loss of shim and the very slow reaction rate observed with very low catalyst loading (less than 4 mol%).

Table 3- 3 The observed third order rate constants for stoichiometric reactions where the [2B] : [1A] ratio = 1 : 1 at 322.8 K

Catalyst loading (mol %)	6.8	8.2	10.5	14.8	16.3	19.9	25.8
[Catalyst]/ 10⁻³ mol dm⁻³	1.03	1.23	1.50	2.24	2.45	3.00	3.83
<i>k</i>_{obs} / mol⁻³ dm⁹ s¹	0.25	0.39	0.44	0.65	0.74	0.89	1.17

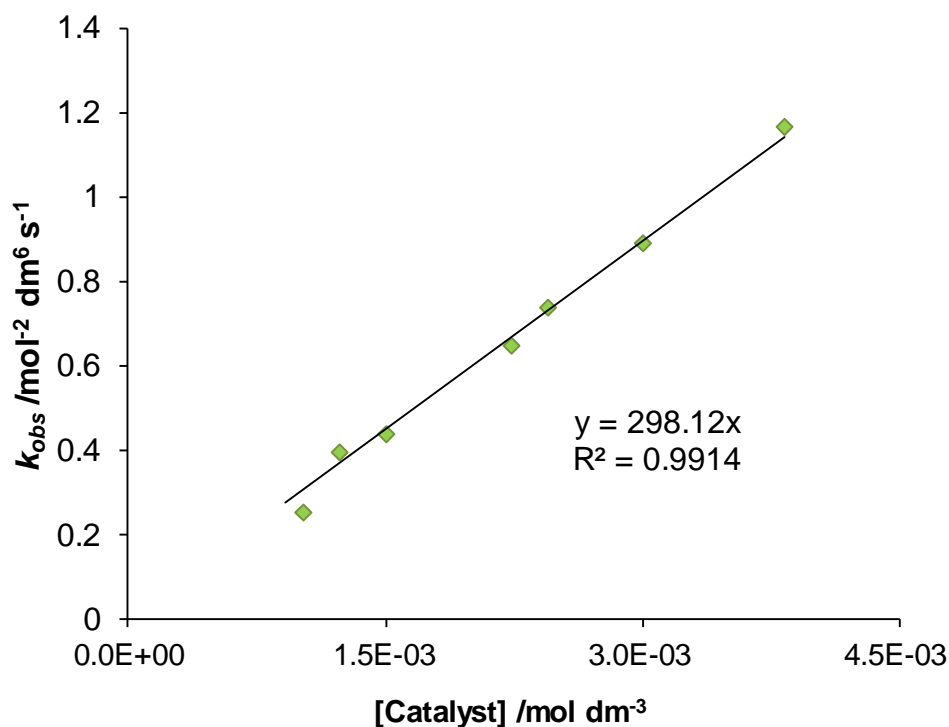


Figure 3-9 A plot of k_{obs} as a function of [catalyst] from the data collected by ¹H-NMR spectroscopy for the hydrofluoroarylation reaction of **1A** with **2B** under different catalyst loading in C₆D₆ at 322.8 K.

The order of the reaction with respect to the catalyst concentration can be graphically shown by RPKA. Data collected from two different experiments under the following conditions are required. The difference in the concentration of reactants should be essentially the same in both

experiments and the catalyst loading is different in individual experiments. The turn over frequencies, TOF (where $\text{TOF} = \text{Rate} / [\text{catalyst}]$) of the individual experiments are plotted as a function of the concentration of the substrate on the same graph. Overlay of the two curves suggests a first order dependence of the rate of the reaction on the concentration of the catalyst.³ This can be expressed as follows from the rate equation (equation 3-14).

$$\frac{v}{[4_{total}]} = \text{TOF} = \frac{k_1 k_2 [2B][1A]}{k_{-1} + k_1 [2B] + k_2 [1A]}$$

equation 3-14³

Three different experiments were carried out to find out the order with respect to the catalyst, (1,5-hexadiene)Ni(IPr) under the following conditions:

- i. Experiments **1c**, **2c** and **3c** $[2B_{1c}] - [1A_{1c}] = [2B_{2c}] - [1A_{2c}] = [2B_{3c}] - [1A_{3c}]$
- ii. Catalyst loading ;
 - a. experiment **1c** – 6.8 mol %
 - b. experiment **2c** – 8.2 mol %
 - c. experiment **3c** – 19.9 mol %

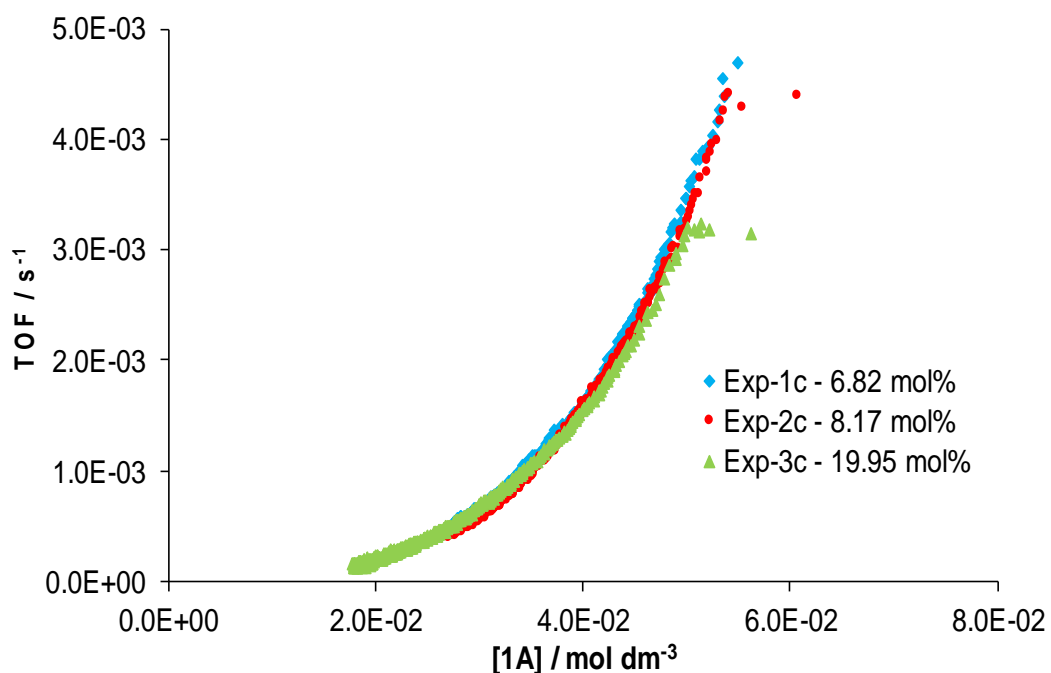


Figure 3-10 A plot of the TOF of the reaction against the substrate concentration constructed from the data collected by ¹H-NMR spectroscopy for reactions of **1A** with **2B**, with different catalyst loading in C₆D₆ at 322.8 K

The TOF was plotted as a function of the concentration of **1A** for all three experiments (Figure 3-10). The graph shows that the curves from all three experiments overlay each other suggesting a first order dependence on the catalyst, (1,5-hexadiene)Ni(IPr) concentration (Figure 3-10). Hence from this it could be deduced that the catalytic cycle is dependent on one molecule of the nickel catalyst. This is in agreement with the first order dependence on the [catalyst] observed from the classical kinetic methods mentioned above.

3.2.8 The order of the reaction with respect to C₆F₅H

3.2.8.1 Isolation method – C₆F₅H order

Experimental methods to identify the order with respect to individual reactants (substrates) involve the use of the isolation method often in combination with the initial rate method. A number of experiments were carried out with **1A** as the limiting reactant and with **2B** added in large excess to ensure the change in the concentration of **2B** is insignificant compared to the concentration change of **1A**. When excess of **2B** to **1A** was increased to 50 fold, the properties of the reaction mixture altered in such a manner that the resonance of the internal standard and the solvent overlapped and the resonance of the **1A** protons and the methyl protons of the arylalkene were indistinguishable. This observation limited the highest excess to 50 fold (see appendix).

A graph plotted treating the data to follow the pseudo 2nd order rate law integrated rate equation

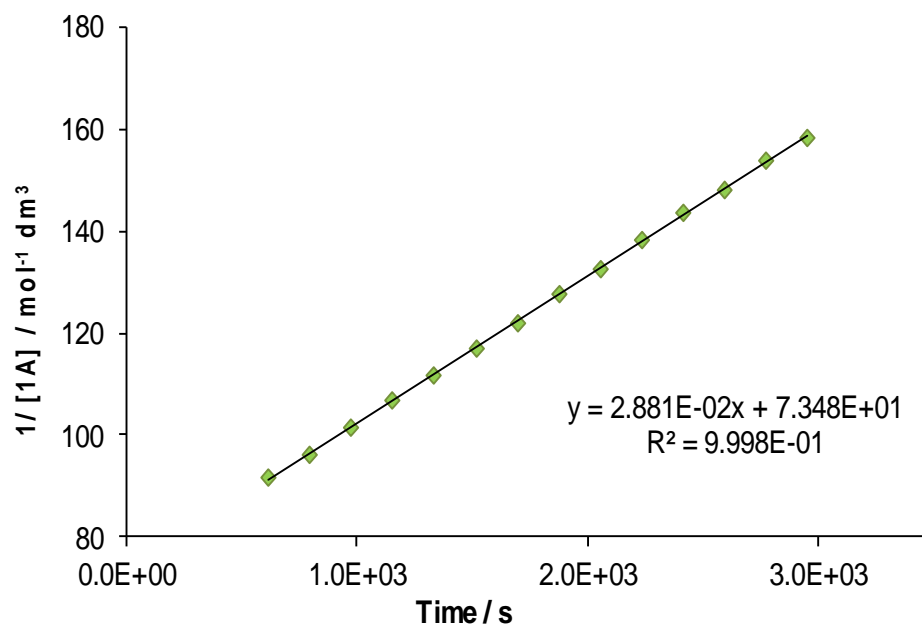


Figure 3-11 A plot of 1/[**1A**] against time constructed from the data collected by ¹H-NMR spectroscopy for the reaction of **1A** with **2B** (ratio 1 : 35) catalysed by (1,5-hexadiene)Ni(IPr) in C₆D₆ at 322.8 K (catalyst loading-12 mol%).

The data thus obtained for individual experiments were fitted for a pseudo zeroth, first, second and third order integrated rate law. The k_{obs} obtained from the best fit graph was used to generate a graph plotting $k_{obs} / [\text{catalyst}]$ as a function of the concentration of **2B**. Different experiments varying the excess of **2B** with respect to **1A** from 16 to 46 fold of the concentration of **1A** were carried out at 322.8 K (Table 3-4). The data obtained was observed to fit with the best linear relationship for a pseudo second order rate equation. The $k_{obs}/[\text{catalyst}]$ was used instead of the k_{obs} to account for errors resulting due to the difference in the catalyst loading in different experiments.

Table 3-4 The observed pseudo second order rate constants for reactions varying the **[2B]: [1A]** ratio by using excess **2B**

[2B] : [1A] ratio	[C₆F₅H] /mol/dm³	$k_{obs}/[\text{catalyst}]$ mol⁻² dm⁶ s⁻¹	Catalyst loading
17	0.255	8.41	12.3
20	0.275	8.96	21.9
25	0.377	12.48	7.5
35	0.521	16.22	11.8
46	0.694	22.28	12.4

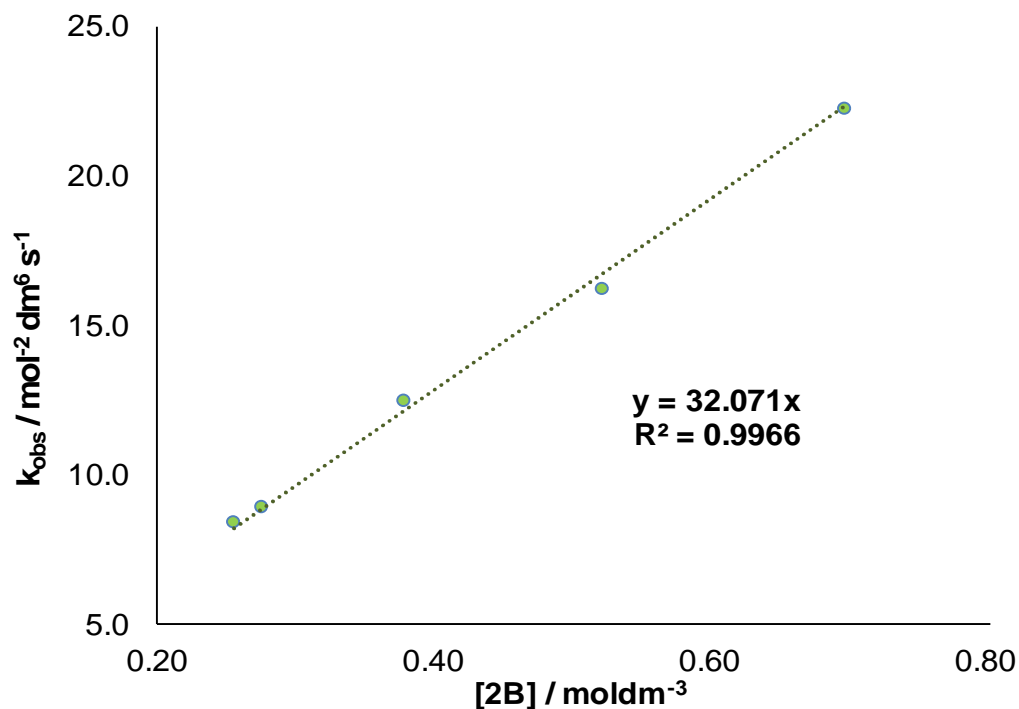


Figure 3-12 A plot of k_{obs} (where, $k_{obs} = k' / [\text{Catalyst}]$) as a function of $[\mathbf{2B}]$ for the reaction of $\mathbf{1A}$ with different excesses of $\mathbf{2B}$ catalysed by (1,5-hexadiene)Ni(IPr), in C_6D_6 at 322.8 K.

$$\text{Rate} = k[\mathbf{1A}]^x[\mathbf{2B}]^y[\text{Cat}]$$

In large excess of $\mathbf{2B}$:

$$\text{Rate} = k_{obs}[\mathbf{1A}]^x, \text{ where } k_{obs} = k[\mathbf{2B}]^y[\text{Cat}]$$

$$\frac{k_{obs}}{[\text{Cat}]} = k[\mathbf{2B}]^y$$

equation 3-15

The graph plotted with the data obtained from different excess of $\mathbf{2B}$ showed a linear relationship with an R^2 of 0.997 when the $k_{obs} / [\text{catalyst}]$ was plotted as a function of $[\mathbf{2B}]$ at 322.8 K. This suggests a first order dependence of the rate on the concentration of $\mathbf{2B}$ from the linear relationship (equation 3-15).

3.2.9 The dependence of the rate of the reaction on concentration of the alkyne

In an attempt to study the order with respect to **1A** at 322.8 K, the conditions of the reaction were altered to make **2B** the limiting substrate. For this the reaction was done under large excess of **1A**, where the concentration change in **1A** is insignificant during the reaction compared to the consumption of **2B**. The best fit was obtained for a pseudo first order rate law graph with the data from the experiment performed with the ratio **2B:1A** = 1:11 (Figure 3-13). The plot of $\ln[2B]$ as a function of time gave a linear fit with a linear regression of 0.998. The linear relationship obtained for a pseudo first order rate equation suggests a first order dependence of the rate on **2B**, which has already been proved earlier. The rate constant for the reaction under excess alkyne conditions, k was calculated as 0.169 s^{-1} from the equation 3-16.

$$\ln[2B]_t = -k_{obs}t + \ln[2B]_0, \text{ where } k_{obs} = k[1A][Cat]$$

equation 3-16

A graph plotted treating data as 1st order using a pseudo 1st order integrated rate equation

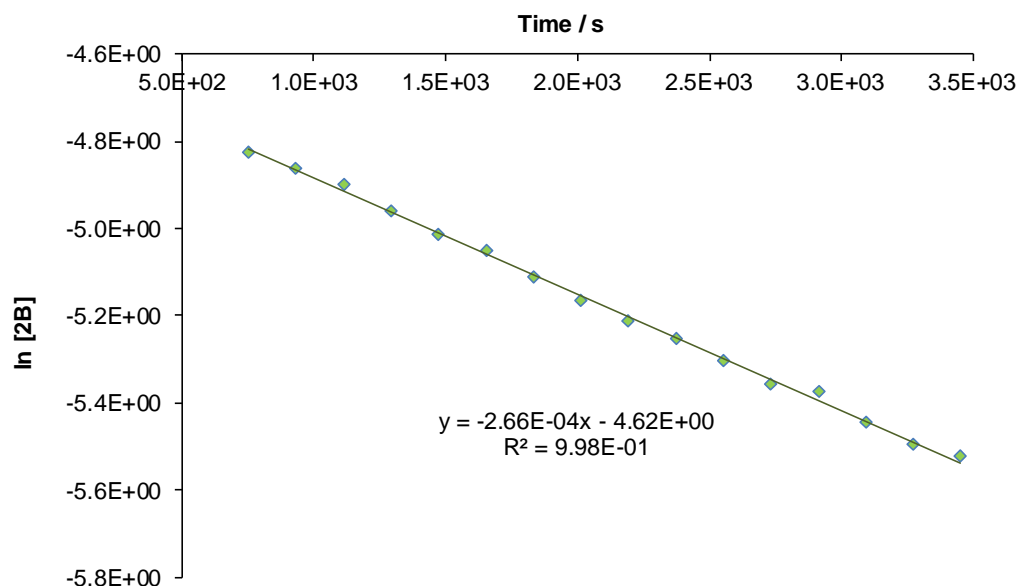


Figure 3-13 A plot of $\ln[2B]$ against time from the data collected by $^1\text{H-NMR}$ spectroscopy for the reaction of **1A** with **2B** (ratio 11 : 1) catalysed by (1,5-hexadiene)Ni(IPr) in C_6D_6 at 322.8 K (catalyst loading 10 mol%).

A second experiment with excess alkyne (where the ratio of **1A**:**2B** was 4.6:1) also showed a best fit for the pseudo first order rate law with a linear regression fit of 0.998. However, the rate was observed to increase quite dramatically with excess alkyne and the highest excess of **1A** was 11 at 322.8 K. Exceeding this gave rise to unsatisfactory results as very few points could be obtained before 55% conversion. This prevented the derivation of the dependence of the rate on **1A** by plotting k_{obs} as a function of the $[\mathbf{1A}]$ at 322.8 K.

To avoid the problem of not being able to collect adequate data when **1A** was in large excess, the temperature of the experiments was lowered from 322.8 K to 306.4 K. A stoichiometric reaction between **2B** and **1A** catalysed by (1,5-hexadiene)Ni(IPr) at 306.4 K exhibited similar behaviour to that at 322.8 K, where the data was observed to show the best linear relationship for a third order integrated rate law.

A graph plotted treating data as third order using third order integrated rate equation

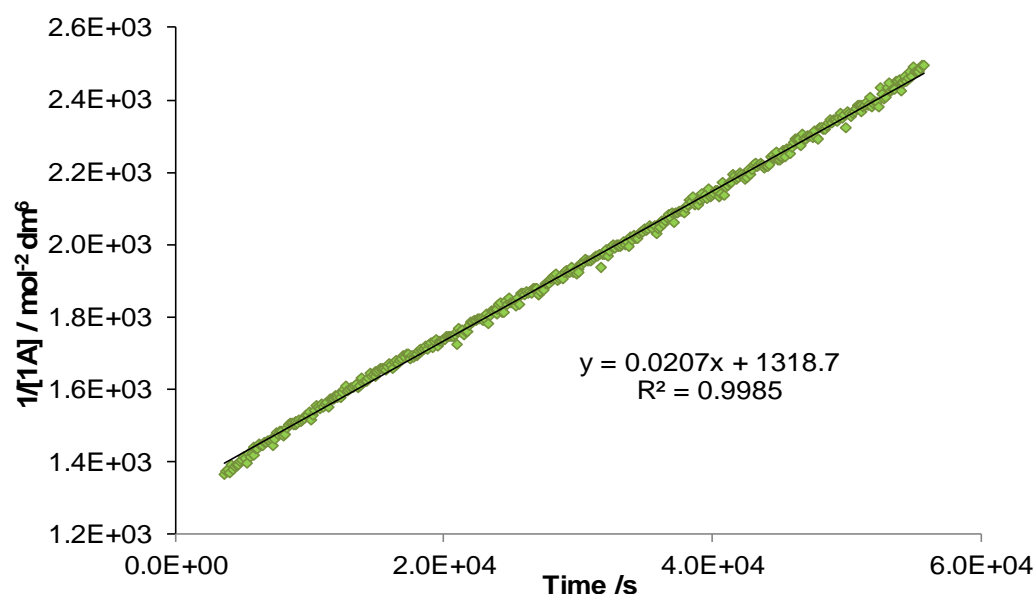


Figure 3-14 A plot of $1/[\mathbf{1A}]^2$ against time constructed from the data collected by $^1\text{H-NMR}$ spectroscopy for the reaction of **1A** with **2B** catalysed by (1,5-hexadiene)Ni(IPr) in C_6D_6 at 306.4 K.

3.2.10 Kinetic analysis at a low temperature to obtain the dependence of the rate of the reaction on alkyne

In order to obtain more information about the dependence of the rate of the reaction on alkyne, different experiments with different excess of **1A** were carried out at 306.4 K. The data obtained from experiments done with 10, 21 and 27 fold excess of **1A** to **2B** at 306.4 K was observed to give a linear fit to a pseudo first order rate law graph (Figure 3-15).

A graph plotted treating data as 1st order using a pseudo 1st order integrated rate equation

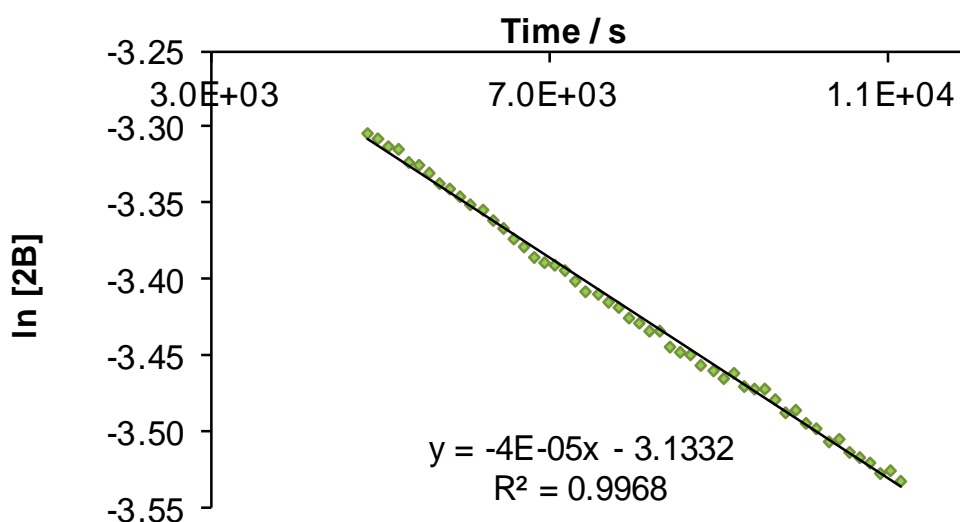


Figure 3-15 A plot of $\ln[2B]$ against time from the data collected by $^1\text{H-NMR}$ spectroscopy for the reaction of **1A** with excess **2B** catalysed by (1,5-hexadiene)Ni(IPr) in C_6D_6 at 306.4 K (catalyst loading 5 mol%).

$$\text{Rate} = k[1A]^x[2B][\text{Cat}]$$

In large excess of **1A**:

$$\text{Rate} = k_{obs}[2B], \text{ where } k_{obs} = k[1A]^x[\text{Cat}]$$

$$\frac{k_{obs}}{[\text{Cat}]} = k[1A]^x$$

equation 3-17

The observed rate constant (k_{obs}) of the three different experiments was plotted as a function of the concentration of **1A** (Table 3-5, Figure 3-16). The graph showed that the rate of the reaction was not dependent on the concentration of **1A** at 306.4 K under the condition when the [**1A**] was 10 fold or more in excess to that of [**2B**], suggesting a zero order with respect to **1A** in the equation 3-17.

Table 3-5 The observed pseudo first order rate constants for reactions varying the [**2B**] : [**1A**] ratio at 306.4 K

[1A] / mol dm ⁻³	[1A] : [2B] ratio	k_{obs} / s
0.29	10	2.35E-02
0.62	21	2.30E-02
1.29	27	2.32E-02

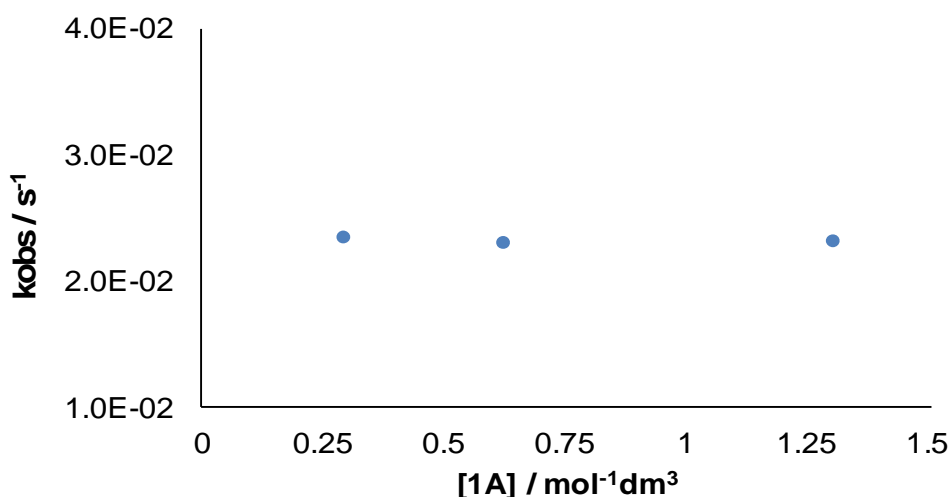
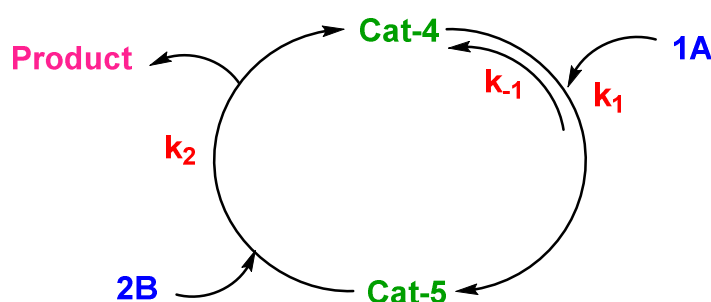


Figure 3-16 A plot of k_{obs} as a function of [**1A**] for the reaction of **2B** with different excesses of **1A** catalysed by (1,5-hexadiene)Ni(IPr), at 306.4 K in C₆D₆.

To obtain further proof and more detailed understanding of the involvement of individual reactants in the mechanism, information from RPKA was sought.

In addition, the methodology was used to understand why the overall order of the reaction observed under stoichiometric conditions was three, although the order with respect to **2B** was observed to be one and with zero with respect to **1A** with isolation conditions. Hence, there appears to be a conflict between the overall order observed in the rate law of the equation and the rate law determined by the isolation method.

3.2.11 Reaction progress kinetic analysis – Excess alkyne conditions



Scheme 3-6 A schematic diagram of the catalytic cycle for the hydrofluoroarylation reaction of **1A** and **2B** catalysed by (1,5-hexadiene)Ni(IPr)

If the rate of the reaction did not depend on the concentration of alkyne, the catalyst resting state would be **Cat-5** (Scheme 3-6) which would be the catalyst coordinated to the alkyne. This is achievable if the k_1 in the catalytic cycle is a large value which will make the term $k_1[1A]$ dominant in the denominator of the rate equation (equation 3-12) and hence the rate equation of the reaction can be modified as follows,

$$v = k_2[4_{total}][2B]$$

equation 3-18

Therefore, the rate of the reaction should exhibit a first order dependence on **2B**. A straight line should be observed when the rate of the reaction is plotted

as a function of **[2B]**. In addition, graphs of different experiments, where the difference in the concentrations of the reactants is different in each individual experiment, should overlay each other (when the rate of the individual reactions are plotted as a function of **[2B]**). Taking this into account, the rates of two reactions with excess of **1A** were plotted on the same graph as a function of **[2B]**.

$$\frac{v}{[4_{total}]} = k_2[2B]$$

equation 3-19

However, the two individual graphs did not overlay each other. This indicates that the rate of the reaction cannot be given by the equation 3-18 under the stoichiometric (or slight excess) conditions. To understand the role of the alkyne in the reaction, two experiments done with different excess of **1A** were chosen for the same analysis mentioned above.

Two different experiments (**1e** and **2e**) were done under the following conditions;

1) Excess alkyne;

a. $[1A_{1e}] : [2B_{1e}] = 11 : 1$

b. $[1A_{2e}] : [2B_{2e}] = 8.5 : 1$

2) $[2B_{1e}] - [1A_{1e}] \neq [2B_{2e}] - [1A_{2e}]$

The rates of the reaction for the two experiments were plotted on the same graph as a function of the concentration of **2B** (Figure 3-17). The curves of experiments **1e** and **2e** overlap each other suggesting a first order dependence of the rate on the concentration of **2B** and saturation kinetics with respect to **1A**. However, this observation is made only in the presence of excess alkyne and not in the stoichiometric reactions. The question of whether similar behaviour is observed for **2B** was answered by plotting the rate of two experiments done with excess **2B** as a function of **[1A]**. In this case however, no such overlay was observed indicating that the reaction did not follow saturation kinetics for **2B** even under excess **2B**. The rate constant

corresponding to the second substrate k_2 was calculated from the equation 3-19 as 0.169 s^{-1}

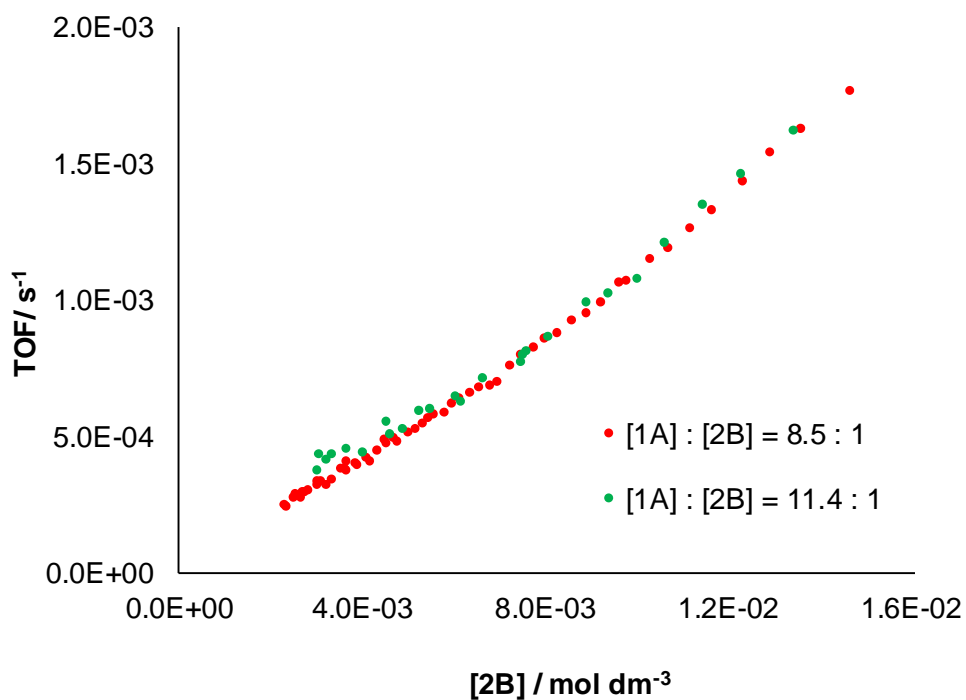


Figure 3-17 A plot of the TOF against $[2B]$ constructed from the data collected by $^1\text{H-NMR}$ spectroscopy for two reactions of $2B$ with excess $1A$ catalysed by (1,5-hexadiene)Ni(IPr) in C_6D_6 at 322.8 K (catalyst loading 10 mol%).

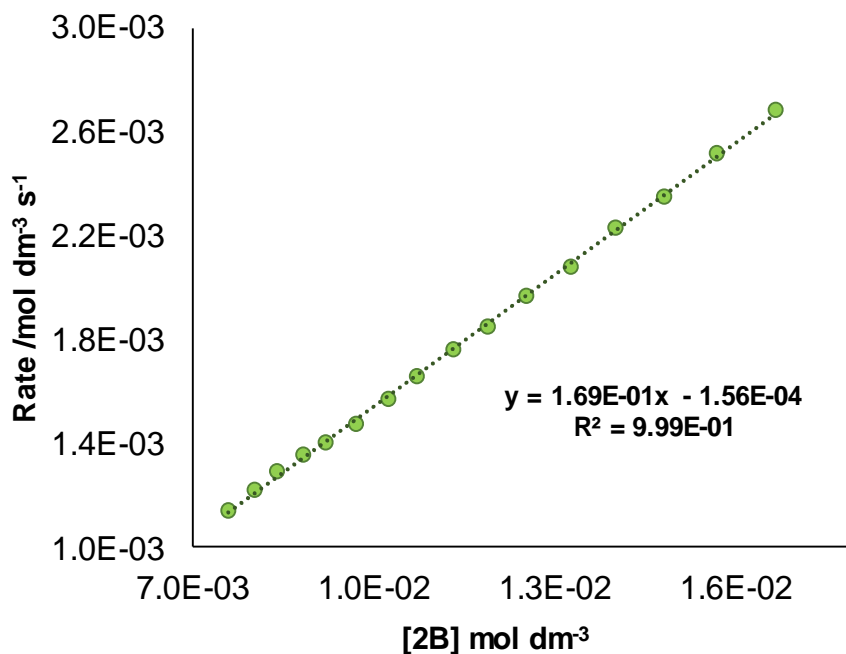


Figure 3-18 A plot of the rate against the concentration of **2B** constructed from the data collected by ¹H-NMR spectroscopy for a reaction with the ratio **2B** : **1A** = 1 : 11 catalysed by (1,5-hexadiene)Ni(IPr) in C₆D₆ at 322.8 K (catalyst loading 10 mol%).

The excess alkyne in the experiments where saturation kinetics has been observed was only of 10 fold excess or less. Hence the argument that the concentration change in **1A** during the course of the reaction is negligible cannot be accepted. This observation made it vital investigate the role of the alkyne further. The kinetic data for various reactions with different ratio of **1A**: **2B** were collected (Table 3-6). The resultant data were fitted for a pseudo first order rate law equation plotting $\ln[2B]$ as a function of time and the observed rate constants were plotted as a function of **[1A]** (Figure 3-19).

Table 3-6 The observed rate constants obtained from pseudo 1st order rate equations for several experiments varying the [1A]:[2B] ratio at 322.8 K

[1A]: [2B] ratio	$k_{\text{obs}} / \text{s}^{-1}$
11.4	1.69E-01
8.9	1.66E-01
6.2	1.49E-01
4.6	1.15E-01
3.4	8.58E-02
2.4	5.63E-02
1.0	1.35E-02

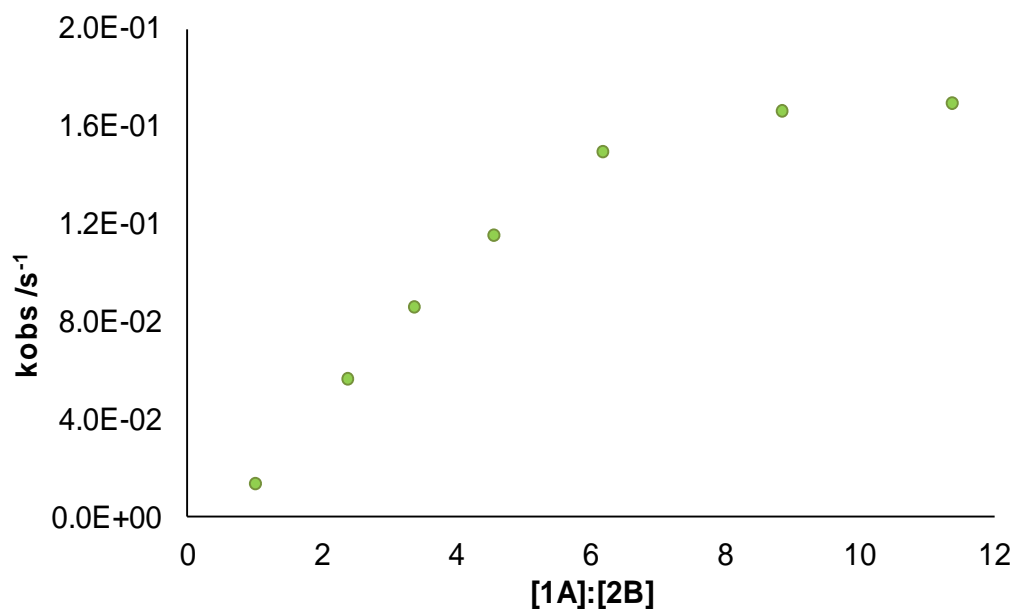


Figure 3-19 A plot of the k_{obs} as a function of the ratio [1A]: [2B] for a series of hydrofluoroarylation reactions with different [1A] catalysed by (1,5-hexadiene)Ni(IPr) in C_6D_6 at 322.8 K.

The ratio of **1A:2B** was changed from 1: 1 to 11:1 in the different experiments used to plot the graph at 322.8 K (Figure 3-19). The graph constructed thus exhibited an initial dependence on **1A** at low excess of **1A** and further increase in the excess leads to saturation kinetics with respect to **1A**. In the experiment where the ratio of **1A:2B** = 1.01, the k_{obs} was obtained from a first order rate law graph for consistency, although the kinetic data best fitted for a third order rate law. However, the data only in the region 20-45% conversion was used for this analysis and the R^2 was observed to be 0.996 for a linear regression line in this region.

The saturation kinetics mentioned above can be linearized by the double reciprocal Lineweaver-Burk equation which was a further development of the Michaelis-Menten equation for enzymatic systems.⁸ The inverse observed rate constants obtained from each of the different experiments varying the ratio of **[1A]: [2B]** at 322.8 K was plotted as a function of $1/[1A]$ (Figure 3-20). The experiment with the ratio of **[1A]: [2B]** = 1: 1 was eliminated from the plot. The V_{max} calculated from the plot was $3.3 \times 10^{-4} \text{ M}^{-1}\text{s}^{-1}$. Thus the rate constant for the second step following the equilibrium (irreversible step with the rate constant k_{cat}) was calculated to be equal to 0.23 s^{-1} ($V_{max} = k_{cat}[\text{Catalyst}]$).

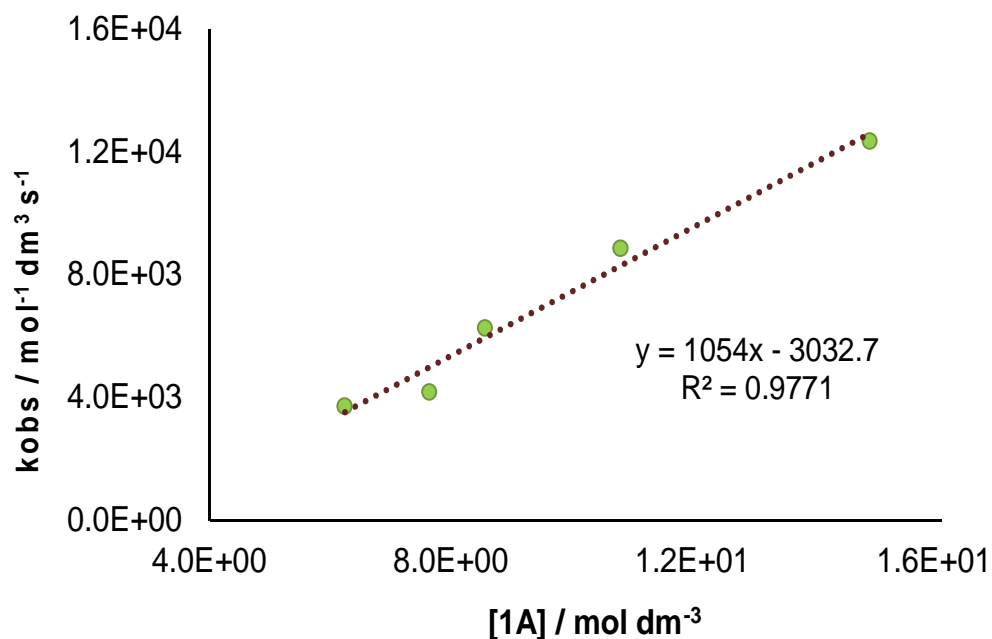
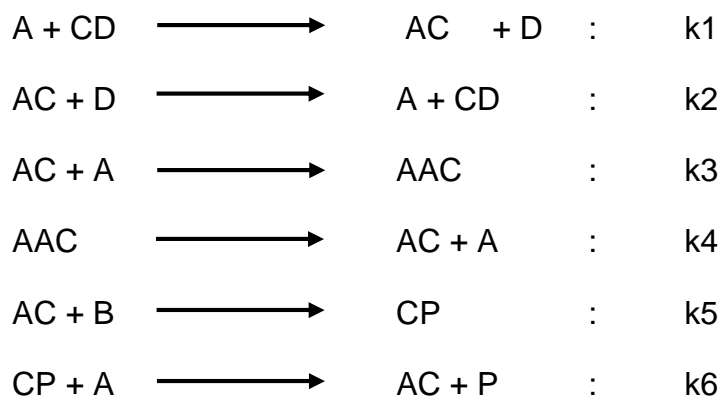


Figure 3-20 A plot of the $1/k_{\text{obs}}$ as a function of $1/[1\mathbf{A}]$ for a series of hydrofluoroarylation reactions with different $[1\mathbf{A}]$ catalysed by (1,5-hexadiene)Ni(IPr) in C_6D_6 at 322.8 K.

3.2.12 Modelled kinetic data

The kinetic data obtained by monitoring the hydrofluoroarylation reaction of **1A** with **2B** catalysed by (1,5-hexadiene)Ni(IPr) using $^1\text{H-NMR}$ spectroscopy was modelled with the modelling and simulation programme, Dynafit4 (version 4.05.103).^a The hydrofluoroarylation reaction catalysed by (1,5-hexadiene)Ni(IPr) at 322.8 K was fitted for the following model, where A and B are the substrates alkyne and fluoroarene respectively, the product P and the catalyst CD. (A = **1A**, B = **2B**, P = arylalkene and CD = (1,5-hexadiene)Ni(IPr), D = 1,5-hexadiene, CP = intermediate).

^a <http://www.biokin.com/dynafit/>



The experimentally obtained kinetic data for a reaction where $[\mathbf{1A}]: [\mathbf{2B}] = 1:1$ was fitted for the above basic model as a preliminary step. The modelled data and the experimentally obtained data are plotted on the graph given below (Figure 3-21). The percentage conversion of the decay of the reactant (in this example $\mathbf{1A}$) is plotted as a function of time. Initially the model was fitted by fixing k_5 as 0.169 s^{-1} which was obtained experimentally. The results from the kinetic analysis pointed out that the step associated with this rate constant (0.169 s^{-1}) was dependent on one molecule of fluoroarene and one molecule of catalyst, hence this rate constant was assigned for the coordination of the fluoroarene in the above model (k_5). Fixing this, the rate constants of the other steps in the above given basic model were obtained from the modelled fit with an estimated confidence level of 95% and are tabulated below in Table 3-7. It was observed that in addition to this, that the model was also found to fit with k_5 as 0.17 s^{-1} , when a different rate constant (other than k_5) was fixed and k_5 was kept as a variable. It was also observed that the experimentally obtained rate constant of 0.169 s^{-1} did not fit any other steps in the model used to fit the data.

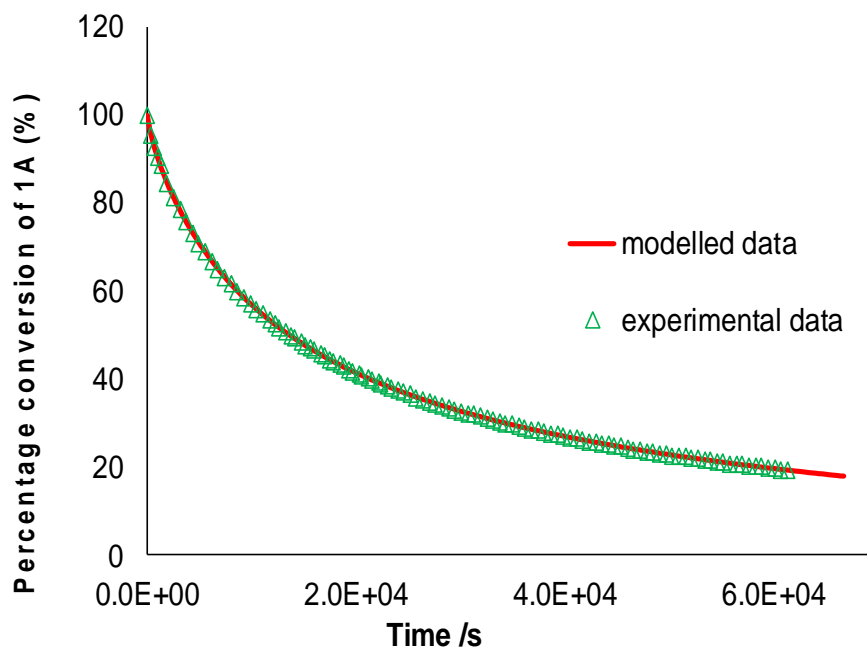


Figure 3-21 The percentage conversion of reactant as a function of time for a stoichiometric reaction of **1A** : **2B** = 1 : 1 at 322.8 K the experimental data and the fit based on the proposed model (catalyst loading 14.8 mol %)

Table 3-7 Rate constants obtained from the model fitting the experimental kinetic data

Catalyst loading	6 mol %	10 mol %	14 mol %	16 mol %	20 mol %
k_1/ s^{-1}	5.5 ± 0.5 $\times 10^{-2}$	5.4 ± 0.1 $\times 10^{-2}$	6.4 ± 0.06 $\times 10^{-2}$	5.8 ± 0.1 $\times 10^{-2}$	2.6 ± 0.2 $\times 10^{-2}$
k_2/ s^{-1}	1.8 ± 0.3	9.6 ± 0.2 $\times 10^{-2}$	1.4 ± 0.04	9.2 ± 0.2 $\times 10^{-1}$	1.2 ± 0.1
k_3/ s^{-1}	5.3 ± 0.2 $\times 10^{-2}$	3.1 ± 0.01 $\times 10^{-2}$	3.6 ± 0.02 $\times 10^{-2}$	4.9 ± 0.06 $\times 10^{-2}$	4.6 ± 0.06 $\times 10^{-2}$
k_4/ s^{-1}	9.3 ± 0.2 $\times 10^{-6}$	3.8 ± 0.06 $\times 10^{-6}$	3.3 ± 0.2 $\times 10^{-6}$	2.4 ± 0.6 $\times 10^{-6}$	8.3 ± 3.6 $\times 10^{-6}$
k_6/ s^{-1}	3.9 ± 0.1 $\times 10^{-2}$	5.9 ± 0.05 $\times 10^{-2}$	5.4 ± 0.07 $\times 10^{-2}$	5.3 ± 0.07 $\times 10^{-2}$	5.9 ± 0.5 $\times 10^{-2}$

The model was further simplified eliminating the first equilibrium between the alkyne and the catalyst. This was done based on the assumption that under the catalytic reaction conditions the alkyne was present in large excess with respect to the catalyst, hence initially the catalyst would be in its AC state (bound to one alkyne displacing the 1,5-hexadiene). This assumption simplifies the model (see below) and reduces the number of variables and eliminates the complication of the 1,5-hexadiene displaced by the alkyne. The model was fitted in a similar manner as mentioned before initially fixing k_5 as a constant at $0.169 \text{ mol}^{-1} \text{ dm}^3 \text{ s}^{-1}$ and the results are tabulated on Table 3-8.

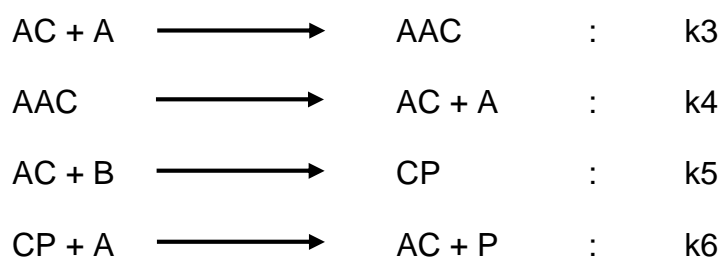


Table 3-8 Rate constants obtained from the simplified model fitting the experimental kinetic data

Catalyst loading	6 mol%	10 mol%	14 mol%	16 mol%	20 mol%
k_3/ s^{-1}	2.3 ± 0.01 $\times 10^{-2}$	2.9 ± 0.03 $\times 10^{-2}$	3.6 ± 0.3 $\times 10^{-2}$	4.1 ± 0.01 $\times 10^{-2}$	5.2 ± 0.01 $\times 10^{-2}$
k_4/ s^{-1}	1.1 ± 0.02 $\times 10^{-5}$	3.7 ± 0.03 $\times 10^{-6}$	3.9 ± 0.2 $\times 10^{-6}$	2.9 ± 0.01 $\times 10^{-6}$	3.2 ± 0.01 $\times 10^{-6}$
k_6/ s^{-1}	2.9 ± 0.02 $\times 10^{-2}$	4.9 ± 0.01 $\times 10^{-2}$	4.2 ± 0.02 $\times 10^{-2}$	4.5 ± 0.02 $\times 10^{-2}$	2.9 ± 0.02 $\times 10^{-2}$

The initial step of the model was proposed to be the coordination of one alkyne molecule, **1A** to nickel in a reversible reaction displacing the

1,5-hexadiene ligand on the catalyst, (1,5-hexadiene)Ni(IPr). The $[\text{CH}_3\text{C}\equiv\text{CC}(\text{CH}_3)_3]\text{Ni}(\text{IPr})$ species resulting from the above step was either in an equilibrium with a species, $[\text{CH}_3\text{C}\equiv\text{CC}(\text{CH}_3)_3]_2\text{Ni}(\text{IPr})$ formed as a result of further coordination with another alkyne molecule or reacts with **2B** to give rise to an intermediate that continued to give the final arylalkene product.

The data did not fit a model where **2B** reacts with the nickel coordinated to two alkynes, $[\text{CH}_3\text{C}\equiv\text{CC}(\text{CH}_3)_3]_2\text{Ni}(\text{IPr})$ and fitted a model only when **2B** reacted with the mono-alkyne nickel species, $[\text{CH}_3\text{C}\equiv\text{CC}(\text{CH}_3)_3]\text{Ni}(\text{IPr})$. However, it was observed that the equilibrium between the mono-alkyne and bis-alkyne nickel species improved the fit to the kinetic data obtained experimentally. The final step of the catalytic cycle which involves a reductive elimination of the product and regeneration of the catalyst was found to coordinate the alkyne to the nickel to give the mono-alkyne nickel species, $[\text{CH}_3\text{C}\equiv\text{CC}(\text{CH}_3)_3]\text{Ni}(\text{IPr})$ and the model did not fit the data when the final step involved coordination of 1,5-hexadiene to regenerate the catalyst added into the reaction mixture. This observation suggests that the resting state of the catalyst in the catalytic cycle is the equilibrium between the alkyne and the mono-alkyne nickel species, $[\text{CH}_3\text{C}\equiv\text{CC}(\text{CH}_3)_3]\text{Ni}(\text{IPr})$. The kinetic data failed to fit a basic model in which **2B** coordinated initially leading to the formation of an intermediate, either the nickel hydride or the Ni-PR₃ η^6 -coordinated to the fluoroarene. The model used to fit the experimental kinetic data is a basic model adapted from some of the steps involved in the mechanism proposed based on the DFT calculation results.¹⁰

3.3 Discussion

Catalysis is often termed a “*purely kinetic phenomenon*”^{1,15} and hence kinetic analysis is sought for true evidence of the mechanism of the reaction. Spectroscopic evidence of plausible intermediates in the catalytic mixtures is not necessarily solid evidence of such intermediates in the true mechanism of the reaction. Proving that such intermediates are kinetically capable of undergoing the reaction reasonably fast, is vital.¹⁶

The kinetic analysis of each reactant involved in the reaction provides information of how the mechanism proceeds. One method to experimentally determine the dependence of the reaction rate on individual reactants is by isolation method in classical kinetic approaches. The isolation method is based on the assumption that the change in the concentration of one reactant is negligible compared to the other. However in our case, the highest excess of reagents that could be used in the isolation method was limited by various factors. The highest excess of **2B** that could be used was limited to 46 times that of **1A**. Further increase in the concentration of **2B** resulted in the change in the polarity of the reaction mixture, that made the chemical shifts of the reactants and the products overlap. The excess of **1A** was more limited than **2B**, because of the dramatic increase in the rate observed with an excess of **1A**, making analysis both difficult and less accurate. Hence a different method, such as the reaction progress kinetic analysis demonstrated by Blackmond, was used to confirm the results observed by classical kinetic methods. Blackmond's review in 2005 discusses and explains a step-by-step analysis of the kinetics of catalytic cycles. This method was adopted to study the kinetics of the hydrofluoroarylation reaction of **1A** with **2B** catalysed by (1,5-hexadiene)Ni(IPr) complex.

3.3.1 The role of the catalyst

The integrated rate law plots do not show the dependence of the rate on the [catalyst] as the total amount of catalyst is always a constant in the catalytic cycle. The dependence of the rate of the reaction on the concentration of the catalyst was analysed both by classical kinetic approaches and reaction progress kinetic analysis. Both analyses showed a first order dependence of the rate of the reaction on [catalyst]. This was observed from graphical rate equation plot, which was plotted with the turn-over frequency as a function of the substrate concentration, where the graphs from different catalyst loading

overlay each other, which is possible when the reaction rate is first order with respect to the [catalyst]. The classical kinetic approaches also showed a first order dependence on the [catalyst] which was derived from observed rate constants obtained for individual reactions with different catalyst loading.

3.3.2 The dependence of the rate of the reaction on the substrates

3.3.2.1 The dependence of the rate on C₆F₅H

The analysis of the experimental data obtained from the isolation method and the analysis of the data obtained for experiments with excess alkyne by RPKA, exhibited a dependence of the rate of the reaction on the concentration of **2B**. Both the classical kinetic analysis approach and RPKA unambiguously highlighted a first order dependence of the rate of the reaction on the concentration of **2B**. This suggests the involvement of one molecule of **2B** in the step in the mechanism which involves the highest energy barrier.

3.3.2.2 The role of the alkyne in the hydrofluoroarylation reaction

The dependence of the rate of the reaction on the concentration of **1A** was more complex, yet more informative of the mechanism than **2B**. Attempts to use the isolation method to identify the order of the reaction with respect to [**1A**] at 322.8 K were not successful due to the very fast rate of reaction. In order to identify the dependence of the reaction with respect to [**1A**] in a similar manner to [**2B**], the data collection was done at 306.4 K. This drop in temperature enabled one to run the experiments under excess **1A** varying the ratio of [**1A**]: [**2B**] from 10 to 30. The experimental results thus obtained showed that the reaction was independent of the concentration of **1A**. This contrasted with the overall third order observed for the rate of the reaction obtained from stoichiometric reactions (**2B**: **1A** = 1:1) at both 322.8 K and

306.4 K, which would suggest a higher order than zero for **1A** (as the order of **2B** has already been shown to be one). However, one has to be aware that the overall rate of the reaction is often misleading and the only way to derive true evidence of the dependence of the rate on individual components is to analyse them individually whenever possible.¹

$$v = \frac{k_1 k_2 [\mathbf{1A}] [\mathbf{2B}] [4_{total}]}{k_{-1} + k_1 [\mathbf{1A}] + k_2 [\mathbf{2B}]}$$

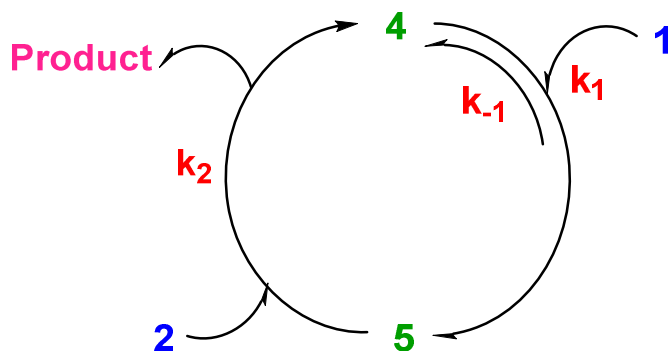
equation 3-20

However, if the reaction is completely independent of **1A**, the rate of the reaction of the stoichiometric reaction plotted as a function of **2B** should exhibit a linear relationship. In addition to this the curves of experiments with different “excess” should overlay each other, when the kinetic data obtained is analysed by RPKA.³ This would be a result of the term $k_1[\mathbf{1A}]$ in the denominator of equation 3-20 becoming the dominating term and hence modify the rate equation to show a linear dependence only on **2B**. However, this is not observed, which suggests that the rate of the reaction is not fully independent of **1A**. The two experiments analysed by RKPA, that exhibited first order dependence on **[2B]** did not have enough excess of **1A** (4.6 fold and 11 fold excess **1A**) for one to argue that the concentration change of **1A** remains a constant during the reaction and hence the observation of saturation kinetics. The fact that saturation kinetics is observed in the presence of a slight excess of **1A** suggests that the step of coordination of alkyne to the catalyst has a significant energy barrier and the rate constant k_1 contributes to the rate of the reaction for low **[1A]**.

Experiments performed with **[1A]:[2B]** ratios varying from 1:1 to 11:1 at 322.8 K provided further evidence for saturation kinetics. The experiments pointed out that as the rate of the reaction did not have any dependence of the alkyne when the alkyne was present in more than 11 folds excess. This behaviour was also observed with the experiments carried out at a lower temperature (306.4 K), where the rate was observed to be independent of the **[1A]** after a 11 folds increase in the concentration of **1A**.

3.3.3 Mechanistic understanding of the hydrofluoroarylation reaction

The kinetic data obtained analysed by classical kinetic methods and by the reaction progress kinetic analysis both provided vital information about the reaction. Both analyses showed a first order dependence on the catalyst and the fluoroarene, suggesting that the step with the highest energy barrier involves one molecule of the catalyst (in its active form) and one molecule of **2B**. The kinetic data analysed by both methods showed that the alkyne did not have a direct role in the step with the highest energy barrier. However, the kinetic data pointed out that the reaction followed saturation kinetics with respect to **1A**.



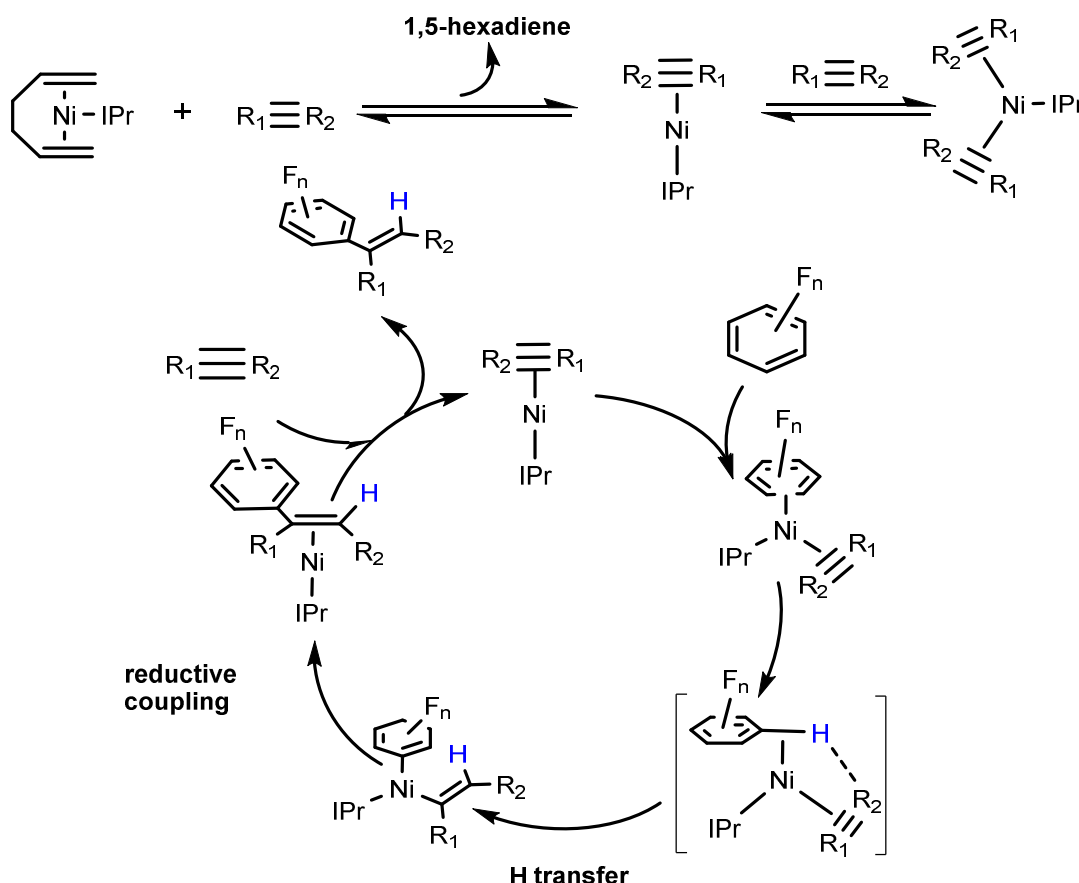
Scheme 3-7 Schematic diagram of a two substrate catalytic system.

The hydrofluoroarylation reaction can be compared to an enzymatic catalytic system (Scheme 3-7) where the second substrate **2** reacts with the catalytic intermediate which is a result of the binding on the first substrate **1** to the free catalyst **4**. The reaction follows a first order rate law with respect to **2B** in the presence of a small excess of **1A**. The equilibrium observed with **1A** and the catalyst (1,5-hexadiene)Ni(IPr) can be compared with the initial binding of the catalyst to the first substrate to give rise to the catalytic intermediate **5** in Scheme 3-7. The equilibrium step requires a slight excess of alkyne to exhibit saturation kinetics. This is observed by the saturation kinetics with respect to **1A** where the rate of the reaction increases with the increase in [**1A**] until an 8-10 fold excess and further increase in the concentration of **1A** has no effect

on the rate of the reaction. This suggests the coordination of alkyne to be in a pre-equilibrium step which precedes the attack of **2B**. This is comparable to the DFT calculation results obtained from the hydrofluoroarylation reaction catalysed by Ni-PR₃, where it was observed that the coordination of the alkyne was preferred to the coordination of fluoroarene in the presence of both.¹⁰

The analysis of the kinetic data of the hydrofluoroarylation reaction catalysed by (1,5-hexadiene)Ni(IPr) suggests a catalytic cycle similar to the one proposed by Perutz et al. The initial coordination of the alkynes replacing the 1,5-hexadiene ligand on the catalyst is added to the mechanism as a pre-equilibrium step. The catalytic cycle is initiated by the coordination of the alkyne and the fluoroarene attacks the Ni-IPr with the alkyne ligated to it. This is seen experimentally by the saturation kinetics similar to enzyme kinetics with respect to alkyne, and the DFT calculations performed on the reaction with the Ni-PR₃ species are also in agreement with this. The hydrogen transfer is postulated to occur via a ligand-to-ligand hydrogen transfer (LLHT) and not through a nickel hydride intermediate. This is based on the observation made in the DFT calculations, where the formation of the nickel alkyne complex is more favourable than to the formation of the nickel hydride. Since the initial coordination observed is that of the alkyne, the formation of the nickel hydride is not possible, hence the hydrogen transfer is proposed to occur via a LLHT. The hydrogen transfer occurring via a LLHT mechanism rather than the formation of the nickel hydride has been proposed in other similar mechanisms in the literature. This observation was made in the mechanistic studies of the hydroarylation of olefins catalysed by the complex, (norbornene)₂Ni(IPr). The calculations performed on the reaction suggested that the hydrogen is transferred via a H-shift where the proton is transferred from the arene to the alkene.¹⁷ The hydrofluoroarylation reaction performed with **1A** and **2B** catalysed by (1,5-hexadiene)Ni(IPr) did not exhibit the formation of a nickel hydride, although this could also be due to its low concentration preventing observation by NMR spectroscopy. The DFT calculation suggests a hydrogen transfer via LLHT when the catalytic

cycle is initiated by the alkyne, and the coordination of the alkyne to the nickel is more favourable than the formation of a nickel-hydride. This initial coordination of alkyne is seen in the kinetic data obtained experimentally and therefore this observation suggests LLHT to be the more likely pathway for hydrogen transfer in the catalytic cycle.



Scheme 3-8 Schematic diagram of the catalytic cycle proposed based on the kinetic analysis of the hydrofluoroarylation of alkynes.

The kinetic data obtained experimentally was observed to give a good fit to a preliminary model similar to the proposed catalytic cycle in Scheme 3-8 using the modelling and simulation program, Dynafit. The kinetic data fitted the model where **2B** reacts with the Ni(0) centre attached to only one alkyne. It was also observed that a model where the **2B** reacts with the Ni(0) centre attached to two alkynes to give the hydrofluoroarylation product, did not fit the kinetic data obtained experimentally. Nevertheless, the equilibrium between the mono-alkyne and bis-alkyne species which gives rise to

$[\text{CH}_3\text{C}\equiv\text{CC}(\text{CH}_3)_3]_2\text{Ni}(\text{IPr})$, was an essential step for the data to fit the model proposed. This observation is comparable to the results obtained from the DFT calculations performed on the hydrofluoroarylation reaction with Ni-PR_3 by Perutz et al.¹⁰ where an equilibrium was observed between the two species, mono and the bis-alkyne complexes, $\text{Ni}(\text{PMe}_3)(\text{MeC}\equiv\text{CMe})$ and $\text{Ni}(\text{PMe}_3)(\text{MeC}\equiv\text{CMe})_2$ with a slight preference for the mono alkyne complex, $\text{Ni}(\text{PMe}_3)(\text{MeC}\equiv\text{CMe})$, which was the active species that continued the catalytic cycle via coordination to the fluoroarene.¹⁰ Therefore although the mono-alkyne complex might be the active nickel species that continues with the catalytic cycle, the equilibrium between the mono and bis-alkyne nickel complexes exists and is significant. The slight preference for the mono-alkyne species over the bis-alkyne species can be explained by the steric factors that play a major role in the formation of Ni-alkyne complexes.¹⁸ Unlike the analogous alkene complexes, the nickel alkyne complexes tend to be reluctant to coordinate more alkynes in their coordination spheres due to the planar geometry adopted.¹⁸ This effect can be expected to be more pronounced in the case where the other ligand on nickel (the IPr in this case) is sterically demanding. The final reductive elimination step that results in the product and the regeneration of the catalyst is proposed to occur via a coordination of the alkyne. This suggestion is made based on the fact that the final step in the model used to fit the kinetic data was found to fit a model with the final coordination of the alkyne and does not fit when the final coordination is with the 1,5-hexadiene found in the reaction mixture.

3.4 Summary

The mechanisms of the hydrofluoroarylation reaction proposed by experimental and DFT calculations for nickel-phosphine complexes differ from one another. The initial coordination of the fluoroarene giving rise to a mechanism that proceeds by a nickel-hydride intermediate which then coordinates the alkyne and transfers the proton from the metal centre to the alkyne, was proposed based on experimental results by Nakao et al.⁹ The mechanism based on the results from the DFT calculations is initiated by the

coordination of the alkyne rather than the fluoroarene. This complex further undergoes a hydrogen transfer via LLHT rather than a nickel-hydride intermediate formation.¹⁰

In this chapter the kinetics of the hydrofluoroarylation reaction was studied using a nickel N-heterocyclic carbene complex, (1,5-hexadiene)Ni(IPr) as the catalyst and C₆F₅H and 4,4-dimethylpentyne as the substrates. The catalytic hydrofluoroarylation reaction resulting from the catalyst and the substrates mentioned before gave a system free of side reactions and free of paramagnetic species enabling in-situ data collection by NMR spectroscopy. The kinetic analysis exhibited evidence for an initial alkyne coordination. The reaction shows saturation kinetics with respect to alkyne and the rate determining step did not depend on the alkyne directly. The step involving the highest energy barrier showed a first order dependence on both the concentration of the fluoroarene and the catalyst. This initial coordination of the alkyne suggests a hydrogen transfer via a LLHT as the formation of the nickel alkyne complex is more favourable than the nickel hydride formation. In addition, the experimentally obtained data was found to fit a model with initial coordination of the alkyne, which subsequently leads to the coordination of the fluoroarene, which supports a hydrogen transfer via a LLHT mechanism as proposed by DFT calculations.

The kinetic analysis of the data obtained for the hydrofluoroarylation reaction catalysed by (1,5-hexadiene)Ni(IPr) is close to the mechanism proposed based on the DFT calculations performed for the same reaction catalysed by Ni-PR₃. However, in order to be able to make a more accurate comparison and to clearly understand the kinetic data and the model that fits the data obtained, it is necessary that the DFT calculations are repeated for the hydrofluoroarylation reaction catalysed by (1,5-hexadiene)Ni(IPr).

3.5 Reference

- (1) Halpern, J. *Inorg. Chim. Acta* **1981**, *50*, 11.
- (2) Atkins, P. W.; Walters, V.; De Paula, J. *Physical Chemistry*; Macmillan Higher Education, **2006**.

- (3) Blackmond, D. G. *Angew Chem Int Ed Engl* **2005**, *44*, 4302.
- (4) Strieter, E. R.; Blackmond, D. G.; Buchwald, S. L. *J. Am. Chem. Soc.* **2005**, *127*, 4120.
- (5) Shekhar, S.; Ryberg, P.; Hartwig, J. F.; Mathew, J. S.; Blackmond, D. G.; Strieter, E. R.; Buchwald, S. L. *J. Am. Chem. Soc.* **2006**, *128*, 3584.
- (6) Mathew, J. S.; Klussmann, M.; Iwamura, H.; Valera, F.; Futran, A.; Emanuelsson, E. A. C.; Blackmond, D. G. *The Journal of Organic Chemistry* **2006**, *71*, 4711.
- (7) Perrin, C. L.; Dwyer, T. J. *Chem. Rev. (Washington, DC, U. S.)* **1990**, *90*, 935.
- (8) Lineweaver, H.; Burk, D. *J. Am. Chem. Soc.* **1934**, *56*, 658.
- (9) Kanyiva, K. S.; Kashihara, N.; Nakao, Y.; Hiyama, T.; Ohashi, M.; Ogoshi, S. *Dalton Trans.* **2010**, *39*, 10483.
- (10) Guihaumé, J.; Halbert, S.; Eisenstein, O.; Perutz, R. N. *Organometallics* **2012**, *31*, 1300.
- (11) Hatnean, J. A.; Beck, R.; Borrelli, J. D.; Johnson, S. A. *Organometallics* **2010**, *29*, 6077.
- (12) Wu, J.; Faller, J. W.; Hazari, N.; Schmeier, T. J. *Organometallics* **2012**, *31*, 806.
- (13) Nakao, Y.; Kashihara, N.; Kanyiva, K. S.; Hiyama, T. *J. Am. Chem. Soc.* **2008**, *130*, 16170.
- (14) Rosenthal, U.; Pulst, S.; Kempe, R.; Pörschke, K.-R.; Goddard, R.; Proft, B. *Tetrahedron* **1998**, *54*, 1277.
- (15) Crabtree, R. H. In *The Organometallic Chemistry of the Transition Metals*; John Wiley & Sons, Inc.: **2005**, p 235.
- (16) Widegren, J. A.; Finke, R. G. *J. Mol. Catal. A: Chem.* **2003**, *198*, 317.
- (17) Bair, J. S.; Schramm, Y.; Sergeev, A. G.; Clot, E.; Eisenstein, O.; Hartwig, J. F. *J. Am. Chem. Soc.* **2014**, *136*, 13098.
- (18) Ozin, G. A.; McIntosh, D. F.; Power, W. J.; Messmer, R. P. *Inorg. Chem.* **1981**, *20*, 1782.

CHAPTER FOUR

INTERMOLECULAR HALOGEN BONDING INTERACTIONS OF NICKEL HALIDE COMPLEXES AND THEIR PENDANT HALOGEN BOND DONORS IN THE SOLID STATE

INTERMOLECULAR HALOGEN BONDING INTERACTIONS OF NICKEL HALIDE COMPLEXES AND THEIR PENDANT HALOGEN BOND DONORS IN THE SOLID STATE

4.1. Introduction

Non-covalent interactions themselves are vital for the very existence of life.¹ Understanding non-covalent interactions is essential due to the central roles played by these interactions in chemistry and biology, specifically in the fields of crystal design, molecular recognition, topochemical reactions, molecular conductors, liquid crystals and in structural biology.²⁻⁴ Halogens are found at the periphery of a wide number of organic and inorganic molecules, and are therefore available for engagement in non-covalent interactions. Depending on the environment halogens are in, they can exhibit Lewis acidic or Lewis basic character, and this enables them to form strong directional intermolecular forces, such as hydrogen bonding and halogen bonding.³ Hydrogen bonding is the most commonly occurring non-covalent interaction and has been known and well documented for many decades, halogen bonding on the other hand, is a relatively new phenomenon, which has now seen more than two flourishing decades.⁵ Halogen bonding is analogous to hydrogen bonding in many ways. The preference for a linear R-X...Y-Z interaction is similar to the observed hydrogen bonding interactions.^{6,7}

4.1.1 A brief look into the history of halogen bonding interactions

Since the 19th century addition complexes of Cl₂, Br₂ and I₂ to Lewis bases has been observed. The interaction observed in these cases were referred to as charge-transfer or electron donor-acceptor interactions.^{4,6} It was later observed that in addition to dihalogens, organic halides too formed similar addition complexes.⁸ The earliest observation reported of a halogen bonding interaction can be tracked to 1863 by Guthrie, in which he described the formation of an addition complex I₂...NH₃.⁹

The first X-ray crystallographic study demonstrating halogen bonding interactions was published by Hassel and Hvoslef in 1954 on a bromine-1,4-dioxane adduct (Figure 4-1).¹⁰ The intermolecular distance between the oxygen atom of the 1,4-dioxane and the bromine atom was found to be 2.71 Å, which was remarkably shorter than the sum of the van der Waals radii 3.35 Å, suggesting a strong non-covalent interaction.¹⁰

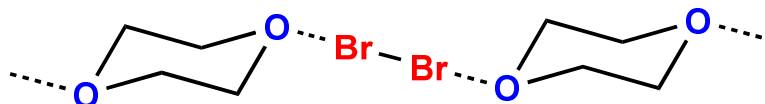


Figure 4-1 Intermolecular halogen bond leading to the formation of the 1:1 adduct of bromine and 1,4-dioxane.¹⁰

The review on halogen bonding interactions by Bent in 1968, intrigued by the presence of such interactions and the crystal structure evidence of halogen bonding interactions by Hassel, is one of the earliest discussions presented on the subject.⁸ The review compares these interactions to hydrogen bonding interactions and the possibility of the presence of such interactions in metal halides in crystals structures.⁸

4.1.2 General features and applications of halogen bonding interactions

Halogens due to their high electronegativity can act as hydrogen bond acceptors or Lewis bases. However, if the halogens are attached to more electron withdrawing environment the halogen atom becomes the Lewis acid and can interact with Lewis bases.⁴ This interaction of halogens with Lewis bases is termed halogen bonding. All five halogens are capable of halogen bonding interactions although the interactions are much less pronounced and not common with less polarizable fluorine and more prominent in larger more polarizable halogens such as iodine and hence the halogen bonding donor

ability decreases $I > Br > Cl > F$.^{4,11} The electron deficient halogen atom acts as the halogen bond donor and the Lewis base acts as the halogen bond acceptor.^{1,4}

An IUPAC task group recommended the definition of halogen bonding interaction as follows;

*“A halogen bond $R-X\cdots Y-Z$ occurs when there is evidence of a net attractive interaction between an electrophilic region on a halogen atom X belonging to a molecule or a molecular fragment $R-X$ (where R can be another atom, including X , or a group of atoms) and a nucleophilic region of a molecule, or molecular fragment, $Y-Z$.”*¹¹

Here the halogen bond donor X , has an electron deficient region and is covalently bound to the atom or molecule, R . The halogen bond acceptor, Y could be an anion or a nucleophilic region, such as lone pair electrons or the π -bond electron pair of the $Y-Z$.¹¹ The halogen bond is generally denoted by three dots between the XB donor and XB acceptor.¹¹

The halogen bonding interaction increases with the decrease in electronegativity of X and the increase in the electron withdrawing ability of R .^{4,11} The characteristic features of a halogen-bonded adduct is the decrease in inter atomic distance between X and Y compared to the sum of the van der Waals radii and the $R-X\cdots Y$ angle tends to be linear (180°).¹¹ Electrostatic attraction is the commonly encountered force in these interactions, but, the dominant force may vary from case to case.¹¹

These XB adducts are often observed to undergo reactions when subjected to different physical conditions and therefore often such halogen bonding interactions are considered as intermediates in chemical reactions. This is seen in the reaction that occurs between dihalogens and alkenes.¹

In the halogen bonding interaction between two halogens of the nature $R-X\cdots X'-R'$, two types of geometries have been observed to be preferred in the literature referred to as type I and type II.^{7,12} Type I geometry is when the two angles θ_1 , θ_2 are equal to each other (θ_1 and θ_2 are the angles $R-X\cdots X'$ and $X\cdots X'-R'$ respectively).¹² The points of interaction of the halogens in type I geometry have the same electrostatic potentials and hence could give rise to electrostatic repulsions. However, a study done by Awwadi and co-workers show that this type of interaction is electrostatically favourable when the angles are in the range, $140 < \theta_1 = \theta_2 < 160$.¹² Type II interactions occur when $\theta_1 = 90^\circ$ and $\theta_2 = 180^\circ$, which agrees with the fact that at the point of interaction the halogens will have different electrostatic potentials.^{7,12}

The usage of halogen bonding interactions in supramolecular structures and solid state was pioneered by the studies done on the self-assembled co-crystals of perfluorocarbon iodides and aliphatic or aromatic amines. The reduction of the van der Waals radii of the $C(\text{PFC})-I\cdots N$, was around 20% indicating a strong halogen bonding interaction between them.³ Halogen bonding involving metal centres and inorganic motifs has also been demonstrated in recent past. One of the earliest reports in the literature on ionic halogen bonding network was reported by Willett and co-workers in 2003.¹³ A series of complexes exhibiting $C-X\cdots X'-M$ ($M = \text{Pt}, \text{Pd}$, $X = \text{Cl}, \text{Br}$; $X' = \text{Cl}, \text{Br}$) interactions was demonstrated by Brammer and co-workers in 2005 (Figure 4-2).¹⁴

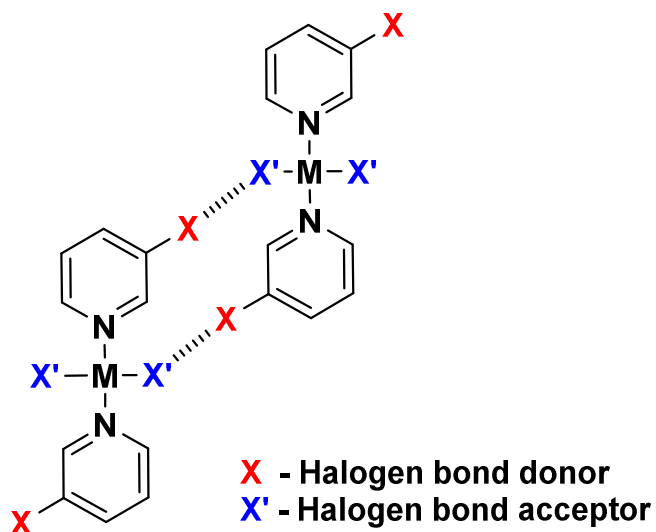


Figure 4-2 Halogen bonding interactions exhibited in metal systems demonstrated by Brammer and co-workers.⁷

More recently a series of pincer palladium halides (PCP)PdX (PCP = 2,6-bis[(di-tert-butylphosphino)methyl]phenyl; X = Br, Cl and I) co-crystallized with various XB donors were reported by Rissanen exhibiting halogen bonding interactions in solid state (Figure 4-3).³ The study performed by Rissanen and co-workers obtained co-crystallised structures of pincer palladium bromide with halogen bond donors I₂, 1,4-C₆F₄I₂ and I(CF₂)₄I.³ The crystal structures exhibiting halogen bonding interactions I₂ and 1,4-C₆F₄I₂ were obtained for the pincer palladium chloride complex and only the crystal structure halogen bonded to I₂ was obtained for the pincer palladium iodide complex.³ The metal complexes showed the general trend of the strength of the halogen bonding interaction decreasing in the order Cl⁻ > Br⁻ > I⁻.³ Out of the three XB donors used, I₂ showed the highest interactions (ranging from 25-19% reduction in the sum of the van der Waals radii from palladium chloride to iodide).³

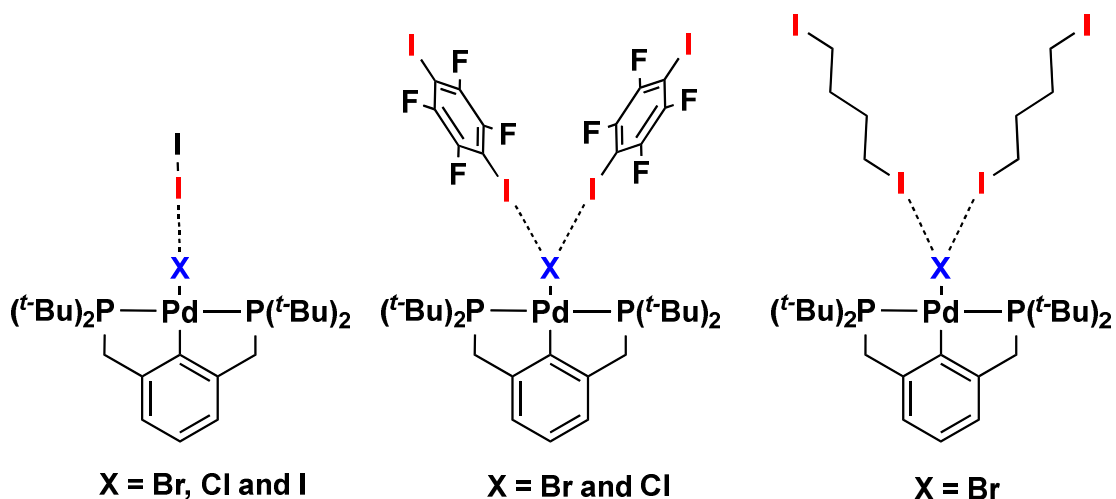


Figure 4-3 Pincer palladium halides acting as halogen bond acceptors with various halogen bond donors.³

Another area of interest that has recently emerged is the application of halogen bonding interactions in solution state including anion recognition and binding.¹⁵⁻¹⁷ One of the earliest works of building organised receptors which include the halogen bond donors for ion-pair recognition was carried out by Resnati, Metrangolo et al.^{4,18} The receptor was able to interact with alkali metals through its podand functionality while the iodoperfluoroarene of the receptor was capable of forming halogen bonding interactions with the anions (Figure 4-4).¹⁸ Compared to the structurally similar receptor which lacks the halogen bond donor, the receptor with the halogen bond donor showed a ~20 fold increase in the affinity in NaI which was determined by ¹H-NMR spectroscopy.^{4,18}

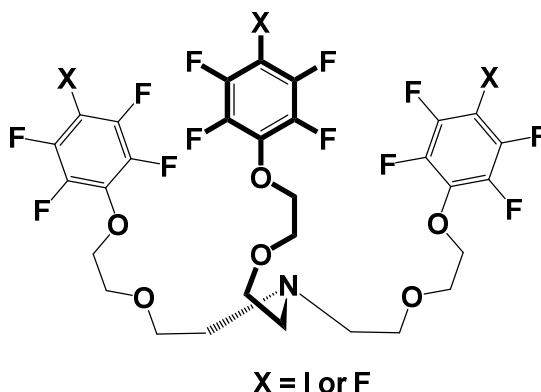


Figure 4-4 Ion-pair recognition receptor designed with podand groups and XB donor site.¹⁸

Taylor and co-workers have demonstrated the use of neutral urea-based receptors which bind to certain anions using both XB and HB interactions.¹⁹ UV-vis and NMR spectroscopic titrations were used to determine the influence of the halogen bonding interaction in the anion affinity by comparing with a receptor where the iodine (XB donor) has been replaced by fluorine.¹⁹

Receptors for anion recognition in polar solvents are more challenging due to the competition from anion solvation.⁴ However, this has been overcome by the use of positively charged receptors in the past.⁴ This was demonstrated by Beer et al. for the cationic receptor bromoimidazoliophane which displayed selective binding to bromide in a polar mixture of CD₃OD-D₂O.²⁰ A comparison conducted using the structurally similar unsubstituted imidazoliophane showed the enhanced anion affinity created by the bromo substituents. The X-ray crystallographic data showed a bidentate halogen bonding interaction, which was demonstrated by a ~14% reduction of the sum of the van der Waals radii between Br...Br.^{4,20}

Recently, Beer et al. were successful in demonstrating the application of halogen bonding interaction in anion binding in water.¹⁶ The work was carried out by comparing the halogen bonding and hydrogen bonding interactions in anion binding of structurally related HB and XB donor receptors.¹⁶ The magnitude of anion binding affinity was shown to double with halogen

bonding interactions in water, which was shown by the possibility of halide recognition in water by acyclic mono-charged XB receptors.¹⁶ The determination of the anion binding with structurally similar XB and HB bond donor receptors were carried by using ¹H-NMR spectroscopic titrations, varying the concentration of various anions (Cl⁻, Br⁻, I⁻ and SO₄²⁻).¹⁶

Halogen bonding interactions have been studied in solution state using group 10 metal fluorides of Ni, Pd and Pt, the details of which is discussed further in the chapter to follow.^{2,21} For the purpose of understanding these interactions in the solid state, a system which demonstrates these interactions in the solid state is needed, crystal structures that would show intermolecular halogen bonding networks. In fact, excluding encapsulated host-guest systems, this reluctance of weakly interacting molecules to co-crystallize is common.²²

Although halogen bonding interactions in metal-halide systems are well known for bromides, chlorides and iodides, metal-fluoride...iodine interactions in the solid state are still absent in the literature, this is despite the fact that the halogen bonding interactions would be much more pronounced when the iodine acts as the halogen bond donor and metal fluoride acts as the Lewis base. Previous attempts to co-crystallise the group 10 metal fluoride complexes with halogen bond donors have been unsuccessful in the Perutz group. As a solution to this, self-complementary molecules that have the halogen bond acceptor and the donor on the same molecule were designed for this purpose (Figure 4-5).

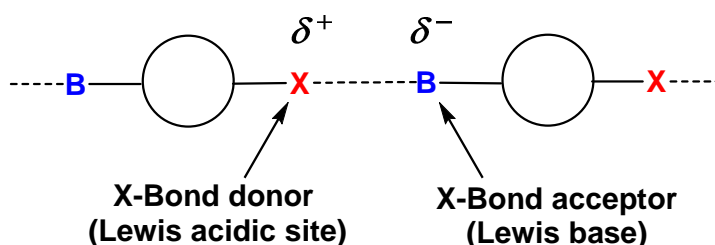
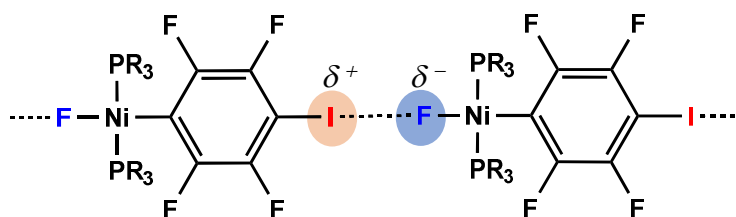


Figure 4-5 Intermolecular halogen bonding network in self-complementary systems.

The model designed for this purpose was a Ni-F with a halogen bond donor atom on the backbone of the molecule, which would enable intermolecular

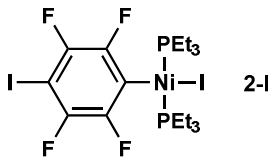
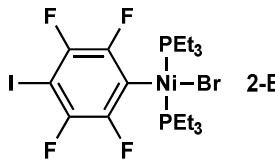
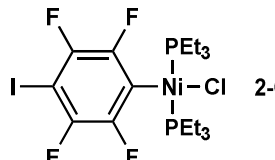
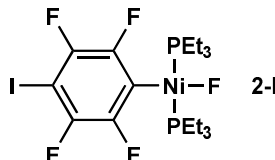
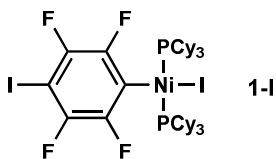
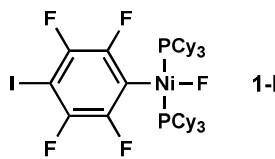
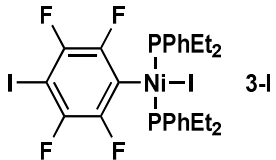
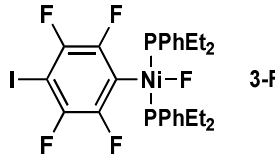
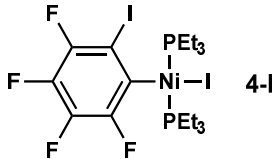
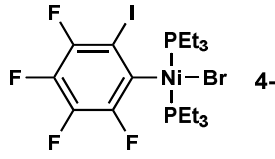
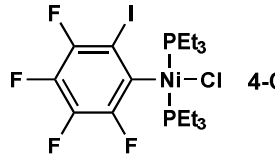
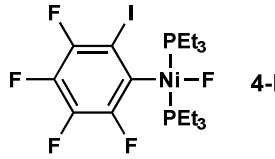
halogen bond networks with the XB acceptor, the nickel-fluoride (Scheme 4-1).



Scheme 4-1 Structural motif targeted in this study that shows the envisaged intermolecular halogen bonding interaction.

A simple synthetic route to arrive at such a system was to perform an oxidative addition on one of the carbon-iodine bonds of diiodotetrafluorobenzene giving rise to a nickel iodide and then convert the iodide into a nickel fluoride by a fluorinating agent. This would result in a molecule with a halogen bond acceptor, the nickel fluoride and a halogen bond donor, the iodine on the backbone of the molecule. A series of complexes with different halogen bond acceptors and different positions of the halogen bond donor and different phosphine groups were prepared to study the halogen bonding interactions in the solid state (Table 4-1).

Table 4-1 Complexes prepared to study the halogen bonding interactions in the solid state.

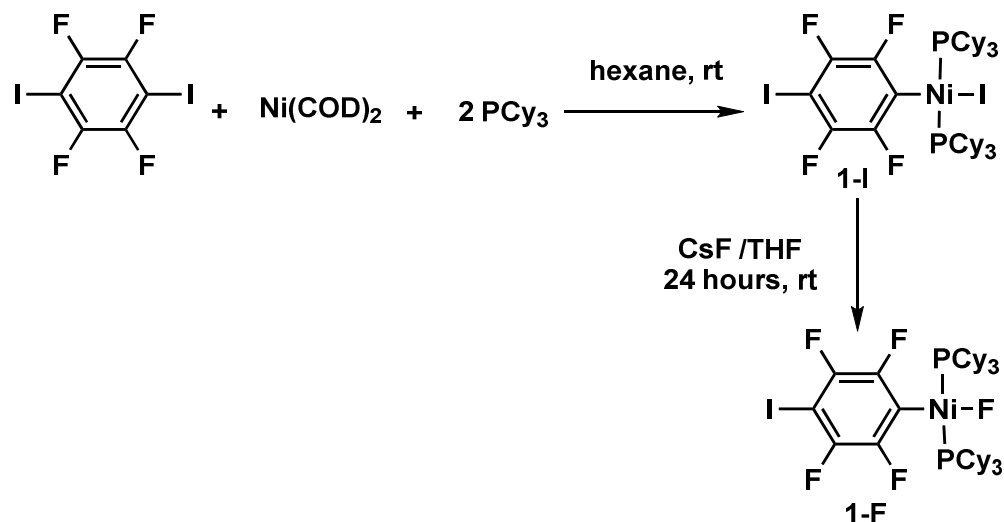
		Iodide	Bromide	Chloride	Fluoride
(1,4-C ₆ F ₄ I ₂)	Triethyl phosphines	 2-I	 2-Br	 2-Cl	 2-F
	Tricyclohexyl phosphines	 1-I			 1-F
	Diethylphenyl phosphine	 3-I			 3-F
(1,2-C ₆ F ₄ I ₂)	Triethyl phosphine	 4-I	 4-Br	 4-Cl	 4-F

4.2. Results

4.1.3 Synthesis and characterization of tricyclohexyl phosphine ligated complexes *trans*-Ni(X)(PCy₃)₂(2,3,5,6-C₆F₄I), X = I, F

4.2.1.1. Synthesis of tricyclohexyl phosphine ligated complexes *trans*-Ni(X)(PCy₃)₂(2,3,5,6-C₆F₄I), X = I, F

Previous studies in the Perutz group have demonstrated that the oxidative addition of carbon-fluorine bonds of fluorinated arenes to nickel centres is facilitated by the presence of electron rich phosphines, for example PCy₃. Therefore our study began by examining the reactivity of tricyclohexyl phosphine ligated nickel species. A solution of Ni(PCy₃)₂ was prepared by reacting Ni(COD)₂ with 2 equivalents of PCy₃ in hexane at room temperature and subsequent addition of 1,4-diiodotetrafluorobenzene immediately gave rise to a red-brown solution (Scheme 4-2). Given the successful generation of the nickel iodide, it was aimed to convert this directly to the fluoride by use of a suitable fluorinating agent. The reaction of *trans*-Ni(I)(PCy₃)₂(2,3,5,6-C₆F₄I) (**1-I**) with caesium fluoride in THF gave rise to a colour change from red to yellow in 5 hours at 50 °C (or alternatively under ambient conditions for 24 hours). (Scheme 4-2).



Scheme 4-2 Formation of **1-I** and **1-F**.

4.2.1.2. Characterisation of *trans*-Ni(I)(PCy₃)₂(2,3,5,6-C₆F₄I)

The resulting red-brown solid was analysed by NMR spectroscopy and LIFDI mass spectrometry at room temperature. The ³¹P-NMR spectrum of the reaction mixture showed two singlet resonances at δ 19.5 and 14.4, in the ratio of 5:1, suggesting two species (Figure 4-6).

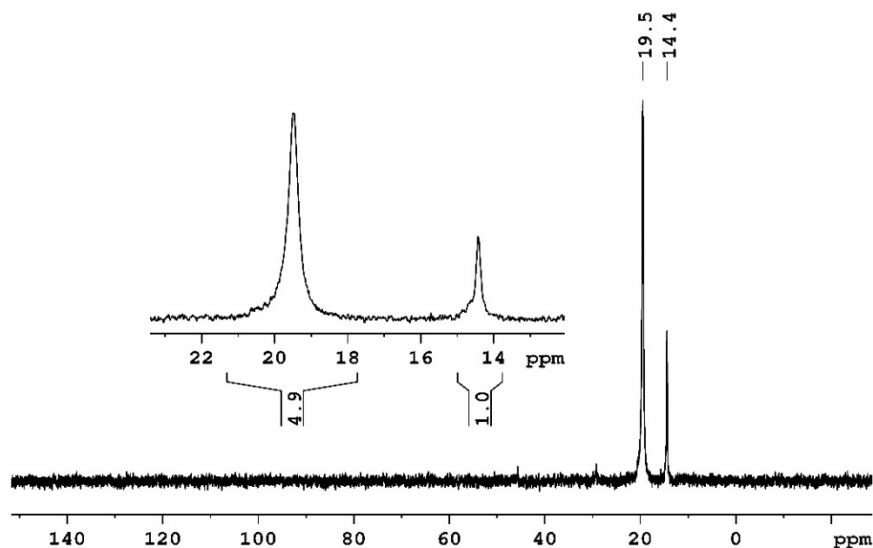


Figure 4-6 ³¹P-NMR (202 MHz) spectrum of the reaction of 1,4-C₆F₄I₂ with Ni(COD)₂ and PCy₃ in C₆D₆.

The LIFDI mass spectrum showed a base peak at 1020.20 (100%) which corresponds to the molecular ion [M]⁺ peak of *trans*-Ni(I)(PCy₃)₂(2,3,5,6-C₆F₄I) (**1-I**). The other peaks were at *m/z* 1022.21, 1023.22 and 1024.22, consistent with the isotopic pattern of **1-I**. A *trans* geometry could be assigned for the two tricyclohexyl phosphine units in **1-I** as suggested by the singlet at δ 19.5 in the ³¹P-NMR spectrum. The resonance at δ 14.4 was due to double oxidative addition on both the C-I bonds of 1,4-C₆F₄I₂, resulting in [Ni(I)(PEt₃)₂]₂(C₆F₄). The ¹⁹F-NMR spectrum shows a singlet resonance at δ -124.7 corresponding to the fluorine atoms on the aromatic ring. The formation of the species of double activation to give [Ni(X)(PR₃)₂]₂(C₆F₄) is confirmed in later sections by LIFDI mass spectrometry and X-ray crystallographic data.

4.2.1.3. Characterization of *trans*-Ni(F)(PCy₃)₂(2,3,5,6-C₆F₄I)

The reaction mixture of **1-I** with caesium fluoride in THF was allowed to settle and the decanted solution was purified by removing the excess caesium fluoride, by re-dissolving the solid in benzene and decanting the solution. The product obtained was analysed by NMR spectroscopy and LIFDI mass spectrometry.

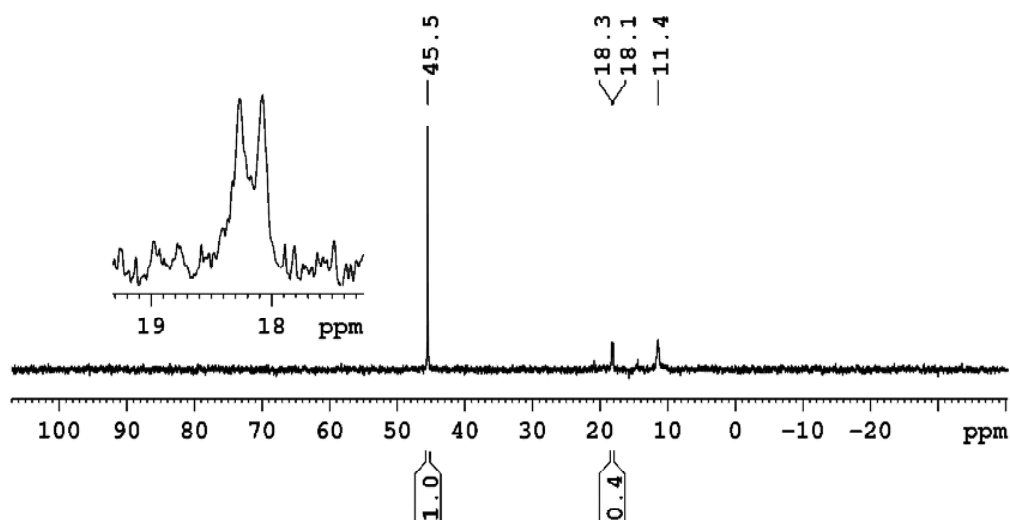


Figure 4-7 ³¹P-NMR (202 MHz) spectrum of the reaction of **1-I** with CsF in C₆D₆.

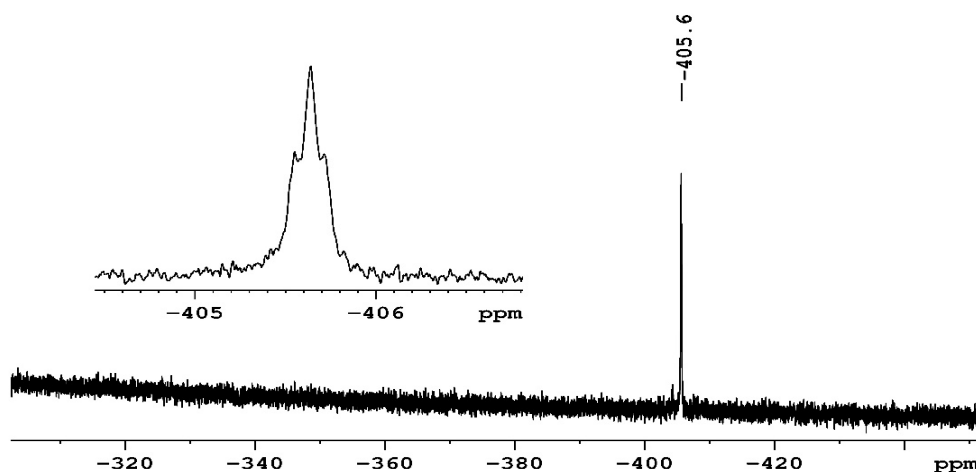


Figure 4-8 ¹⁹F-NMR (470 MHz) spectrum (in the region δ -300 to -440) of the reaction of reaction of **1-I** with CsF in C₆D₆.

The ^{19}F -NMR spectrum exhibited a triplet resonance at δ -405.6, coupled to the two phosphorus atoms of the PCy_3 units, with coupling constants of $J = 38$ Hz, indicating the formation of a nickel-fluoride (Figure 4-7). The ^{31}P -NMR spectrum exhibited a doublet resonance at δ 18.2, coupled to the fluoride with a coupling constant of $J = 38$ Hz (Figure 4-8). From the ^{19}F -NMR spectrum, and the ^{31}P -NMR spectrum, it could be concluded that the reaction of the *trans*-Ni(I)(PCy_3)₂(C_6F_4) with CsF gave rise to, *trans*-Ni(F)(PCy_3)₂(2,3,5,6- C_6F_4) (**1-F**), and the two phosphine units could be assigned a *trans* geometry. The LIFDI mass spectrum showed a molecular ion peak at (m/z) 912.29, which corresponds to the molecular mass of **1-F**. The other peaks were at m/z 913.28, 914.30, 915.28 and 916.26 which matches the isotopic pattern of **1-F**.

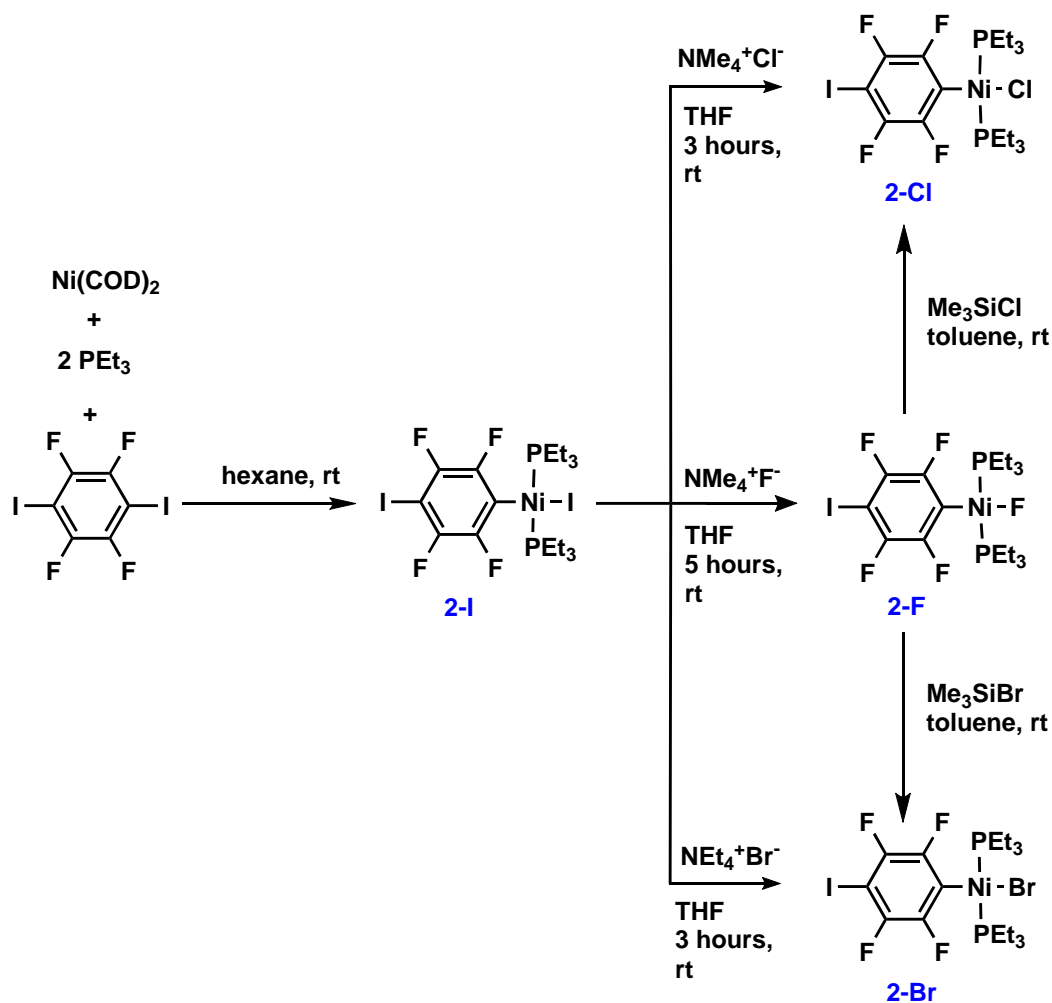
The ^{31}P -NMR spectrum showed that the product of interest, **1-F** formed in low yields and the major product exhibited a peak at δ 45.5 in the ^{31}P -NMR spectrum. A control reaction with the 1,4-diodotetrafluorobenzene and PCy_3 heated at 50 °C gave rise to white precipitate that showed a similar peak at δ 45.4 in the ^{31}P -NMR spectrum, suggesting that this species was not a Ni containing species, but rather a species formed by the reaction of the fluoroarene and the phosphine, probably a phosphonium salt of the nature [$\text{PCy}_3(\text{C}_6\text{F}_4)$]⁺ I⁻.

If the peak in the ^{31}P -NMR spectrum was due to [$\text{PCy}_3(\text{C}_6\text{F}_4)$]⁺ I⁻, changing the phosphine to a less basic phosphine should lower the formation of this species. Hence, the phosphine was changed from PCy_3 to PEt_3 .²³ In addition to this, there were also other advantages of changing the phosphine to triethylphosphine. Ni(F)(PEt_3)₂(C_6F_4) would be easier to crystallise than Ni(F)(PCy_3)₂(C_6F_4). Also the halogen bonding interaction studies using group 10 metals have been done using PEt_3 as the phosphine, and the new studies would be therefore comparable to the earlier studies.

4.1.4 Synthesis and characterization of *trans*-Ni(X)(PEt₃)₂(2,3,5,6-C₆F₄I), X = I, Br, Cl, F

4.2.1.4. Synthesis of *trans*-Ni(X)(PEt₃)₂(2,3,5,6-C₆F₄I), X = I, Br, Cl, F

To suppress the double oxidative addition on diiodotetrafluorobenzene, the tricyclohexyl phosphine was replaced with triethyl phosphine. A solution of Ni(PEt₃)₂(COD)²⁴ was prepared at room temperature by reacting Ni(COD)₂ with 2 equivalents of PEt₃ in hexane. The reaction of 1,4-diiodotetrafluorobenzene with the freshly prepared Ni(PEt₃)₂ in hexane at room temperature immediately gave rise to a red solution from which the product precipitated as a brown-red solid (Scheme 4-3). In successive independent reactions, the nickel iodide was converted to the fluoride, chloride and bromide using suitable fluorinating, chlorinating and brominating agents respectively (Scheme 4-3).



Scheme 4-3 The formation of complexes **2-I**, **2-F**, **2-Cl** and **2-Br**.

4.2.1.5. Characterization of *trans*-Ni(I)(PEt₃)₂(2,3,5,6-C₆F₄)

The precipitated brown-red solid from the reaction of $\text{Ni(PEt}_3)_2$ with 1,4-diodotetrafluorobenzene in hexane was washed with cold pentane and analysed by NMR spectroscopy and LIFDI mass spectrometry at room temperature. The change of the phosphine from PCy_3 to PEt_3 brought significant improvement in the yields of both steps, the nickel-iodide and the fluoride formation. The reaction resulted in *trans*-Ni(I)(PEt₃)₂(2,3,5,6-C₆F₄) **2-I** as the major product in a good yield (84%).

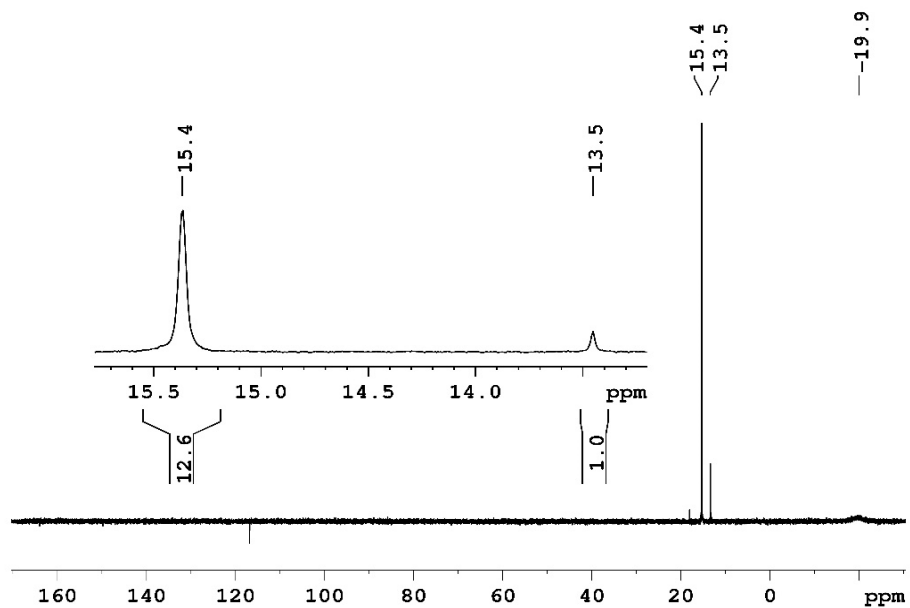


Figure 4-9 ^{31}P -NMR (202 MHz) spectrum of **2-I** in C_6D_6 .

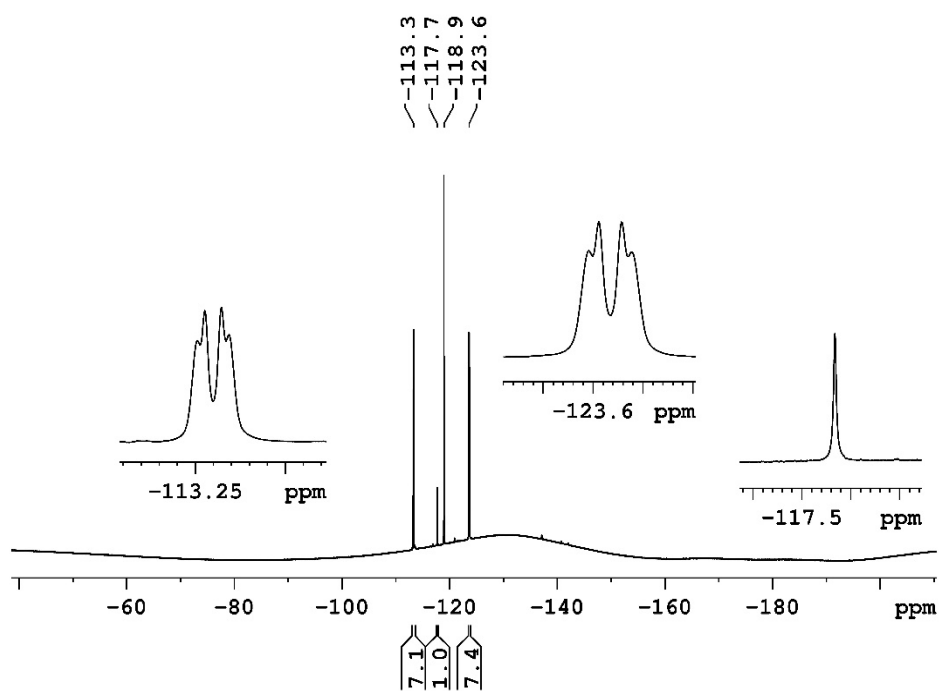


Figure 4-10 ^{19}F -NMR (470 MHz) spectrum of **2-I** in C_6D_6 .

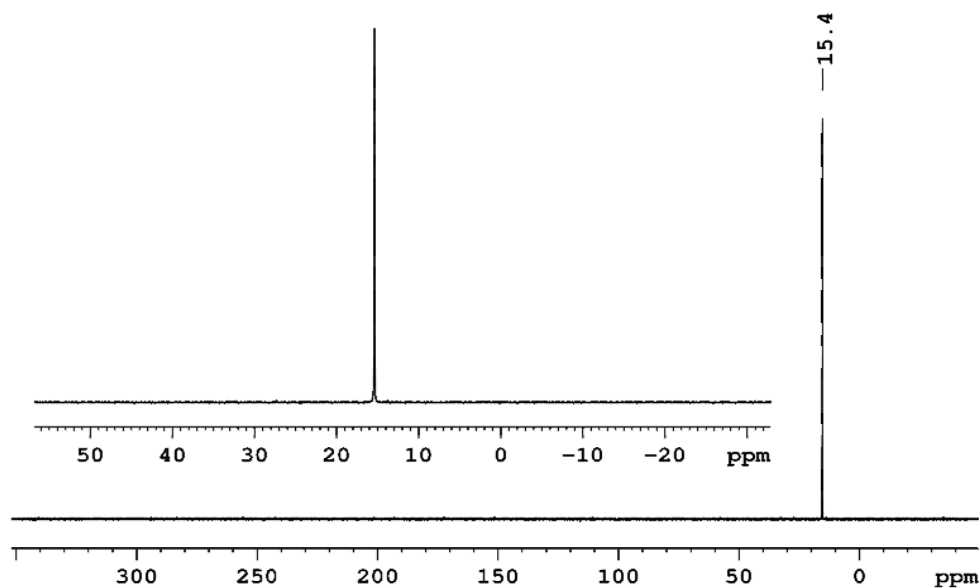


Figure 4-11 ^{31}P -NMR (202 MHz) spectrum of **2-I** in C_6D_6 after purification

The ^{31}P -NMR spectrum showed a singlet at δ 15.4 for the two phosphorus atoms in chemically and magnetically equivalent environment of the major product **2-I**, and hence a trans geometry could be assigned for the two phosphine groups on nickel. (Figure 4-9). The fluorine atoms of the aromatic ring of **2-I** were seen in the ^{19}F -NMR spectrum as two second order multiplets, AA'XX' at δ -113.3 and δ -123.6, resulting from the ortho and para coupling of the neighbouring magnetically inequivalent fluorine atoms on the ring (Figure 4-10). The additional peak observed at δ -118.9, is due to the excess of 1,4- $\text{C}_6\text{F}_4\text{I}_2$ from the reaction. The peak at 695.93 in the LIFDI mass spectrum was identified as the molecular ion $[\text{M}]^+$ base peak (100%) of *trans*-Ni(I)(PEt₃)₂(2,3,5,6- $\text{C}_6\text{F}_4\text{I}$). The other peaks were at m/z 696.92, 697.92, 698.93 and 699.93 corresponding to the isotopes of **2-I**. In addition to this the ^{31}P -NMR spectrum showed a singlet at δ 13.5, which was due to a minor product resulting from the reaction (Figure 4-9). The ^{19}F -NMR spectrum too displayed a singlet at δ -117.7 (Figure 4-10). This species was identified as the *trans*-[Ni(I)(PEt₃)₂]₂(2,3,5,6- C_6F_4), which would arise from the oxidative addition of both the iodine atoms on the 1,4-diiodotetrafluorobenzene (Figure 4-12). The symmetrical compound

Halogen bonding interaction studies in solid state *trans*-[Ni(I)(PEt₃)₂]₂(2,3,5,6-C₆F₄) agrees with the singlet observed in the ³¹P-NMR spectrum and the singlet seen in the ¹⁹F-NMR spectrum. The identity of this species was demonstrated by the peak at 990.17 in the LIFDI mass spectrum which corresponds to the molecular ion [M]⁺ base peak (100%) of *trans*-[Ni(I)(PEt₃)₂]₂(2,3,5,6-C₆F₄). The other peaks were at m/z 991.18, 992.17, 993.17, 994.17, 995.17 and 996.16 corresponding to the isotopes of *trans*-[Ni(I)(PEt₃)₂]₂(2,3,5,6-C₆F₄) (Figure 4-13).

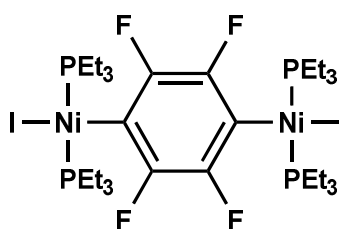


Figure 4-12 *trans*-[Ni(I)(PEt₃)₂]₂(2,3,5,6-C₆F₄)

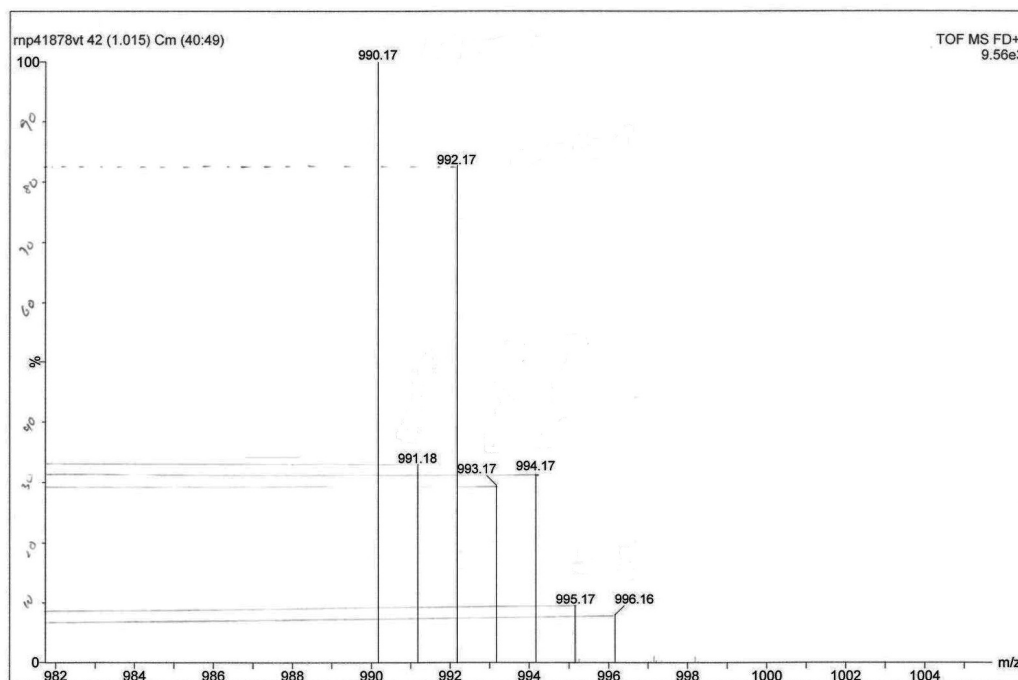


Figure 4-13 LIFDI mass spectrum showing the isotopic pattern of *trans*-[Ni(I)(PEt₃)₂]₂(2,3,5,6-C₆F₄) (see appendix for calculated spectrum of C₃₀H₆₀F₄Ni₂P₄I₂).

4.2.1.6. X-ray crystallographic studies of 2-I

Layering of a saturated solution of **2-I** in THF, with hexane gave rise to dark red crystals at the interface of the two solvents at room temperature suitable for X-ray crystallographic studies (Figure 4-14). The X-ray crystallographic analysis of the single crystal confirmed the structure of **2-I**. The nickel centre exhibited a square planar geometry consistent with its +2 oxidation state. The square planar geometry around the metal centre consisted of two PEt₃ groups trans to each other and the iodide and the C₆F₄I trans to each other. Selected intramolecular bond lengths are given in Table 4-2. The intermolecular distance between the nickel iodide and the iodine on the aromatic ring was observed to be 3.4970(6) Å. The Ni-I(1)-I(2) angle was observed to be 139.2°.

Table 4-2 Selected bond lengths (Å) and angles (°) of **2-I**.

I2-C4	2.093(6)	C6-C1	1.376(9)
Ni1-P1	2.224(2)	F1-C2	1.341(7)
Ni1-I1	2.5221(9)	F2-C3	1.350(7)
Ni1-C1	1.877(6)	C4-I2-I1	168.0(2)
P2-C17	1.838(7)	I2-I1-Ni1	139.2(2)
C5-C6	1.381(8)	C15-P2-C13	103.3(3)
C5-C4	1.394(9)	I1-Ni1-C1	178.3(2)
C13-C14	1.51(1)	P1-Ni1-P2	178.33(7)

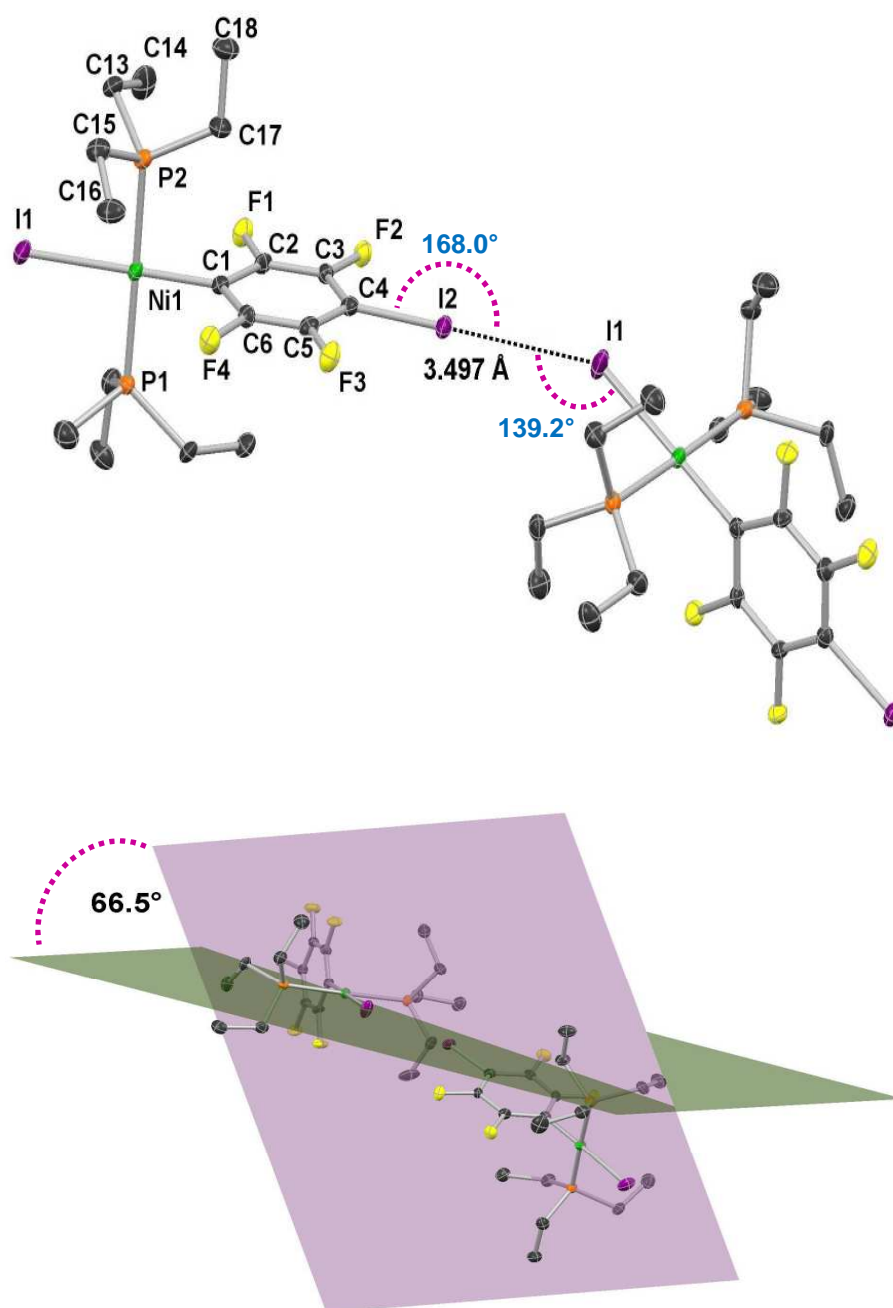


Figure 4-14 (Top) Molecular structure of **2-I**. Thermal ellipsoids set at 50% level and hydrogen atoms are omitted for clarity. (Below) Torsional angle between the two adjacent metal centre planes of **2-I**.

4.2.1.7. Characterization of *trans*-Ni(F)(PEt₃)₂(2,3,5,6-C₆F₄I)

The reaction of *trans*-Ni(I)(PEt₃)₂(2,3,5,6-C₆F₄I) with tetramethylammonium fluoride in THF gave a colour change from red to yellow in 5 hours at room temperature. The reaction mixture was passed through a short column of Celite inside the glove-box, and the unreacted tetramethylammonium fluoride subsequently removed by precipitating from benzene. The residual unreacted **2-I** was removed by washing with pentane to leave a yellow solid isolated in 71% yield (Scheme 4-4).

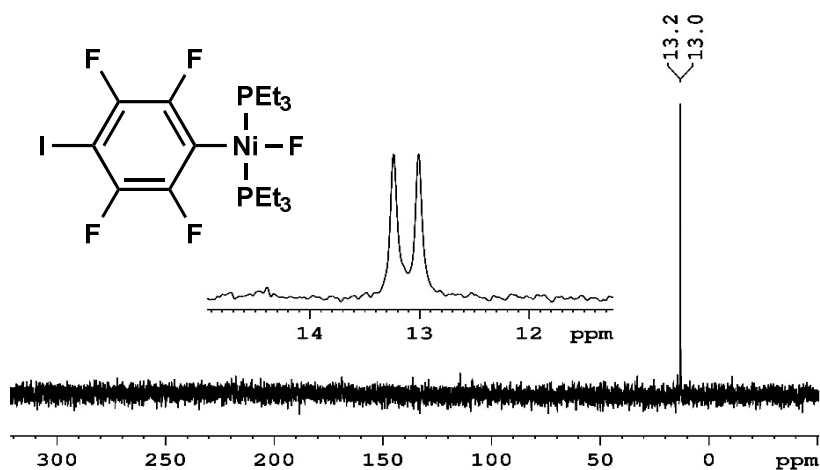


Figure 4-15 ³¹P-NMR (202 MHz) spectrum of **2-F** in C₆D₆.

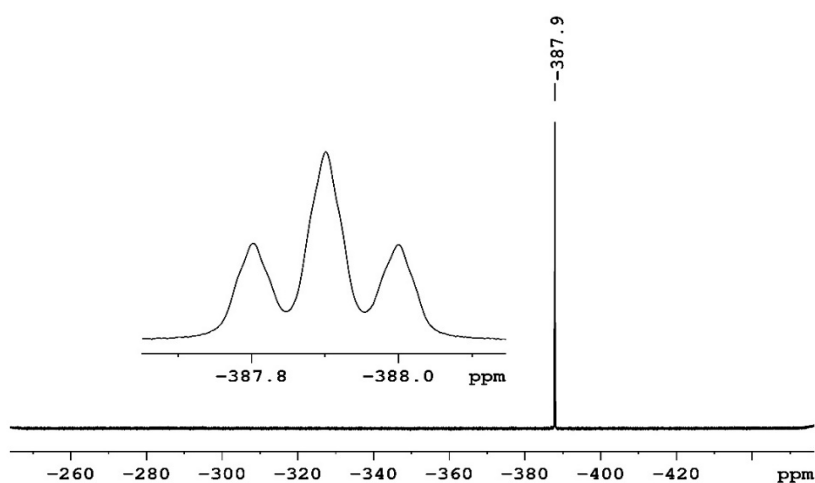


Figure 4-16 ¹⁹F-NMR (470 MHz) spectrum of **2-F** in C₆D₆.

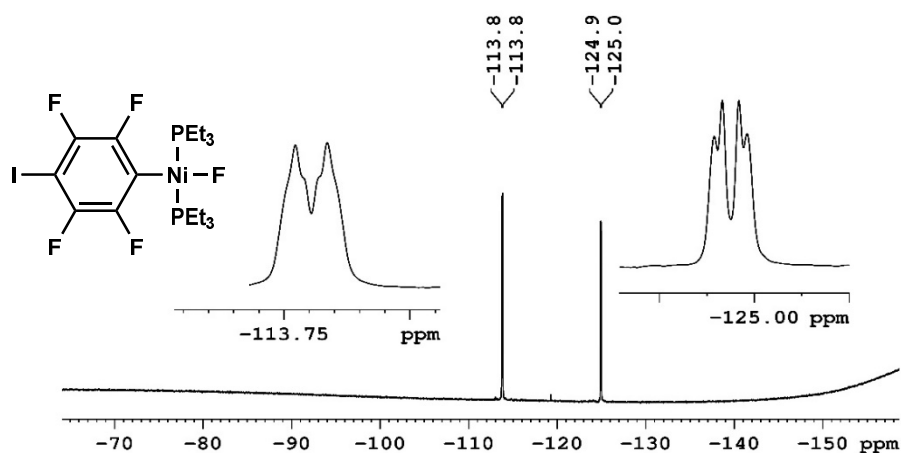


Figure 4-17 ^{19}F -NMR (470 MHz) spectrum of **2-F** in C_6D_6 .

The yield of the reaction of **2-I** with tetramethylammonium fluoride was seen to improve significantly compared to the same reaction using CsF as the fluorinating reagent. The major product of the reaction was the *trans*- $\text{Ni}(\text{F})(\text{PEt}_3)_2(2,3,5,6\text{-C}_6\text{F}_4\text{I})$ (**2-F**), which was isolated in good yield (71%). Analysis of the major product by ^{31}P -NMR spectroscopy showed a resonance at δ 13.1 as a doublet $J = 46$ Hz, corresponding to the two equivalent phosphorus atoms on the two phosphine groups on nickel. The coupling of an appropriate magnitude for an expected $^2J_{\text{P-F}}$ coupling.²⁴

The ^{19}F -NMR spectrum of the purified product showed two resonances at δ -113.8 and δ -124.9 for the four aromatic fluorine atoms with second order multiplets AA'XX' spin system, suggesting magnetic inequivalence for the fluorine atoms on the ring. The fluoride resonance of the complex was observed as a triplet at δ -387.9, $J = 46$ Hz, which was further split into an un-resolved triplet by the ortho fluorine atoms in the ^{19}F -NMR spectrum, characteristic of a nickel fluoride resonance (Figure 4-16).²⁴ The LIFDI mass spectrum showed a molecular ion $[\text{M}^+]$ base peak (100%) at 587.99 with appropriate isotopic peaks, corresponding to the molecular mass of *trans*- $\text{Ni}(\text{F})(\text{PEt}_3)_2(2,3,5,6\text{-C}_6\text{F}_4\text{I})$ (Figure 4-18).

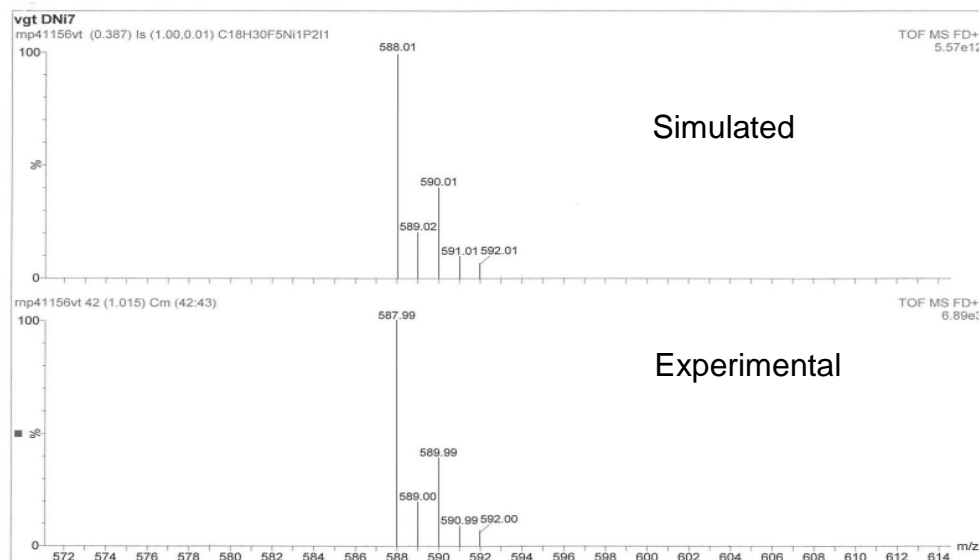


Figure 4-18 LIFDI mass spectrum showing the isotopic pattern of **2-F**.

4.2.1.8. X-ray crystallographic studies of **2-F**

Single crystals of **2-F** suitable for X-ray crystallographic studies were obtained by slow diffusion of hexane into a saturated solution of **2-F** in THF/benzene at room temperature. The X-ray crystallographic analysis of the single crystal confirmed the structure of **2-F**. The crystal showed a highly orderly packing and twinning was also seen, where the triethyl groups of the phosphine of the above and below layer falls into the pocket created by the fluoroaromatic ring which is perpendicular to the square plane of the metal centre. Selected bond lengths are given in Table 4-3. The intermolecular distance between the nickel fluoride and the iodine on the aromatic ring was observed to be 2.655(5) Å. The Ni-F(1)-I(1) angle was observed to be 180.00(4)°.

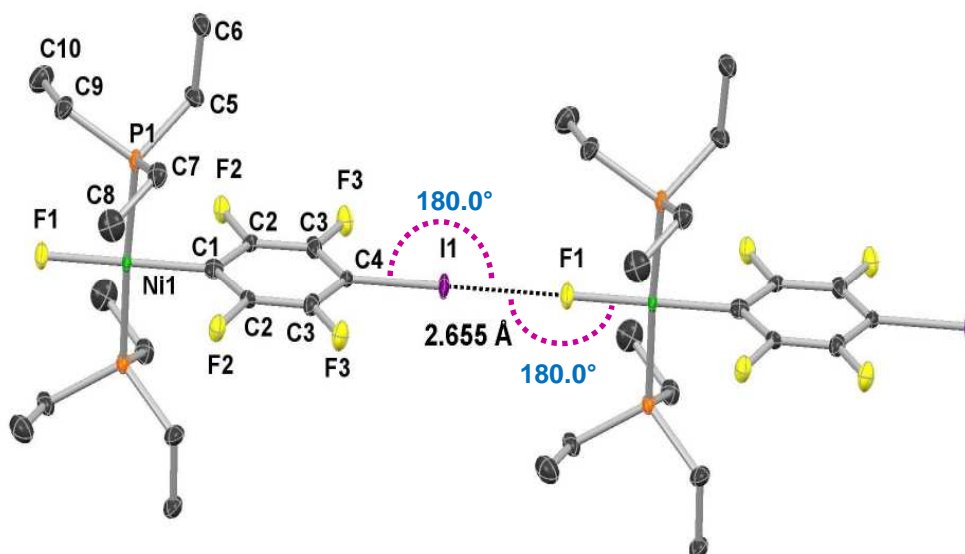


Figure 4-19 Molecular structure of **2-F**. Thermal ellipsoids set at 50% level. Hydrogen atoms are omitted for clarity.

Table 4-3 Selected bond lengths (Å) and angles (°) of **2-F**.

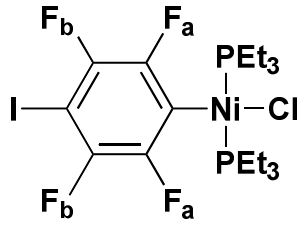
I1-C1	2.103(7)	C5-F1	1.34(1)
Ni1-P1	2.209(2)	C7-F6	1.35(1)
Ni1-F2	1.827(5)	P1-C5	1.830(7)
Ni1-C1	1.852(9)	C3-C2-F2	117.0(6)
F3-C6	1.362(9)	P1-Ni1-F1	91.5
C5-C6	1.571(7)	P1-Ni1-C1	88.5

4.2.1.9. Synthesis and characterization of *trans*-Ni(Cl)(PEt₃)₂(2,3,5,6-C₆F₄)

The reaction of **2-I** with tetramethylammonium chloride in THF at room temperature gave rise to a yellow solution in 3 hours (Scheme 4-3). The resulting product was analysed by NMR spectroscopy (Table 4-4) and LIFDI mass spectrometry after the purification process. The LIFDI mass

Halogen bonding interaction studies in solid state spectrum showed a molecular ion $[M^+]$ base peak (100%) at 604.00, corresponding to the molecular mass of **2-Cl**. Alternatively complex **2-Cl** could be synthesised rapidly and more efficiently by reacting a solution of **2-F** in toluene with chlorotrimethylsilane, which resulted in complex **2-Cl** within 15 minutes of stirring at room temperature. The resulting by products Me_3SiF and excess reagent were removed *in vacuo*.

Table 4-4 ^{31}P and ^{19}F -NMR data for complex **2-Cl**.

	^{31}P -NMR	δ 14.3
	^{19}F -NMR	δ -113.1 (2 F_a)
		δ -124.1 (2 F_b)

4.2.1.10. X-ray crystallographic studies of **2-Cl**

Single crystals of **2-Cl** suitable for X-ray crystallography were obtained by slow diffusion of hexane in a saturated solution of **2-Cl** in THF/benzene and slow evaporation, simultaneously at room temperature over a fortnight, which resulted in bright yellow crystal blocks (Figure 4-20). The X-ray crystallographic analysis of the single crystal confirmed the structure of **2-Cl** (Table 4-5). The intermolecular distance between the nickel chloride and the iodine on the aromatic ring was observed to be 3.2414(5) Å. The Ni-Cl(1)-I(1) angle was observed to be 146.83 (2)°.

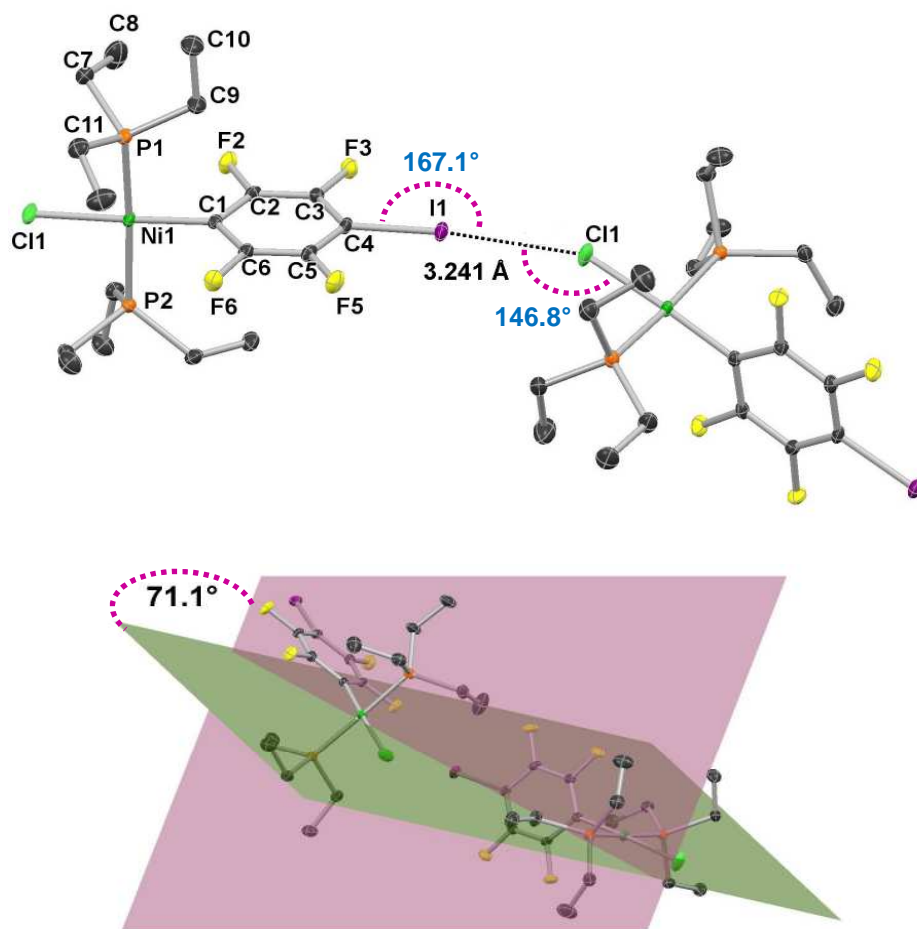


Figure 4-20 Molecular structure of **2-Cl** (top). Thermal ellipsoids set at 50% level and hydrogen atoms are omitted for clarity. (Below) Torsional angle between the two adjacent metal centre planes of **2-Cl**.

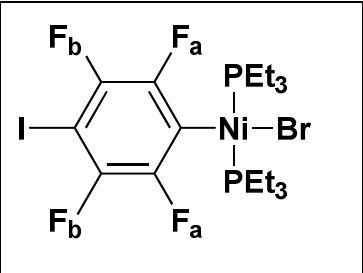
Table 4-5 Selected bond lengths (Å) and angles (°) of **2-Cl**.

C1-C2	1.382(2)	Cl1-Ni1	2.2037(5)
C1-Ni1	1.881(2)	Ni1-P1	2.2086(5)
C2-C3	1.381(2)	C7-C8	1.515(3)
C2-F2	1.361(2)	C4-I1-Cl1	167.1(5)
C3-C4	1.385(2)	I1-Cl1-Ni1	146.8(2)
C3-F3	1.350(2)	C7-P1-C11	103.12(9)
C4-I1	2.082(2)	C8-C7-P1	113.9(1)
C7-P1	1.825(2)	Cl1-Ni1-C1	175.83(5)

4.2.1.11. Characterization of *trans*-Ni(Br)(PEt₃)₂(2,3,5,6-C₆F₄I)

The reaction of *trans*-Ni(I)(PEt₃)₂(2,3,5,6-C₆F₄I) with tetraethylammonium bromide in THF gave a colour change from red to yellow-orange in 3 hours at room temperature (Scheme 4-3). The product resulting from the reaction was analysed by NMR spectroscopy (Table 4-6) and LIFDI mass spectrometry after the purification process. The LIFDI mass spectrum showed a molecular ion [M⁺] base peak (100%) at 649.94, corresponding to the molecular mass of *trans*-Ni(Br)(PEt₃)₂(2,3,5,6-C₆F₄I). Alternatively complex **2-Br** could be synthesised rapidly and more efficiently by reacting a solution of **2-F** in toluene with bromotrimethylsilane, which resulted in complex **2-Br** within 15 minutes of stirring at room temperature. The resulting by-products Me₃SiF and excess reagent were removed *in vacuo*.

Table 4-6 ³¹P and ¹⁹F-NMR data for complex **2-Br**.

	³¹ P-NMR	δ 14.4
	¹⁹ F-NMR	δ -112.9 (2 F _a)
δ -123.8 (2 F _b)		

4.2.1.12. X-ray crystallographic studies of **2-Br**

Single crystals of **2-Br** suitable for X-ray crystallography were obtained at room temperature by slow diffusion of hexane in a saturated solution of **2-Br** in benzene, which resulted in bright yellow crystal blocks (Figure 4-21). The X-ray crystallographic analysis of the single crystal confirmed the structure of **2-Br** (Table 4-7). The intermolecular distance between the

Halogen bonding interaction studies in solid state nickel bromide and the iodine on the aromatic ring was observed to be 3.3320(2) Å. The Ni-I(1)-I(2) angle was observed to be 143.31(1)°.

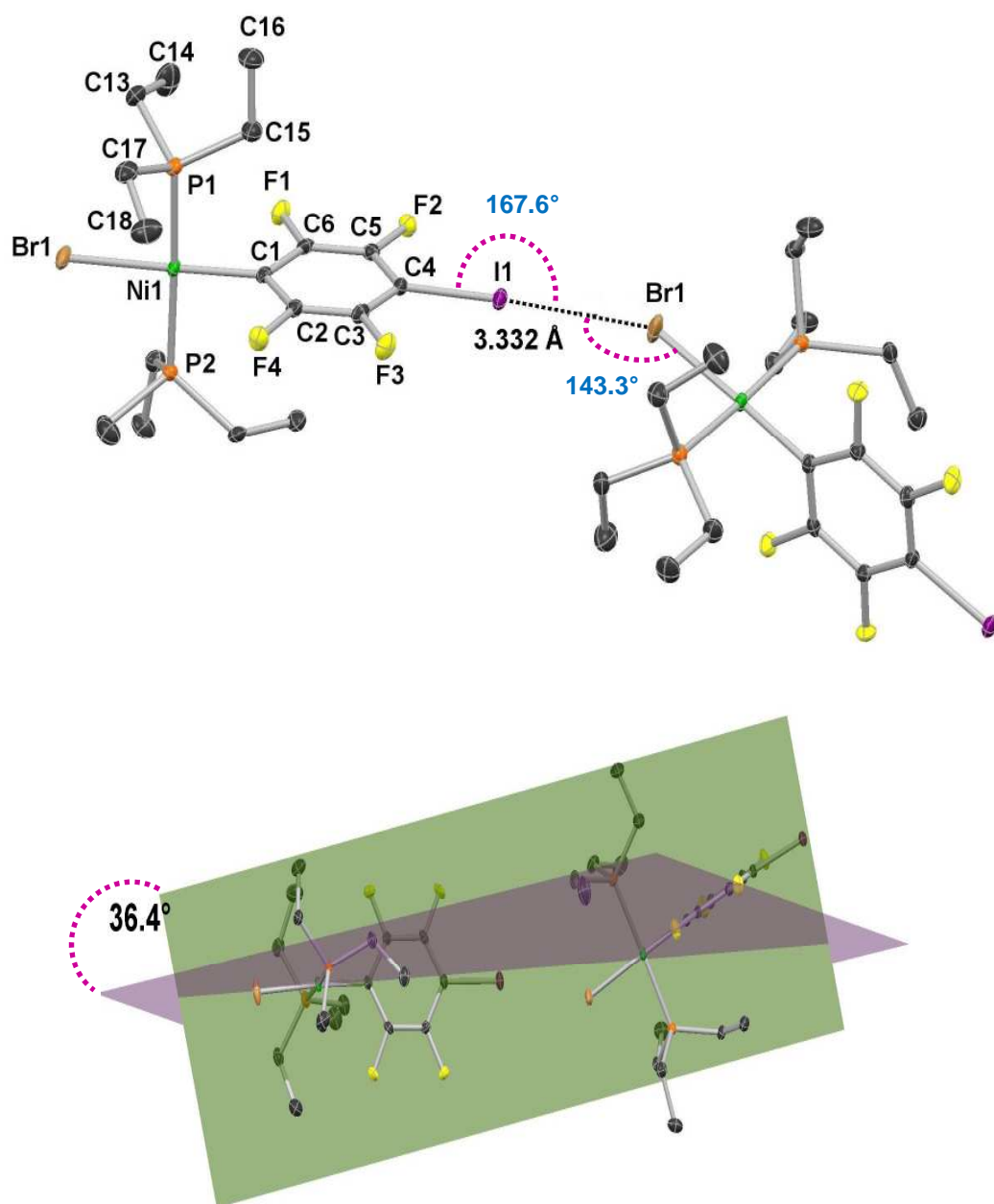


Figure 4-21 Molecular structure of **2-Br** (top). Thermal ellipsoids set at 50% level. Hydrogen atoms are omitted for clarity. (Below) Torsional angle between the two adjacent metal centre planes of **2-Br**.

Table 4-7 Selected bond lengths (Å) and angles (°) of **2-Br**.

I1-C4	2.082(2)	C3-C4	1.372(3)
Ni1-Br1	2.3384(3)	C2-C3	1.384(3)
Ni1-P2	2.2176(6)	C13-C14	1.512(4)
Ni1-C1	1.881(2)	Br1-Ni1-C1	176.61(6)
F1-C6	1.359(2)	C4-I2-Br1	167.6(6)
F2-C5	1.349(2)	I2-Br1-Ni1	143.3(1)
C1-C2	1.382(3)	C13-P1-C17	103.3(1)

4.2.1.13. Formation of $[\text{Ni}(\text{Br})(\text{PEt}_3)_2]_2(\text{C}_6\text{F}_4)$

The product arising from the oxidative addition of both iodine atoms on 1,4- $\text{C}_6\text{F}_4\text{I}_2$, $[\text{Ni}(\text{I})(\text{PEt}_3)_2]_2(2,3,5,6\text{-C}_6\text{F}_4)$, when reacted with tetramethylammonium bromide gave rise to $[\text{Ni}(\text{Br})(\text{PEt}_3)_2]_2(2,3,5,6\text{-C}_6\text{F}_4)$, the identity of which was confirmed by X-ray crystallographic studies. Single crystals of the complex were grown from hexane.

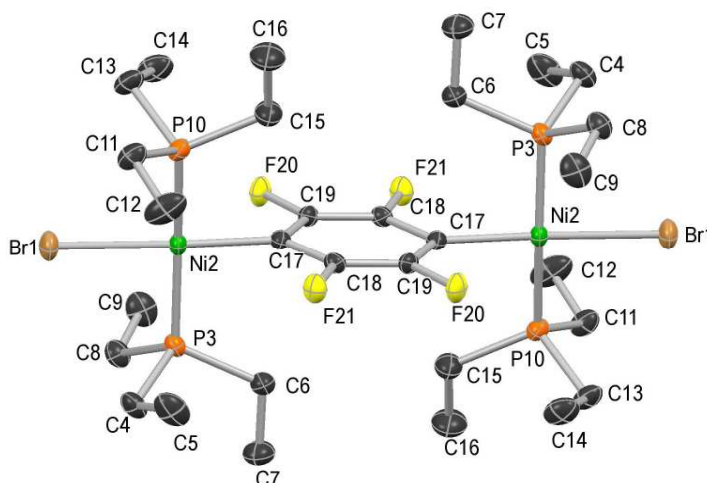


Figure 4-22 Molecular structure of $[\text{Ni}(\text{Br})(\text{PEt}_3)_2]_2(2,3,5,6\text{-C}_6\text{F}_4)$, thermal ellipsoids set at 50% level and hydrogen atoms are omitted for clarity. (structure refinement data - see appendix)

Table 4-8 Selected bond lengths (Å) and angles (°) of complex [Ni(Br)(PEt₃)₂]₂(2,3,5,6-C₆F₄).

Br1-Ni2	2.3547(3)	C18-F21	1.370(3)
Ni2-P3	2.2165(7)	Br1-Ni2-C17	172.87(7)
Ni2-P10	2.2147(7)	P3-Ni2-P10	172.36(3)
Ni2-C17	1.898(2)	Ni2-C17-C19	122.5(2)
P3-C4	1.829(3)	F21-C18-C17	118.8(2)
C17-C18	1.392(3)	P10-Ni2-C17	92.21(7)

The data collected from the X-ray crystallography of [Ni(Br)(PEt₃)₂]₂(2,3,5,6-C₆F₄), showed two nickel centres bound to the fluoroaromatic ring, C₆F₄, para to each other. Two triethyl phosphine groups trans to each other and a bromide completed the square planar geometry around the metal centres. The square planar plane of the metal coordination centre and the plane of the aromatic ring were near perpendicular to each other (88.2°). Selected bond lengths and angles are given in Table 4-8.

Table 4-9 Crystal data for complexes **2-I**, **2-F**, **2-Cl** and **2-Br**.

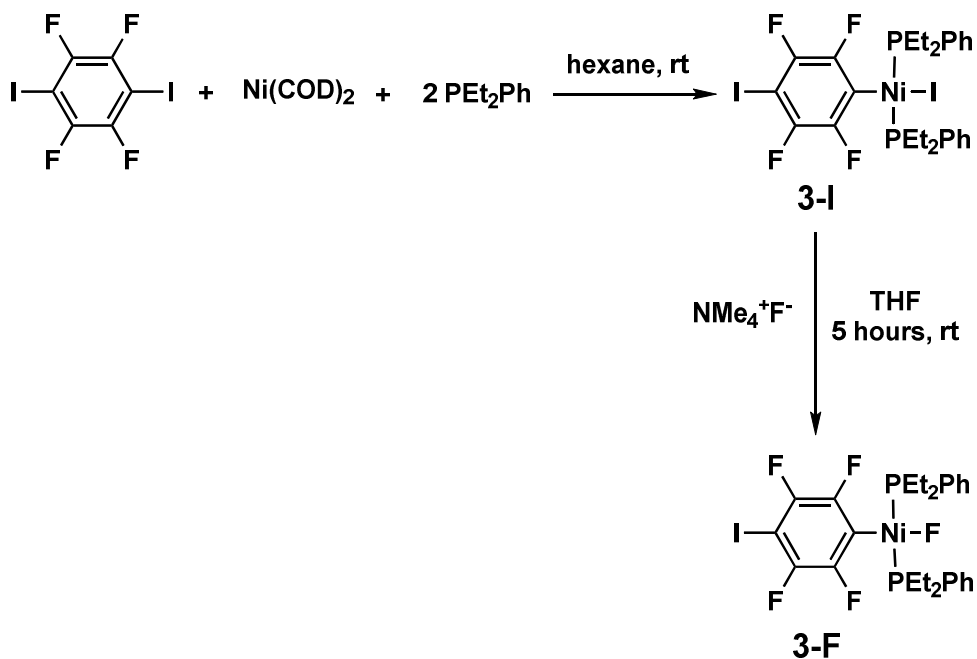
	2-I	2-F	2-Cl	2-Br
M	696.87	588.97	605.42	649.88
a/ Å	9.9032(3)	7.8675(5)	9.95341(11)	9.95422(18)
b/ Å	16.1922(6)	11.3291(3)	16.0611(2)	16.0712(3)
c/ Å	15.2884(7)	12.9347(6)	15.04577(13)	15.0877(3)
Vol/ Å ³	2445.85(17)	1149.51(10)	2387.31(4)	2401.41(8)
T/ K	110.1(2)	110.05(10)	110.05(10)	110.05(10)
α /°	90.00	90	90.00	90.00
β /°	93.913(4)	94.392(5)	97.0034(9)	95.7803(19)
γ /°	90.00	90	90.00	90.00
Space gp	P2 ₁ /c	I2	P2 ₁ /c	P2 ₁ /c
Z	4	2	4	4
μ (Mo K α mm ⁻¹)	0.7107	0.7107	0.7107	0.7107
Reflections collected	12397	5693	18822	22833
Ind reflections	6325	2011	7680	7765
R _(int)	0.0326	0.0382	0.0244	0.0346
Final R ind [I>2 σ (I)]	R ₁ = 0.0578	R ₁ = 0.0255	R ₁ = 0.0254	R ₁ = 0.0277
	wR ₂ = 0.101	wR ₂ = 0.0592	wR ₂ = 0.0497	wR ₂ = 0.0543
Final R ind [all data]	R ₁ = 0.0816	R ₁ = 0.0266	R ₁ = 0.0254	R ₁ = 0.0277
	wR ₂ = 0.109	wR ₂ = 0.0595	wR ₂ = 0.0497	wR ₂ = 0.0543

4.1.5 Synthesis and characterization of *trans*-Ni(X)(PEt₂Ph)₂(2,3,5,6-C₆F₄I), X = I and F

4.2.1.14. Synthesis of *trans*-Ni(X)(PEt₂Ph)₂(2,3,5,6-C₆F₄I), X = I and F

The electronic structure of the other ligands on the metal centre has a significant effect on the halogen bonding interaction, which has been demonstrated by earlier work done in the group ². To be able to investigate this further the triethyl phosphine groups on the complexes were replaced with diethylphenyl phosphines, which would obtain a better understanding of the effect of phosphine groups on the halogen bonding interactions in the solid state.

The Ni(PEt₂Ph)₂ species was prepared in solution by reacting Ni(COD)₂ with 2 equivalents of PEt₂Ph in hexane at room temperature. The reaction of 1,4-diiodotetrafluorobenzene with the freshly prepared Ni(PEt₂Ph)₂ in hexane at room temperature gave rise to a red-brown solution after stirring for 30 minutes. The reaction mixture was allowed to stand for an hour whereupon the product precipitated as a red-brown solid. The solid was analysed by NMR spectroscopy at room temperature (Scheme 4-4). The nickel iodide obtained was converted to the nickel fluoride. The reaction of *trans*-Ni(I)(PEt₂Ph)₂(2,3,5,6-C₆F₄I) with tetramethylammonium fluoride in THF gave rise to a colour change from red to yellow in 5 hours at room temperature.



Scheme 4-4 Formation of complexes **3-I** and **3-F** at room temperature.

4.2.1.15. Characterisation of *trans*-Ni(I)(PEt₂Ph)₂(2,3,5,6-C₆F₄I)

The reaction of 1,4-C₆F₄I with Ni(COD)₂ and PEt₂Ph in hexane at room temperature gave rise to *trans*-Ni(I)(PEt₂Ph)₂(2,3,5,6-C₆F₄I). The ³¹P-NMR spectrum exhibited a singlet at δ 16.2, for the two equivalent phosphorus atoms on the PEt₂Ph groups on the metal. (Figure 4-23). The ¹⁹F-NMR spectrum showed two second order multiplets AA'XX' spin systems at δ -114.4 and δ -123.6. (Figure 4-24). The LIFDI mass spectrum showed a molecular ion [M⁺] base peak (100%) at 791.90, corresponding to the molecular mass of **3-I**.

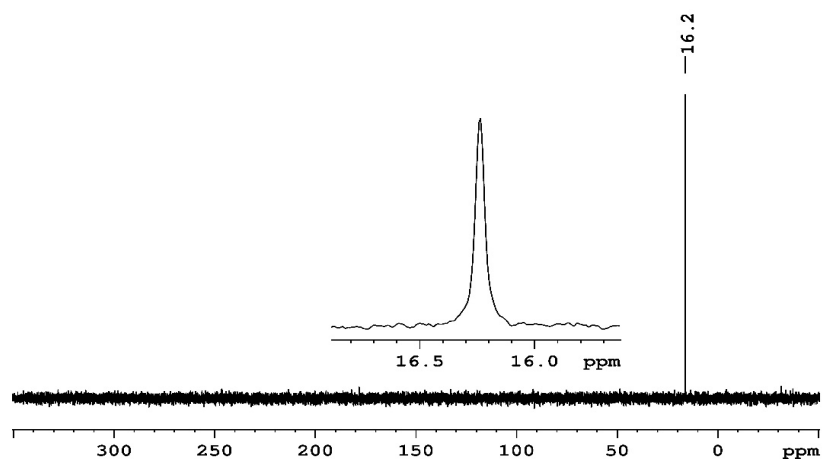


Figure 4-23 ^{31}P -NMR (202 MHz) spectrum of **3-I** in C_6D_6 .

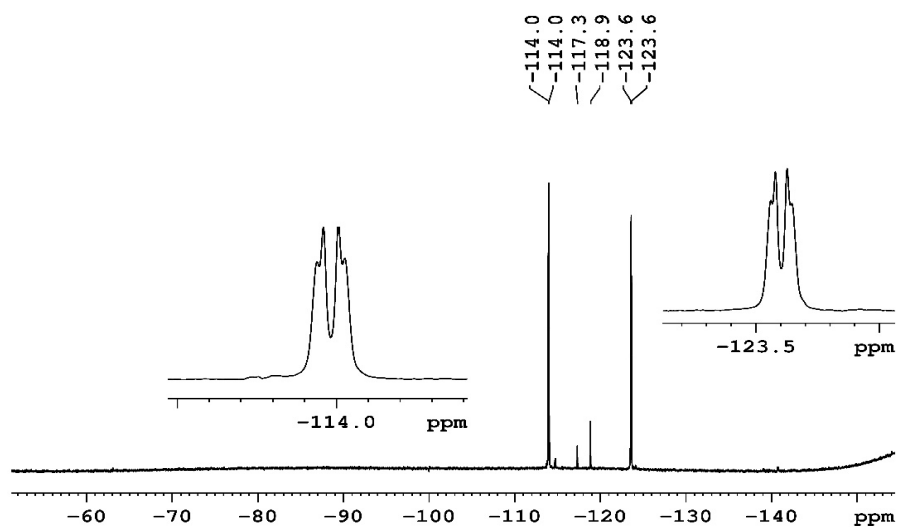


Figure 4-24 ^{19}F -NMR (470 MHz) spectrum of **3-I** in C_6D_6 .

4.2.1.16. X-ray crystallographic studies of **3-I**

Single crystals of **3-I** suitable for X-ray crystallography were obtained by slow diffusion of hexane into a saturated solution of **3-I** in THF/benzene, which resulted in dark deep crystal blocks (Figure 4-25). The X-ray crystallographic analysis of the single crystal confirmed the structure of **3-I**. The three aromatic rings present in the structure orient themselves away

Halogen bonding interaction studies in solid state from each other and the two phenyl groups twist away from the molecule to lessen steric hindrance (Table 4-2). The intermolecular distance between the nickel iodide and the iodine on the aromatic ring was observed to be 3.6791(4) Å. The Ni(1)-I(1)-I(2) angle was observed to be 158.22(1)°.

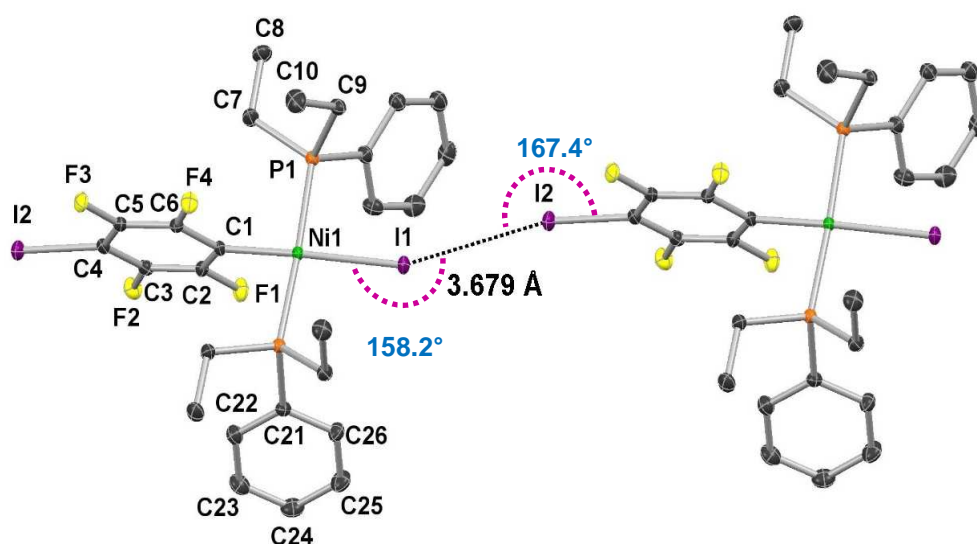


Figure 4-25 Molecular structure of **3-I**. Thermal ellipsoids set at 50% level. Hydrogen atoms are omitted for clarity.

Table 4-10 Selected bond lengths (Å) and angles (°) of **3-I**.

I1-Ni1	2.5347(4)	C4-C5	1.381(4)
I2-C4	2.089(2)	C1-C6	1.387(3)
Ni1-P1	2.2194(6)	C5-C6	1.388(3)
Ni1-C1	1.901(2)	C4-C3	1.390(3)
P1-C7	1.839(2)	C4-I2-I1	167.4(7)
P2-C19	1.839(2)	I2-I1-Ni1	158.2(1)
F1-C2	1.354(2)	C9-P1-C16	105.8(1)
C7-C8	1.521(3)	I1-Ni1-C1	172.92(7)

4.2.1.17. Characterization of *trans*-Ni(F)(PEt₂Ph)₂(2,3,5,6-C₆F₄I)

The product was purified from solid material by passing through a short column of Celite inside the glove-box, and the unreacted tetramethylammonium fluoride was removed by precipitating in benzene and the unreacted **3-I** was removed by washing with pentane. The product of the reaction was analysed by NMR spectroscopy (Figure 4-26 to Figure 4-27) and mass spectrometry after the purification process.

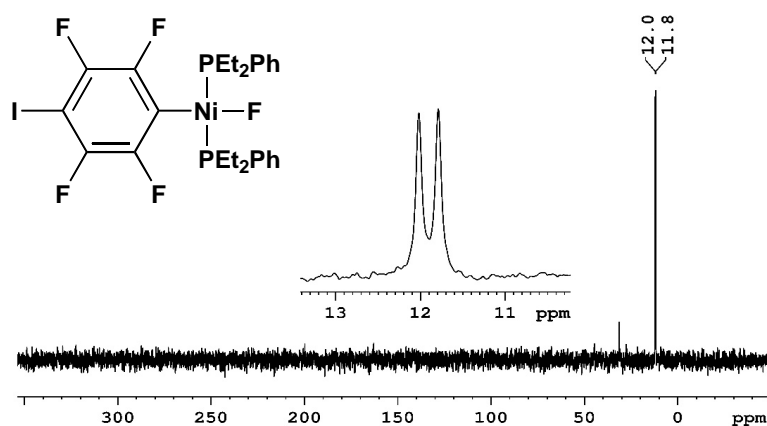


Figure 4-26 ³¹P-NMR (202 MHz) spectrum of **3-F** in C₆D₆.

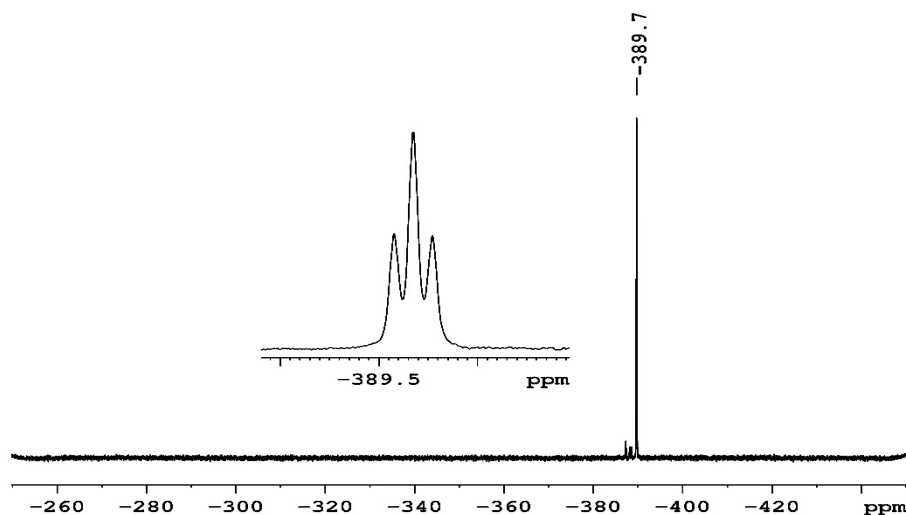
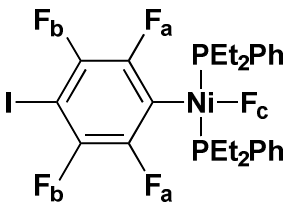


Figure 4-27 ¹⁹F-NMR (470 MHz) spectrum of **3-F** in C₆D₆.

Halogen bonding interaction studies in solid state

The reaction of **3-I** with NMe_4^+F^- , gave rise to *trans*-Ni(F)(PEt₂Ph)₂(C₆F₄I) in reasonable yield (64%). The LIFDI mass spectrum showed a molecular ion [M⁺] base peak (100%) at 684.00, corresponding to the molecular mass of **3-F**. All attempts taken to obtain single crystals suitable for X-ray crystallography were fruitless.

	³¹ P-NMR	δ 11.9 (d, J = 45 Hz)
	¹⁹ F-NMR	δ -389.7 (dd, J = 45 Hz, 9 Hz, F _c)
		δ -115.2 (AA'XX', 2 F _a)
		δ -126.5 (AA'XX', 2 F _b)

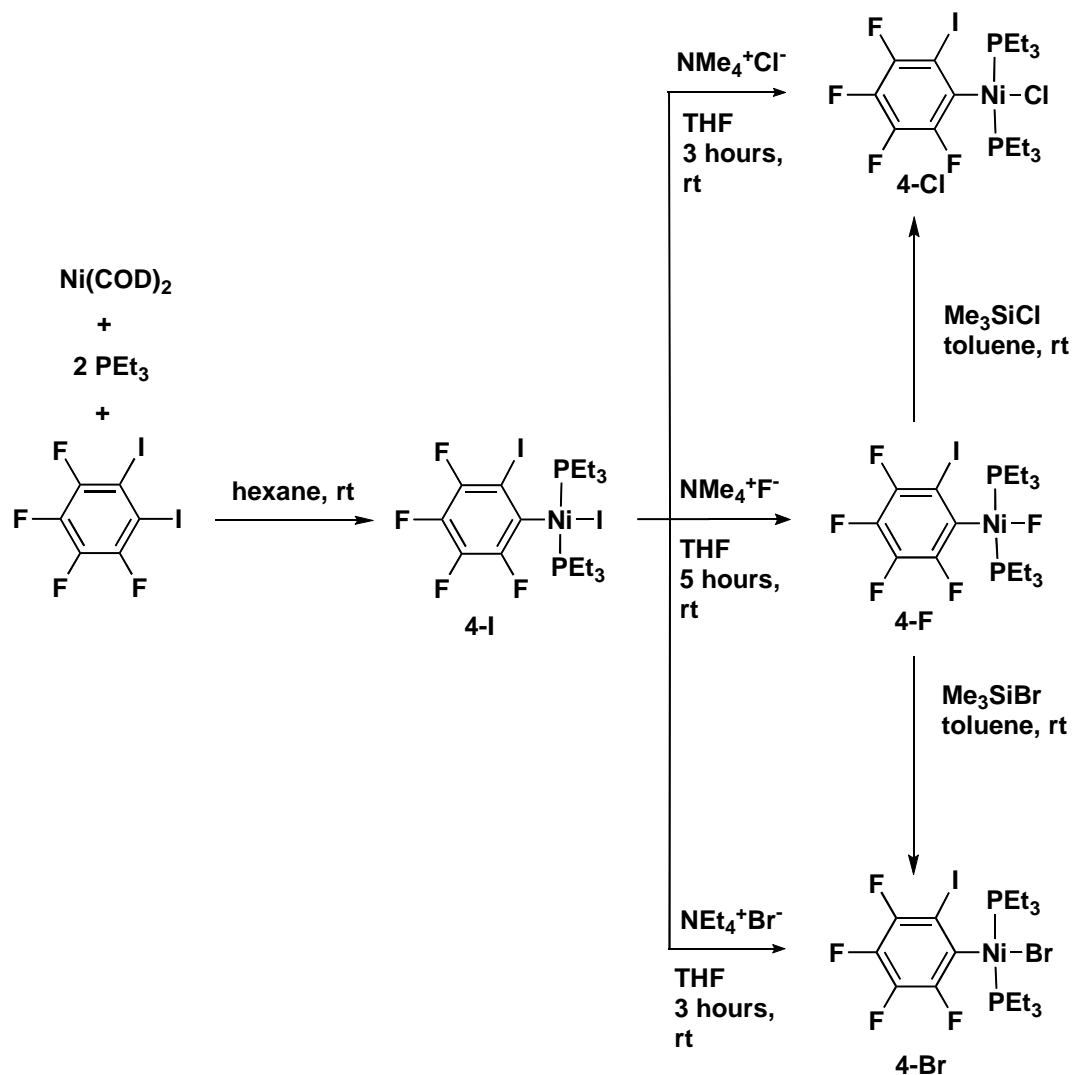
4.1.6 Synthesis and characterization of *trans*-Ni(X)(PEt₃)₂(2,3,4,5-C₆F₄I), X = I, Br, Cl and F

4.2.1.18. Synthesis of *trans*-Ni(X)(PEt₃)₂(2,3,4,5-C₆F₄I), X = I, Br, Cl and F

Our next point of interest was to model systems changing the position of the halogen bond donor on the fluoroaromatic ring, to be able to compare the effect of the electron withdrawing fluorine atoms ortho to the σ -hole, the iodine. The 1,2-diiodotetrafluorobenzene was used replacing the 1,4-diiodotetrafluorobenzene, which was anticipated to give a series of complexes with the σ -hole, ortho to only one fluorine atom and the metal centre. In addition to this the σ -hole being positioned ortho to the metal centre would enable the investigation of a different orientation of the halogen bond formation.

Halogen bonding interaction studies in solid state

The $\text{Ni}(\text{PEt}_3)_2$ was prepared in solution by reacting $\text{Ni}(\text{COD})_2$ with 2 equivalents of PEt_3 in hexane at room temperature. The reaction of 1,2-diodotetrafluorobenzene with the freshly prepared $\text{Ni}(\text{PEt}_3)_2$ in hexane at room temperature immediately gave rise to a black-red solution which was left in the freezer at $-30\text{ }^\circ\text{C}$ overnight to give rise to crystalline red product, which was filtered and washed. The solid was analysed by NMR spectroscopy at room temperature (Scheme 4-5). The iodide thus purified was used in the formation of the fluoride, chloride and the bromide in separate steps. The reaction of **4-I** with tetramethylammonium fluoride in THF gave rise to a colour change from red to yellow in 5 hours at room temperature (Scheme 4-5). The reaction of **4-I** with tetramethylammonium chloride in THF at room temperature gave rise to a bright yellow solution in less than 3 hours (Scheme 4-5). The reaction of **4-I** with tetraethylammonium bromide in THF gave a colour change from red to yellow-orange in 3 hours at room temperature (Scheme 4-5).



Scheme 4-5 Synthesis of complexes **4-I**, **4-F**, **4-Cl** and **4-Br**.

4.2.1.19. Characterisation of *trans*-Ni(I)(PEt₃)₂(2,3,4,5-C₆F₄I)

The reaction of Ni(PEt₃)₂ with 1,2-diodotetrafluorobenzene gave rise to *trans*-Ni(I)(PEt₃)₂(2,3,4,5-C₆F₄I) in a reasonable yield at room temperature (67%). The ³¹P-NMR spectrum of the product exhibited a singlet resonance at δ 10.3, for the two equivalent phosphorus atoms *trans* to each other on the metal centre.

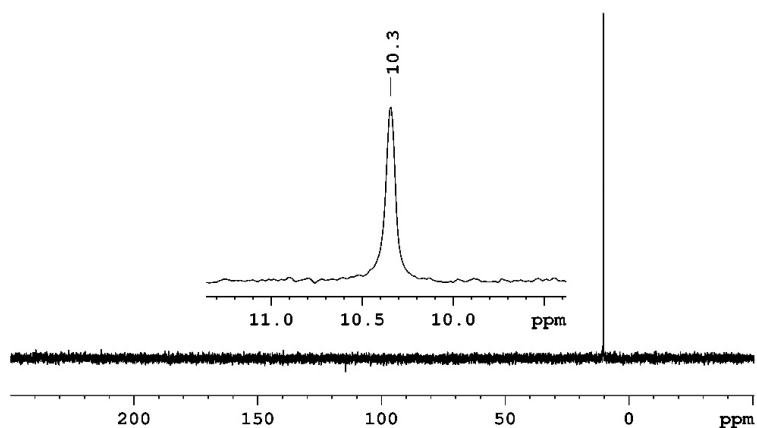


Figure 4-28 ^{31}P -NMR (202 MHz) spectrum of **4-I** in C_6D_6 .

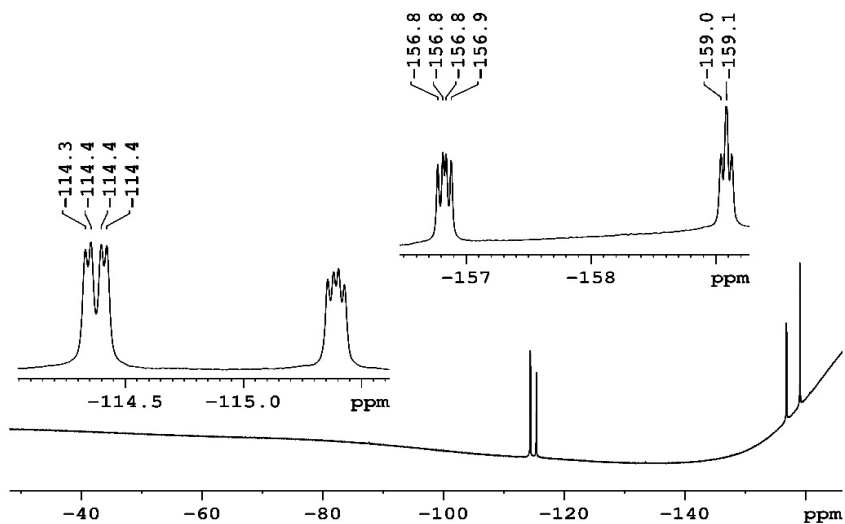


Figure 4-29 ^{19}F -NMR (470 MHz) spectrum of **4-I** in C_6D_6 .

The ^{19}F -NMR spectrum revealed four resonances for the four aromatic fluorine atoms at δ -114.4 (dd, $J = 11$ Hz, 32 Hz, 1 F), δ -115.4 (dd, $J = 12$ Hz, 22 Hz, 1 F), δ -156.8 (dd, $J = 21$ Hz, 32 Hz, 1 F), δ -159.1 (t, $J = 21$ Hz, 1 F).

4.2.1.20. X-ray crystallographic studies of 4-I

Single crystals of **4-I** were obtained from a saturated hexane solution of **4-I** at $-30\text{ }^{\circ}\text{C}$ over-night. The deep red crystals were washed with cold pentane and analysed by X-ray crystallography confirming the structure of **4-I** (Figure 4-30). Selected bond lengths are given in Table 4-2.

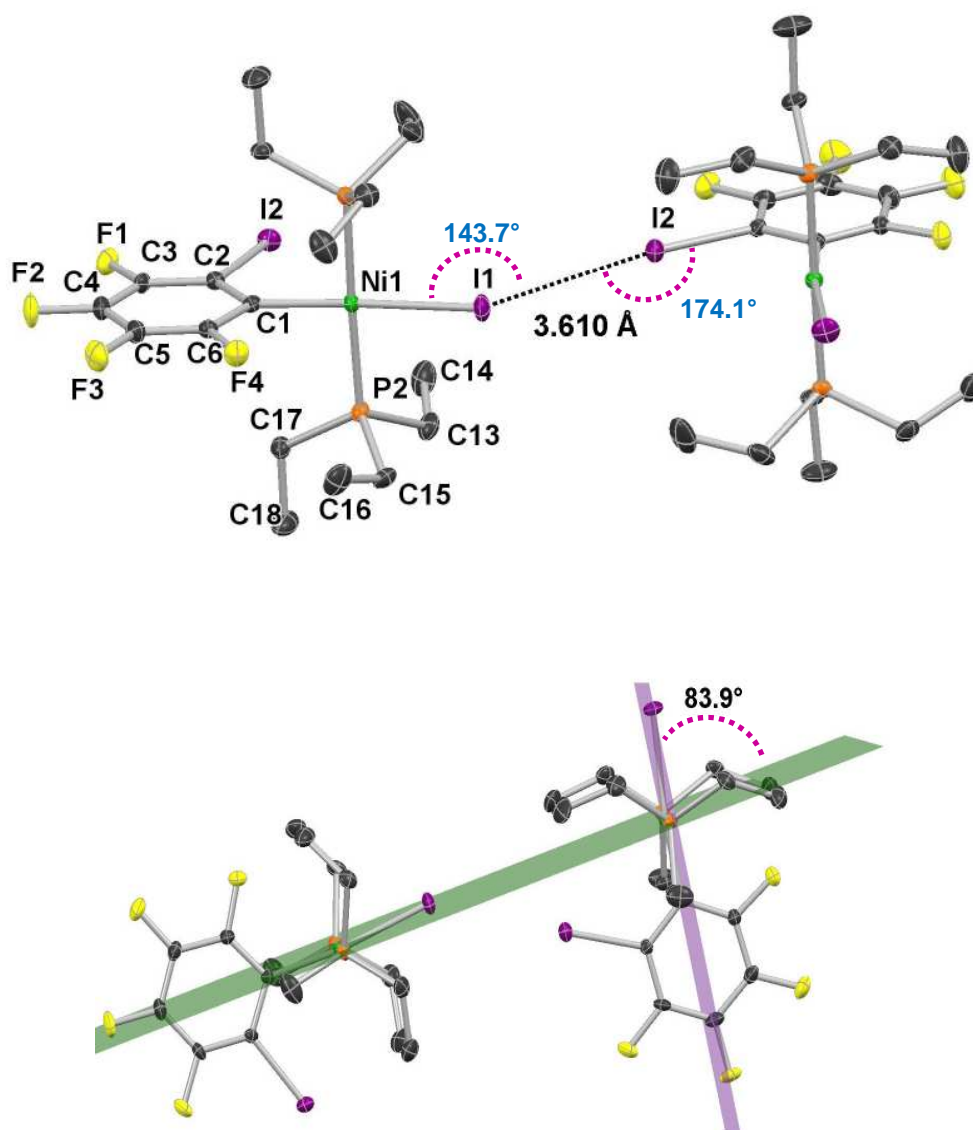


Figure 4-30 Molecular structure of **4-I** (top), Thermal ellipsoids set at 50% level and hydrogen atoms are omitted for clarity. (Below) Torsional angle between the two adjacent metal centre planes of **4-I**.

Table 4-11 Selected bond lengths (Å) and angles (°) of **4-I**.

C1-C2	1.402(4)	Ni1-P2	2.2251(8)
C1-C6	1.388(4)	I1-Ni1	2.5339(4)
C1-Ni1	1.908(3)	C2-C3	1.379(4)
C2-I2	2.098(3)	C2-I2-I1	174.10(7)
C3-F1	1.359(3)	Ni-I1-I2	143.66(1)
C6-F4	1.355(3)	C13-P2-C15	101.0(1)
C17-P2	1.824(3)	I1-Ni1-C1	173.84(8)
C13-C14	1.520(5)	P1-Ni1-P2	177.32(3)

The intermolecular distance between the nickel fluoride and the iodine on the aromatic ring was observed to be 3.6100(3) Å. The Ni(1)-I(1)-I(2) angle was observed to be 143.66(1)°. The iodide on nickel bends slightly out of the plane, enabling the iodine of the neighbouring molecule to interact at an angle.

4.2.1.21. Characterization of *trans*-Ni(F)(PEt₃)₂(2,3,4,5-C₆F₄I)

The product of the reaction between **4-I** and NMe₄⁺F⁻ initially was purified in a similar manner to the *trans*-Ni(F)(PEt₃)₂(2,3,5,6-C₆F₄I), mentioned before. After which the product was re-crystallised twice to isolate pure **4-F**. The product of the reaction was analysed by NMR spectroscopy and mass spectrometry after the purification process

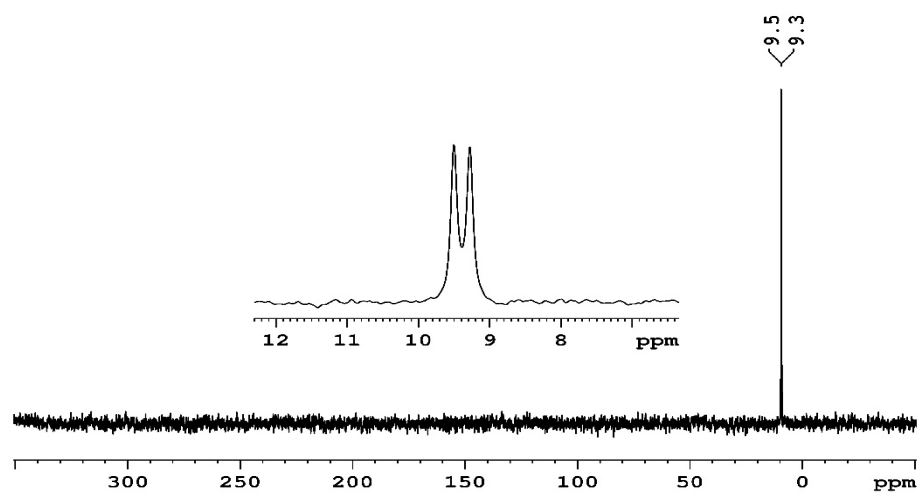


Figure 4-31 ^{31}P -NMR (202 MHz) spectrum of 4-F in C_6D_6 .

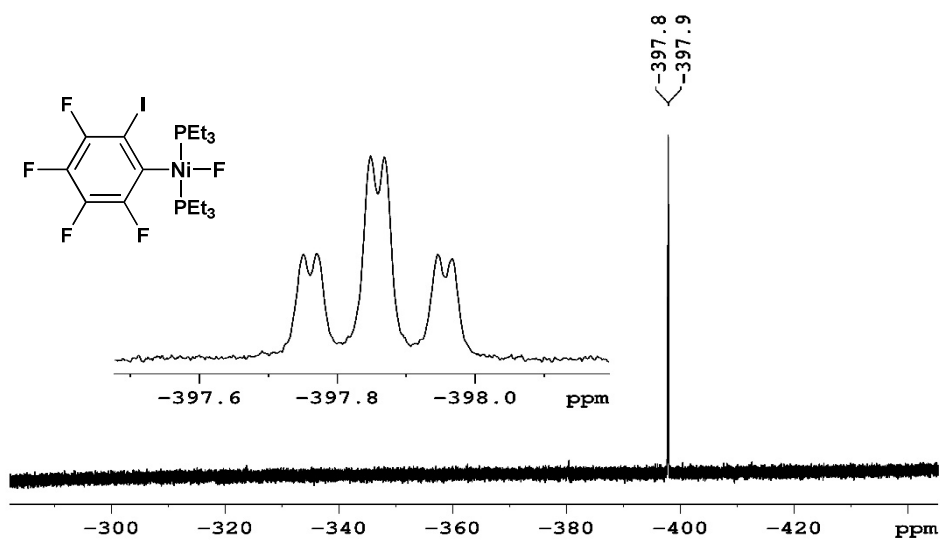


Figure 4-32 ^{19}F -NMR (470 MHz) spectrum of 4-F in C_6D_6 .

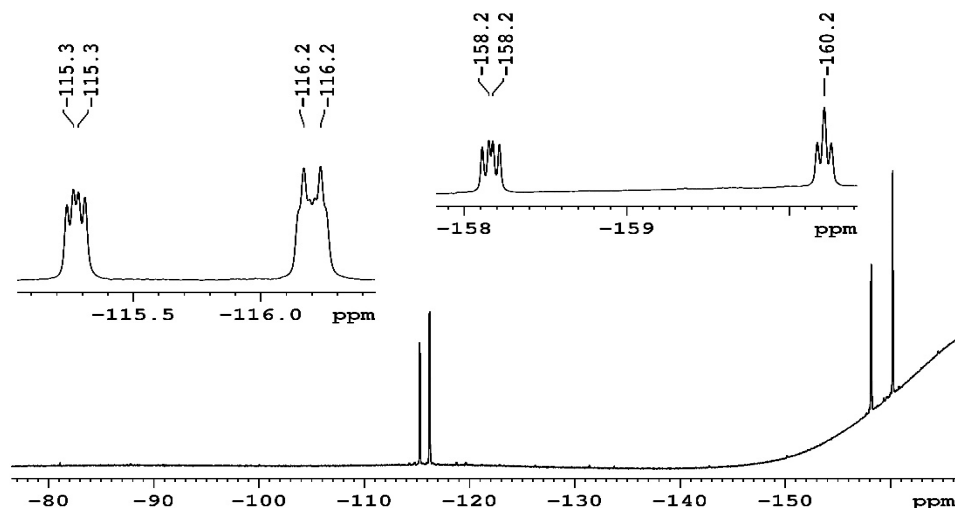


Figure 4-33 ^{19}F -NMR (470 MHz) spectrum of **4-F** in C_6D_6 .

The reaction gave rise to *trans*-Ni(F)(PEt₃)₂(2,3,4,5-C₆F₄I) within five hours at room temperature (Figure 4-33). The fluoride resonance was observed in the ^{19}F -NMR spectrum at δ -397.8 (Figure 4-32) as a doublet of triplets as a result phosphorus coupling ($J_{\text{F-P}} = 46$ Hz), and a three bond coupling to the aromatic fluorine ortho to the metal centre ($J_{\text{F-F}} = 9$ Hz).

Table 4-12 ^{31}P and ^{19}F -NMR data for complex **4-F**.

	^{31}P -NMR	δ 9.4 (d, $J = 46$ Hz, 2 P)
	^{19}F -NMR	δ -397.9 (dd, $J = 46$ Hz, 9 Hz, F _e)
		δ -115.3 (dd, $J = 20$ Hz, 11 Hz, F _a)
		δ -116.2 (dt, $J = 31$ Hz, 11 Hz, F _d)
		δ -158.2 (dd, $J = 31$ Hz, 19 Hz, F _c)
		δ -160.2 (t, $J = 20$ Hz, F _b)

4.2.1.22. X-ray crystallographic studies of 4-F.

Single crystals suitable for X-ray crystallography were obtained by slow diffusion of hexane into a saturated solution of **4-F** in benzene in the freezer at -30 °C over a fortnight. Selected bond lengths are given in Table 4-2.

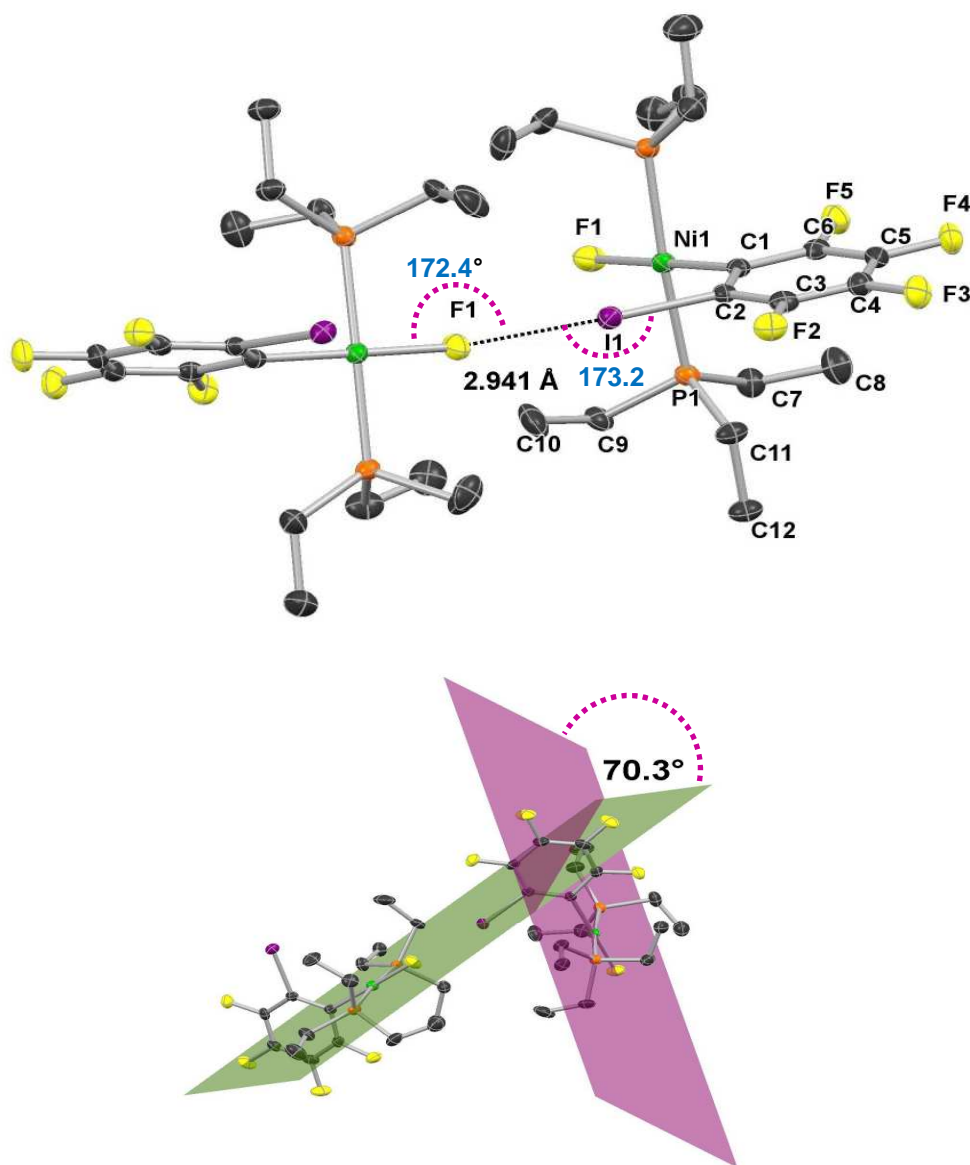


Figure 4-34 Molecular structure of **4-F**. Thermal ellipsoids set at 50% level and hydrogen atoms are omitted for clarity. (Below) Torsional angle between the two adjacent metal centre planes of **4-F**.

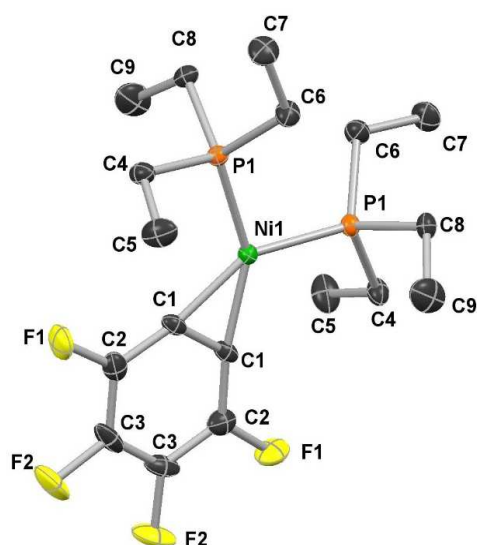
Table 4-13 Selected bond lengths (Å) and angles (°) of **4-F**.

C1-C2	1.39(1)	F1-Ni1	1.841(5)
C1-Ni1	1.891(7)	Ni1-P1	2.218(2)
C2-C3	1.39(1)	C1-C6	13.95(9)
C2-I1	2.110(7)	C7-P1	1.829(9)
C3-C4	1.39(1)	P1-Ni1-P2	173.12(8)
C3-F2	1.341(9)	F1-Ni1-C1	179.3(3)
C4-C5	1.35(1)	Ni1-F1-I1	172.4(3)
C4-F3	1.361(9)	C2-I1-F1	173.2(2)
C5-C6	1.38(1)	C7-P1-C11	104.5(4)

The X-ray crystallographic analysis of the single crystal confirmed the structure of **4-F**. The intermolecular distance between the nickel fluoride and the iodine on the aromatic ring was observed to be 2.941(5) Å. The Ni-F(1)-I(1) angle was observed to be 172.4(3)°.

4.2.1.23. Unexpected Formation of Ni(PEt₃)₂(C₆F₄)

A solution of **4-F** in hexane/benzene left to crystallize in the freezer gave rise to another complex which was identified as a η^2 tetra-fluoro-benzene complex bounded to Ni(PEt₃)₂ giving rise to Ni(PEt₃)₂(C₆F₄) (Figure 4-35).



C1-C1	1.359(5)
C1-C2	1.364(5)
C2-C3	1.386(5)
C2-F1	1.365(4)
C3-F2	1.356(4)
C4-P1	1.824(3)
Ni1-P1	2.1678
Ni1-C1	1.869
C2-C1-C1	121.6(3)
Ni1-C1-C1	68.7
C1-Ni1-P1	106.3
C1-Ni1-C1	42.6
C1-Ni1-P1	148.9

Figure 4-35 Molecular structure of $\text{Ni}(\text{PEt}_3)_2(\text{C}_6\text{F}_4)$. Thermal ellipsoids set at 50% level and hydrogen atoms are omitted for clarity. Selected bond lengths (\AA) and angles ($^\circ$) given in table above for $\text{Ni}(\text{PEt}_3)_2(\text{C}_6\text{F}_4)$. (structure refinement data – see appendix)

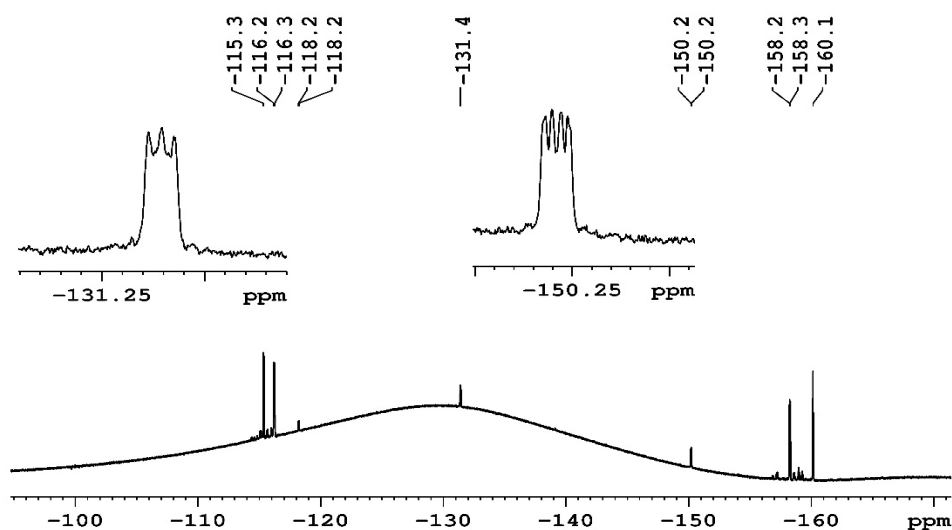


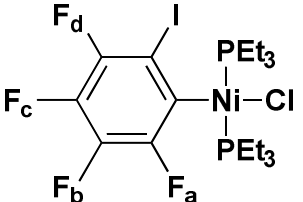
Figure 4-36 ^{19}F -NMR (470 MHz) spectrum of the sample containing $\text{Ni}(\text{PEt}_3)_2(\text{C}_6\text{F}_4)$.

The sample containing the crystals of $\text{Ni}(\text{PEt}_3)_2(\text{C}_6\text{F}_4)$ was re-dissolved in C_6D_6 and analysed by NMR spectroscopy. The ^{19}F -NMR spectrum of the sample showed that the major component in the mixture to be **4-F**. Excluding the signals of complex **4-F**, two additional peaks were observed at δ -131.4 and at δ -150.2 in the ^{19}F -NMR spectrum and an additional peak at δ 27.3 in the ^{31}P -NMR spectrum. These data fit the structure $\text{Ni}(\text{PEt}_3)_2(\text{C}_6\text{F}_4)$, and this is in agreement with the nickel-benzynes complexes observed in the literature. For example Bennett and co-workers report the complex $\text{Ni}(\text{PEt}_3)_2(\text{C}_6\text{H}_4)$, which was obtained by the reduction of $\text{Ni}(\text{Br})(2\text{-BrC}_6\text{H}_4)(\text{PEt}_3)_2$ by lithium in ether, showed a broad singlet at δ 28.5 at room temperature.^{25,26}

4.2.1.24. Characterization of *trans*- $\text{Ni}(\text{Cl})(\text{PEt}_3)_2(2,3,4,5\text{-C}_6\text{F}_4\text{I})$

The reaction of **4-I** and $\text{NMe}_4^+\text{Cl}^-$ gave a bright yellow confirmed by NMR spectroscopy as **4-Cl** (Table 4-14). Alternatively complex **4-Cl** could be synthesised rapidly and more efficiently, in a similar manner to **2-Cl**, by reacting **4-F** with chlorotrimethylsilane in toluene, giving in complex **4-Cl** within 15 minutes of stirring at room temperature. The resulting by products and excess reagent were removed *in vacuo*.

Table 4-14 ^{31}P and ^{19}F -NMR spectroscopy data for complex **4-Cl**.

	^{31}P -NMR	δ 9.5 (s, 2 P)
	^{19}F -NMR	δ -115.8 (dd, J = 31 Hz, 12 Hz, F_a)
		δ -116.8 (dd, J = 21 Hz, 12 Hz, F_d)
		δ -159.3 (dd, J = 31 Hz, 20 Hz, F_c)
		δ -162.0 (t, J = 20 Hz, F_b)

4.2.1.25. X-ray crystallographic studies of 4-Cl.

Single crystals suitable for X-ray crystallography were obtained by slow diffusion of hexane into a saturated solution of **4-Cl** in THF/toluene in the freezer at -30 °C over a fortnight (Figure 4-37). The X-ray crystallographic analysis of the single crystal confirmed the structure of **4-Cl**. However, the structure solved showed disorder on the ethyl groups of the phosphine groups and hence the methyl groups has been omitted from the structure for clarity. Attempts made to obtain better quality crystals were fruitless. Some of the selected bond lengths are given in Table 4-2. The intermolecular distance between the nickel chloride and the iodine on the aromatic ring was observed to be 3.31(1) Å. The Ni-Cl(4)-I(1) angle was observed to be 160.7°.

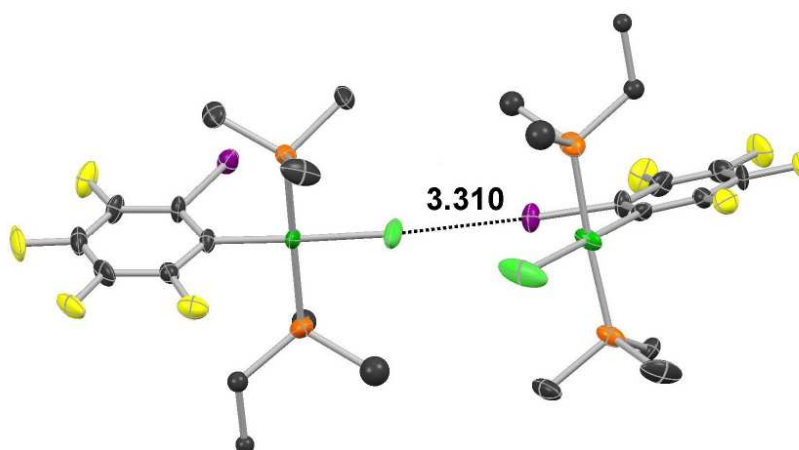


Figure 4-37 Molecular structure of **4-Cl**. Thermal ellipsoids set at 50% level. Hydrogen atoms and the end methyl groups are omitted for clarity.

Table 4-15 Selected bond lengths (Å) and angles (°) of **4-Cl**.

I1-C13	2.09(3)	I1-C13	2.09(3)
Ni2-P3	2.220(7)	Ni2-C12	1.88(2)
Ni2-C14	2.19(1)	F6-C5	1.34(4)
P3-C18	1.85(7)	C13-I1-Cl4	171.5(7)
F8-C9	1.32(3)	Ni2-Cl4-I1	160.7(5)

4.2.1.26. Characterization of *trans*-Ni(Br)(PEt₃)₂(2,3,4,5-C₆F₄I)

The product resulting from the reaction between **4-I** and NEt₄⁺Br⁻ was analysed by NMR spectroscopy (Table 4-16) after the purification process (Scheme 4-5). Alternatively complex **4-Br** could be synthesised, in a similar manner to **4-Cl**, rapidly and more efficiently by reacting a solution of **4-F** in toluene with bromotrimethylsilane, which resulted in complex **4-Br** within 15 minutes of stirring at room temperature. The resulting by products and excess reagent were removed *in vacuo*. Single crystals were grown by slow diffusion of hexane into a solution of saturated solution of **4-Br** in benzene. However, the quality of the X-ray crystallographic data collected from the crystals were too poor.

Table 4-16 ³¹P and ¹⁹F-NMR data for complex **4-Br**.

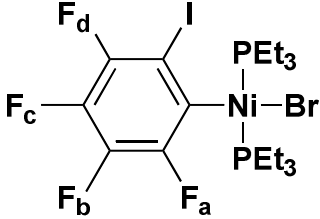
	³¹ P-NMR	δ 9.3 (s, 2 P)
	¹⁹ F-NMR	δ -115.2 (dd, J = 32 Hz, 11 Hz, F _a)
		δ -116.2 (dd, J = 33 Hz, 12 Hz, F _d)
		δ -159.3 (dd, J = 33 Hz, 21 Hz, F _c)
		δ -160.1 (t, J = 20 Hz, F _b)

Table 4-17 Crystal data for complexes **3-I**, **4-I**, **4-F** and **4-Cl**.

	3-I	4-I	4-F	4-Cl
M	792.95	696.87	588.97	605.42
a/ Å	7.8141(3)	14.8011(4)	9.4116(5)	9.2736(2)
b/ Å	12.9211(4)	12.6196(2)	12.7010(8)	13.2118(3)
c/ Å	14.7784(5)	13.2994(2)	9.7270(5)	9.8170(2)
Vol/ Å ³	1401.12(9)	2484.12(8)	1157.62(11)	1197.81(5)
T/ K	110.05(10)	110.05(10)	110.05(10)	110.05(10)
α /°	76.749(3)	90	90	90
β /°	79.700(3)	90	95	95
γ /°	76.748(3)	90	90	90
Space gp	P-1	Pna2 ₁	P2 ₁	P2 ₁
Z	2	4	2	2
Reflections collected	17424	16658	7725	10869
Independent reflections	8876	7396	7725	6245
Final R ind [I>>2 σ (I)]	R ₁ = 0.0248	R ₁ = 0.0252	R ₁ = 0.0333	R ₁ = 0.0288
	wR ₂ = 0.0526	wR ₂ = 0.0479	wR ₂ = 0.0846	wR ₂ = 0.0636
Final R ind [all data]	R ₁ = 0.0310	R ₁ = 0.0310	R ₁ = 0.0333	R ₁ = 0.0288
	wR ₂ = 0.0566	wR ₂ = 0.0512	wR ₂ = 0.0845	wR ₂ = 0.0636

4.1.7 Solid State NMR spectroscopic studies

Solid state magic angle spinning NMR spectroscopy offered an opportunity to learn more about the halogen bonding interactions. Fortunately, the fluoride on the metal centre can act as a ^{19}F -MAS SSNMR spectroscopic handle and appears at high field with no overlap from other resonances. In addition to this, the fluoride resonance is very sensitive to its environment.² Therefore, solid state NMR spectroscopy was used to understand and analyse the self-complementary interactions of these complexes. ^{19}F -MAS SSNMR spectroscopy was used to analyse the effect on the fluoride resonance of halogen bonding interactions in complexes **2-F** and **4-F**. The complex *trans*-Ni(F)(PEt₃)₂(C₆F₅) known in the literature,²⁴ which doesn't have a halogen bond donor atom on its backbone was also analysed by ^{19}F -MAS SSNMR spectroscopy for comparison purposes.

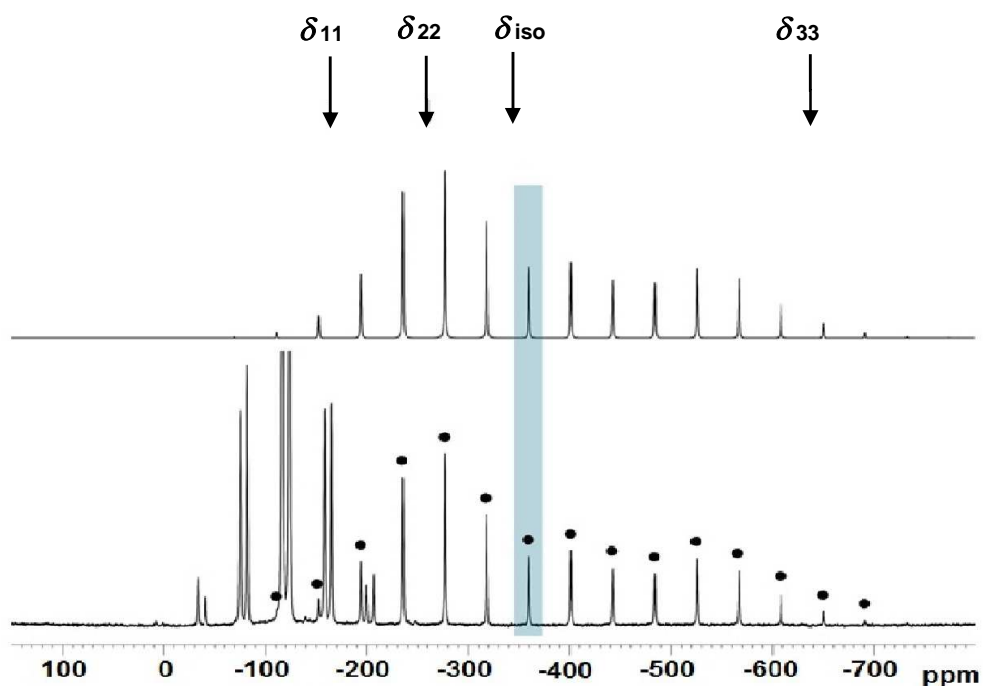


Figure 4-38 ^{19}F -MAS SSNMR spectrum of complex **2-F**. The black dots indicate the peaks corresponding to the fluoride resonance.

The peaks arising due to the fluoride resonance of **2-F** are marked with black dots in Figure 4-38. The other peaks in the range of δ -100 to -160 arise from the resonance of the fluorine atoms on the aromatic ring. The isotropic chemical shift δ_{iso} of the fluoride resonance was identified by obtaining several spectra varying the rate of spinning. The δ_{iso} of the fluoride resonance in **2-F** was observed at δ -359.8 ppm. The components of the anisotropic chemical shift tensor are labelled as δ_{11} , δ_{22} and δ_{33} , where δ_{11} , is the least shielded component and δ_{33} is the most shielded component ($\delta_{11} \geq \delta_{22} \geq \delta_{33}$).²⁷ For the complex **2-F** the least shielded component of the anisotropic chemical shift tensor δ_{11} is observed at δ -165 ppm and the most shielded δ_{33} is observed at δ -645 ppm. The isotropic chemical shift δ_{iso} of the fluoride resonance of *trans*-Ni(F)(PEt₃)₂(C₆F₅) was observed at δ -393.9 in the ¹⁹F-MAS NMR spectrum (Figure 4-40). This was in good agreement with the solution state fluoride resonance at δ -394.3 (in C₆D₆) for the same complex. The solution state fluoride resonance of **2-F** appeared ~29 ppm to higher field at δ -388.3 than its solid state isotropic chemical shift (δ_{iso} of **2-F** was observed at δ -359.8 in the ¹⁹F-MAS SSNMR). The isotropic chemical shift δ_{iso} of the fluoride resonance of complex **4-F** was observed at δ -373.0 in the ¹⁹F-MAS NMR spectrum. The solution state fluoride resonance of **4-F** was observed ~25 ppm higher field at δ -397.9. Attempts to obtain information about the J_{P-F} coupling from the ³¹P-MAS SSNMR of the above mentioned complexes was fruitless due to the spectrum being poorly resolved and further experiments conducted to improve the situation were equally unrewarding.

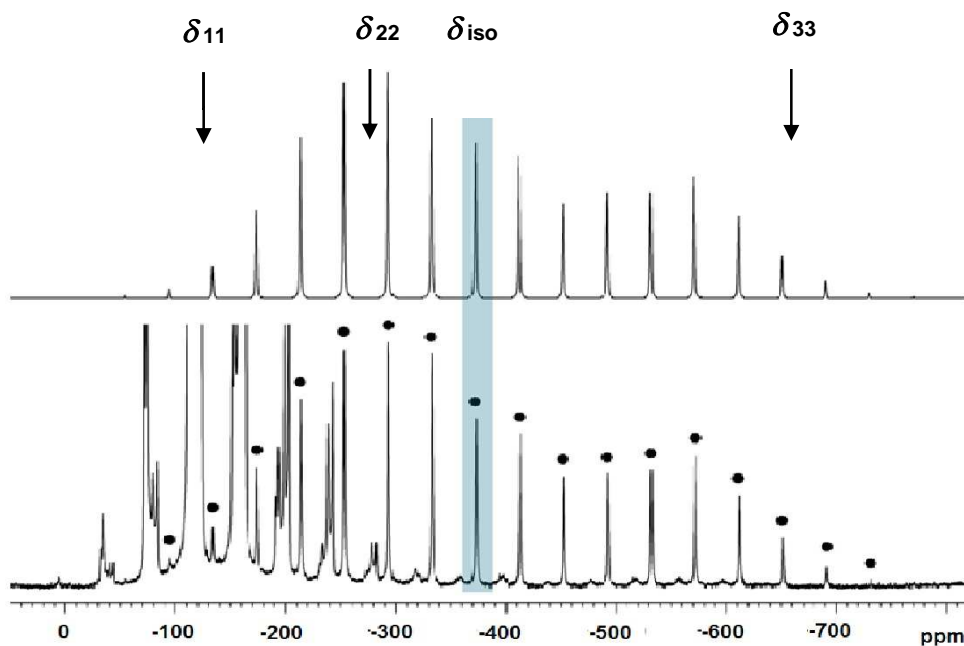


Figure 4-39 ^{19}F -MAS SSNMR spectrum of complex **4-F**. The black dots indicate the peaks corresponding to the fluoride resonance.

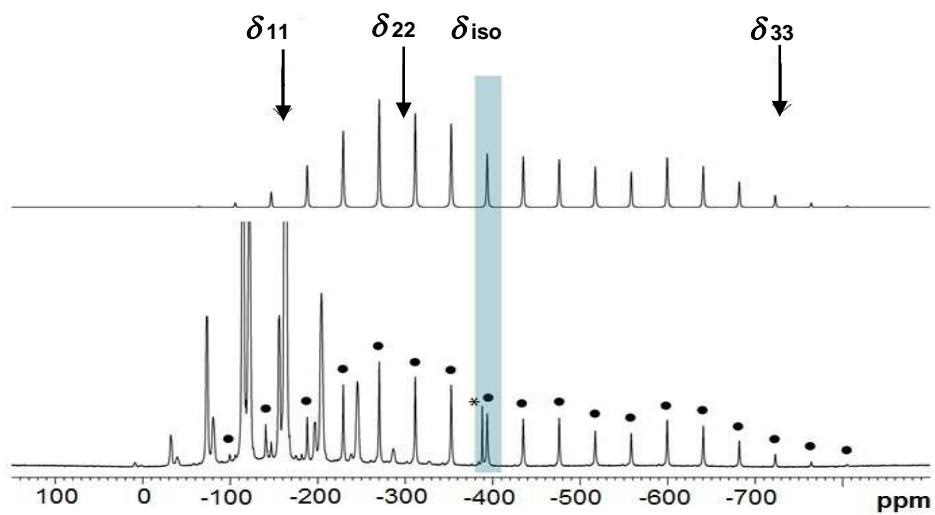


Figure 4-40 ^{19}F -MAS SSNMR spectrum of *trans*-Ni(F)(PEt₃)₂(C₆F₅). The black dots indicate the peaks corresponding to the fluoride resonance.

Table 4-18 Isotropic chemical shifts of *trans*-Ni(F)(PEt₃)₂(C₆F₅), **2-F** and **4-F** in solution and solid state NMR spectroscopy.

Sample		δ_{iso} (ppm)
<i>trans</i> -Ni(F)(PEt ₃) ₂ (C ₆ F ₅)	Solid	-393.9(1)
	Solution (~40 μ M) in C ₆ D ₆	-394.3
<i>trans</i> -Ni(F)(PEt ₃) ₂ (2,3,5,6-C ₆ F ₄)	Solid	-359.8(2)
	Solution (~40 μ M) in C ₆ D ₆	-388.3
<i>trans</i> -Ni(F)(PEt ₃) ₂ (2,3,4,5-C ₆ F ₄)	Solid	-373.0(2)
	Solution (~40 μ M) in C ₆ D ₆	-397.9

Table 4-19 ¹⁹F-MAS-SSNMR parameters for *trans*-Ni(F)(PEt₃)₂(C₆F₅), **2-F** and **4-F**

Sample	δ_{iso} (ppm)	Ω (ppm)	K	δ_{11} (ppm)	δ_{22} (ppm)	δ_{33} (ppm)
<i>trans</i> -Ni(F)(PEt ₃) ₂ (C ₆ F ₅)	-393.9(2)	575(10)	0.50(3)	-154	-298	-729
<i>trans</i> -Ni(F)(PEt ₃) ₂ (2,3,4,5-C ₆ F ₄)	-373.0(2)	530(10)	0.40(3)	-143	-302	-673
<i>trans</i> -Ni(F)(PEt ₃) ₂ (2,3,5,6-C ₆ F ₄)	-359.8(2)	480(10)	0.58(3)	-165	-266	-645

δ_{iso} = Isotropic chemical shift, $\delta_{\text{iso}} = (\delta_{11} + \delta_{22} + \delta_{33}) / 3$

Ω = Span, the breadth of the CSA powder pattern, $\Omega = \delta_{33} - \delta_{11}$

K = Skew, measures the asymmetry of the powder pattern,

$$K = (\delta_{\text{iso}} - \delta_{22}) / \Omega^{27}$$

4.1.8 Variable Temperature X-ray crystallographic studies of 2-F.

Halogen bonding interactions, similar to all weak non-covalent forces are dependent on temperature. In order to understand the effect of temperature on these interactions in the solid state, X-ray crystallographic data were collected at various temperatures. Crystals of complex **2-F** were used for this study as they showed the highest X-Bonding interaction in the series of complexes prepared. The intermolecular distance between Ni-F of the metal centre and I-C of the aromatic ring at different temperatures are tabulated below. Other selected distances in the crystal structure are also given for the purpose of comparison (Table 4-20).

Table 4-20 Variable temperature X-ray crystallographic data for complex **2-F**, selected intermolecular bond lengths are given for comparison purposes.

Temperature/ K	111 K	199 K	240 K
Intermolecular Ni-F...I-C distance / Å	2.652(3)	2.683(5)	2.707(7)
Ni-F / Å	1.83	1.83	1.85
Ni-C / Å	1.87	1.88	1.88
Ni-P / Å	2.21	2.21	2.20
C-I / Å	2.09	2.10	2.13
C-F / Å	1.35	1.36	1.36

Halogen bonding interaction studies in solid state

The intermolecular distance between the fluoride on the metal centre and the iodine on the fluoroaromatic ring increased with increasing temperature (Table 4-20). The highest temperature attained was limited to 240 K due to difficulty in attaining reliable data caused by thermal motions and to avoid phase transitions. The lowest temperature was limited to 111 K due to the fact that nitrogen was used as a coolant.

Table 4-21 Crystal data and structure refinement for **2-F** at variable temperatures.

T / K	111	199	240
Crystal system	monoclinic	monoclinic	monoclinic
Space group	I2	I2	Cc
a/Å	7.8920(5)	8.0074(4)	17.1652(15)
b/Å	11.3325(4)	11.3665(4)	8.5185(13)
c/Å	12.9439(5)	12.9665(5)	16.935(2)
α /°	90	90	90
β /°	94.434(5)	94.616(4)	96.803(10)
γ /°	90	90	90
Volume/Å ³	1154.19(9)	1176.34(8)	2458.8(5)
Z	2	2	4
Reflections collected	4467	4258	5903
Goodness-of-fit on F ²	0.969	1.035	1.077
Final R indexes [I ≥ 2σ (I)]	R ₁ = 0.0312, wR ₂ = 0.0611	R ₁ = 0.0287, wR ₂ = 0.0783	R ₁ = 0.0559, wR ₂ = 0.1623
Final R indexes [all data]	R ₁ = 0.0364, wR ₂ = 0.0622	R ₁ = 0.0312, wR ₂ = 0.0801	R ₁ = 0.0769, wR ₂ = 0.1825

Table 4-22 Intermolecular distances and the angles of complexes **2-I**, **2-F**, **2-Cl**, **2-Br**, **3-I**, **4-I**, **4-F** and **4-Cl**.

Compound	Intermolecular I-X distance / Å	Normalized ratio $d_{I-X} / (r_I + r_X)$	Percentage reduction of the van der Waals radii / %	C-XB _{donor} -XB _{acceptor} angle/°	M-XB _{acceptor} -XB _{donor} angle/°	Torsion angle for adjacent metal plane
<i>trans</i> -Ni(I)(PEt ₃) ₂ (2,3,5,6-C ₆ F ₄ I) 2-I	3.4970(6)	0.86	14.3	168.0(2)	139.2(3)	66.5
<i>trans</i> -Ni(Br)(PEt ₃) ₂ (2,3,5,6-C ₆ F ₄ I) 2-Br	3.3320(2)	0.85	15.4	167.6(6)	143.3(1)	36.4
<i>trans</i> -Ni(Cl)(PEt ₃) ₂ (2,3,5,6-C ₆ F ₄ I) 2-Cl	3.2414(5)	0.84	16.0	167.1(5)	146.8(2)	71.1
<i>trans</i> -Ni(F)(PEt ₃) ₂ (2,3,5,6-C ₆ F ₄ I) 2-F	2.655(5)	0.76	24.3	180.0	180.00(4)	0.0

Halogen bonding interaction studies in solid state

Compound	Intermolecular I-X distance/ Å	Normalized distance $d_{I-X} / (r_I + r_X)$	Percentage reduction of the van der Waals radii / %	C-XB _{donor} -XB _{acceptor} angle/°	M-XB _{acceptor} -XB _{donor} angle/°	Torsion angle-adjacent metal planes
<i>trans</i> -Ni(I)(PEt ₂ Ph) ₂ (2,3,5,6-C ₆ F ₄ I) 3-I	3.6791(4)	0.90	9.8	167.4(6)	158.2(1)	0.0
<i>trans</i> -Ni(I)(PEt ₃) ₂ (2,3,4,5-C ₆ F ₄ I) 4-I	3.6100(3)	0.89	11.5	174.1(7)	143.7(1)	83.9
<i>trans</i> -Ni(Cl)(PEt ₃) ₂ (2,3,4,5-C ₆ F ₄ I) 4-Cl	3.31(1)	0.86	-	171.5(7)	160.7(5)	64.4
<i>trans</i> -Ni(F)(PEt ₃) ₂ (2,3,4,5-C ₆ F ₄ I) 4-F	2.941(5)	0.84	15.9	173.2(2)	172.4(3)	70.3

4.3. Discussion

Halogen bonding interactions have been explained in most cases by the σ -hole model. The σ -hole is an electron deficient region created on heavier halogen atoms resulting from higher polarizability.⁴ This electron deficiency is enhanced by strong electron withdrawing groups attached to the site. This σ -hole readily interacts with Lewis bases, to give rise to halogen bonding interactions. One method frequently used to estimate halogen bonding interactions in the solid state is the percentage reduction of the sum of the van der Waals radii or the normalized radii (distance between the $\text{XB}_{\text{donor}}\cdots\text{XB}_{\text{acceptor}}$ / sum of the van der Waals radii of individual atoms).^{3,4,28,29} The strength of these interactions is estimated by how much the sum of the van der Waals radii is reduced and these interactions also exhibit a characteristic angle preference of 180° for $\text{R-XB}_{(\text{donor})}\cdots\text{XB}_{(\text{acceptor})}$ in a strong interaction³. Some of the supramolecular complexes exhibiting the best defined halogen bonding interactions are obtained by using iodine atoms bound to electron withdrawing groups, for example $\text{C}_6\text{F}_5\text{I}$.^{3,29}

The van der Waals radii used to calculate the percentage reduction of the sum of the van der Waals radii in Table 4-22, are based on the van der Waals radii calculated by statistical analysis of intermolecular contacts in X-ray crystal structures, which was initiated by Rowland and Taylor for a few main group elements,³⁰ and further adopted by Alvarez.³¹

For all of the halogen bond donor-acceptor complexes synthesised a bonding interaction is apparent between the interacting halogens. The strength of the halogen bonding interaction is indicated by the percentage reduction of the sum of the van der Waals radii between the X-Bond donor and X-Bond acceptor atoms. When comparing between the series of complexes prepared from 1,4-diodotetrafluorobenzene (para-iodo complexes) and 1,2-diodotetrafluorobenzene (ortho-iodo complexes), the highest X-Bonding interaction is observed for the para-iodo complexes

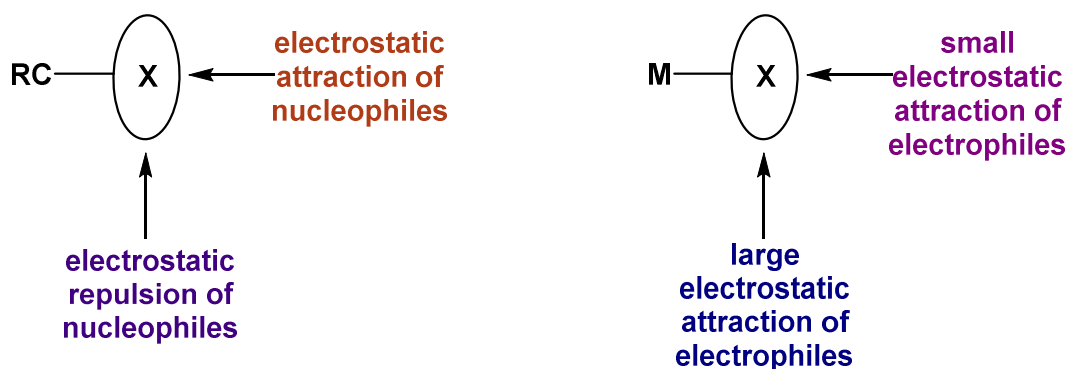
Halogen bonding interaction studies in solid state (Table 4-22). This observation could be rationalised both electronically and sterically. Firstly based on the fact that the complexes with the X-Bond donor para to the metal centre has two fluorine atoms ortho to it, which makes the σ -hole (the electron deficient region of the X-Bond donor ⁴) more electron deficient, which in turn would enhance the X-bonding interaction. Secondly, the σ -hole of the X-Bond donor atom is more accessible to the X-Bond acceptor atom in the complexes where the X-bond donor is para to the metal centre, compared to the complexes where the X-Bond donor is ortho to the metal centre and hence hindered by the ethyl groups on the phosphine.

The two series of complexes **2-I** (PEt₃ as the phosphine ligand) and **3-I** (PEt₂Ph as the phosphine ligand) offer an opportunity to compare the effect of altering the phosphine on the solid state halogen bonds. The phosphine groups on the metal centre have a significant effect on the X-Bonding interactions. It has been shown by Perutz and co-workers ²¹ in 2011, that the enthalpies of the X-Bonding interactions were significantly affected by the change of the phosphine groups on the metal centre. The electronic effects of the phosphine substituents was studied by comparing nickel complexes with PCy₃ and PEt₃ and platinum complexes of PCy₃ and P^{*i*}-Pr₃ and it was found that the PCy₃ had the largest enthalpy in both cases. When comparing the complexes **2-I** (Ni-I...I distance 3.497 Å) and **3-I** (Ni-I...I distance 3.679 Å), where the X-Bond acceptor is the same and the X-Bond donor is para to the metal centre in both complexes (Table 4-22), the X-Bond interaction is higher for **2-I** (14.3% reduction of the sum of the van der Waals radii) than for **3-I** (9.8% reduction of the sum of the van der Waals radii). This observation could be rationalized by the fact that, when one of the ethyl groups is replaced by a less electron donating phenyl ring, the electron donating ability of the phosphine is reduced, hence the electronegativity of the X-Bond acceptor (iodide) is reduced and therefore the X-Bonding interaction is less in **3-I** than in **2-I**. In addition to this the X-Bond acceptor atom is more sterically hindered to approach the

Halogen bonding interaction studies in solid state X-Bond donor by the phenyl groups on the phosphine groups in **3-I** making its X-Bonding interaction less than for **2-I**.

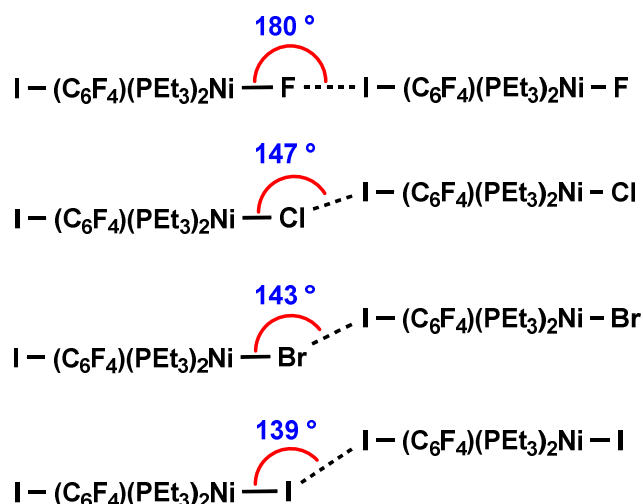
In both the series of complexes prepared from 1,4-diodotetrafluorobenzene and 1,2-diodotetrafluorobenzene, the highest X-Bond interaction is seen when fluoride acts as the X-Bond acceptor, which is indicated by the percentage reduction of the sum of the van der Waals radii (Table 4-22). For complex **2-F** a 24.3% reduction of the sum of the van der Waals radii, and a 16.0% reduction of the sum of the van der Waals radii for complex **4-F** (Table 4-22). The percentage reduction of the van der Waals radii could be seen to decrease in the order $F^- > Br^- > Cl^- > I^-$, suggesting the XB interaction decreasing in the same manner. This is in agreement with the fact the more electronegative halogen atoms show the highest interaction when the halogen atoms attached to the metal centres act as XB acceptors. This sequence indicates that the electrostatic potentials have an important role the X-Bonding interactions in such systems, as the fluoride shows the highest negative potential.³

Halogen bonding interactions are directional forces. This directionality arises mainly due to the anisotropic charge distribution around the nucleus of halogen atoms, resulting in a positive potential, which is more pronounced in the less electronegative atoms especially iodine. This anisotropic charge distribution is compressed along the axis of the C- X_{donor} , creating the positive potential trans to the C- X_{donor} ^{7,29} (Scheme 4-6).



Scheme 4-6 Scheme of the anisotropic charge distribution around the halogen depending on their environment and the resulting electrostatic attraction of electrophiles or nucleophiles respectively.⁷

The closer the C-XB(donor)⋯XB(acceptor) angle is to 180°, the greater the interaction between the X-Bond donor and the acceptor is. In the series of complexes synthesized where the X-Bond donor is para to the metal centre, complex **2-F** showed a C-I(donor)⋯X(acceptor) angle closest to 180°, (C-I⋯F angle 180.0°) (Table 4-22) indicating the highest X-Bond interaction when the nickel-fluoride acts as the XB acceptor. In the same series complexes, the nickel-iodide has a Ni-I⋯I angle of 139°, the Ni-Br⋯I angle of 143°, and the Ni-Cl⋯I angle of 147° (Scheme 4-7).



Scheme 4-7 Schematic diagram of the Ni-X⋯I angles of the para-iodo complexes.

Halogen bonding interaction studies in solid state

This could be explained by the fact that large polarisable atoms such as iodine would have an electron deficient region in the direction trans to the Ni-iodide bond, and therefore the σ -hole of the halogen bond cannot interact at a 180° angle, due to the fact that both the halogens will have identical electrostatic potential at the point of interaction and therefore will result in repulsions (Scheme 4-6). Therefore when the X-Bond acceptor is a heavy polarizable halogen the X-Bond donor will interact with its electron rich region. However in the case of the Ni-F \cdots I angle of the nickel-fluorides, the angles observed are closer to 180° . This is because fluorine is the least polarisable of the halides and hence does not have an electron deficient region created therefore the σ -hole of the XB donor would interact at an 180° in the Ni-Fluoride case.

To be able to study and compare the self-complementary interactions of complex **2-F** or **4-F**, with the existing studies done on halogen bonding using group 10 metal fluorides a solution phase titration using solution phase ^{19}F -NMR spectroscopy was attempted.²¹ However, to be able to obtain reliable data the concentration used must be quite high. However, the solubility of both complexes **2-F** and **4-F** proved insufficient to obtain a high concentration making it difficult to obtain reliable data. (Over a 20 fold increase in concentration, a change in chemical shift of 0.7 ppm).

In recent years the application of solid state NMR to the study of hydrogen and halogen bonding interactions has increased. An example of such magic angle spinning solid state NMR spectroscopy study is the determination of the ^{15}N - ^1H bond lengths in crystalline histidine, where intermolecular hydrogen bonding led to elongation of one of the imidazole N-H bonds.³² Multinuclear solid state NMR spectroscopy (^{31}P and ^{77}Se) has been used in studying halogen bonding interactions,^{28,33} such as the interaction in P=Se \cdots I motifs. The distances were determined based on the change observed in J couplings with halogen bonding interactions.³⁴ The fluoride resonance in the ^{19}F -MAS NMR spectra of **2-F** and **4-F** both show

Halogen bonding interaction studies in solid state a downfield shift compared to their respective resonances in the solution state ^{19}F -NMR spectra (Table 4-18). The fluoride chemical shift in the solution state NMR spectrum of the analogous complex $\text{Ni}(\text{F})(\text{PEt}_3)_2(\text{C}_6\text{F}_5)$, where the halogen bond donor is absent, (δ -393.9) is very similar to the fluoride chemical shift in the solution state NMR spectrum (δ -394.3). This observation can be rationalised by the self-complementary halogen bonding interactions found in complexes **2-F** and **4-F**, which reduces the electron cloud shielding the fluoride and hence shifts the resonance downfield. Halogen bonding interactions which can be compared to a Lewis acid base interaction, make the fluoride, the halogen bond acceptor, resonate at a lower field. The higher the interaction the more downfield the fluoride resonance appears. This is seen in the order of ascending frequency of the fluoride resonance, $\text{Ni}(\text{F})(\text{PEt}_3)_2(\text{C}_6\text{F}_5) < \text{Ni}(\text{F})(\text{PEt}_3)_2(2,3,4,5\text{-C}_6\text{F}_4\text{I}) < \text{Ni}(\text{F})(\text{PEt}_3)_2(2,3,5,6\text{-C}_6\text{F}_4\text{I})$. This observation is in agreement with the X-ray crystallography data, where the para-iodo complex shows the highest halogen bonding interactions.

The effect of temperature and pressure on halogen bonding interactions of similar systems has been studied previously namely the halogen bonding interactions with $\text{C-X}\cdots\text{X}'\text{-M}$ halogen bonds have been studied by Brammer and co-workers in 2008, illustrating the compressibility of these non-covalent interactions.^{7,35} These studies demonstrated that the application of high pressure had a more significant effect than the change in the temperature. There was a *ca.* 5% reduction of the unit cell volume when the temperature was varied from 300 down to 30 K, and a more significant 19% reduction in unit cell volume upon varying the pressure from atmospheric pressure to *ca.* 4 GPa. Also it was shown that the high pressure studies can be used to discriminate between strong and weak interactions in halogen bonds and hydrogen bonds.⁷ The variable temperature X-ray crystallography data of complex **2-F** shows a change in the unit cell volume with the temperature change. A 4.5% reduction in the unit cell volume is observed when the temperature is changed from 240 K

Halogen bonding interaction studies in solid state to 200 K and *ca* 2% reduction in the unit cell volume is observed from 200 K to 111 K, overall *ca* 6.5% reduction is observed in the unit cell volume when the temperature is changed from 240 K to 111 K. Based on the observations made by Brammer and co-workers, further studies are currently undertaken to obtain variable pressure X-ray crystallographic data for the complexes. Preliminary results obtained for the complex **2-Br** exhibited a ~20% reduction in the unit cell volume when the pressure was changed from 0 GPa to 3.6 GPa and the Ni-Br...I distance was observed to undergo a ~9% reduction. Further studies are carried out to obtain data for complexes **2-F**, **2-I** and **2-Cl**.

When comparing the results obtained our systems to the work done by Rissanen,³ the X-Bonding interaction seen in the crystal structures of 2-Cl and 2-Br are in good agreement with their system where the X-Bond acceptor was the (PCP)Pd-X (PCP = (2,6-bis[(di-*t*-butylphosphino)-methyl]-phenyl)palladium halide, where X = Cl & Br), and the X-Bond donor the 1,4-(C₆F₄I₂). He reports a 13% reduction of the van der Waals radii, which is comparable to our system with the complexes 2-Cl and 2-Br which show a *ca* 13% (using van der Waals radii as proposed by Bondi) reduction of the van der Waals radii.

4.4. Summary

The model chosen to work with has proven to be quite successful in demonstrating quite thoroughly several different aspects of self-complementary metal-halide halogen bonding interactions. It has been shown that the highest interaction is feasible when halogen atoms with higher negative potential act as the halogen bond acceptor, which is in agreement with the fact that the electrostatic contribution plays the important role in metal halide acceptor systems. The interaction is more pronounced when the X-Bond donor is attached to highly electron

Halogen bonding interaction studies in solid state withdrawing groups, as shown by the stronger interactions seen for the para iodo complexes compared to the ortho iodo complexes. The halogen bonding interactions of metal halide systems can be improved by designing metal centres with more electron donating ligands, which are also not sterically demanding. This is true for our systems where triethyl phosphines showing greater interactions than diethylphenyl phosphines and for other systems observed in the literature.³ In addition to X-ray crystallography, solid state NMR spectroscopy has proved to be a useful tool to study non-covalent interactions of this nature. The spectroscopic resonances of the fluorides, which are very sensitive to their environment, show a change in their chemical shift which is dependent on the halogen bonding interaction.

4.5. References

- (1) Metrangolo, P.; Neukirch, H.; Pilati, T.; Resnati, G. *Acc. Chem. Res.* **2005**, *38*, 386.
- (2) Libri, S.; Jasim, N. A.; Perutz, R. N.; Brammer, L. *J. Am. Chem. Soc.* **2008**, *130*, 7842.
- (3) Johnson, M. T.; Džolić, Z.; Cetina, M.; Wendt, O. F.; Öhrström, L.; Rissanen, K. *Cryst. Growth Des.* **2011**, *12*, 362.
- (4) Beale, T. M.; Chudzinski, M. G.; Sarwar, M. G.; Taylor, M. S. *Chem. Soc. Rev.* **2013**, *42*, 1667.
- (5) Legon, A. C. *Phys. Chem. Chem. Phys.* **2010**, *12*, 7736.
- (6) Politzer, P.; Lane, P.; Concha, M.; Ma, Y.; Murray, J. *Journal of Molecular Modeling* **2007**, *13*, 305.
- (7) Brammer, L.; Minguez Espallargas, G.; Libri, S. *CrystEngComm* **2008**, *10*, 1712.
- (8) Bent, H. A. *Chem. Rev. (Washington, DC, U. S.)* **1968**, *68*, 587.
- (9) Guthrie, F. *Journal of the Chemical Society* **1863**, *16*, 239.

- (10) Hassel, O.; Hvoslef, J.; Vihovde, E. H.; Sørensen, N. A. *Acta Chem. Scand.* **1954**, *8*, 873.
- (11) Desiraju Gautam, R.; Legon Anthony, C.; Ho Shing, P.; Kloo, L.; Marquardt, R.; Metrangolo, P.; Politzer, P.; Resnati, G.; Rissanen, K. In *Pure Appl. Chem.* 2013; Vol. 85, p 1711.
- (12) Awwadi, F. F.; Willett, R. D.; Peterson, K. A.; Twamley, B. *Chemistry – A European Journal* **2006**, *12*, 8952.
- (13) Willett, R. D.; Awwadi, F.; Butcher, R.; Haddad, S.; Twamley, B. *Cryst. Growth Des.* **2003**, *3*, 301.
- (14) Zordan, F.; Brammer, L.; Sherwood, P. *J. Am. Chem. Soc.* **2005**, *127*, 5979.
- (15) Caballero, A.; Zapata, F.; Beer, P. D. *Coord. Chem. Rev.* **2013**, *257*, 2434.
- (16) Langton, M. J.; Robinson, S. W.; Marques, I.; Félix, V.; Beer, P. D. *Nat Chem* **2014**, *6*, 1039.
- (17) Robinson, S. W.; Mustoe, C. L.; White, N. G.; Brown, A.; Thompson, A. L.; Kennepohl, P.; Beer, P. D. *J. Am. Chem. Soc.* **2015**, *137*, 499.
- (18) Mele, A.; Metrangolo, P.; Neukirch, H.; Pilati, T.; Resnati, G. *J. Am. Chem. Soc.* **2005**, *127*, 14972.
- (19) Chudzinski, M. G.; McClary, C. A.; Taylor, M. S. *J. Am. Chem. Soc.* **2011**, *133*, 10559.
- (20) Caballero, A.; White, N. G.; Beer, P. D. *Angewandte Chemie International Edition* **2011**, *50*, 1845.
- (21) Beweries, T.; Brammer, L.; Jasim, N. A.; McGrady, J. E.; Perutz, R. N.; Whitwood, A. C. *J. Am. Chem. Soc.* **2011**, *133*, 14338.
- (22) Siegbahn, P. E. M.; Eisenstein, O.; Rheingold, A. L.; Koetzle, T. F. *Acc. Chem. Res.* **1996**, *29*, 348.
- (23) Henderson, W. A.; Streuli, C. A. *J. Am. Chem. Soc.* **1960**, *82*, 5791.
- (24) Cronin, L.; Higgitt, C. L.; Karch, R.; Perutz, R. N. *Organometallics* **1997**, *16*, 4920.
- (25) Bennett, M. A.; Wenger, E. *Organometallics* **1995**, *14*, 1267.

- (26) Edwards, A. J.; Willis, A. C.; Wenger, E. *Organometallics* **2002**, *21*, 1654.
- (27) Saitô, H.; Ando, I.; Ramamoorthy, A. *Prog. Nucl. Magn. Reson. Spectrosc.* **2010**, *57*, 181.
- (28) Weingarth, M.; Raouafi, N.; Jouvelet, B.; Duma, L.; Bodenhausen, G.; Boujlel, K.; Schollhorn, B.; Tekely, P. *Chem. Commun. (Cambridge, U. K.)* **2008**, 5981.
- (29) Lommerse, J. P. M.; Stone, A. J.; Taylor, R.; Allen, F. H. *J. Am. Chem. Soc.* **1996**, *118*, 3108.
- (30) Rowland, R. S.; Taylor, R. *The Journal of Physical Chemistry* **1996**, *100*, 7384.
- (31) Alvarez, S. *Dalton Trans.* **2013**, *42*, 8617.
- (32) Zhao, X.; Sudmeier, J. L.; Bachovchin, W. W.; Levitt, M. H. *J. Am. Chem. Soc.* **2001**, *123*, 11097.
- (33) Viger-Gravel, J.; Leclerc, S.; Korobkov, I.; Bryce, D. L. *Journal of the American Chemical Society* **2014**, *136*, 6929.
- (34) Viger-Gravel, J.; Meyer, J. E.; Korobkov, I.; Bryce, D. L. *CrystEngComm* **2014**, *16*, 7285.
- (35) Mínguez Espallargas, G.; Brammer, L.; Allan, D. R.; Pulham, C. R.; Robertson, N.; Warren, J. E. *J. Am. Chem. Soc.* **2008**, *130*, 9058.

CHAPTER FIVE

**SOLUTION STUDIES OF
HYDROGEN AND HALOGEN BONDING
TOWARDS NICKEL FLUORIDES**

The work presented in this chapter was a continuation of previous work done by Dr. Torsten Beweries and has been carried out in conjunction with Dr. Dan A Smith

SOLUTION STUDIES OF HYDROGEN AND HALOGEN BONDING TOWARDS NICKEL FLUORIDES

5.1 Introduction

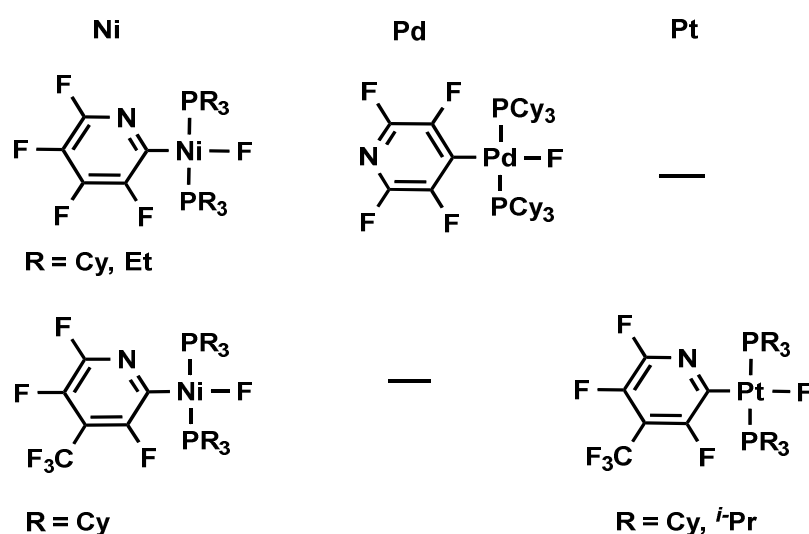
Non-covalent interactions such as hydrogen and halogen bonding have been studied extensively due to their growing applications in various fields of crystal engineering, biochemistry and in understanding catalytic cycles.¹ Although structural evidence of such interactions has been common in literature over half a decade,² the quantification of these interactions have only recently been investigated by several groups.³ IR spectroscopy, UV-Visible spectroscopy, rotational spectroscopy and NMR spectroscopy are some of the most commonly used techniques to quantify the binding energies of these interactions.^{1,4-7}

Hydrogen bonding, which plays an important role in catalytic cycles, biochemistry and crystal engineering, is described as an interaction that arises when an electrophilic hydrogen atom, $H^{\delta+}$ from a motif, H-R, in which R is more electronegative than H, interacts with a Lewis base.^{4,8} The strength of the hydrogen bonding to metal-hydrides was quantified in 1995, in the range 10-30 kJ/mol.⁹

IR spectroscopic studies of haloalkynes acting as halogen bond donors to Lewis bases conducted by Laurence and co-workers, was one of the earliest thermodynamic data published for organic halogen bond donors.¹⁰ Over the past few decades, transition metal fluorides have acquired great interest, due to their unique properties in catalytic cycles and to their involvement in C-F activation.^{1,6,11,12} Metal halides are known to behave as Lewis bases, by acting as acceptors for hydrogen and halogen bonding.^{13,14} Perutz and co-workers have been able to use ¹⁹F-NMR spectroscopy for a detailed study on hydrogen and halogen bonding interactions of transition metal fluorides, quantifying the

interactions^{1,11} They have also been able to use multinuclear NMR spectroscopy for the measurements of the energetics of group 5 and 6 metal hydrides binding to halogen bond donors.⁶ Previous studies in our group focusing on the thermodynamic studies of non-covalent interactions of group 10 metal fluorides using C₆F₅I, as the halogen bond donor, and indole, as the hydrogen bond donor, revealed that halogen bond was weaker in comparison to the hydrogen bond.¹

A series of group 10 metal mono-fluoride complexes, which were structurally closely related were prepared to study the halogen bonding interactions of group 10 metal fluorides. Solubility in nonpolar solvents, was additionally required from the complexes to avoid electrostatic competition arising with Lewis basic solvents and polar solvents.^{7,15} The complexes prepared were *trans*-Ni(F)(PCy₃)₂(2-C₅NF₄) and its analogue *trans*-Pd(F)(PCy₃)₂(4-C₅NF₄), *trans*-Pt(F)(PR₃)₂[2-C₅NF₂H(CF₃)] (where R = Cy or *i*-Pr) and its analogue *trans*-Ni(F)(PCy₃)₂[2-C₅NF₂H(CF₃)] (Scheme 5-1).



Scheme 5-1 Group 10 metal fluorides used for halogen bonding interactions studies.¹¹

The enthalpy of halogen bonding ($-\Delta H^\circ$) was observed to increase in the order Ni < Pd < Pt and quantified in the range -16 to -25 kJ/mol. Through these experiments it was also established that the fluoropyridyl ligand had a negligible effect on the thermodynamic parameters, whereas the phosphine

ligand on the metal centre had a significant effect on the enthalpies. The electronic effects of the phosphine substituents was studied by comparing the PCy₃ and PEt₃ complexes of nickel and the PCy₃ and P^{*i*}-Pr₃ complexes of platinum, and it was found that the PCy₃ complexes had the largest binding in both cases. It was also shown that the value of the spin-spin coupling constants $J_{\text{Pt-F}}$ increases with the adduct formation. DFT calculations were in good agreement with the experimental data obtained. In addition, it also suggested that the region of negative potential around the fluoride is slightly more radially extended in the case of Pt, and the potential minimum along the extension of the M-F vector is deeper for Pt-F. These differences additively caused a stronger electrostatic interaction with the σ -hole of the iodine centre in the case of the Pt-F.¹¹

The choice of solvent plays an important role in these non-covalent interactions. Previous work done in our group has proven that there was an increment in the values for K, $|\Delta H|$, $|\Delta S|$ when the solvent was changed from toluene to heptane. This was attributed in part to the formation of the π -stack adducts between fluorinated and non-fluorinated arenes.¹

5.2 NMR spectroscopic studies of halogen bonding interactions of Ni(F)(PEt₃)₂(2-C₅F₄N) with iodoperfluorohexane

5.2.1 Background /Aim

The halogen bonding interaction of *trans*-Ni(F)(PEt₃)₂(2-C₅F₄N) has been quantified with C₆F₅I as the halogen bond donor, in previous studies in our group.¹ Having achieved this, it was of interest to compare the binding energy of this metal complex to different halogen bond donors. In addition to this, it was also necessary to investigate sources of errors in the methods of determining the equilibrium constants.

5.2.2 Results

The halogen bonding interaction of $\text{Ni}(\text{F})(\text{PEt}_3)_2(2\text{-C}_5\text{F}_4\text{N})^{\text{a}}$ with a stronger halogen bond donor, compared to $\text{C}_6\text{F}_5\text{I}$, was investigated by NMR spectroscopic titration. For this purpose, 1-iodoperfluorohexane, a stronger halogen bond donor than $\text{C}_6\text{F}_5\text{I}$ was used.⁶ The ^{19}F -NMR spectroscopic titration was done at 300 K, measuring the downfield shift in the resonance of the fluoride, with increasing concentration of the halogen bond donor, $\text{C}_6\text{F}_{13}\text{I}$. The experiment was done in duplicate (experiments **a** and **b**) and the data was fitted to 1: 1 host-guest adduct formation model using a Microsoft Excel macro program developed by Professor Christopher Hunter (University of Cambridge) (Figure 5-1).

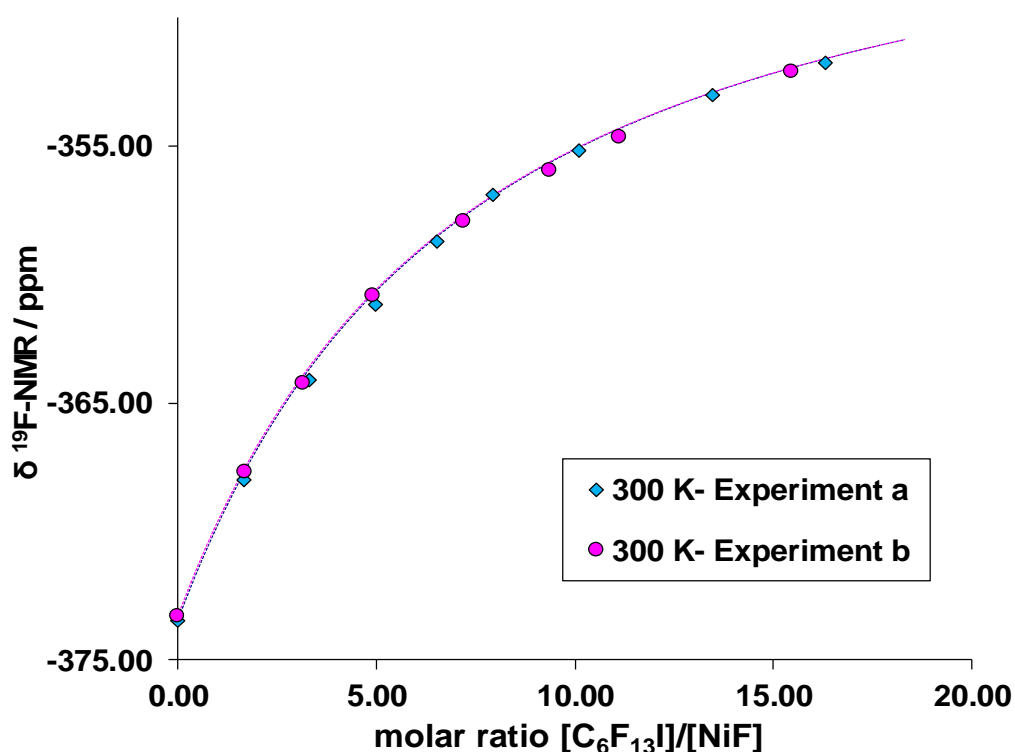


Figure 5-1 Fit of the titration curves at 300 K showing $\Delta\delta_{\text{F}}$ versus the ratio of the molar concentrations of $\text{C}_6\text{F}_{13}\text{I}$ and $\text{Ni}(\text{F})(\text{PEt}_3)_2(\text{C}_5\text{F}_4\text{N})$ in toluene- d_8 .

^a Complex, $\text{Ni}(\text{F})(\text{PEt}_3)_2(2\text{-C}_5\text{F}_4\text{N})$ was prepared by Dr. Dan A Smith as reported in literature. (12) Cronin, L.; Higgitt, C. L.; Karch, R.; Perutz, R. N. *Organometallics* **1997**, *16*, 4920.

The data points obtained from the two NMR spectroscopic titrations were fitted independently for the equilibrium constant (K_{eq}) and the downfield shift of the co-ordinated fluoride resonance from that of the free fluoride resonance ($\Delta\delta_F$). The values are given in Table 5-1 for both experiments a and b.

Table 5-1 Summary of the thermodynamic data for halogen bonding for complex $Ni(F)(PEt_3)_2(C_5F_4N)$ with $C_6F_{13}I$ at 300 K in toluene- d_8 .

	$K_{300} / \text{mol dm}^{-3}$	$\Delta\delta_F$
Exp- a	6.58 ± 0.02	30.96
Exp- b	6.58 ± 0.04	30.65

5.3 NMR spectroscopy studies of $Ni(F)(i\text{-Pr}_2\text{Im})_2(C_6F_5)$ as a Halogen and Hydrogen bond acceptor.

5.3.1 Introduction

Previous study in our group has shown that the mono-fluoride complex *trans*- $Ni(F)(PR_3)_2(C_5NF_4)$ (R = cyclohexyl and ethyl) acts as a Lewis base enabling hydrogen and halogen bonding interactions with hydrogen and halogen bond donors respectively.¹

As a continuation of the studies of halogen and hydrogen bonding interactions with group 10 metal fluorides in our group, a series of isostructural compounds were prepared, replacing the phosphine groups on the metal centre with N-heterocyclic carbenes, both literature known Ni-complex¹⁶ and isostructural Pt, and Pd complexes. These complexes, soluble in most organic solvents were used as the metal fluorides for the measurement of hydrogen and halogen bonding. The fluoride resonance appears up-field in the ^{19}F -NMR spectrum (δ - 376.3), free of overlap from other fluorine resonances and is highly sensitive to its environment and hence provides a direct spectroscopic tool for this measurement. The hydrogen bond donor used for the measurements was

indole, which is known to be a good hydrogen bond donor but a poor hydrogen bond acceptor. Iodopentafluorobenzene, which is a well-established halogen bond donor, ^{1,8,11} was used for the halogen bonding measurements (Scheme 5-2). The experimental results obtained from the previous study in the group are given in Table 5-2 .

Table 5-2 Thermodynamic data for hydrogen and halogen bonding for complexes $\text{Ni}(\text{F})(i\text{-Pr}_2\text{Im})_2(\text{C}_6\text{F}_5)$ from previous studies in the group.^b

	ΔH° / kJ/mol	ΔS° / J/(mol·K)	$\Delta\delta_{\text{F}}$
$\text{Ni}(\text{F})(i\text{-Pr}_2\text{Im})_2(\text{C}_6\text{F}_5)/ \text{C}_6\text{F}_5\text{I}$	-9.1(9)	-3(3)	52.1
$\text{Ni}(\text{F})(i\text{-Pr}_2\text{Im})_2(\text{C}_6\text{F}_5)/ \text{indole}$	5.8(2)	63(1)	36.2

However the thermodynamic data obtained from these experiments did not show the expected trend. Previous studies of the halogen bonding interaction of $\text{Ni}(\text{F})(\text{PEt}_3)_2(\text{C}_5\text{NF}_4)$, resulted in an enthalpy change of (ΔH°) -16 kJ/mol for the halogen bonding interaction with $\text{C}_6\text{F}_5\text{I}$ and an enthalpy change of (ΔH°) -23.4 kJ/mol for the hydrogen bonding interaction with indole.¹ In the above observation however the hydrogen bonding interaction had a positive enthalpy change indicating an endothermic reaction, and the entropy change was observed to be a large positive value. For these reasons the reliability of the results obtained was questionable. In retrospect it was hypothesised that the stronger interactions seen in these systems might be a reason for the unreliable data obtained from the experiments that were analogous to the experiments done previously with $\text{Ni}(\text{F})(\text{PEt}_3)_2(\text{C}_5\text{NF}_4)$. Therefore to obtain reliable data from such strongly interacting systems, the working concentrations of both guest and host must be lowered (Figure 5-2). The graph is generated by plotting the percentage binding against the ratio of guest: host.

^b The data presented was obtained from the experiments performed by Dr. Torsten Beweries, as a continuation of the XB studies on group 10 metal fluoride complexes. However, the work has not yet been published due to the unreliability of the thermodynamic data obtained via experiments.

The three solid lines in the graph are for the same equilibrium constant ($K = 1430$) but different concentrations of host. The curve for the highest concentration (33.6 mmol/dm^3) reaches saturation early and therefore makes it difficult to obtain as many data points in the region of binding. The curve with the lowest concentration (1.68 mmol/dm^3) gives the opportunity to obtain more data points before saturation occurs. The two dotted lines are plotted with a 10% increase in the equilibrium constant. The highest concentration with the higher K value (shown with the black dotted line) clearly overlaps with the curve with the lower K value, making it difficult to distinguish between the K values. However, the lowest concentration curve with the higher K (green dotted lines) does not overlap in the binding region with the lower K curve (blue solid line), making the two K values distinguishable from each other, and therefore gives the opportunity to obtain a more accurate measurement. Hence, the working concentrations of both guest and host species were lowered to be able to obtain reliable thermodynamic data for these systems.

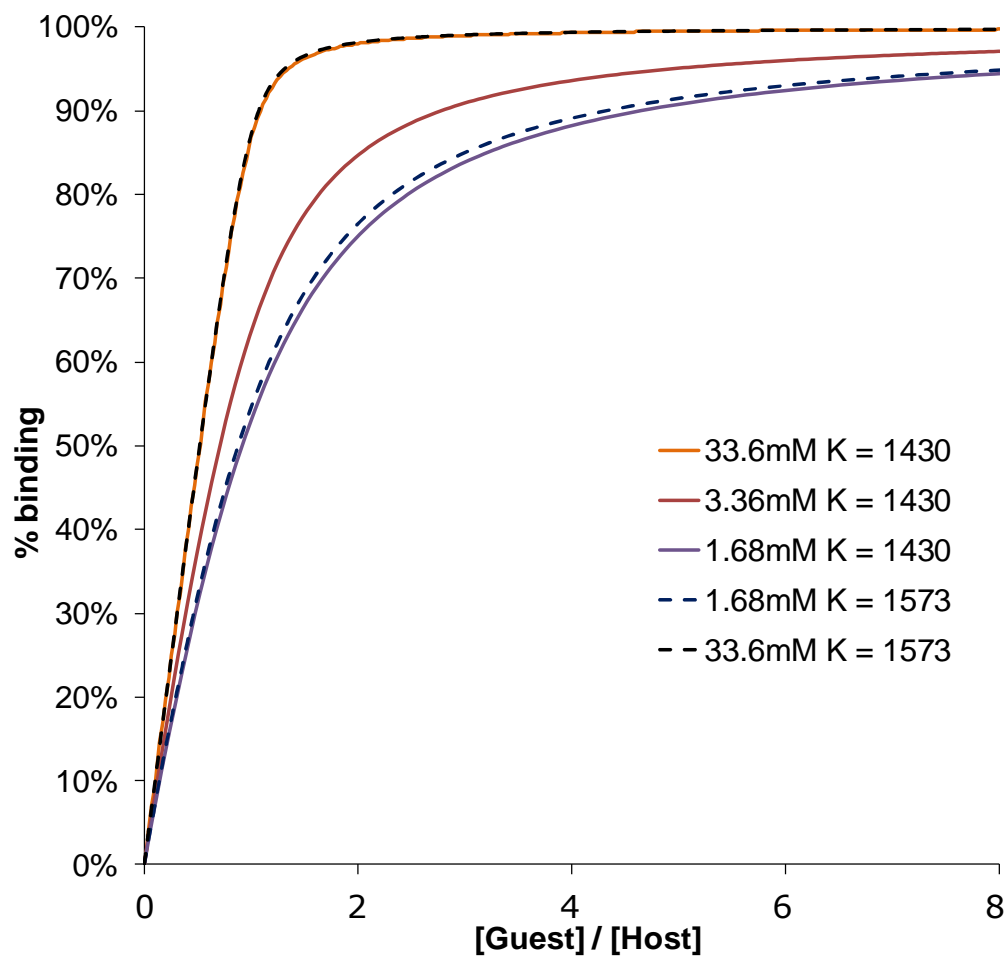


Figure 5-2 Predicted curves for a 1:1 host-guest binding system, for different concentrations of host and guest.

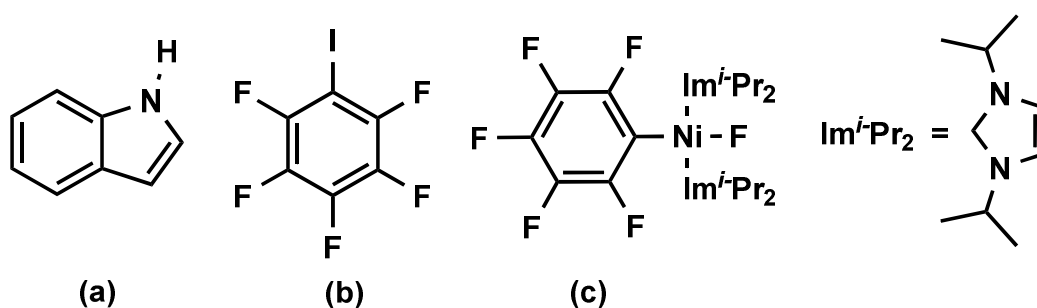
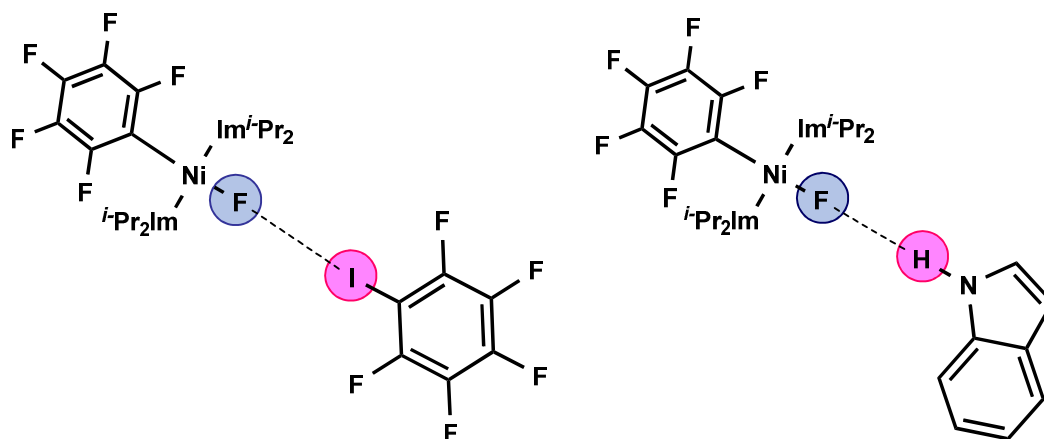


Figure 5-3 Species used for the study. (a) indole, (b) iodopentafluorobenzene, (c) *trans*-Ni(F)(*i*-Pr₂Im)₂(C₆F₅)



Scheme 5-2 *trans*-Ni(F)(*i*-Pr₂Im)₂(C₆F₅) acting as a Lewis base towards C₆F₅I and indole.

5.3.2 Results

5.3.2.1 NMR spectroscopy studies of Halogen bonding of *trans*-Ni(F)(*i*-Pr₂Im)₂(C₆F₅)

For *trans*-Ni(F)(*i*-Pr₂Im)₂(C₆F₅)^c, a downfield shift was observed in the fluoride resonance upon the introduction of the halogen bond donor, C₆F₅I. The variation in the shift was dependent on both the temperature and the amount of halogen-bond donor present. This shift in the resonance of the fluoride resonance was used to obtain the equilibrium constant for the formation of the halogen bonded adduct. A ¹⁹F-NMR spectroscopic titration was performed in toluene-d₈, varying the temperature from 260 K to 310 K. The data thus obtained were fitted to a 1: 1 host-guest adduct formation model (Figure 5-4). The concentration of the host complex, *trans*-Ni(F)(*i*-Pr₂Im)₂(C₆F₅) used for the experiments was 7 mmol/dm⁻³. The enthalpy change and entropy change for the adduct formation was obtained from the van't Hoff plot (Figure 5-5).



^c Complex, *trans*-Ni(F)(*i*-Pr₂Im)₂(C₆F₅) was taken from the laboratory stock, prepared according to the literature procedure. (16) Schaub, T.; Fischer, P.; Steffen, A.; Braun, T.; Radius, U.; Mix, A. *J. Am. Chem. Soc.* **2008**, *130*, 9304.

The two parameters fitted for the data points obtained were the equilibrium constant (K_{eq}) and the downfield shift of the co-ordinated fluoride resonance from that of the free fluoride resonance ($\Delta\delta_F$) (Table 5-3). The equilibrium constants obtained at different temperatures from the NMR spectroscopic data gave a linear regression fit ($R^2 = 0.999$) in van't Hoff plot (Figure 5-5), from which the entropy change ΔS° was calculated as -50.2 ± 1.2 J/(mol·K) and the enthalpy change ΔH° was calculated as -23.9 ± 0.3 kJ/mol. The temperature of the NMR spectrometer has been calibrated using methodology known in literature.¹⁷

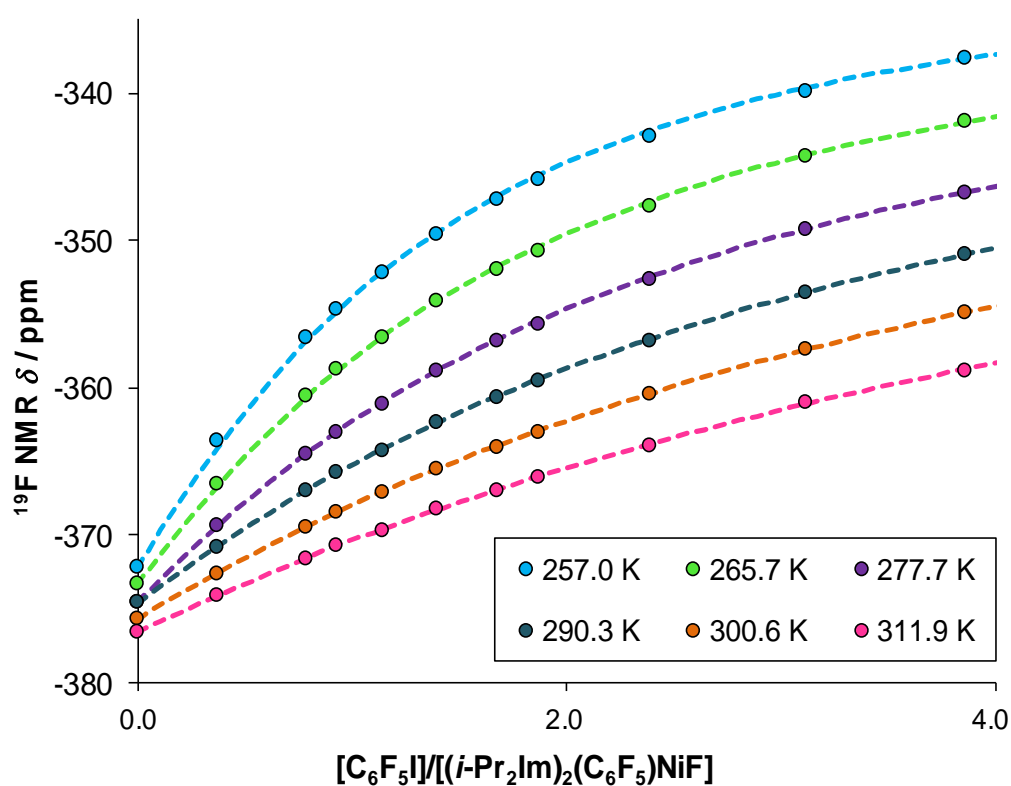


Figure 5-4 Fit of the titration curves for different temperatures showing $\Delta\delta_F$ versus the ratio of the molar concentrations of C₆F₅I and *trans*-Ni(F)(*i*-Pr₂Im)₂(C₆F₅) (~7 mM) in toluene-d₈.

Table 5-3 Equilibrium constants and the downfield shift of the co-ordinated fluoride resonance from that of the free fluoride resonance measured at various temperatures for adduct formation between *trans*-Ni(F)(*i*-Pr₂Im)₂(C₆F₅) and C₆F₅I in toluene.

Temperature /K	Equilibrium constant K _{eq}	$\Delta\delta_F$
257.0	171.0	43.5
265.7	114.2	43.3
277.7	73.7	43.7
290.3	45.7	41.6
300.6	33.0	45.9
311.9	24.1	46.8

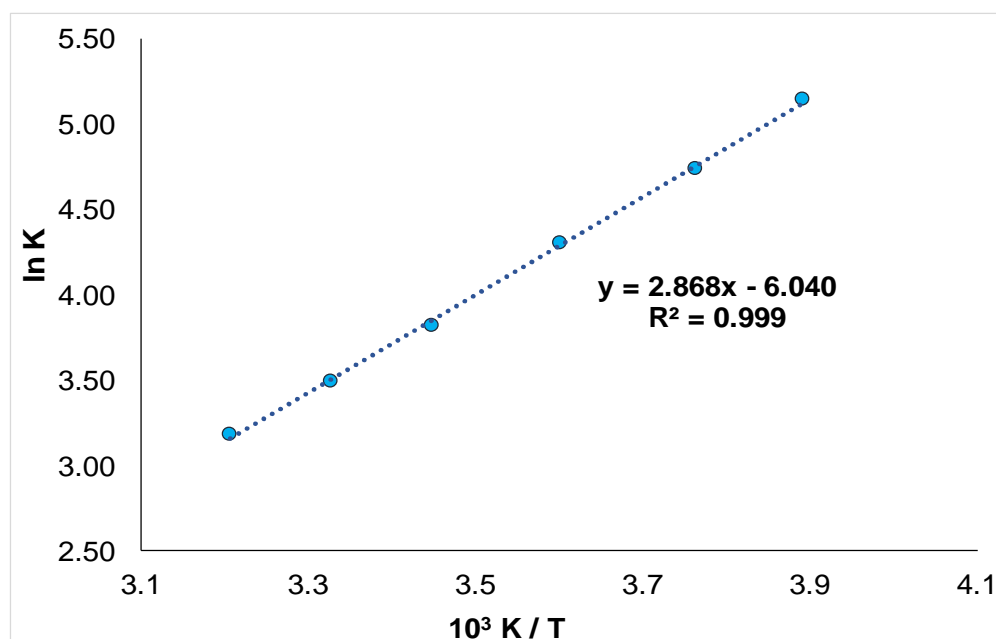


Figure 5-5 van't Hoff plot of the equilibrium constants from the NMR titration of C₆F₅I and Ni(F)(*i*-Pr₂Im)₂(C₆F₅) in toluene-d₈.

5.3.2.2 NMR spectroscopy studies of Hydrogen bonding of *trans*-Ni(F)(*i*-Pr₂Im)₂(C₆F₅).

A downfield shift was observed in the fluoride resonance when indole was introduced to the metal complex *trans*-Ni(F)(*i*-Pr₂Im)₂(C₆F₅). The equilibrium constant of the hydrogen bonding interaction of *trans*-Ni(F)(*i*-Pr₂Im)₂(C₆F₅) with indole was measured by a ¹⁹F-NMR spectroscopy titration, similar to the titration above mentioned. The variation in the shift of the fluoride resonance was measured over a temperature range of 270 K to 320 K. The data points thus obtained was fitted to a 1: 1 host-guest adduct formation model, similar to the halogen bonding interaction mentioned above. (Figure 5-6), fitting the equilibrium constants and the downfield shift of the co-ordinated fluoride resonance from that of the free fluoride resonance ($\Delta\delta_F$) (Table 5-4). (Concentration of the host, *trans*-Ni(F)(*i*-Pr₂Im)₂(C₆F₅) ~1.6mmol/dm⁻³).

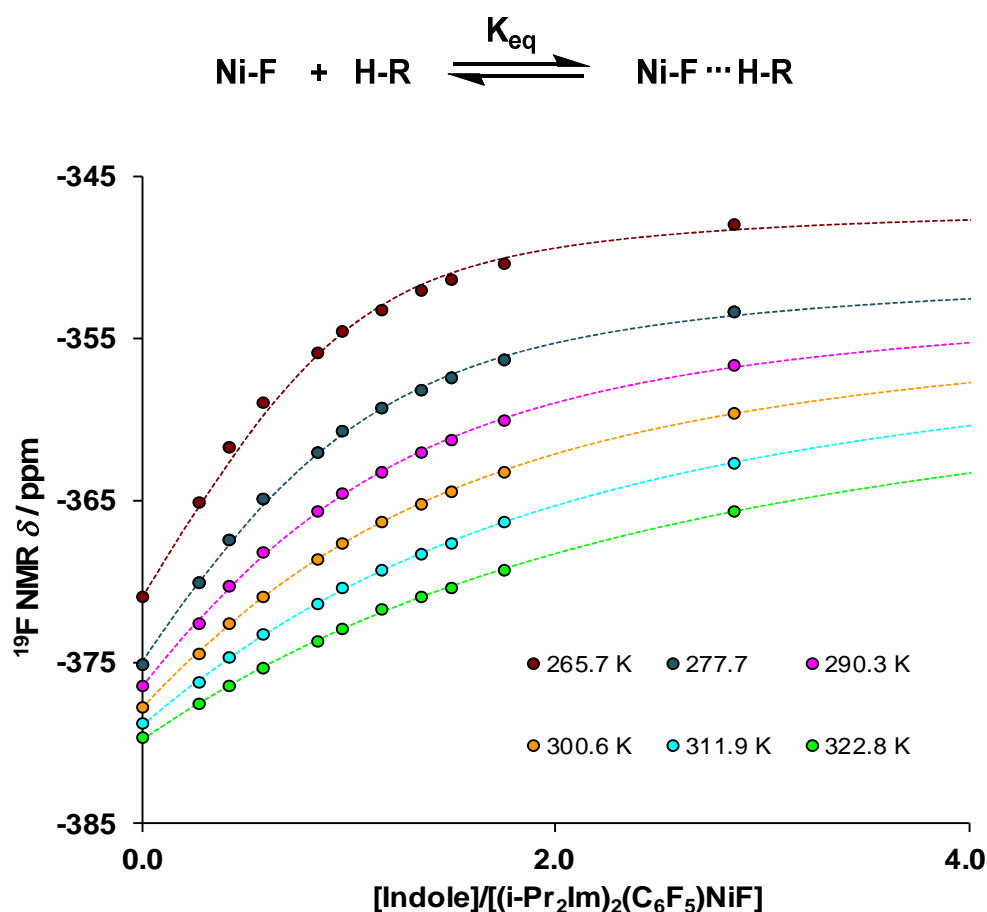


Figure 5-6 Fit of the titration curves for different temperatures showing $\Delta\delta_F$ versus the ratio of the molar concentrations of indole and Ni(F)(*i*-Pr₂Im)₂(C₆F₅) (~1.6 mM) in toluene-d₈.

The equilibrium constants at different temperatures were used to plot the van't Hoff plot (Figure 5-7), which gave rise to a linear regression line ($R^2 = 0.999$). From the gradient and the intercept of the van't Hoff plot the change in the bond formation enthalpy was calculated as -32.7 ± 0.5 kJ/mol, and the change in the entropy was calculated as -53.6 ± 1.7 J/ (mol·K).

Table 5-4 Equilibrium constants and the downfield shift of the coordinated fluoride resonance from that of the free fluoride resonance measured at various temperatures for adduct formation with indole in toluene.

Temperature /K	Equilibrium constant $K_{eq} / 10^2$	$\Delta\delta_F$
265.7	41.6	23.5
277.7	20.8	24.6
290.3	11.3	25.0
300.6	7.2	25.5
311.9	4.4	26.3
322.8	3.1	26.3

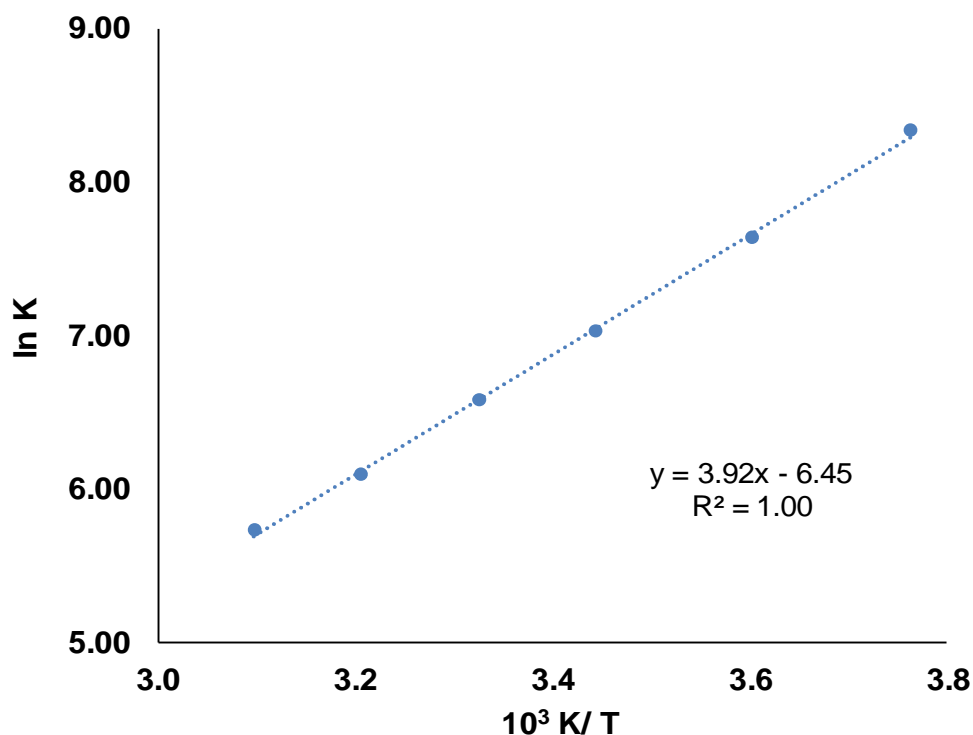


Figure 5-7 van't Hoff plot of the equilibrium constants from the NMR titration of indole and $\text{Ni}(\text{F})(i\text{-Pr}_2\text{Im})_2(\text{C}_6\text{F}_5)$ in toluene- d_8 .

Table 5-5 Summary of the thermodynamic data obtained for hydrogen and halogen bonding of $\text{Ni}(\text{F})(i\text{-Pr}_2\text{Im})_2(\text{C}_6\text{F}_5)$ with indole and $\text{C}_6\text{F}_5\text{I}$ respectively, in toluene- d_8 .

Lewis Acid	K_{300}	$\Delta H^\circ / \text{kJ/mol}$	$\Delta S^\circ / \text{J}/(\text{mol}\cdot\text{K})$
$\text{C}_6\text{F}_5\text{I}$	33.0	-23.9 ± 0.3	-50.2 ± 1.2
Indole	716.7	-32.7 ± 0.5	-53.6 ± 1.7

5.4 Discussion

N-heterocyclic carbenes are electron-rich neutral σ -donating ligands, which are well known for their ability to form very strong bonds with several metals. N-heterocyclic carbenes are often used as alternatives for phosphine ligands in catalysis.^{18,19} The results obtained in this study show that the enthalpy of interaction for $\text{Ni}(\text{F})(i\text{-Pr}_2\text{Im})_2(\text{C}_6\text{F}_5)$ with indole (-32.7 kJ/mol) is stronger than

that with C₆F₅I (-23.9 kJ/mol), indicating a preference of hydrogen bonding over halogen bonding, when C₆F₅I and indole are used as the halogen and hydrogen bond donor respectively (Table 5-5). This is consistent with the previous observation made in our group for the hydrogen and halogen bonding of analogous phosphine attached complex, Ni(F)(PEt₃)₂(C₅NF₄) (Table 5-6).¹ However, in order to be able to predict the preference of binding between HB donors and XB donors of these metal fluoride complexes in general, comparison studies must be carried out with structurally similar XB and HB donors.

Table 5-6 Thermodynamic data for hydrogen and halogen bonding for complexes Ni(F)(*i*-Pr₂Im)₂(C₆F₅) studies here and the literature values for Ni(F)(PCy₃)₂(C₅NF₄)¹¹ and Ni(F)(PEt₃)₂(C₅NF₄)¹ in toluene.

	Indole		C ₆ F ₅ I	
	ΔH°/ kJ/mol	ΔS°/ J/(mol·K)	ΔH°/ kJ/mol	ΔS°/ J/(mol·K)
Ni(F)(<i>i</i> -Pr ₂ Im) ₂ (C ₆ F ₅)	-32.7	-53.6	-23.9	-50.2
Ni(F)(PCy ₃) ₂ (C ₅ NF ₄) ¹¹	-	-	-18.6(4)	-54(2)
Ni(F)(PEt ₃) ₂ (C ₅ NF ₄) ¹	-23.4(2)	-44.5(8)	-16(1)	-42(4)

The significant feature of the above table is that the experimentally obtained enthalpies of both halogen bond and hydrogen bond formation of *trans*-Ni(F)(*i*-Pr₂Im)₂(C₆F₅), with C₆F₅I and indole respectively, are higher than the bond formation enthalpies obtained for the analogous phosphine attached metal complexes *trans*-Ni(F)(PEt₃)₂(C₅NF₄) and the tricyclohexyl phosphine complex *trans*-Ni(F)(PCy₃)₂(C₅NF₄) in toluene experimentally.^{1,11} This can be attributed mainly due to the difference in the other ligands on the metal centres of the

two complexes which do not have a direct participation in the formation of the halogen or hydrogen bond.

It is known from previous experiments in our group, that the strength of the halogen binding interaction increased with the basicity of the phosphine groups attached to the metal centre in the metal fluoride complex (Table 5-6).¹¹ Substituting the phosphine groups with N-heterocyclic carbene groups resulted in stronger halogen bonding interaction than both the analogous phosphine ligated complexes as expected. N-heterocyclic carbenes are known to be stronger σ -donors than highly basic phosphine groups as a result of the highly directional sp^2 -type lone pair on the carbon atom.^{18,19} In addition to this, the π -back donation of the N-heterocyclic carbenes with the metal centre, though not negligible, is less pronounced compared to phosphine groups. These differences make the metal more electron rich when the phosphine groups on the metal are replaced by N-heterocyclic carbene groups, thus enabling stronger interactions for the metal-fluoride.

The other difference in the structure of the two complexes compared is the fluoroarene ring. Previous studies in our group with a series of group 10 metal fluoride complexes showed that changing the fluoroarene ring from tetrafluoropyridyl in *trans*-[Ni(F)(C₅NF₄)(PCy₃)₂] ($\Delta H^\circ = -18.6$ kJ/mol) to 3,5-difluoro-4-trifluoromethylpyridyl in *trans*-Ni(F)(PCy₃)₂[C₅NF₂H(CF₃)] ($\Delta H^\circ = -18.9$ kJ/mol) had an insignificant change in the strength of the halogen bonding interaction, compared to the change of the phosphine group from triethyl phosphine ($\Delta H^\circ = -16$ kJ/mol) to tricyclohexyl phosphine ($\Delta H^\circ = -18.6$ kJ/mol). However, unlike the above mentioned example, where the change is in the substituent on the fluoropyridyl ring, the change is more complicated in our comparison, as the change is from a fluoropyridyl ring to a fluorophenyl ligand, and not negligible. However, despite this it could be concluded that the major contribution to the strengthening of the halogen bond adduct formation is the metal centre made more electron rich, by the attached N-heterocyclic carbene groups.

The equilibrium constant at 300 K, obtained for the halogen bond adduct formation between the Ni(F)(PEt₃)₂(C₅F₄N) and C₆F₁₃I (K_{eq} = 6.58(1)) is higher than the analogous interaction with C₆F₅I (K_{eq} = 3.41(9)).¹ This stronger interaction is due to the halogen bond donor C₆F₁₃I being a stronger halogen bond donor than C₆F₅I.

5.5 Summary

The previous work done with the metal complex *trans*-Ni(F)(*i*-Pr₂Im)₂(C₆F₅), to study the halogen and hydrogen bonding interaction, gave thermodynamic data that was anomalous, but the thermodynamic data obtained in this study has proved to be fruitful and more reliable, as the results show the expected trend. The N-heterocyclic carbene complex, *trans*-Ni(F)(*i*-Pr₂Im)₂(C₆F₅), has been shown to have a stronger halogen bonding and hydrogen bonding interaction than the analogous complex Ni(F)(PEt₃)₂(C₅F₄N), which is demonstrated by the larger enthalpy change associated with the binding. This can be attributed mainly to the halogen bond acceptor, the fluoride made more electron rich by the strong σ -donation from the N-heterocyclic carbene.

5.6 References

- (1) Libri, S.; Jasim, N. A.; Perutz, R. N.; Brammer, L. *J. Am. Chem. Soc.* **2008**, *130*, 7842.
- (2) Hassel, O.; Hvoslef, J.; Vihovde, E. H.; Sørensen, N. A. *Acta Chem. Scand.* **1954**, *8*, 873.
- (3) Beale, T. M.; Chudzinski, M. G.; Sarwar, M. G.; Taylor, M. S. *Chem. Soc. Rev.* **2013**, *42*, 1667.
- (4) Arunan, E.; Desiraju Gautam, R.; Klein Roger, A.; Sadlej, J.; Scheiner, S.; Alkorta, I.; Clary David, C.; Crabtree Robert, H.; Dannenberg Joseph, J.; Hobza, P.; Kjaergaard Henrik, G.; Legon Anthony, C.; Mennucci, B.; Nesbitt David, J. In *Pure Appl. Chem.* 2011; Vol. 83, p 1619.
- (5) Legon, A. C.; Millen, D. J. *Faraday Discussions of the Chemical Society* **1982**, *73*, 71.
- (6) Smith, D. A.; Brammer, L.; Hunter, C. A.; Perutz, R. N. *J. Am. Chem. Soc.* **2014**, *136*, 1288.

- (7) Robertson, C. C.; Perutz, R. N.; Brammer, L.; Hunter, C. A. *Chem. Sci.* **2014**, *5*, 4179.
- (8) Nguyen, H. L.; Horton, P. N.; Hursthouse, M. B.; Legon, A. C.; Bruce, D. W. *J. Am. Chem. Soc.* **2003**, *126*, 16.
- (9) Peris, E.; Lee, J. C.; Rambo, J. R.; Eisenstein, O.; Crabtree, R. H. *J. Am. Chem. Soc.* **1995**, *117*, 3485.
- (10) Laurence, C.; Queignec-Cabanetos, M.; Dziembowska, T.; Queignec, R.; Wojtkowiak, B. *J. Am. Chem. Soc.* **1981**, *103*, 2567.
- (11) Beweries, T.; Brammer, L.; Jasim, N. A.; McGrady, J. E.; Perutz, R. N.; Whitwood, A. C. *J. Am. Chem. Soc.* **2011**, *133*, 14338.
- (12) Cronin, L.; Higgitt, C. L.; Karch, R.; Perutz, R. N. *Organometallics* **1997**, *16*, 4920.
- (13) Brammer, L.; Bruton, E. A.; Sherwood, P. *Cryst. Growth Des.* **2001**, *1*, 277.
- (14) Aullon, G.; Bellamy, D.; Guy Orpen, A.; Brammer, L.; Eric, A. B. *Chem. Commun. (Cambridge, U. K.)* **1998**, 653.
- (15) Sarwar, M. G.; Dragisic, B.; Salsberg, L. J.; Gouliaras, C.; Taylor, M. S. *J. Am. Chem. Soc.* **2010**, *132*, 1646.
- (16) Schaub, T.; Fischer, P.; Steffen, A.; Braun, T.; Radius, U.; Mix, A. *J. Am. Chem. Soc.* **2008**, *130*, 9304.
- (17) Ammann, C.; Meier, P.; Merbach, A. *Journal of Magnetic Resonance (1969)* **1982**, *46*, 319.
- (18) Wilson, D. J. D.; Couchman, S. A.; Dutton, J. L. *Inorg. Chem.* **2012**, *51*, 7657.
- (19) Fortman, G. C.; Nolan, S. P. *Chem. Soc. Rev.* **2011**, *40*, 5151.

CHAPTER SIX

CONCLUSIONS

AND

FURTHER DEVELOPMENT

CONCLUSIONS AND FURTHER DEVELOPMENT**HYDROFLUOROARYLATION OF ALKYNES****The objective of the study -**

The study was motivated by the difference in the mechanisms proposed in literature for the hydrofluoroarylation of alkynes catalysed by Ni(COD)₂ using phosphines as the ligands. Thus the main objective of the study was to investigate the mechanism in more detail. For this purpose a suitable system to gain experimental data that could be kinetically analysed was sought.

Conclusions based on this study –

- The project was started with a search for a system to study the hydrofluoroarylation reaction in detail. For this purpose, initially the literature known nickel bis-phosphine complex Ni(PCy₃)₂(alkyne) (alkyne = 3-hexyne, PhC≡CPh) and nickel mono-phosphine complex (1,5-hexadiene)Ni(PR₃) (R = *i*-Pr, Cy) were chosen.^{1,2} The bis-phosphine complex Ni(PR₃)₂(alkyne) on reacting with C₆F₅H gave rise to side reactions resulting in C-H and C-F bond activation in addition to the hydrofluoroarylation. The reaction of Ni(PCy₃)₂(alkyne) with C₆F₅H gave *trans*-Ni(H)(PCy₃)₂(C₆F₅) as a product of C-H bond activation. The products resulting from C-F activation were *trans*-Ni(F)(PCy₃)₂(C₆F₄H) and Ni(F)(PCy₃)₂(C₆F₄(R₁)C=C(R₁)H) (R₁ = Ph, CH₂CH₂CH₃). Experimental results suggest Ni(F)(PCy₃)₂(C₆F₄(R₁)C=C(R₁)H) is formed via a C-F bond activation of the para position of the arylalkene, resulting from the hydrofluoroarylation reaction.
- The mono-phosphine complex, (1,5-hexadiene)Ni(PR₃) behaved as a bis-phosphine nickel source. This was believed to be a result of the phosphine ligated to nickel being labile and therefore easily detached from the metal source to form the bis-phosphine nickel source.

- The alternative literature known complex, (1,5-hexadiene)Ni(IPr) has been shown to catalyse the hydrofluoroarylation reaction in this study. It was also observed that symmetrical and unsymmetrical alkynes behaved differently in the hydrofluoroarylation reaction where the symmetrical alkynes gave rise to trimerization of the alkynes in the presence of the catalyst, (1,5-hexadiene)Ni(IPr). The hydrofluoroarylation reaction catalysed by (1,5-hexadiene)Ni(IPr) proved to be free of paramagnetic species and was monitored in-situ by NMR spectroscopy.
- The hydrofluoroarylation reaction of $\text{CH}_3\text{C}\equiv\text{CC}(\text{CH}_3)_3$ with $\text{C}_6\text{F}_5\text{H}$ catalysed by (1,5-hexadiene)Ni(IPr) was used as the system to collect experimental data for kinetic analysis. This reaction proved to be free of side reactions and the reactants were consumed to give only the desired product (only one isomer was observed to form). Data was collected using $^1\text{H-NMR}$ spectroscopy. This data was analysed by classical kinetic methods and by reaction progress kinetic analysis.³ In addition to this, the experimental data was fitted with a modelling and simulation program.
- The kinetic analysis of the reaction of $\text{CH}_3\text{C}\equiv\text{CC}(\text{CH}_3)_3$ and $\text{C}_6\text{F}_5\text{H}$ catalysed by (1,5-hexadiene)Ni(IPr) provided evidence for an initial alkyne coordination. The kinetic analysis suggests that the reaction follows saturation kinetics with respect to alkyne and the rate of the reaction is not directly dependent on the alkyne when alkyne is present in excess.
- The kinetic analysis also suggests a first order dependence on both the fluoroarene and the catalyst. The initial coordination of alkyne suggests a hydrogen transfer by ligand-to-ligand hydrogen transfer according to the DFT calculations performed on the hydrofluoroarylation reaction catalysed by Ni-PR₃ reported in literature.⁴
- The model also suggested an equilibrium between the mono and bis-alkyne nickel complexes, (IPr)Ni(alkyne)₂ and (IPr)Ni(alkyne). The active species involved in the catalytic cycle, however, was the mono-alkyne complex, (IPr)Ni(alkyne). This observation too is in agreement

to the DFT calculation results reported in literature. The final reductive elimination step which gives the product involves the coordination of fresh alkyne rather than the 1,5-hexadiene in the medium. The kinetic analysis performed on the hydrofluoroarylation reaction is more closely related to the mechanism proposed based on the computational calculations⁵ than the mechanism proposed based on experimental data.⁶

HALOGEN BONDING INTERACTION STUDIES

Intermolecular halogen bonding interactions of nickel halide complexes and their pendant halogen bond donors in the solid state

The objective of the project –

Crystal structures of metal-halide systems exhibiting halogen bonding interactions are reported for chloride, bromide and iodide but metal-fluoride halogen bonding interactions in the solid state were still absent. Therefore a system exhibiting a metal fluoride interaction with a halogen was targeted for the study. A series of self-complementary molecules were prepared for this purpose.

Conclusions based on this study –

- The model chosen for study, *trans*-Ni(X)(L)₂(C₆F₄I) [where, X = F, Cl, Br and I; L = PEt₃ and P(Et₂Ph)₃] proved to be quite successful in thoroughly demonstrating a halogen bonded self-complementary metal-halide system.
- The model as expected showed the greatest reduction of intermolecular distance when normalised to the van der Waals radii, when the metal fluoride was used as the XB acceptor. This is in agreement with the observation made by Rissanen, where the electrostatic contribution plays a vital role when the XB acceptors are metal halides.⁷

- The anisotropic charge distribution found in large polarizable halogens is demonstrated by the halogen bonding interactions occurring at an angle of 139° to 147° for Ni-X...I when the halides are I, Br and Cl and the angle of interaction was found to be 180°, for Ni-F...I, which is attributable to the absence of a significant anisotropic charge distribution in fluoride.
- The interaction was found to be more prominent with the para iodo complexes than the ortho iodo complexes, this observation can be rationalised by the number of fluorine atoms ortho to the iodine. More fluorine atoms ortho to the halogen bond donor, makes the σ -hole more electron deficient.
- A higher interaction was seen when the metal was ligated to triethyl phosphine groups than when ligated to less electron donating and more sterically demanding diethylphenyl phosphine groups.
- In addition to X-ray crystallographic techniques, solid state NMR spectroscopy has been employed to study the interactions using ^{19}F -solid state NMR spectroscopy. The fluoride resonances were found to show a significant shift depending on the strength of the halogen bonding interaction. This was compared to the analogous system without the halogen bonding interaction.
- A variable temperature X-ray crystallographic study showed a 4.5 % reduction in the unit cell volume when the temperature is changed from 240 K to 200 K and ca 2 % reduction in the unit cell volume from 200 K to 111 K. Overall ca 6.5 % reduction is observed in the unit cell volume when the temperature is changed from 240 K to 111 K.

Solution studies of hydrogen and halogen bonding towards nickel fluoride complexes

- The solution-state studies performed via ^{19}F -NMR spectroscopic titrations, of the halogen bonding and hydrogen bonding interactions of the N-heterocyclic carbene complex, *trans*-Ni(F)(*i*-Pr₂Im)₂(C₆F₅) (*i*-Pr₂Im = 1,3-bis(isopropyl)imidazolin-2-ylidene), has been shown to have a stronger halogen bonding and hydrogen bonding interaction than the analogous complex Ni(F)(PEt₃)₂(2-C₅F₄N). This was demonstrated by the larger enthalpy change associated with the binding. This observation can be attributed mainly to the halogen bond acceptor, the fluoride made more electron rich by the strong σ -donation from the N-heterocyclic carbene.⁸ The importance of using very dilute solutions of the guest and host for determination of strong binding was demonstrated.

Further development

- Mechanism of hydrofluoroarylation - The mechanistic understanding derived from the kinetic analysis of the experimentally obtained data for the hydrofluoroarylation reaction is similar to the mechanism postulated based on the DFT calculations. However, the repetition of the calculations for the hydrofluoroarylation reaction catalysed by the N-heterocyclic complex, (1,5-hexadiene)Ni(IPr) instead of the Ni-PR₃ would enable one to obtain much clearer insight into the mechanism and a more accurate comparison can be made to the experimentally obtained results.
- Solid state halogen bonding interactions – Solid state interactions have been demonstrated with metal-fluorides as the halogen bond acceptors. The work has been performed by fluorinating the nickel iodide Ni(I)(PEt₃)₂(C₆F₄I) which was obtained by oxidative addition of one iodine in diiodotetrafluorobenzene. This can be extended to model systems with bidentate phosphine ligands or a different group of ligand

to change the geometry and the strength of the halogen bonding interactions. Similarly the fluoroarene can be changed to exhibit different results.

- The solution state studies of the halogen bonding and hydrogen bonding interactions towards *trans*-Ni(F)(*i*-Pr₂Im)₂(C₆F₅) has been demonstrated that it is a far more potent Lewis base than its analogue Ni(F)(PEt₃)₂(2-C₅F₄N). The work detailed in chapter 5 has been previously done with the N-heterocyclic carbene complexes of Ni, Pd and Pt in the group giving thermodynamic data that was not reliable. The complexes with Ni has been studied again in this work demonstrating the possibility of more reliable results by working at lower concentration. This can be extended to complete the series of complexes of the group 10 metals to obtain a complete comparison.

References

- (1) Wu, J.; Faller, J. W.; Hazari, N.; Schmeier, T. J. *Organometallics* **2012**, *31*, 806.
- (2) Hatnean, J. A.; Beck, R.; Borrelli, J. D.; Johnson, S. A. *Organometallics* **2010**, *29*, 6077.
- (3) Blackmond, D. G. *Angew Chem Int Ed Engl* **2005**, *44*, 4302.
- (4) Guihaumé, J.; Halbert, S.; Eisenstein, O.; Perutz, R. N. *Organometallics* **2012**, *31*, 1300.
- (5) Guihaume, J.; Halbert, S.; Eisenstein, O.; Perutz, R. N. *Organometallics* **2012**, *31*, 1300.
- (6) Kanyiva, K. S.; Kashihara, N.; Nakao, Y.; Hiyama, T.; Ohashi, M.; Ogoshi, S. *Dalton Trans.* **2010**, *39*, 10483.
- (7) Johnson, M. T.; Džolić, Z.; Cetina, M.; Wendt, O. F.; Öhrström, L.; Rissanen, K. *Cryst. Growth Des.* **2011**, *12*, 362.
- (8) Crabtree, R. H. *J. Organomet. Chem.* **2005**, *690*, 5451.

CHAPTER SEVEN

EXPERIMENTAL

1 Experimental

1.1 General considerations

All experiments involving oxygen and water sensitive materials were done under an argon or nitrogen atmosphere, in an argon filled glove box or standard Schlenk (10^{-2} mbar) techniques or high vacuum lines (10^{-4} mbar). General use solvents (AR grade) were dried over sodium, distilled and stored under argon. Solvents such as hexane and THF were collected from the solvent purification system (removes oxygen and water) and were further dried and distilled. Deuterated solvents were dried over potassium and distilled prior to use. Normal laboratory nitrogen was dried further by passing through a column filled with activated molecular sieves.

1.2 Solution NMR spectroscopy and mass spectrometry

All standard NMR spectra were recorded on Bruker AMX500 spectrometers, unless otherwise stated, in tubes fitted with Young's PTFE stopcocks. All ^1H and ^{13}C chemical shifts are reported in ppm (δ) relative to tetramethylsilane and referenced using the chemical shifts of residual protio solvent resonances (benzene, δ 7.16), unless otherwise stated. The $^{31}\text{P}\{^1\text{H}\}$ -NMR spectra were referenced to external H_3PO_4 .

LIFDI mass spectra were obtained from a Waters Micromass GCT Premier orthogonal time-of-flight instrument set to one scan per second with resolution power of 6000 FWHM and equipped with a LIFDI probe from LINDEN GmbH. Toluene was used for tuning the instrument. The polyethylene glycol probe was kept at ambient temperature with the emitter potential at 12 kV. Activated tungsten wire LIFDI emitters (13 μm tungsten from LINDEN) were ramped manually up to 100 mA for the emitter heating current during the experiment. The m/z values are accurate to 0.01 Da.

1.3 Solid State NMR spectroscopy

The MAS rotors and caps were pumped under high vacuum for 24 hours then stored in the glove box where they remained for at least a week before use. The ^{19}F -MAS NMR spectra were acquired at 9.4T (376.48 MHz) using a Bruker Avance III HD console and a Bruker 2.5mm H(F)/X double-resonance probe. A 30° tip-angle pulse was used to acquire the spectra to ensure sufficient radio frequency bandwidth to yield undistorted spinning sideband intensities. Relaxation delays of 4-7 s were used. Spectra were collected at 296 K unless stated otherwise. All shifts are reported relative to CFCl_3 and were calibrated using solid sodium fluoride ($d_{\text{iso}} = -224.2$ ppm) as a secondary external reference. Isotropic chemical shifts were determined by comparison of three or more spectra acquired over a range of rotation frequencies (9-30 kHz). Simulation of the shielding tensors was performed using the CSA tensor module (Eichele/Wasylishen) within the WSolids NMR Simulation Package (ver. 1.20.18).

1.4 CHAPTER 2

THE SEARCH FOR A SYSTEM TO STUDY THE MECHANISM OF HYDROFLUOROARYLATION OF ALKYNES

1.4.1 General considerations

All air and moisture sensitive steps were performed inside the glove box or in a Schlenk line. Tricyclohexylphosphine (Sigma-aldrich) was used from the laboratory stock and tricyclopentylphosphine was purchased from Sigma-Aldrich and used as received. Diphenylacetylene were purchased from Sigma-Aldrich and was stored in the glove box after the removal of oxygen. $\text{C}_6\text{F}_5\text{H}$, $\text{C}_5\text{F}_5\text{N}$ and 1,4- $\text{C}_6\text{F}_4\text{H}_2$ (Sigma-Aldrich) were stored in ampoules over molecular sieves after the removal of oxygen. Alkynes, 4-octyne, 3-hexyne,

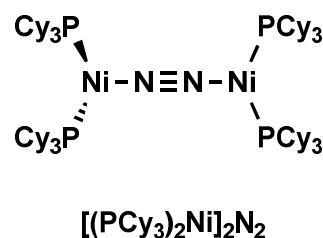
$\text{PhC}\equiv\text{CSiMe}_3$ (Sigma-Aldrich) and $\text{CH}_3\text{C}\equiv\text{CC}(\text{CH}_3)_3$ (Alfa-aesar) were subjected to removal of oxygen by freeze-pump-thaw cycles and stored in the glove box over molecular sieves. Allylmagnesium chloride and P^iPr_3 were purchased from Sigma-Aldrich and used as received.

$\text{Ni}(\text{COD})_2$ was prepared as reported in literature¹ from $\text{NiCl}_2 \cdot 6\text{H}_2\text{O}$ (20.0g, 84.2mmol) which was taken in a Schlenk flask and dissolved in ethanol (250 mL). To the resulting solution pyridine (40 mL) was added and stirred for 2 hours. The resulting blue solid product was filtered and dried (46 g, 68.7% yield). The product $\text{Ni}(\text{Py}_4)\text{Cl}_2$ (5g, 1.74mmol) was taken in a Schlenk flask and was dissolved in THF (50 mL) and to this 1,5-cyclooctadiene (2.5 mL, 20.4 mmol) was added. While stirring a slight excess of sodium (0.5 g) was added and was allowed to stir for another 3 hours. The solvent was removed under vacuum and the resulting solid was extracted with benzene. The solvent was removed under vacuum and the resulting solid was washed with methanol (3 mL x 3) to remove the black impurity present in the reaction mixture. The resulting yellow solid was dried under vacuum and stored in the glove box (0.2 g, 41.9% yield). Experiments were also carried out using commercially available $\text{Ni}(\text{COD})_2$ (Sigma-Alrich).

1.4.2 Synthesis of Bis(bis-(tricyclohexylphosphine)nickel) dinitrogen

The synthesis was performed as reported in literature.^{2,3} All glassware was heated under vacuum prior to the synthesis, to ensure them moisture free. Normal laboratory nitrogen was dried further by passing through a column filled with molecular sieves, which was heated and dried under vacuum trapping the moisture over a week, prior to drying nitrogen. In a Schlenk flask, a solution of $\text{Ni}(\text{acac})_2$ (previously prepared and sublimed and stored in the glove box 2.0 g, 7.8 mmol) and PCy_3 (4.4 g, 15.7mmol) was prepared in toluene (12 mL) inside the glove box. This was taken out connected to nitrogen on the Schlenk line and cooled to $-20\text{ }^\circ\text{C}$, to this $\text{Al}(\text{CH}_3)_3$ (2 M in toluene, 7.8 mL) was added slowly by a cannula over an hour while bubbling in nitrogen. The resulting mixture was allowed to reach room temperature slowly and this was stirred further for

another 24 hours under nitrogen. The solution was cooled in an ice and the solvent was filtered giving a deep red solid as the final product (0.78 mg, 16 %). The solid thus obtained was taken into a nitrogen filled glove box and samples for NMR spectroscopy and IR spectroscopy were prepared.



IR, toluene: 2030.3 cm^{-1} (2028 cm^{-1} reported in literature)³ : **^{31}P -NMR** (500 MHz, C_6D_6) δ 46.1

1.4.3 Synthesis of $(PCy_3)_2Ni(\eta^2-PhC\equiv CPh)$

The preparation of $(PCy_3)_2Ni(\eta^2-PhC\equiv CPh)$ was performed similarly to the analogous compound known in literature.⁴ A suspension of $Ni(COD)_2$ (138 mg, 0.5 mmol) was prepared in pentane (3 mL) To this, PCy_3 (280 mg, 1.0 mmol) was added and left to stir till dissolved, after which diphenylacetylene (89 mg, 0.5 mmol) was added and allowed to stir at room temperature for a further 30 minutes. Upon cooling the resulting solution in an ice bath for 30 minutes an orange coloured solid precipitated. The solid was separated by decanting and washed with cold pentane. After drying the resulting solid in vacuo the solid was analysed by NMR spectroscopy and mass spectrometry. (369 mg, 92.7 % yield).

^{31}P -NMR (C_6D_6 , 298 K): δ 41.2 (s, 2 P): **MS** (LIFDI 100 % M^+) 796.51

1.4.4 Synthesis of $(PCy_3)_2Ni(\eta^2-CH_3CH_2CH_2C\equiv CCH_2CH_2CH_3)$

A similar procedure to that used in the synthesis of $(PCy_3)_2Ni(\eta^2-PhC\equiv CPh)$ was followed.¹¹ The resulting bright yellow solid (80 mg, 91.5 % yield) was analysed by NMR spectroscopy and mass spectrometry.

^{31}P -NMR (C_6D_6 , 298 K): δ 44.4 (s, 2 P): **MS** (LIFDI 100 % M^+) 728.53

1.4.5 Reaction of $(\text{PCy}_3)_2\text{Ni}(\eta^2\text{-alkyne})$ with $\text{C}_6\text{F}_5\text{H}$ (where, alkyne = 4-octyne and $\text{PhC}\equiv\text{CPh}$)

1.4.5.1 Reaction (i)

The reactions with $(\text{PCy}_3)_2\text{Ni}(\eta^2\text{-PhC}\equiv\text{CPh})$ are given in detail in this section, however, the common procedure for both complexes $(\text{PCy}_3)_2\text{Ni}(\eta^2\text{-PhC}\equiv\text{CPh})$ and $(\text{PCy}_3)_2\text{Ni}(\eta^2\text{-CH}_3\text{CH}_2\text{CH}_2\text{C}\equiv\text{CCH}_2\text{CH}_2\text{CH}_3)$ was the same. The complex, $(\text{PCy}_3)_2\text{Ni}(\eta^2\text{-PhC}\equiv\text{CPh})$ (0.010 g, 0.012 mmol) was dissolved in 5 mL C_6D_6 . To this pentafluorobenzene (0.0014 mL, 0.012 mmol) was added. The reaction was monitored by NMR after 1 hour at room temperature, after heating at 50 °C for an hour and after 24 hours, and heated at 80 °C for 3 hours.

1.4.5.2 Reaction (ii)

The same reaction mentioned above was repeated using hexane as the solvent. The reaction mixture upon heating at 50 °C for two days a yellow solid precipitated. The resulting solid was separated by decanting the solvent and was purified as follows: The solid was washed with cold hexane, dried and was re-dissolved in benzene. The resulting solution was passed through a short column packed with Celite inside the glove box and the solvent was evaporated in vacuo. The resulting solid was washed with cold pentane twice and evaporated and was analysed by multinuclear NMR spectroscopy and LIFDI mass spectrometry.

The solvent decanted from the initial reaction mixture was evaporated and re-dissolved in C_6D_6 and analysed by multinuclear NMR spectroscopy and LIFDI mass spectrometry. The analysis showed the presence of two fluorides present in the sample. All attempts made to separate the two fluorides present in the solvent decanted were fruitless. Attempts to obtain a single crystal for X-ray analysis were equally unsuccessful.

1.4.6 Reaction of $(PCy_3)_2Ni(\eta^2-PhC\equiv CPh)$ with 1,2,4,5- $C_6F_4H_2$

Complex $(PCy_3)_2Ni(\eta^2-PhC\equiv CPh)$ (0.010 g, 0.012 mmol) was dissolved in C_6D_6 (5 mL) and to this 1,2,4,5- $C_6F_4H_2$ (0.0014 mL, 0.012 mmol) was added. The reaction was monitored by NMR spectroscopy after an hour at room temperature, after heating at 50 °C for an hour and after 24 hours, and further heated at 80 °C for 3 hours.

1.4.7 Reaction of $Ni(PCy_3)_2$ and C_6F_5H with $PhC\equiv CPh$

Tricyclohexylphosphine (10 mg, 0.036 mmol) was added to a Schlenk flask containing a suspension of $Ni(COD)_2$ (5 mg, 0.018 mmol) in C_6D_6 and allowed to stir at room temperature until the completely dissolved inside the glove box. To this mixture, pentafluorobenzene (2 μ L, 0.018 mmol) was added and allowed to stir for a minute. This was taken out of the glove box and was heated at 50° C for 2 hours and analysed by multinuclear NMR spectroscopy. To this one equivalent of $PhC\equiv CPh$ (3.2 mg, 0.018 mmol) was added and was further heated for a day at 50° C. The reaction mixture was analysed by multinuclear NMR spectroscopy and LIFDI mass spectrometry.

1.4.8 Reaction of $Ni(COD)_2$ and PCy_3 with pentafluoro(4-octenyl)benzene

The arylalkene product, pentafluoro(4-octenyl)benzene was prepared according to literature^{5,6} by reacting C_6F_5H with 1.5 equivalents of 4-octyne, in the presence of the 3 mol % catalyst separately made by reacting $Ni(COD)_2$ and $PCyp_3$ in toluene (1 mL). The resulting mixture was heated at 80° C for 3 hours. The product was purified by column chromatography (eluent – hexane: ethyl acetate = 9: 1) and further passing through a short column of Celite to remove paramagnetic species. The solvent from the resulting reaction mixture was removed in vacuo re-dissolved in C_6D_6 and analysed by multinuclear NMR spectroscopy. The resulting arylalkene was treated with a slight excess of $Ni(COD)_2$ and PCy_3 and heated further at 50 °C for two days followed by

heating at 80 °C for several days. The reaction mixture was monitored using multinuclear NMR spectroscopy at regular intervals.

1.4.9 Reaction of *trans*-Ni(F)(PCy₃)₂(C₆F₄H) with (PCy₃)₂Ni(η^2 -PhC≡CPh)

The nickel fluoride, *trans*-Ni(F)(PCy₃)₂(C₆F₄H) was prepared according to literature known procedures⁷ by reacting pentafluorobenzene (0.002 mL, 0.018 mmol) with a suspension of Ni(COD)₂ (5 mg, 0.018 mmol) and PCy₃ (10.2 mg, 0.036 mmol) in C₆D₆. The reaction mixture was heated at 50° C for 3 days and analysed by multinuclear NMR spectroscopy. To this reaction mixture a slight excess of (PCy₃)₂Ni(η^2 -PhC≡CPh) (15.8 mg, 0.02 mmol) was added, and heated at 50° C for two days. The reaction mixture was analysed by multinuclear NMR spectroscopy and LIFDI mass spectroscopy.

1.4.10 Synthesis of (1,5-hexadiene)Ni(L)

1.4.10.1 Synthesis of (1,5-hexadiene)Ni(PR₃) where R = *i*-Pr and Cy

The complex, (1,5-hexadiene)Ni(P^{*i*}Pr)₃ was synthesised according to the known literature procedure⁸ by reacting allylmagnesium chloride (0.334 mL, 3.3 mmol) with nickel(II) chloride (200 mg, 1.54 mmol) and P^{*i*}Pr₃ (0.29 mL, 1.54 mmol) in 2 mL ether. The resulting product was separated as an oil and was analysed by multinuclear NMR spectroscopy.

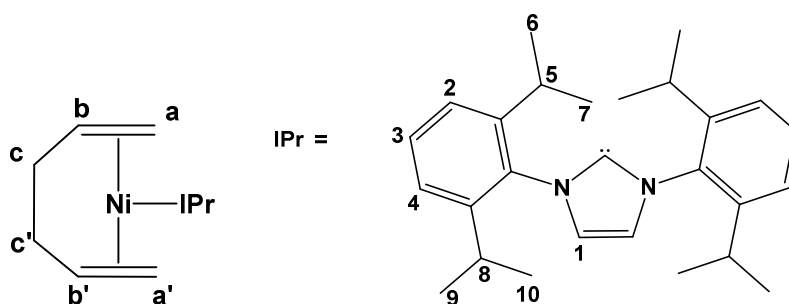
The analogous complex, (1,5-hexadiene)Ni(PCy₃) was synthesised in a similar manner by reacting allylmagnesium chloride (0.334 mL, 3.3 mmol) with a stirred suspension of nickel(II) chloride (200 mg, 1.54 mmol) and PCy₃ (430 mg, 1.54 mmol) in 2 mL ether. The mixture was stirred for 30 minutes at room temperature. The volatiles were removed under vacuum and the residue was extracted with pentane (3 x 4 mL) and filtered through Celite. The pentane was removed under vacuum and the resulting residue was dissolved in 3 mL benzene and heated for 7 hours at 50 °C. The solvent was removed under vacuum and the resulting residue was extracted with pentane (3 x 5 mL) and

filtered through Celite. The pentane was removed under vacuum. On addition of cold hexane to the solid a yellow solid product precipitated out. This solid was further purified by washing with cold hexane (4.2 mg, 64 % yield).

$^{31}\text{P-NMR}$ (C_6D_6 , 298 K): δ 54.4 (s): **MS** (LIFDI 100 % M^+) 420.25

1.4.10.2 Synthesis of (1,5-hexadiene)Ni(IPr)

Complex (1,5-hexadiene)Ni(IPr) was synthesised as described in literature⁸ using IPr from the laboratory stock resulting in a reasonable yield. The orange-brown solid product obtained from the reaction was analysed by NMR spectroscopy and LIFDI mass spectrometry. The complex was found to be stable at room temperature for 48 hours and 3-4 months when stored at $-30\text{ }^\circ\text{C}$.



$^1\text{H-NMR}$ (C_6D_6 , 298 K): δ 7.18 (t, J = 7.7 Hz, 2 H_3), δ 7.07 (d, J = 7.8 Hz, 2 H_2 and 2 H_4), δ 6.64 (s, 2 H_1), δ 4.11 (m, 2 H_b), δ 3.23 (m, 2 H_5 and 2 H_8), δ 2.60 (m, 2 H_c), δ 2.58 (d, J = 9 Hz, 2 H_a), δ 2.21 (d, J = 13.3 Hz, 2 $\text{H}_{a'}$), δ 1.51 (m, 2 H_c), δ 1.32 and δ 1.09 (d, J = 6.8 Hz, 3 H_6 , 3 H_7 , 3 H_9 and 3 H_{10}) : **MS** (LIFDI 100 % M^+) 528.30

1.4.11 Reaction of (1,5-hexadiene)Ni(PR₃) with Fluoroaromatics (where R = Cy₃ and ⁱPr₃)

1.4.11.1 Reaction of (1,5-hexadiene)Ni(PR₃) with C₆F₅H

Complex (1,5-hexadiene)Ni(PCy₃) (4 mg, 1 mmol) was taken in a Young's NMR tube and was dissolved in C₆D₆. To this C₆F₅H (0.11 mL, 1 mmol) was added and analysed immediately by multinuclear NMR spectroscopy. The same procedure was followed for (1,5-hexadiene)Ni(PⁱPr₃).

1.4.11.2 Reaction of (1,5-hexadiene)Ni(PR₃) with C₅F₅N

In a Young's NMR tube, complex (1,5-hexadiene)Ni(PCy₃) (4 mg, 1 mmol) was dissolved in C₆D₆ and to this C₅F₅N (0.11 mL, 1 mmol) was added at room temperature and was analysed immediately by multinuclear NMR spectroscopy. The same procedure was followed for (1,5-hexadiene)Ni(PⁱPr₃).

¹⁹F-NMR (C₆D₆, 298 K): δ -378.8 (t, J= 38 Hz, F), ³¹P-NMR (C₆D₆, 298 K): δ 19.2 (d, J= 37 Hz, 2 P)

1.4.12 Reaction of (1,5-hexadiene)Ni(PR₃) with Alkynes (where R = Cy and ⁱPr₃)

1.4.12.1 Reaction of (1,5-hexadiene)Ni(PR₃) with PhC≡CPh

In a Schlenk flask, complex (1,5-hexadiene)Ni(PCy₃) (4 mg, 1 mmol) was dissolved in C₆D₆. To this PhC≡CPh (0.18 mg, 1 mmol) was added at room temperature and allowed to stir for 30 minutes. The resulting solution when analysed by LIFDI mass spectrometry. Analysis by NMR spectroscopy was not possible even after purification of the solution due to inadequate shimming which may have resulted from paramagnetic species formed in the reaction mixture. The same procedure was followed for (1,5-hexadiene)Ni(PⁱPr₃).

MS (LIFDI 100 % M⁺) 872.4

1.4.12.2 Reaction of (1,5-hexadiene)Ni(PR₃) with PhC≡CSi(CH₃)₃

The complex (1,5-hexadiene)Ni(PCy₃) (4 mg, 1 mmol) was taken in a Schlenk flask and dissolved in toluene. To this PhC≡CSi(CH₃)₃ (0.20 mL, 1 mmol) was added at room temperature. Upon addition of the alkyne to the complex, the complex was observed to decompose and further analysis on the reaction mixture was not possible. The reaction was repeated at -40 °C, as an attempt to avoid decomposition at room temperature.⁹ However, the complex was observed to decompose and further analysis was not possible. The same procedure was followed for (1,5-hexadiene)Ni(PⁱPr₃) and the same results were observed.

1.4.13 Hydrofluoroarylation reaction in the presence of (1,5-hexadiene)Ni(IPr)

The hydrofluoroarylation reaction catalysed by (1,5-hexadiene)Ni(IPr) was performed in a procedure similar to the hydrofluoroarylation reaction catalysed by Ni(COD)₂ and PCyp₃ reported in literature.^{5,6} In a Young's NMR tube, C₆F₅H (4 μL, 0.04 mmol) was taken in 4 mL C₆D₆ inside the glove box. To this the alkyne (y mmol, see table below) was added at room temperature. The complex, (1,5-hexadiene)Ni(IPr) (x mol %, see table below) was added to the reaction mixture and was analysed immediately and at frequent intervals heating at 55 °C for 24 hours or at room temperature for 24 hours by multinuclear NMR spectroscopy.

Table 1 Conditions used in the hydrofluoroarylation reaction carried out with different alkynes

Alkyne	Conditions	y	x mol %
3-hexyne	Stoichiometric, rt, 16 hrs	5 μL , 0.04 mmol	100
	Catalytic, 55 $^{\circ}\text{C}$, 24 hrs	5 μL , 0.04 mmol	5
4-octyne	Stoichiometric, rt, 16 hrs	6 μL , 0.04 mmol	100
	Catalytic, 55 $^{\circ}\text{C}$, 20 hrs	6 μL , 0.04 mmol	10
$\text{PhC}\equiv\text{CSi}(\text{CH}_3)_3$	Stoichiometric, rt, 36 hrs	4 μL , 0.04 mmol	100
	Catalytic, 55 $^{\circ}\text{C}$, 24 hrs	4 μL , 0.04 mmol	10

1.5 CHAPTER 3

KINETIC STUDIES OF HYDROFLUOROARYLATION REACTION USING Ni(0)-NHC COMPLEX

1.5.1 General considerations

The catalyst (1,5-hexadiene)Ni(IPr) was prepared following the literature procedure,⁸ purified and isolated as a solid analysed by NMR spectroscopy and LIFDI mass spectrometry and stored in the freezer attached to the glove box at -30 $^{\circ}\text{C}$, under an argon atmosphere. The catalyst used for the kinetic

experiments was not stored longer than 3 months. The solvent C_6D_6 was dried over Na/K over a week and transferred into an ampoule with a Young's cap on the high vacuum line and stored in the glove box. The reagents C_6F_5H and $CH_3C\equiv CC(CH_3)_3$ were purchased from Sigma-Aldrich and Alfa-aesar respectively. Oxygen was removed via freeze-pump-thaw cycles and stored in the glove box over molecular sieves. The internal standard 1,4- $(CF_3)_2C_6H_4$ was purchased from Sigma-Aldrich and was subjected to the same procedure mentioned above for the substrates. All experimental samples were prepared inside the glove box with stock solutions of individual reactants and catalyst. The NMR spectra for the kinetic analysis were collected using a AMX 500 MHz spectrometer. The temperatures of the spectrometer mentioned in the kinetic experiments were obtained from calibration done by a group member^a using standard techniques.^{10,11}

1.5.2 Preparation of stock solutions

Individual samples for each kinetic experiment were prepared from stock solutions. All glassware was heated under vacuum to remove any residual moisture. All stock solutions were prepared inside the glove box and if necessary stored in the freezer attached to the glove box at $-30\text{ }^\circ\text{C}$. The stock solutions were prepared by measuring the masses of the individual substrates, catalyst and the solvent added. The mass of the internal standard added to the substrate stock solution was measured.

1.5.3 Preparation of samples for kinetic analysis

The samples for the kinetic analysis were prepared inside the glove box in NMR tubes, fitted with Young's caps. The individual sample tubes were

^a Calibration of temperature was performed by Dr. Dan A Smith which was also used for the NMR titration performed in order to study the solution state halogen and hydrogen bonding studies in Chapter 5

prepared by measuring the mass of the substrate stock solution added and the catalyst stock solution added. The time was recorded immediately when the catalyst was added. For consistency, deuterated solvent was added to the samples to make up to 500 μL . The sample was allowed to stand in the spectrometer for 2 minutes to reach the temperature of the spectrometer.

1.5.4 Stoichiometric reactions

All the stock solutions (excluding the experiments for the isolation techniques) were prepared by a 1 : 1 stoichiometry of $\text{C}_6\text{F}_5\text{H}$ and $\text{CH}_3\text{C}\equiv\text{CC}(\text{CH}_3)_3$ in C_6D_6 inside the glove box, in vials that were heated and subjected to vacuum prior to use. The masses of the individual substrates, internal standard and solvent used to make the stock solutions are as follows:

	$\text{C}_6\text{F}_5\text{H}$	$\text{CH}_3\text{C}\equiv\text{CC}(\text{CH}_3)_3$	$\text{CF}_3\text{C}_6\text{H}_4\text{CH}_3$	C_6D_6
Mass /mg	61.2	35.1	81.2	5017.1
Moles /mmol	0.36	0.37	0.38	
Concentration /mol/dm ³	0.073	0.073	0.076	

1.5.5 Preparation of the catalyst stock solution

The stock solution of the catalyst, (1,5-hexadiene)Ni(IPr) was prepared in C_6D_6 inside the glove box in a 5 mL vial by measuring the mass of the catalyst and solvent added, the data is tabulated below;

Catalyst Stock Solution	
mass of cat/mg =	10.3
n Catalyst/mmol	0.019
[catalyst]/mmol/mL	0.019
mass of benzene/mg	927
mass total/mg	937.3

1.5.6 Order with respect to the catalyst

In order to find the dependence of the rate of the reaction on the catalyst, several reactions with different catalyst loading were performed at 322.8 K where the stoichiometry between $[C_6F_5H]$: $[CH_3C\equiv CC(CH_3)_3]$ was 1:1. In a Young's NMR tube, the stock solution containing the reactants and internal standard was added measuring the mass. To this the catalyst stock solution was added measuring the mass and the time was measured. Several experiments with different catalyst loadings were prepared as tabulated below, varying the catalyst loading from 7 – 26 mol %. Due to the very slow rate, the reactions with catalyst loadings less than 5 mol % did not give reliable data as the shimming parameters were changed with time.

Catalyst loading (mol %)	6.8	8.2	10.5	14.8	16.3	19.9	25.8
$[CH_3C\equiv CC(CH_3)_3]$ / mmol/dm³	15.1	15.1	14.3	14.9	15.1	14.9	15.2
[Catalyst]/ mmol/dm³	1.03	1.23	1.50	2.24	2.45	3.00	3.83

1.5.7 Order with respect to substrates

1.5.7.1 Isolation methods

To prepare the series of reactant solutions, the same stock solution was used and from this a 0.10 mL was taken for each experiment measuring the mass of the stock solution added into the NMR tubes fitted with Young's caps. To this excess amounts of C_6F_5H or $CH_3C\equiv C(CH_3)_3$ were added depending on the species whose dependence was studied. Alternatively, when the quantities needed to be added were small, stock solutions varying the ratio of $[C_6F_5H]:[CH_3C\equiv CC(CH_3)_3]$ were prepared measuring the masses. This stock solutions were taken in the NMR tubes, to which the catalyst stock solution was added.

1.5.7.2 Order with respect to pentafluorobenzene – 322.8 K

In a NMR tube fitted with a Young's cap, the stock solution containing 1:1 stoichiometric amount of C_6F_5H and $CH_3C\equiv CC(CH_3)_3$ (approximately 0.10 mL, exact mass was measured for each experiment) was taken. To this excess C_6F_5H was added, measuring the mass added. In this manner, the excess of total C_6F_5H was varied from 17 fold excess to 46 as indicated in the table below. The data was collected at 322.8 K.

$[C_6F_5H] :$ $[CH_3C\equiv CC(CH_3)_3]$ ratio	Excess mass of C_6F_5H /mg	$[C_6F_5H_{total}]$ /mol/dm ³	Catalyst loading /mol %
17	20.2	0.26	12.3
20	23.1	0.28	21.9
25	30.7	0.38	7.5
35	42.5	0.52	11.8
46	57.1	0.69	12.4

1.5.7.3 Order with respect to $\text{CH}_3\text{C}\equiv\text{CC}(\text{CH}_3)_3$ – 322.8 K

The same procedure followed to obtain the order with respect to $\text{C}_6\text{F}_5\text{H}$ was followed. The mass of excess alkyne added is given in the table below. The data collection was done at 322.8 K.

$[\text{CH}_3\text{C}\equiv\text{CC}(\text{CH}_3)_3]$: $[\text{C}_6\text{F}_5\text{H}]$ ratio	mass of $\text{CH}_3\text{C}\equiv\text{CC}(\text{CH}_3)_3$ /mg	Catalyst loading /mol %
11.4	7.4	10.6
8.9	5.6	10.9
4.6	3.8	15.6

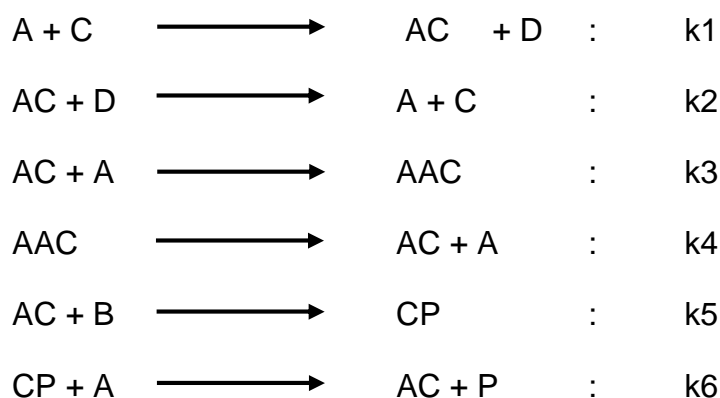
1.5.7.4 Order with respect to $\text{CH}_3\text{C}\equiv\text{CC}(\text{CH}_3)_3$ – 306.4 K

The kinetic analysis at 306.4 K was performed in a similar manner to the analysis done at 322.8 K. The mass of the excess alkyne added is given in the table below.

$[\text{CH}_3\text{C}\equiv\text{CC}(\text{CH}_3)_3]$: $[\text{C}_6\text{F}_5\text{H}]$ ratio	$[\text{CH}_3\text{C}\equiv\text{CC}(\text{CH}_3)_3]$ / mol dm^{-3}	Catalyst loading / mol %
10	0.29	4
21	0.62	5
27	1.29	3

1.5.7.5 Modelled kinetic data

To model the kinetic data the modelling and simulation fitting program Dynafit version 4.05.103 was used.^b The kinetic data obtained via ¹H-NMR spectroscopy for the hydrofluoroarylation reaction of $\text{CH}_3\text{C}\equiv\text{CC}(\text{CH}_3)_3$ with $\text{C}_6\text{F}_5\text{H}$ catalysed by (1,5-hexadiene)Ni(IPr) at 322.8 K was used as the experimental data. The model of the catalytic cycle used to fit the data is as follows; (A = $\text{CH}_3\text{C}\equiv\text{CC}(\text{CH}_3)_3$; C = (1,5-hexadiene)Ni(IPr); B = $\text{C}_6\text{F}_5\text{H}$; D = 1,5-hexadiene; P = product; CP = intermediate).



The concentration of the reactants and catalyst in the reaction mixture at 322.8 K;

Concentration / mmol dm ⁻³	[$\text{CH}_3\text{C}\equiv\text{CC}(\text{CH}_3)_3$] / mmol dm ⁻³	[$\text{C}_6\text{F}_5\text{H}$] /mmol dm ⁻³	[(1,5-hexadiene)Ni(IPr)] /mmol dm ⁻³
6 mol%	15.1	14.8	0.5
10 mol%	14.3	14.2	1.5
14 mol%	15.1	14.8	2.2
16 mol%	15.0	14.8	2.5
20 mol%	14.6	14.4	3.0

^b <http://www.biokin.com/dynafit/>

1.6 CHAPTER 4

INTERMOLECULAR HALOGEN BONDING INTERACTIONS OF NICKEL HALIDE COMPLEXES AND THEIR PENDANT HALOGEN BOND DONORS IN THE SOLID STATE

1.6.1 General considerations

Ni(COD)₂ was purchased from Sigma-Aldrich. 1,4-C₆F₄I₂, 1,2-C₆F₄I₂ (Fluorochem), Me₃SiCl and Et₃SiBr (Sigma-Aldrich) were distilled and were stored over molecular sieves. Commercially available tetramethylammonium fluoride tetrahydrate (Sigma-Aldrich) was dried similarly to the literature methodology used by Christe et al.¹² Triethylphosphine was purchased from Fluorochem.

1.6.2 Synthesis of nickel halide complexes

1.6.2.1 Synthesis of *trans*-Ni(I)(PCy₃)₂(2,3,5,6-C₆F₄I)

A solution of Ni(PCy₃)₂ was prepared by adding PCy₃ (101 mg, 0.36 mmol) to a stirred suspension of Ni(COD)₂ (50 mg, 0.18 mmol) in 10 mL of hexane, in a 25 mL Schlenk flask inside the glove box. The resulting mixture was stirred further to obtain a clear orange solution. A solution of 1,4-C₆F₄I₂ (108 mg, 0.27 mmol) was prepared separately in 5 mL of hexane in a 50 mL Schlenk flask, to this the Ni(PCy₃)₂ solution prepared was added drop-wise while stirring. The resulting red solution was left stirring further for 15 minutes and then allowed to stand for an hour, after which a red solid precipitated from the reaction mixture. The solution on top was decanted and the solid was washed with cold pentane twice and dried under vacuum. The solid was analysed by NMR spectroscopy and LIDFI mass spectrometry.

³¹P-NMR (C₆D₆, 298 K): δ 19.5 (s, 2 P); ¹⁹F-NMR (C₆D₆, 298 K): δ -113.3 (AA'XX', 2 F), δ -123.6 (AA'XX', 2 F). MS (LIFDI 100 % M⁺) 1020.20

1.6.2.2 Synthesis of *trans*-Ni(F)(PCy₃)₂(2,3,5,6-C₆F₄I) using CsF

An excess quantity of CsF (65 mg, 0.43 mmol) was added into a 250 mL Schlenk flask containing *trans*-Ni(I)(PCy₃)₂(2,3,5,6-C₆F₄I) (100.2 mg, 0.09 mmol) dissolved in 50 mL of THF and heated at 50 °C for 5 hours. The resulting yellow reaction mixture was allowed to settle for an hour and the solution was decanted into a Schlenk flask and evaporated to dryness. The remaining solid was re-dissolved in toluene and allowed to settle for 15 minutes. The solution on top was decanted into another Schlenk flask and the solvent was removed by evaporation. The resulting yellow solid was analysed by NMR spectroscopy and LIFDI mass spectrometry.

³¹P-NMR (C₆D₆, 298 K): δ 18.2 (d, 38 Hz, 2 P); **¹⁹F-NMR (C₆D₆, 298 K):** δ -405.6 (t, 38 Hz, 1 F), δ -113.3 (AA'XX', 2 F), δ -123.6 (AA'XX', 2 F). **MS (LIFDI 100 % M⁺):** 912.29.

1.6.2.3 Synthesis of *trans*-Ni(I)(PEt₃)₂(2,3,5,6-C₆F₄I) (2-I)

A solution of Ni(PEt₃)₂(COD) was prepared by adding PEt₃ (69 μ L, 0.36 mmol) to a stirred suspension of Ni(COD)₂ (50 mg, 0.18 mmol) in 10 mL of hexane, in a 25 mL Schlenk flask inside the glove box. The resulting mixture was stirred further to obtain a clear orange solution. A solution of 1,4-C₆F₄I₂ (106 mg, 0.26 mmol) was prepared separately in 5 mL of hexane in a 50 mL Schlenk flask, to this the Ni(PEt₃)₂(COD) solution prepared was added drop-wise while stirring. The resulting red-brown solution was left stirring further for 15 minutes and then allowed to stand for an hour upon which a red-brown solid precipitated from the reaction mixture. The solution on top was decanted and the solid was washed with cold pentane twice and dried under vacuum. (105.1 mg, 84 % yield). The solid was analysed by NMR spectroscopy and LIFDI mass spectrometry. NMR spectroscopy characterization was done in C₆D₆. Single crystals for X-ray crystallographic studies were obtained by layering of a saturated solution of **2-I** in THF, with hexane which gave dark red crystals at the interface of the two solvents at room temperature.

³¹P-NMR (C₆D₆, 298 K): δ 15.4 (s, 2 P): **¹⁹F-NMR (C₆D₆, 298 K):** δ -113.3 (AA'XX', 2 F), δ -124.1 (AA'XX', 2 F): **MS** (LIFDI, 100 % M⁺) 695.93: **EA:** Found: C, 31.12 H, 4.32 %, Calc for C₁₈H₃₀F₄I₂NiP₂. C, 31.02; H, 4.34 %.

1.6.2.4 Synthesis of *trans*-Ni(F)(PEt₃)₂(2,3,5,6-C₆F₄I) (2-F)

An excess of tetramethylammonium fluoride (150 mg, 1.6 mmol) was added into a 250 mL Schlenk flask containing a solution of *trans*-Ni(I)(PEt₃)₂(2,3,5,6-C₆F₄I) (100 mg, 0.14 mmol) dissolved in 50 mL of THF, and stirred at room temperature for 5 hours. The resulting reaction mixture was allowed to settle for an hour and the yellow solution on top was decanted and passed through a short column of Celite into another Schlenk flask and the solvent was evaporated under vacuum. The resulting solid was re-dissolved in benzene and allowed to settle for 30 minutes. The solution on top was decanted and was passed through a short column of Celite into another Schlenk flask. The solvent was evaporated under vacuum. The resulting yellow solid product was washed with cold pentane twice and dried under vacuum. (60.1 mg, 71.1% yield) The solid was analysed by NMR spectroscopy and LIDFI mass spectrometry. The fluorination using CsF of Ni(I)(PEt₃)₂(2,3,5,6-C₆F₄I) resulted in poor yields. Single crystals of **2-F** suitable for X-ray crystallographic studies were obtained by slow diffusion of hexane into a saturated solution of **2-F** in THF/benzene at room temperature.

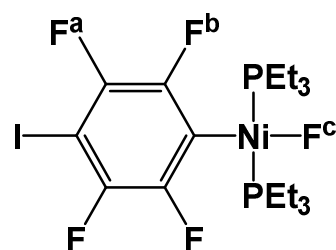
³¹P-NMR (C₆D₆, 298 K): δ 13.1 (d, 46 Hz, 2 P):

¹⁹F-NMR (C₆D₆, 298 K): δ -387.9 (t, 46 Hz, 1 F^c), δ -

113.8 (AA'XX', 2 F^b), δ -123.6 (AA'XX', 2 F^a): **MS**

(LIFDI, 100 % M⁺) 587.99: **EA:** Found: C, 36.59 H,

5.06 %, Calc for C₁₈H₃₀F₅INiP₂. C, 36.71; H, 5.13 %.

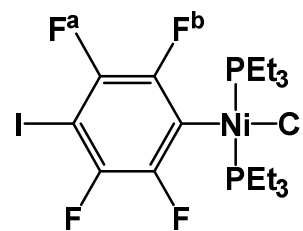


1.6.2.5 Synthesis of *trans*-Ni(Cl)(PEt₃)₂(2,3,5,6-C₆F₄) (**2-Cl**)

An excess of tetramethylammonium chloride (150 mg, 1.4 mmol) was added into a 250 mL Schlenk flask containing a solution of *trans*-Ni(I)(PEt₃)₂(2,3,5,6-C₆F₄) (100 mg, 0.14 mmol) dissolved in 50 mL of THF, and stirred at room temperature for 3 hours. The resulting reaction mixture was allowed to settle for an hour and the yellow solution on top was decanted and passed through a short column of Celite into another Schlenk flask and the solvent was evaporated under vacuum. The resulting solid was re-dissolved in benzene and allowed to settle for 30 minutes. The solution on top was decanted and was passed through a short column of Celite into another Schlenk flask. The solvent was evaporated under vacuum. The resulting yellow solid product was washed with cold pentane twice and dried under vacuum. (55.2 mg, 63.5 % yield) The solid was analysed by NMR spectroscopy and LIDFI mass spectrometry. NMR spectroscopy characterization was done in C₆D₆. The conversion of Ni(I)(PEt₃)₂(2,3,5,6-C₆F₄) using CsCl resulted in longer reaction times and poor yields compared to the reaction with NMe₄⁺Cl⁻.

Alternatively *trans*-Ni(Cl)(PEt₃)₂(2,3,5,6-C₆F₄) was synthesised from *trans*-Ni(F)(PEt₃)₂(2,3,5,6-C₆F₄). Chlorotrimethylsilane (13 μL, 0.1 mmol) was added into a solution of THF containing *trans*-Ni(F)(PEt₃)₂(2,3,5,6-C₆F₄), (50 mg, 0.08 mmol) and stirred for an hour. The solvent and excess reagents and by-products were removed under vacuum, washed with pentane and dried. (47 mg, 92 % yield). Single crystals of **2-Cl** suitable for X-ray crystallography were obtained by slow diffusion of hexane in a saturated solution of **2-Cl** in THF/benzene and slow evaporation, simultaneously at room temperature over a fortnight, which resulted in bright yellow crystal blocks.

$^{31}\text{P-NMR}$ (C_6D_6 , 298 K): δ 14.3 (s, 2 P): $^{19}\text{F-NMR}$ (C_6D_6 , 298 K): δ -113.1 (AA'XX', 2 F^b), δ -124.1 (AA'XX', 2 F^a): **MS** (LIFDI, 100 % M⁺) 604.00: **EA**: Found: C, 36.29 H, 4.87 %, Calc for $\text{C}_{18}\text{H}_{30}\text{F}_4\text{IClNiP}_2$. C, 35.71; H, 4.99 %.

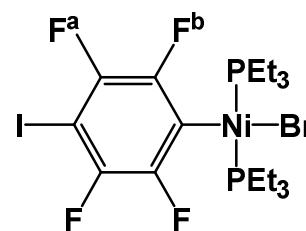


1.6.2.6 Synthesis of *trans*-Ni(Br)(PEt₃)₂(2,3,5,6-C₆F₄I) (**2-Br**)

An excess of tetraethylammonium bromide (200 mg, 0.9 mmol) was added into a 250 mL Schlenk flask containing a solution of *trans*-Ni(I)(PEt₃)₂(2,3,5,6-C₆F₄I) (100 mg, 0.14 mmol) dissolved in 50 mL of THF, and stirred at room temperature for 3 hours. The resulting reaction mixture was allowed to settle for an hour and the yellow-orange solution on top was decanted and passed through a short column of Celite into another Schlenk flask and the solvent was evaporated under vacuum. The resulting solid was re-dissolved in toluene and allowed to settle for 30 minutes. The solution on top was decanted and was passed through a short column of Celite into another Schlenk flask. The solvent was evaporated under vacuum. The resulting yellow-orange solid product was washed with cold pentane twice and dried under vacuum. (64.3 mg, 70.7 % yield) The solid was analysed by NMR spectroscopy and LIDFI mass spectrometry. NMR spectroscopy characterization was done in C₆D₆.

Alternatively *trans*-Ni(Br)(PEt₃)₂(2,3,5,6-C₆F₄I) was synthesised from *trans*-Ni(F)(PEt₃)₂(2,3,5,6-C₆F₄I). Bromotriethylsilane (17 μL , 0.1 mmol) was added into a solution of THF containing *trans*-Ni(F)(PEt₃)₂(2,3,5,6-C₆F₄I), (50 mg, 0.08 mmol) and stirred for an hour. The solvent and excess reagents and by-products were removed under vacuum, washed with pentane and dried. (50 mg, 90 % yield). Single crystals of **2-Br** suitable for X-ray crystallographic studies were obtained at room temperature by slow diffusion of hexane in a saturated solution of **2-Br** in benzene, which resulted in bright yellow crystal blocks.

$^{31}\text{P-NMR}$ (C_6D_6 , 298 K): δ 14.4 (s, 2 P): $^{19}\text{F-NMR}$ (C_6D_6 , 298 K): δ -112.9 (AA'XX', 2 F^b), δ -123.8 (AA'XX', 2 F^a): **MS** (LIFDI, 100 % M⁺) 649.94: **EA**: Found: C, 33.41 H, 4.56 %, Calc for $\text{C}_{18}\text{H}_{30}\text{F}_4\text{I}\text{Br}\text{NiP}_2$. C, 33.27; H, 4.65 %.



1.6.2.7 Synthesis of *trans*-Ni(I)(PEt₂Ph)₂(2,3,5,6-C₆F₄I) (3-I)

A solution of Ni(PEt₂Ph)₂ was prepared by adding PEt₂Ph (62.7 μL , 0.36 mmol) to a stirred suspension of Ni(COD)₂ (50 mg, 0.18 mmol) in 10 mL of hexane, in a 25 mL Schlenk flask inside the glove box. The resulting mixture was stirred further to obtain a clear orange solution. A solution of 1,4-C₆F₄I₂ (106 mg, 0.26 mmol) was prepared separately in 5 mL of hexane in a 50 mL Schlenk flask, to this the Ni(PEt₂Ph)₂(COD) solution prepared was added drop-wise while stirring. The resulting red-brown solution was left stirring further for 15 minutes and then allowed to stand for an hour upon which a red-brown solid precipitated from the reaction mixture. The solution on top was decanted and the solid was washed with cold pentane twice and dried under vacuum. (92 mg, 64 % yield). The solid was analysed by NMR spectroscopy and LIDFI mass spectrometry. Single crystals of **3-I** suitable for X-ray crystallographic studies were obtained by slow diffusion of hexane into a saturated solution of **3-I** in THF/benzene, which resulted the formation of dark deep crystal blocks.

$^{31}\text{P-NMR}$ (C_6D_6 , 298 K): δ 16.2 (s, 2 P): $^{19}\text{F-NMR}$ (C_6D_6 , 298 K): δ -114.4 (AA'XX', 2 F), δ -123.6 (AA'XX', 2 F): **MS** (LIFDI, 100 % M⁺) 791.90:

1.6.2.8 Synthesis of *trans*-Ni(F)(PEt₂Ph)₂(2,3,5,6-C₆F₄I) (3-F)

An excess of tetramethylammonium fluoride (150 mg, 1.6 mmol) was added into a 250 mL Schlenk flask containing a solution of *trans*-Ni(I)(PEt₂Ph)₂(2,3,5,6-C₆F₄I) (100 mg, 0.13 mmol) dissolved in 50 mL of THF, and stirred at room temperature for 5 hours. The resulting reaction mixture was

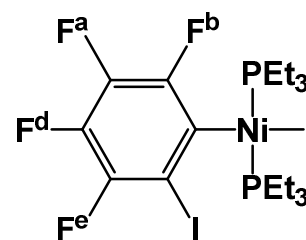
allowed to settle for an hour and the yellow solution on top was decanted and passed through a short column of Celite into another Schlenk flask and the solvent was evaporated under vacuum. The resulting solid was re-dissolved in benzene and allowed to settle for 30 minutes. The solution on top was decanted and was passed through a short column of Celite into another Schlenk flask. The solvent was evaporated under vacuum. The resulting yellow solid product was washed with cold pentane twice and dried under vacuum. (55.4 mg, 64.1 % yield) The solid was analysed by NMR spectroscopy and LIDFI mass spectrometry. NMR spectroscopy characterization was done in C₆D₆.

³¹P-NMR (C₆D₆, 298 K): δ 11.9 (d, 45 Hz, 2 P): **¹⁹F-NMR (C₆D₆, 298 K):** δ -389.7 (t, 45 Hz, 1 F) δ -115.2 (AA'XX', 2 F), δ -126.5 (AA'XX', 2 F): **MS** (LIFDI, 100 % M⁺) 684.00

1.6.2.9 Synthesis of *trans*-Ni(I)(PEt₃)₂(2,3,4,5-C₆F₄I) (**4-I**)

A solution of Ni(PEt₃)₂(COD) was prepared by adding PEt₃ (69 μ L, 0.36 mmol) to a stirred suspension of Ni(COD)₂ (50 mg, 0.18 mmol) in 10 mL of hexane, in a 25 mL Schlenk flask inside the glove box. The resulting mixture was stirred further to obtain a clear orange solution. A solution of 1,2-C₆F₄I₂ (106 mg, 0.26 mmol) was prepared separately in 5 mL of hexane in a 50 mL Schlenk flask, to this the Ni(PEt₃)₂(COD) solution prepared was added drop-wise while stirring. The resulting black-brown solution was left stirring further for 15 minutes. The reaction mixture was left in the freezer at -30 °C overnight for recrystallization. The dark solution on top was decanted and the red crystals were washed with cold pentane twice and dried under vacuum. (85.4 mg, 67.4 % yield). The solid was analysed by NMR spectroscopy and LIDFI mass spectrometry. NMR spectroscopy characterization was done in C₆D₆. Single crystals of **4-I** were obtained from a saturated **4-I** hexane solution at -30 °C overnight. The deep red crystals were washed with cold pentane and analysed by X-ray crystallography.

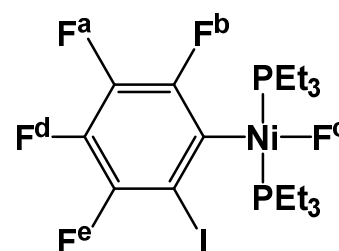
³¹P-NMR (C₆D₆, 298 K): δ 10.3 (s, 2 P) **¹⁹F-NMR:** δ -114.4 (dd, 30 Hz, 11 Hz, 1 F^b), δ -115.4 (dd, 23 Hz, 12 Hz, 1 F^e), δ -156.8 (dd, 32 Hz, 21 Hz, 1 F^d), δ -159.1 (t, 20 Hz, 1 F^a) : **EA:** Found: C, 31.01 H, 4.22 %, Calc for C₁₈H₃₀F₄I₂NiP₂. C, 31.02; H, 4.34 %.



1.6.2.10 Synthesis of *trans*-Ni(F)(PEt₃)₂(2,3,4,5-C₆F₄I) (4-F)

An excess of tetramethylammonium fluoride (150 mg, 1.6 mmol) was added into a 250 mL Schlenk flask containing a solution of *trans*-Ni(I)(PEt₃)₂(2,3,4,5-C₆F₄I) (100 mg, 0.14 mmol) dissolved in 50 mL of THF, and stirred at room temperature for 5 hours. The resulting reaction mixture was allowed to settle for an hour and the yellow solution on top was decanted and passed through a short column of Celite into another Schlenk flask and the solvent was evaporated under vacuum. The resulting solid was re-dissolved in benzene and allowed to settle for 30 minutes. The solution on top was decanted and was passed through a short column of Celite into another Schlenk flask. The solvent was evaporated under vacuum. The resulting yellow solid product was washed with cold pentane twice and dried under vacuum. (52 mg, 63 % yield) The solid was analysed by NMR spectroscopy and LIDFI mass spectrometry. Single crystals suitable for X-ray crystallography were obtained by slow diffusion of hexane into a saturated solution of **4-F** in benzene in the freezer at -30 °C over a fortnight.

³¹P-NMR (C₆D₆, 298 K): δ 9.4 (d, 46 Hz, 2 P): **¹⁹F-NMR (C₆D₆, 298 K):** δ -397.9 (dd, J = 46 Hz, 9 Hz, F^c), δ -115.3 (dd, 20 Hz, 11 Hz, 1 F^b), δ -116.2 (dd, 31 Hz, 11 Hz, 1 F^e), δ -158.2 (dd, 31 Hz, 19 Hz, 1 F^d), δ -160.2 (t, 19 Hz, 1 F^a) : **EA:** Found: C, 36.69 H, 5.13 %, Calc for C₁₈H₃₀F₅INiP₂. C, 36.71; H, 5.13 %.

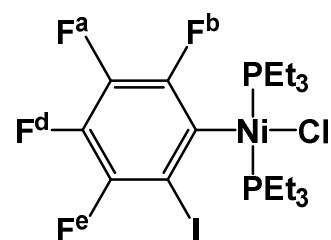


1.6.2.11 Synthesis of *trans*-Ni(Cl)(PEt₃)₂(2,3,4,5-C₆F₄I) (4-Cl)

An excess of tetramethylammonium chloride (150 mg, 1.4 mmol) was added into a 250 mL Schlenk flask containing a solution of *trans*-Ni(I)(PEt₃)₂(2,3,4,5-C₆F₄I) (100 mg, 0.14 mmol) dissolved in 50 mL of THF, and stirred at room temperature for 2 hours. The resulting reaction mixture was allowed to settle for an hour and the yellow solution on top was decanted and passed through a short column of Celite into another Schlenk flask and the solvent was evaporated under vacuum. The resulting solid was re-dissolved in benzene and allowed to settle for 30 minutes. The solution on top was decanted and was passed through a short column of Celite into another Schlenk flask. The solvent was evaporated under vacuum. The resulting yellow solid product was washed with cold pentane twice and dried under vacuum. (59 mg, 69 % yield) The solid was analysed by NMR spectroscopy and LIDFI mass spectrometry. NMR spectroscopy characterization was done in C₆D₆. Single crystals suitable for X-ray crystallography were obtained by slow diffusion of hexane into a saturated solution of **4-Cl** in THF/toluene in the freezer at -30 °C over a fortnight.

Alternatively *trans*-Ni(Cl)(PEt₃)₂(2,3,4,5-C₆F₄I) was synthesised from *trans*-Ni(F)(PEt₃)₂(2,3,4,5-C₆F₄I). Chlorotrimethylsilane (13 μL, 0.1 mmol) was added into a solution of THF containing *trans*-Ni(F)(PEt₃)₂(2,3,4,5-C₆F₄I), (50 mg, 0.08 mmol) and stirred for an hour. The solvent and excess reagents and by-products were removed under vacuum, washed with pentane and dried. (48 mg, 93 % yield).

³¹P-NMR (C₆D₆, 298 K): δ 9.5 (s, 2 P): ¹⁹F-NMR (C₆D₆, 298 K): δ -115.8 (dd, 31 Hz, 12 Hz, 1 F^b), δ -116.8 (dd, 22 Hz, 12 Hz, 1 F^e), δ -159.3 (dd, 31 Hz, 20 Hz, 1 F^d), δ -162.0 (t, 21 Hz, 1 F^a): **EA**: Found: C, 36.68 H, 4.87 %, Calc. C, 35.71; H, 4.99 %.

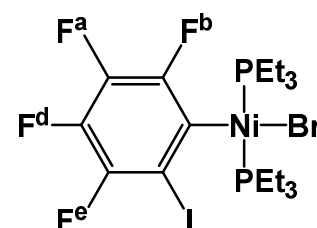


1.6.2.12 Synthesis of *trans*-Ni(Br)(PEt₃)₂(2,3,4,5-C₆F₄I) (4-Br)

An excess of tetraethylammonium bromide (200 mg, 0.9 mmol) was added into a 250 mL Schlenk flask containing a solution of *trans*-Ni(I)(PEt₃)₂(2,3,4,5-C₆F₄I) (100 mg, 0.14 mmol) dissolved in 50 mL of THF, and stirred at room temperature for 2 hours. The resulting reaction mixture was allowed to settle for an hour and the orange solution on top was decanted and passed through a short column of Celite into another Schlenk flask and the solvent was evaporated under vacuum. The resulting solid was re-dissolved in toluene and allowed to settle for 30 minutes. The solution on top was decanted and was passed through a short column of Celite into another Schlenk flask. The solvent was evaporated under vacuum. The resulting orange solid product was washed with cold pentane twice and dried under vacuum. (62 mg, 68 % yield) The solid was analysed by NMR spectroscopy and LIDFI mass spectrometry. NMR spectroscopy characterization was done in C₆D₆.

Alternatively *trans*-Ni(Br)(PEt₃)₂(2,3,4,5-C₆F₄I) was synthesised from *trans*-Ni(F)(PEt₃)₂(2,3,4,5-C₆F₄I). Bromotriethylsilane (17 μL, 0.1 mmol) was added into a solution of THF containing *trans*-Ni(F)(PEt₃)₂(2,3,4,5-C₆F₄I), (50 mg, 0.08 mmol) and stirred for an hour. The solvent and excess reagents and by-products were removed under vacuum, washed with pentane and dried. (53 mg, 96 % yield).

³¹P-NMR (C₆D₆, 298 K): δ 9.3 (s, 2 P): ¹⁹F-NMR (C₆D₆, 298 K): δ -115.2 (dd, 32 Hz, 11 Hz, 1 F^b), δ -116.2 (dd, 33 Hz, 12 Hz, 1 F^e), δ -157.5 (dd, 33 Hz, 21 Hz, 1 F^d), δ -160.1 (t, 20 Hz, 1 F^a): EA: Found: C, 33.36 H, 4.54 %, Calc. C, 33.27; H, 4.65 %.



1.7 CHAPTER 5

SOLUTION STUDIES OF HYDROGEN AND HALOGEN BONDING TOWARDS NICKEL FLUORIDES

1.7.1 Common procedure for NMR titrations

The complexes *trans*-Ni(F)(PEt₃)₂(C₅F₄N) and *trans*-Ni(F)(*i*-Pr₂Im)₂(C₆F₅) were prepared according to literature known procedure or taken from the laboratory stock.^{7,13} The stock solutions of host and guest were prepared by measuring the mass of the host, guest and the solvent added. The procedure for NMR spectroscopic titrations followed was similar to the previously reported titrations performed in the group.^{11,14,15} The samples for the titration were prepared in NMR tubes fitted with Young's caps inside the glove box, by measuring the exact mass of the host and the guest added. The solvent was added to make the total volume 6 mL. The samples were then allowed to thermostat in a cold bath which was approximately in the temperature required. The sample was allowed to stand inside the spectrometer for 2 minutes to allow the sample to attain the required temperature.

1.7.2 Stock solution preparation

	Host		Guest	
	Mass of host /mg	Mass of solvent /mg	Mass of guest /mg	Mass of solvent /mg
Ni(F)(PEt₃)₂(C₅F₄N) vs C₆F₁₃I	55.9	3558.9	463.6	536.7
Ni(F)(<i>i</i>-Pr₂Im)₂(C₆F₅) vs C₆F₅I	39.6	4590.5	85.6	2919.0
Ni(F)(<i>i</i>-Pr₂Im)₂(C₆F₅) vs indole	8.1	5190.1	10.7	4926.5

1.7.3 Sample preparation for titration

Ni(F)(PEt₃)₂(C₅F₄N) vs C₆F₁₃I		Ni(F)(ⁱPr₂Im)₂(C₆F₅) vs C₆F₅I		Ni(F)(ⁱPr₂Im)₂(C₆F₅) vs indole	
Host /mg	Guest /mg	host	guest	host	Guest
419.88	0.00	331.93	0.00	400.42	0.00
417.60	12.03	337.21	19.88	395.69	16.38
412.25	23.76	327.46	40.55	394.19	25.38
420.79	36.53	339.04	49.64	393.84	34.95
431.60	49.13	332.51	59.86	393.15	50.53
444.81	61.53	338.70	74.35	393.26	57.79
437.29	77.16	336.18	88.73	394.07	69.56
437.07	102.84	332.85	97.94	396.61	81.21
430.46	122.75	337.89	127.36	396.84	90.21
		338.47	166.34	397.07	105.32
		341.45	207.67	395.92	171.65
		341.33	242.26		
		333.88	294.71		

1.7.4 Fitting of the titration data

The titration data obtained from the ^{19}F -NMR spectra were used to fit the formation of a 1:1 adduct between the halogen or hydrogen bond donor and the nickel fluoride, as shown below;



where, Y-R = is either the halogen bond donor or the hydrogen bond donor

The downfield shift of the co-ordinated fluoride resonance from that of the free fluoride resonance ($\Delta\delta_{\text{F}}$) and the equilibrium constant associated with the adduct formation are the two parameters fitted for the different temperatures the titration has been done. The two parameters were fitted with a Microsoft Excel macro program developed by Professor Christopher Hunter (University of Cambridge). From the equilibrium constants obtained at different temperatures, the van't Hoff plot was constructed which gave ΔH_0 and ΔS_0 .

1.1. References

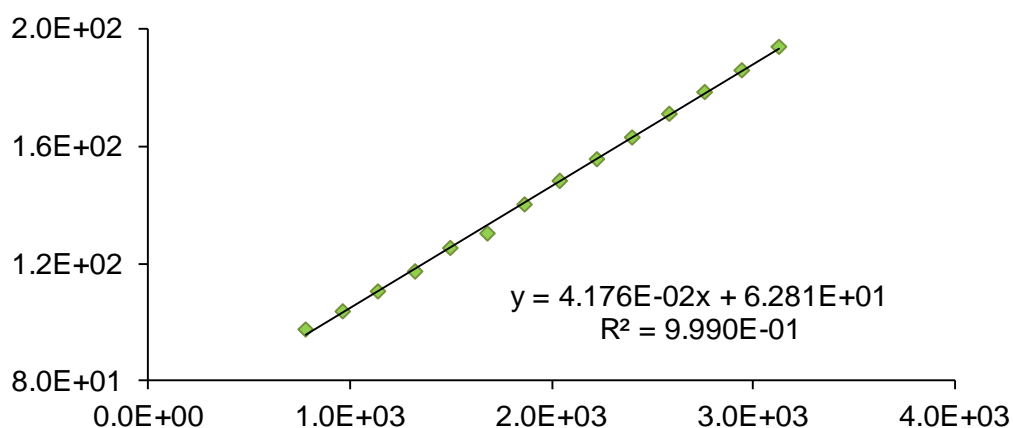
- (1) Otsuka, S.; Rossi, M. *Journal of the Chemical Society A: Inorganic, Physical, Theoretical* **1968**, 2630.
- (2) Jolly, P. W.; Jonas, K.; Krüger, C.; Tsay, Y. H. *J. Organomet. Chem.* **1971**, 33, 109.
- (3) Darensbourg, M. Y.; Ludwig, M.; Riordan, C. G. *Inorg. Chem.* **1989**, 28, 1630.
- (4) Hatnean, J. A.; Beck, R.; Borrelli, J. D.; Johnson, S. A. *Organometallics* **2010**, 29, 6077.
- (5) Nakao, Y.; Kashiwara, N.; Kanyiva, K. S.; Hiyama, T. *J. Am. Chem. Soc.* **2008**, 130, 16170.
- (6) Kanyiva, K. S.; Kashiwara, N.; Nakao, Y.; Hiyama, T.; Ohashi, M.; Ogoshi, S. *Dalton Trans.* **2010**, 39, 10483.

- (7) Cronin, L.; Higgitt, C. L.; Karch, R.; Perutz, R. N. *Organometallics* **1997**, *16*, 4920.
- (8) Wu, J.; Faller, J. W.; Hazari, N.; Schmeier, T. J. *Organometallics* **2012**, *31*, 806.
- (9) Poerschke, K. R. *J. Am. Chem. Soc.* **1989**, *111*, 5691.
- (10) Ammann, C.; Meier, P.; Merbach, A. *Journal of Magnetic Resonance (1969)* **1982**, *46*, 319.
- (11) Smith, D. A.; Brammer, L.; Hunter, C. A.; Perutz, R. N. *J. Am. Chem. Soc.* **2014**, *136*, 1288.
- (12) Christe, K. O.; Wilson, W. W.; Wilson, R. D.; Bau, R.; Feng, J. A. *J. Am. Chem. Soc.* **1990**, *112*, 7619.
- (13) Schaub, T.; Radius, U. *Chemistry – A European Journal* **2005**, *11*, 5024.
- (14) Libri, S.; Jasim, N. A.; Perutz, R. N.; Brammer, L. *J. Am. Chem. Soc.* **2008**, *130*, 7842.
- (15) Beweries, T.; Brammer, L.; Jasim, N. A.; McGrady, J. E.; Perutz, R. N.; Whitwood, A. C. *J. Am. Chem. Soc.* **2011**, *133*, 14338.

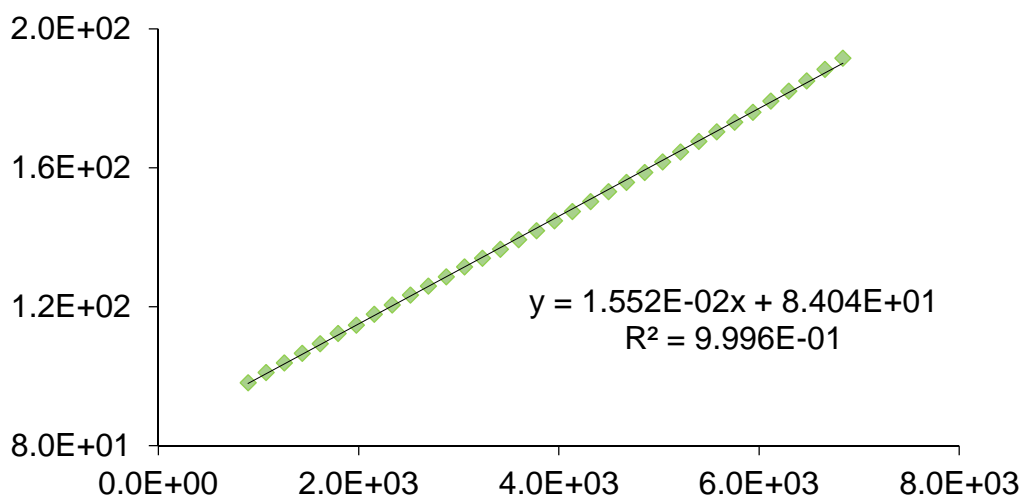
CHAPTER 3

Isolation method – Determination of the dependence of the rate on $[\text{C}_6\text{F}_5\text{H}]$

Graphs plotted treating the data to follow the pseudo 2nd order rate law integrated rate equation

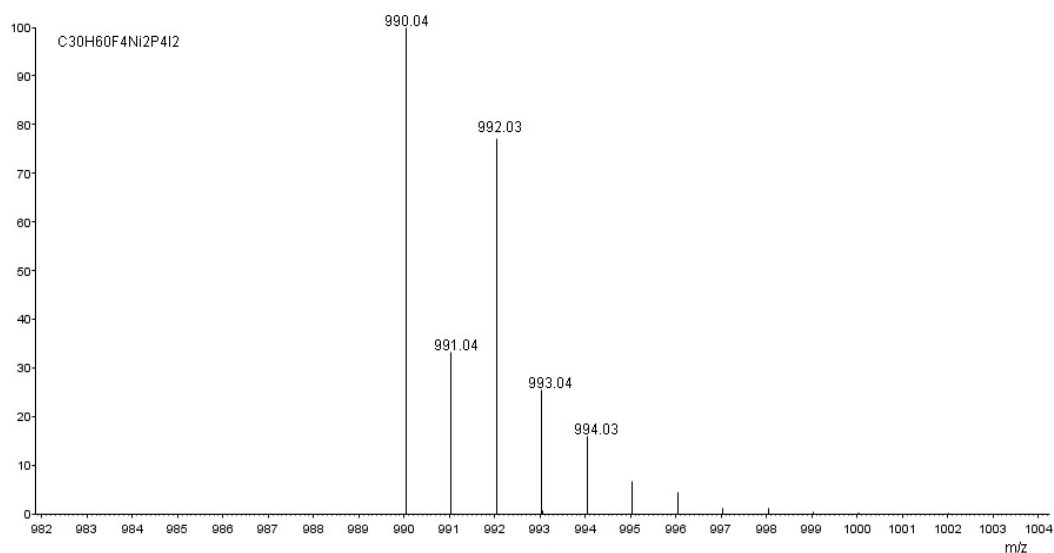


A plot of $1/[1\text{A}]$ against time constructed from the data collected by $^1\text{H-NMR}$ spectroscopy for the reaction of **1A** with **2B** (ratio 1 : 46) catalysed by (1,5-hexadiene)Ni(IPr) in C_6D_6 at 322.8 K.



A plot of $1/[1\text{A}]$ against time constructed from the data collected by $^1\text{H-NMR}$ spectroscopy for the reaction of **1A** with **2B** (ratio 1 : 17) catalysed by (1,5-hexadiene)Ni(IPr) in C_6D_6 at 322.8 K.

Chapter 4

Figure 1 Simulated mass spectrum showing the isotopic pattern of the chemical formula $C_{30}H_{60}F_4Ni_2P_4I_2$.**Table 1** Crystal structure data for complexes, $Ni(PEt_3)_2(C_6F_4)$ and $[Ni(PEt_3)_2]_2C_6F_4$

	$Ni(PEt_3)_2(C_6F_4)$	$[Ni(PEt_3)_2]_2C_6F_4$
$a/\text{\AA}$	8.1337(19)	11.0590(5)
$b/\text{\AA}$	8.1345(4)	12.1681(6)
$c/\text{\AA}$	31.6126(17)	15.1847(8)
$Vol/\text{\AA}^3$	2091.61	1982.25
T/K	110	123
$\alpha/^\circ$	90.000(4)	75.960(3)
$\beta/^\circ$	90.021(3)	89.526(2)
$\gamma/^\circ$	90.020(3)	89.997(2)
R-factor (%)	5.57	2.52

ABBREVIATIONS

Chemicals

Me	methyl, -CH ₃
Et	ethyl, -CH ₂ CH ₃
<i>i</i> Pr	iso-propyl, -CH(CH ₃) ₂
Ph	phenyl, C ₆ H ₅
Dppe	diphenylphosphinoethane
IMes	2,5-Mes ₂ -N ₂ C ₃ H ₂
COD	1,5-cyclooctadiene
Cy	cyclohexyl
Cyp	cyclopentyl
Ar ^F	fluorinated aromatic ring
THF	tetrahydrofuran
IPr	1,3-bis(2,6-diisopropylphenyl)-4,5-dihydro-2H-imidazol-2-ylidene
<i>i</i> Pr ₂ Im	1, 3-bis(isopropyl)imidazolin-2-ylidene
DME	dimethoxyethane
NHC	N-heterocyclic carbene
ⁿ Bu	<i>n</i> -butyl
^t Bu	<i>tert</i> -butyl
dmpe	1,2-bis(dimethylphosphino)ethane

Units

Å	ångström
atm	atmosphere
Hz	hertz
h	hours
K	kelvin
s	second
J	joule
mol	mole
g	gram
mg	milligram
°	degree
°C	degree Celsius

Spectroscopy

IR	infra-red
UV	ultra violet
Vis	visible
MS	mass spectroscopy
LIFDI	liquid injection field desorption ionization
NMR	nuclear magnetic resonance
COSY	correlation spectroscopy
MAS	magic angle spinning
δ	chemical shift (in ppm)

ppm	parts per million
J	coupling constant
s	singlet
d	doublet
t	triplet
q	quartet
m	multiplet
br	broad
dd	doublet of doublets
dt	doublet of triplets

Special terms

DFT	density functional theory
KIE	kinetic isotopic effect
RPKA	reaction progress kinetic analysis
XB	halogen bonding
HOMO	highest occupied molecular orbital
LUMO	lowest unoccupied molecular orbital
LLHT	ligand to ligand hydrogen transfer
VT	variable temperature
vs.	versus
ca	<i>circa</i> -approximately
e.g.	<i>exempli gratia</i>

References

Chapter 1

- (1) Wang, J.; Sánchez-Roselló, M.; Aceña, J. L.; del Pozo, C.; Sorochinsky, A. E.; Fustero, S.; Soloshonok, V. A.; Liu, H. *Chem. Rev. (Washington, DC, U. S.)* **2014**, *114*, 2432.
- (2) Fried, J.; Sabo, E. F. *J. Am. Chem. Soc.* **1954**, *76*, 1455.
- (3) Sun, A. D.; Love, J. A. *Dalton Trans.* **2010**, *39*, 10362.
- (4) Braun, T.; Perutz, R. N. In *Perspectives in Organometallic Chemistry*; Screttas, C. G., Steele, B. R., Eds.; The Royal Society of Chemistry: 2003, p 136.
- (5) Kuehnel, M. F.; Lentz, D.; Braun, T. *Angew Chem Int Ed Engl* **2013**, *52*, 3328.
- (6) Keyes, L.; Love, J. A. In *C-H and C-X Bond Functionalization: Transition Metal Mediation*; The Royal Society of Chemistry: 2013, p 159.
- (7) Grushin, V. V. *Acc. Chem. Res.* **2010**, *43*, 160.
- (8) Weaver, J.; Senaweera, S. *Tetrahedron* **2014**, *70*, 7413.
- (9) Braun, T.; Izundu, J.; Steffen, A.; Neumann, B.; Stammler, H.-G. *Dalton Trans.* **2006**, 5118.
- (10) Ahrens, T.; Kohlmann, J.; Ahrens, M.; Braun, T. *Chem. Rev. (Washington, DC, U. S.)* **2015**, *115*, 931.
- (11) Champagne, P. A.; Desroches, J.; Hamel, J.-D.; Vandamme, M.; Paquin, J.-F. *Chem. Rev. (Washington, DC, U. S.)* **2015**.
- (12) Hughes, R. P. *Eur. J. Inorg. Chem.* **2009**, *2009*, 4591.
- (13) Clot, E.; Besora, M.; Maseras, F.; Megret, C.; Eisenstein, O.; Oelckers, B.; Perutz, R. N. *Chem. Commun. (Cambridge, U. K.)* **2003**, 490.
- (14) Nakao, Y. *The Chemical Record* **2011**, *11*, 242.
- (15) Kiso, Y.; Tamao, K.; Kumada, M. *J. Organomet. Chem.* **1973**, *50*, C12.
- (16) Crabtree, R. H. *J. Organomet. Chem.* **2005**, *690*, 5451.
- (17) Crabtree, R. H. In *The Organometallic Chemistry of the Transition Metals*; John Wiley & Sons, Inc.: 2005, p 235.
- (18) Tolman, C. A. *Chem. Rev. (Washington, DC, U. S.)* **1977**, *77*, 313.

- (19) Gusev, D. G. *Organometallics* **2009**, *28*, 763.
- (20) Fahey, D. R.; Mahan, J. E. *J. Am. Chem. Soc.* **1977**, *99*, 2501.
- (21) Cronin, L.; Higgitt, C. L.; Karch, R.; Perutz, R. N. *Organometallics* **1997**, *16*, 4920.
- (22) Tsou, T. T.; Kochi, J. K. *J. Am. Chem. Soc.* **1979**, *101*, 6319.
- (23) Jasim, N. A.; Perutz, R. N.; Whitwood, A. C.; Braun, T.; Izundu, J.; Neumann, B.; Rothfeld, S.; Stammler, H.-G. *Organometallics* **2004**, *23*, 6140.
- (24) Crespo, M.; Martinez, M.; Sales, J. *Organometallics* **1993**, *12*, 4297.
- (25) Braun, T.; Perutz, R. N.; Sladek, M. I. *Chem. Commun. (Cambridge, U. K.)* **2001**, 2254.
- (26) Steffen, A.; Sladek, M. I.; Braun, T.; Neumann, B.; Stammler, H.-G. *Organometallics* **2005**, *24*, 4057.
- (27) A. Widdowson, D.; Wilhelm, R. *Chem. Commun. (Cambridge, U. K.)* **1999**, 2211.
- (28) Manabe, K.; Ishikawa, S. *Synthesis* **2008**, *2008*, 2645.
- (29) Lafrance, M.; Rowley, C. N.; Woo, T. K.; Fagnou, K. *J. Am. Chem. Soc.* **2006**, *128*, 8754.
- (30) Johnson, S. A.; Huff, C. W.; Mustafa, F.; Saliba, M. *J. Am. Chem. Soc.* **2008**, *130*, 17278.
- (31) Kanyiva, K. S.; Kashihara, N.; Nakao, Y.; Hiyama, T.; Ohashi, M.; Ogoshi, S. *Dalton Trans.* **2010**, *39*, 10483.
- (32) Reinhold, M.; McGrady, J. E.; Perutz, R. N. *J. Am. Chem. Soc.* **2004**, *126*, 5268.
- (33) Hatnean, J. A.; Beck, R.; Borrelli, J. D.; Johnson, S. A. *Organometallics* **2010**, *29*, 6077.
- (34) Nakao, Y.; Kashihara, N.; Kanyiva, K. S.; Hiyama, T. *J. Am. Chem. Soc.* **2008**, *130*, 16170.
- (35) Johnson, S. A.; Taylor, E. T.; Cruise, S. J. *Organometallics* **2009**, *28*, 3842.
- (36) Doster, M. E.; Hatnean, J. A.; Jetic, T.; Modi, S.; Johnson, S. A. *J. Am. Chem. Soc.* **2010**, *132*, 11923.

- (37) Nakamura, Y.; Yoshikai, N.; Ilies, L.; Nakamura, E. *Org. Lett.* **2012**, *14*, 3316.
- (38) Yoshikai, N.; Mashima, H.; Nakamura, E. *J. Am. Chem. Soc.* **2005**, *127*, 17978.
- (39) Yoshikai, N.; Matsuda, H.; Nakamura, E. *J. Am. Chem. Soc.* **2009**, *131*, 9590.
- (40) Nova, A.; Reinhold, M.; Perutz, R. N.; Macgregor, S. A.; McGrady, J. E. *Organometallics* **2010**, *29*, 1824.
- (41) Nova, A.; Erhardt, S.; Jasim, N. A.; Perutz, R. N.; Macgregor, S. A.; McGrady, J. E.; Whitwood, A. C. *J. Am. Chem. Soc.* **2008**, *130*, 15499.
- (42) Hatnean, J. A.; Johnson, S. A. *Organometallics* **2012**, *31*, 1361.
- (43) Igau, A.; Grutzmacher, H.; Baceiredo, A.; Bertrand, G. *J. Am. Chem. Soc.* **1988**, *110*, 6463.
- (44) Arduengo, A. J.; Harlow, R. L.; Kline, M. *J. Am. Chem. Soc.* **1991**, *113*, 361.
- (45) Herrmann, W. A.; Elison, M.; Fischer, J.; Köcher, C.; Artus, G. R. *J. Angew Chem Int Ed Engl* **1995**, *34*, 2371.
- (46) Herrmann, W. A.; Goossen, L. J.; Köcher, C.; Artus, G. R. *J. Angew Chem Int Ed Engl* **1996**, *35*, 2805.
- (47) Perrin, L.; Clot, E.; Eisenstein, O.; Loch, J.; Crabtree, R. H. *Inorg. Chem.* **2001**, *40*, 5806.
- (48) Love, J. A.; Sanford, M. S.; Day, M. W.; Grubbs, R. H. *J. Am. Chem. Soc.* **2003**, *125*, 10103.
- (49) Hillier, A. C.; Sommer, W. J.; Yong, B. S.; Petersen, J. L.; Cavallo, L.; Nolan, S. P. *Organometallics* **2003**, *22*, 4322.
- (50) Schaub, T.; Radius, U. *Chemistry – A European Journal* **2005**, *11*, 5024.
- (51) Schaub, T.; Backes, M.; Radius, U. *J. Am. Chem. Soc.* **2006**, *128*, 15964.
- (52) Ohashi, M.; Saijo, H.; Shibata, M.; Ogoshi, S. *Eur. J. Org. Chem.* **2013**, *2013*, 443.

- (53) Wu, J.; Faller, J. W.; Hazari, N.; Schmeier, T. J. *Organometallics* **2012**, *31*, 806.
- (54) Iglesias, M. J.; Blandez, J. F.; Fructos, M. R.; Prieto, A.; Álvarez, E.; Belderrain, T. R.; Nicasio, M. C. *Organometallics* **2012**, *31*, 6312.
- (55) Bair, J. S.; Schramm, Y.; Sergeev, A. G.; Clot, E.; Eisenstein, O.; Hartwig, J. F. *J. Am. Chem. Soc.* **2014**, *136*, 13098.

Chapter 2

- (1) Nakao, Y.; Kashihara, N.; Kanyiva, K. S.; Hiyama, T. *J. Am. Chem. Soc.* **2008**, *130*, 16170.
- (2) Kanyiva, K. S.; Kashihara, N.; Nakao, Y.; Hiyama, T.; Ohashi, M.; Ogoshi, S. *Dalton Trans.* **2010**, *39*, 10483.
- (3) Hatnean, J. A.; Beck, R.; Borrelli, J. D.; Johnson, S. A. *Organometallics* **2010**, *29*, 6077.
- (4) Lafrance, M.; Rowley, C. N.; Woo, T. K.; Fagnou, K. *J. Am. Chem. Soc.* **2006**, *128*, 8754.
- (5) Do, H.-Q.; Daugulis, O. *J. Am. Chem. Soc.* **2008**, *130*, 1128.
- (6) Nova, A.; Reinhold, M.; Perutz, R. N.; Macgregor, S. A.; McGrady, J. E. *Organometallics* **2010**, *29*, 1824.
- (7) Braun, T.; Perutz, R. N. In *Perspectives in Organometallic Chemistry*; Screttas, C. G., Steele, B. R., Eds.; The Royal Society of Chemistry: 2003, p 136.
- (8) Jolly, P. W.; Jonas, K.; Krüger, C.; Tsay, Y. H. *J. Organomet. Chem.* **1971**, *33*, 109.
- (9) Guihaumé, J.; Halbert, S.; Eisenstein, O.; Perutz, R. N. *Organometallics* **2012**, *31*, 1300.
- (10) Rosenthal, U.; Pulst, S.; Kempe, R.; Pörschke, K.-R.; Goddard, R.; Proft, B. *Tetrahedron* **1998**, *54*, 1277.
- (11) Poerschke, K. R. *J. Am. Chem. Soc.* **1989**, *111*, 5691.
- (12) Green, M.; Grove, D. M.; Howrd, J. A.; Spencer, J. L.; Stone, F. G. A. *J. Chem. Soc., Chem. Commun.* **1976**, 759.

- (13) Upton, T. H.; Goddard, W. A. *J. Am. Chem. Soc.* **1978**, *100*, 321.
- (14) Ozin, G. A.; McIntosh, D. F.; Power, W. J.; Messmer, R. P. *Inorg. Chem.* **1981**, *20*, 1782.
- (15) Guo, L.; Bradshaw, J. D.; Tessier, C. A.; Youngs, W. J. *Organometallics* **1995**, *14*, 586.
- (16) Johnson, S. A.; Taylor, E. T.; Cruise, S. J. *Organometallics* **2009**, *28*, 3842.
- (17) Cronin, L.; Higgitt, C. L.; Karch, R.; Perutz, R. N. *Organometallics* **1997**, *16*, 4920.
- (18) Wu, J.; Faller, J. W.; Hazari, N.; Schmeier, T. J. *Organometallics* **2012**, *31*, 806.
- (19) Hatnean, J. A.; Johnson, S. A. *Organometallics* **2012**, *31*, 1361.
- (20) Ateşin, T. A.; Li, T.; Lachaize, S.; García, J. J.; Jones, W. D. *Organometallics* **2008**, *27*, 3811.
- (21) Darensbourg, M. Y.; Ludwig, M.; Riordan, C. G. *Inorg. Chem.* **1989**, *28*, 1630.

Chapter 3

- (1) Halpern, J. *Inorg. Chim. Acta* **1981**, *50*, 11.
- (2) Atkins, P. W.; Walters, V.; De Paula, J. *Physical Chemistry*; Macmillan Higher Education, **2006**.
- (3) Blackmond, D. G. *Angew Chem Int Ed Engl* **2005**, *44*, 4302.
- (4) Strieter, E. R.; Blackmond, D. G.; Buchwald, S. L. *J. Am. Chem. Soc.* **2005**, *127*, 4120.
- (5) Shekhar, S.; Ryberg, P.; Hartwig, J. F.; Mathew, J. S.; Blackmond, D. G.; Strieter, E. R.; Buchwald, S. L. *J. Am. Chem. Soc.* **2006**, *128*, 3584.
- (6) Mathew, J. S.; Klusmann, M.; Iwamura, H.; Valera, F.; Futran, A.; Emanuelsson, E. A. C.; Blackmond, D. G. *The Journal of Organic Chemistry* **2006**, *71*, 4711.

- (7) Perrin, C. L.; Dwyer, T. J. *Chem. Rev. (Washington, DC, U. S.)* **1990**, *90*, 935.
- (8) Lineweaver, H.; Burk, D. *J. Am. Chem. Soc.* **1934**, *56*, 658.
- (9) Kanyiva, K. S.; Kashihara, N.; Nakao, Y.; Hiyama, T.; Ohashi, M.; Ogoshi, S. *Dalton Trans.* **2010**, *39*, 10483.
- (10) Guihaumé, J.; Halbert, S.; Eisenstein, O.; Perutz, R. N. *Organometallics* **2012**, *31*, 1300.
- (11) Hatnean, J. A.; Beck, R.; Borrelli, J. D.; Johnson, S. A. *Organometallics* **2010**, *29*, 6077.
- (12) Wu, J.; Faller, J. W.; Hazari, N.; Schmeier, T. J. *Organometallics* **2012**, *31*, 806.
- (13) Nakao, Y.; Kashihara, N.; Kanyiva, K. S.; Hiyama, T. *J. Am. Chem. Soc.* **2008**, *130*, 16170.
- (14) Rosenthal, U.; Pulst, S.; Kempe, R.; Pörschke, K.-R.; Goddard, R.; Proft, B. *Tetrahedron* **1998**, *54*, 1277.
- (15) Crabtree, R. H. In *The Organometallic Chemistry of the Transition Metals*; John Wiley & Sons, Inc.: **2005**, p 235.
- (16) Widegren, J. A.; Finke, R. G. *J. Mol. Catal. A: Chem.* **2003**, *198*, 317.
- (17) Bair, J. S.; Schramm, Y.; Sergeev, A. G.; Clot, E.; Eisenstein, O.; Hartwig, J. F. *J. Am. Chem. Soc.* **2014**, *136*, 13098.
- (18) Ozin, G. A.; McIntosh, D. F.; Power, W. J.; Messmer, R. P. *Inorg. Chem.* **1981**, *20*, 1782.

Chapter 4

- (1) Metrangolo, P.; Neukirch, H.; Pilati, T.; Resnati, G. *Acc. Chem. Res.* **2005**, *38*, 386.
- (2) Libri, S.; Jasim, N. A.; Perutz, R. N.; Brammer, L. *J. Am. Chem. Soc.* **2008**, *130*, 7842.
- (3) Johnson, M. T.; Džolić, Z.; Cetina, M.; Wendt, O. F.; Öhrström, L.; Rissanen, K. *Cryst. Growth Des.* **2011**, *12*, 362.

- (4) Beale, T. M.; Chudzinski, M. G.; Sarwar, M. G.; Taylor, M. S. *Chem. Soc. Rev.* **2013**, *42*, 1667.
- (5) Legon, A. C. *Phys. Chem. Chem. Phys.* **2010**, *12*, 7736.
- (6) Politzer, P.; Lane, P.; Concha, M.; Ma, Y.; Murray, J. *Journal of Molecular Modeling* **2007**, *13*, 305.
- (7) Brammer, L.; Minguez Espallargas, G.; Libri, S. *CrystEngComm* **2008**, *10*, 1712.
- (8) Bent, H. A. *Chem. Rev. (Washington, DC, U. S.)* **1968**, *68*, 587.
- (9) Guthrie, F. *Journal of the Chemical Society* **1863**, *16*, 239.
- (10) Hassel, O.; Hvoslef, J.; Vihovde, E. H.; Sørensen, N. A. *Acta Chem. Scand.* **1954**, *8*, 873.
- (11) Desiraju Gautam, R.; Legon Anthony, C.; Ho Shing, P.; Kloo, L.; Marquardt, R.; Metrangolo, P.; Politzer, P.; Resnati, G.; Rissanen, K. In *Pure Appl. Chem.* 2013; Vol. 85, p 1711.
- (12) Awwadi, F. F.; Willett, R. D.; Peterson, K. A.; Twamley, B. *Chemistry – A European Journal* **2006**, *12*, 8952.
- (13) Willett, R. D.; Awwadi, F.; Butcher, R.; Haddad, S.; Twamley, B. *Cryst. Growth Des.* **2003**, *3*, 301.
- (14) Zordan, F.; Brammer, L.; Sherwood, P. *J. Am. Chem. Soc.* **2005**, *127*, 5979.
- (15) Caballero, A.; Zapata, F.; Beer, P. D. *Coord. Chem. Rev.* **2013**, *257*, 2434.
- (16) Langton, M. J.; Robinson, S. W.; Marques, I.; Félix, V.; Beer, P. D. *Nat Chem* **2014**, *6*, 1039.
- (17) Robinson, S. W.; Mustoe, C. L.; White, N. G.; Brown, A.; Thompson, A. L.; Kennepohl, P.; Beer, P. D. *J. Am. Chem. Soc.* **2015**, *137*, 499.
- (18) Mele, A.; Metrangolo, P.; Neukirch, H.; Pilati, T.; Resnati, G. *J. Am. Chem. Soc.* **2005**, *127*, 14972.
- (19) Chudzinski, M. G.; McClary, C. A.; Taylor, M. S. *J. Am. Chem. Soc.* **2011**, *133*, 10559.
- (20) Caballero, A.; White, N. G.; Beer, P. D. *Angew Chem Int Ed Engl* **2011**, *50*, 1845.

- (21) Beweries, T.; Brammer, L.; Jasim, N. A.; McGrady, J. E.; Perutz, R. N.; Whitwood, A. C. *J. Am. Chem. Soc.* **2011**, *133*, 14338.
- (22) Siegbahn, P. E. M.; Eisenstein, O.; Rheingold, A. L.; Koetzle, T. F. *Acc. Chem. Res.* **1996**, *29*, 348.
- (23) Henderson, W. A.; Streuli, C. A. *J. Am. Chem. Soc.* **1960**, *82*, 5791.
- (24) Cronin, L.; Higgitt, C. L.; Karch, R.; Perutz, R. N. *Organometallics* **1997**, *16*, 4920.
- (25) Bennett, M. A.; Wenger, E. *Organometallics* **1995**, *14*, 1267.
- (26) Edwards, A. J.; Willis, A. C.; Wenger, E. *Organometallics* **2002**, *21*, 1654.
- (27) Saitô, H.; Ando, I.; Ramamoorthy, A. *Prog. Nucl. Magn. Reson. Spectrosc.* **2010**, *57*, 181.
- (28) Weingarth, M.; Raouafi, N.; Jouvelet, B.; Duma, L.; Bodenhausen, G.; Boujlel, K.; Schollhorn, B.; Tekely, P. *Chem. Commun. (Cambridge, U. K.)* **2008**, 5981.
- (29) Lommerse, J. P. M.; Stone, A. J.; Taylor, R.; Allen, F. H. *J. Am. Chem. Soc.* **1996**, *118*, 3108.
- (30) Rowland, R. S.; Taylor, R. *The Journal of Physical Chemistry* **1996**, *100*, 7384.
- (31) Alvarez, S. *Dalton Trans.* **2013**, *42*, 8617.
- (32) Zhao, X.; Sudmeier, J. L.; Bachovchin, W. W.; Levitt, M. H. *J. Am. Chem. Soc.* **2001**, *123*, 11097.
- (33) Viger-Gravel, J.; Leclerc, S.; Korobkov, I.; Bryce, D. L. *Journal of the American Chemical Society* **2014**, *136*, 6929.
- (34) Viger-Gravel, J.; Meyer, J. E.; Korobkov, I.; Bryce, D. L. *CrystEngComm* **2014**, *16*, 7285.
- (35) Mínguez Espallargas, G.; Brammer, L.; Allan, D. R.; Pulham, C. R.; Robertson, N.; Warren, J. E. *J. Am. Chem. Soc.* **2008**, *130*, 9058.

Chapter 5

- (1) Libri, S.; Jasim, N. A.; Perutz, R. N.; Brammer, L. *J. Am. Chem. Soc.* **2008**, *130*, 7842.
- (2) Hassel, O.; Hvoslef, J.; Vihovde, E. H.; Sørensen, N. A. *Acta Chem. Scand.* **1954**, *8*, 873.
- (3) Beale, T. M.; Chudzinski, M. G.; Sarwar, M. G.; Taylor, M. S. *Chem. Soc. Rev.* **2013**, *42*, 1667.
- (4) Arunan, E.; Desiraju Gautam, R.; Klein Roger, A.; Sadlej, J.; Scheiner, S.; Alkorta, I.; Clary David, C.; Crabtree Robert, H.; Dannenberg Joseph, J.; Hobza, P.; Kjaergaard Henrik, G.; Legon Anthony, C.; Mennucci, B.; Nesbitt David, J. In *Pure Appl. Chem.* 2011; Vol. 83, p 1619.
- (5) Legon, A. C.; Millen, D. J. *Faraday Discussions of the Chemical Society* **1982**, *73*, 71.
- (6) Smith, D. A.; Brammer, L.; Hunter, C. A.; Perutz, R. N. *J. Am. Chem. Soc.* **2014**, *136*, 1288.
- (7) Robertson, C. C.; Perutz, R. N.; Brammer, L.; Hunter, C. A. *Chem. Sci.* **2014**, *5*, 4179.
- (8) Nguyen, H. L.; Horton, P. N.; Hursthouse, M. B.; Legon, A. C.; Bruce, D. W. *J. Am. Chem. Soc.* **2003**, *126*, 16.
- (9) Peris, E.; Lee, J. C.; Rambo, J. R.; Eisenstein, O.; Crabtree, R. H. *J. Am. Chem. Soc.* **1995**, *117*, 3485.
- (10) Laurence, C.; Queignec-Cabanetos, M.; Dziembowska, T.; Queignec, R.; Wojtkowiak, B. *J. Am. Chem. Soc.* **1981**, *103*, 2567.
- (11) Beweries, T.; Brammer, L.; Jasim, N. A.; McGrady, J. E.; Perutz, R. N.; Whitwood, A. C. *J. Am. Chem. Soc.* **2011**, *133*, 14338.
- (12) Cronin, L.; Higgitt, C. L.; Karch, R.; Perutz, R. N. *Organometallics* **1997**, *16*, 4920.
- (13) Brammer, L.; Bruton, E. A.; Sherwood, P. *Cryst. Growth Des.* **2001**, *1*, 277.
- (14) Aullon, G.; Bellamy, D.; Guy Orpen, A.; Brammer, L.; Eric, A. B. *Chem. Commun. (Cambridge, U. K.)* **1998**, 653.
- (15) Sarwar, M. G.; Dragisic, B.; Salsberg, L. J.; Gouliaras, C.; Taylor, M. S. *J. Am. Chem. Soc.* **2010**, *132*, 1646.

- (16) Schaub, T.; Fischer, P.; Steffen, A.; Braun, T.; Radius, U.; Mix, A. *J. Am. Chem. Soc.* **2008**, *130*, 9304.
- (17) Ammann, C.; Meier, P.; Merbach, A. *Journal of Magnetic Resonance (1969)* **1982**, *46*, 319.
- (18) Wilson, D. J. D.; Couchman, S. A.; Dutton, J. L. *Inorg. Chem.* **2012**, *51*, 7657.
- (19) Fortman, G. C.; Nolan, S. P. *Chem. Soc. Rev.* **2011**, *40*, 5151.

Chapter 6

- (1) Wu, J.; Faller, J. W.; Hazari, N.; Schmeier, T. J. *Organometallics* **2012**, *31*, 806.
- (2) Hatnean, J. A.; Beck, R.; Borrelli, J. D.; Johnson, S. A. *Organometallics* **2010**, *29*, 6077.
- (3) Blackmond, D. G. *Angew Chem Int Ed Engl* **2005**, *44*, 4302.
- (4) Guihaumé, J.; Halbert, S.; Eisenstein, O.; Perutz, R. N. *Organometallics* **2012**, *31*, 1300.
- (5) Guihaume, J.; Halbert, S.; Eisenstein, O.; Perutz, R. N. *Organometallics* **2012**, *31*, 1300.
- (6) Kanyiva, K. S.; Kashihara, N.; Nakao, Y.; Hiyama, T.; Ohashi, M.; Ogoshi, S. *Dalton Trans.* **2010**, *39*, 10483.
- (7) Johnson, M. T.; Džolić, Z.; Cetina, M.; Wendt, O. F.; Öhrström, L.; Rissanen, K. *Cryst. Growth Des.* **2011**, *12*, 362.
- (8) Crabtree, R. H. *J. Organomet. Chem.* **2005**, *690*, 5451.

Chapter 7

- (1) Otsuka, S.; Rossi, M. *Journal of the Chemical Society A: Inorganic, Physical, Theoretical* **1968**, 2630.
- (2) Jolly, P. W.; Jonas, K.; Krüger, C.; Tsay, Y. H. *J. Organomet. Chem.* **1971**, *33*, 109.
- (3) Darensbourg, M. Y.; Ludwig, M.; Riordan, C. G. *Inorg. Chem.* **1989**, *28*, 1630.
- (4) Hatnean, J. A.; Beck, R.; Borrelli, J. D.; Johnson, S. A. *Organometallics* **2010**, *29*, 6077.

- (5) Nakao, Y.; Kashihara, N.; Kanyiva, K. S.; Hiyama, T. *J. Am. Chem. Soc.* **2008**, *130*, 16170.
- (6) Kanyiva, K. S.; Kashihara, N.; Nakao, Y.; Hiyama, T.; Ohashi, M.; Ogoshi, S. *Dalton Trans.* **2010**, *39*, 10483.
- (7) Cronin, L.; Higgitt, C. L.; Karch, R.; Perutz, R. N. *Organometallics* **1997**, *16*, 4920.
- (8) Wu, J.; Faller, J. W.; Hazari, N.; Schmeier, T. J. *Organometallics* **2012**, *31*, 806.
- (9) Poerschke, K. R. *J. Am. Chem. Soc.* **1989**, *111*, 5691.
- (10) Ammann, C.; Meier, P.; Merbach, A. *Journal of Magnetic Resonance (1969)* **1982**, *46*, 319.
- (11) Smith, D. A.; Brammer, L.; Hunter, C. A.; Perutz, R. N. *J. Am. Chem. Soc.* **2014**, *136*, 1288.
- (12) Christe, K. O.; Wilson, W. W.; Wilson, R. D.; Bau, R.; Feng, J. A. *J. Am. Chem. Soc.* **1990**, *112*, 7619.
- (13) Schaub, T.; Radius, U. *Chemistry – A European Journal* **2005**, *11*, 5024.
- (14) Libri, S.; Jasim, N. A.; Perutz, R. N.; Brammer, L. *J. Am. Chem. Soc.* **2008**, *130*, 7842.
- (15) Beweries, T.; Brammer, L.; Jasim, N. A.; McGrady, J. E.; Perutz, R. N.; Whitwood, A. C. *J. Am. Chem. Soc.* **2011**, *133*, 14338.